THE UNIVERSITY *of* EDINBURGH

Phage therapy for *Escherichia coli* urinary tract infections: selecting therapeutic phages and understanding resistance mechanisms in urine

Alba Park de la Torriente

Thesis presented for the degree of Doctor of Philosophy

The University of Edinburgh

2023

Declaration

I hereby declare that this thesis has been written and composed by me. Except where stated otherwise, the work presented here is my own and has not been submitted for any degree or professional qualification.

Alba Park de la Torriente June 2023

Abstract

Urinary tract infections (UTIs) affect a large proportion of the human and canine population. Due to rising levels of antibiotic resistance, empirical treatment with conventional antibiotics may fail, which can increase the probabilities of recurrence and severe complications. The most common species causing UTIs is uropathogenic *Escherichia coli* (UPEC), from which a clonal complex of particular concern is the O25:H4-ST131 as it is associated with the global emergence of multidrug-resistant and highly pathogenic urinary tract and bloodstream infections. Phage therapy is regarded as a promising alternative to antibiotics and could be especially useful to treat multidrug-resistant bacteria such as ST131 strains. This work aimed to find phages that could target strain EC958: a well characterised member of the ST131 group; and to dissect the causes of resistance that could lead to unsuccessful treatment. First, the optimisation of an artificial urine (AU) that could be used to study the phage-bacterium interaction was carried out, with the intention of obtaining results that could be translated to human and veterinary medicine. Then, different phages and phage combinations were screened against EC958 in the AU and standard lab media (LB). Finding a phage cocktail that could inhibit EC958 in LB was relatively easy, whereas none of the combinations tested in AU could prevent its growth for more than 8 hours. To understand what was causing the resistance, the infection assays were analysed by media and by timepoint using the phage LUC4. For this, individual colonies were isolated from the surviving population after phage exposure and re-challenged with the phage. The majority of the resistant variants recovered from LB assays were insensitive to the phage in the subsequent infections, which indicated that they had a fixed resistance to the phage. In AU, two different phenotypes were found in the resistant population. Some of the single colonies gave rise to a fixed phage-resistant culture, and others were still susceptible to the phage, despite having survived the initial challenge. Analysis of short and long read sequencing data indicated that mutations led to loss of expression of the

primary phage receptor—OmpC—in the fixed resistant variants. The transient resistance, which is also observed in pooled canine urine but not in LB, was accelerated when the bacteria were cultured in the supernatant of an EC958 culture, and this was not due to significant changes in the phage adsorption rate. It was concluded that the productive phage infection was highly dependent on the culture conditions and the physiological state of the bacterial culture, which validated the effort to develop the AU for *E. coli*-phage interaction studies. The mechanism underlying the transient resistance could not be fully deciphered in the time available, but various hypotheses are discussed in the thesis and are currently being tested.

Towards testing phage therapy for *E. coli* ST131 UTIs, three pilot studies were carried out in pigs: the first one with the aim of testing the safety of therapeutic phages produced from a detoxified *E. coli* strain; the second to establish a porcine model of UTI with ST131, and the third one used the UTI model to observe the efficacy of the phage. This study was also useful to analyse a phage treatment of EC958 infection *in vivo*, and *ex vivo*, by challenging the infected urine samples with phage. Preliminary data from these pilot studies suggested that pigs can be a good model to study *E. coli* UTIs and phage therapy. The phage preparations did not cause any significant inflammatory response in the pigs. *E. coli* ST131 strain EC958 was able to colonise and establish a UTI after intravesical instillation, with some evidence of macroscopical lesions in the bladder mucosa such as petechias. However, it is speculated that the infection was starting to self-resolve after a week. Phage LUC4 showed little impact to treat the UTI *in vivo*, with only a very short-lived reduction in bacterial counts in the urine of one of two animals. In line with the *in vitro* studies using AU and pooled urine, analysis of the surviving bacteria showed that they retained sensitivity to phage LUC4 when tested under laboratory conditions. This indicated that transient resistance was also the main issue preventing an effective intervention *in vivo*, for which it is important to understand the mechanism behind this resistance in order to achieve a safe and effective phage therapy for a multidrug-resistant UPEC such as ST131 EC958.

Lay Summary

Urinary tract infections (UTIs) are common in humans and companion animals. The bacterial species that causes the majority of these infections is *Escherichia coli*. Most UTIs can be treated with antibiotics, but there is a concerning rise in antibiotic resistance which increases the risk of failed treatments and more severe outcomes including bloodstream infections and sepsis. This threat calls for the research and development of alternative strategies to prevent and treat bacterial infections, such as vaccines, probiotics, immune modulators and bacteriophages (or phages). Phages are viruses that exclusively infect and can kill bacteria, which gives them potential to be administered in humans and animals with bacterial infections. The use of phages for medical purposes is called phage therapy (PT) and has been used in some countries for several decades. Still, some features of PT make it a challenge for widescale adoption and commercialisation. Unlike antibiotics, phages often have a narrow spectrum; and as with antibiotics, bacteria can have resistance that allows them to escape phage killing. For these reasons, prescribing the right phage for a particular infection can be difficult, and even with prior confirmation of susceptibility, the therapy can still fail. The aim of this project was to address some of these issues. Using a well-studied multidrug-resistant *E. coli* strain, EC958, a range of phages and phage cocktails were tested. The results showed that this strain is highly resistant to phage infection in urine and therefore the causes of resistance were investigated. By analysing the bacteria surviving phage infection, it was shown that more than one resistance mechanism is in place. Genetic mutations can lead to changes on the surface of the bacterium that prevent the attachment of the phage to the bacterial host, which is the first requirement for infection. On the other hand, it is hypothesised that changes in bacterial physiology as a consequence of growing in urine can cause resistance of the bacterial culture to phage. This type of resistance is not observed in lab culture conditions and this is not due to a lack of phage recognition at the bacterial cell surface. The latter mechanism could not be characterised further, but its significance was supported in a pilot study using an animal model of UTI.

Acknowledgements

Finishing this work has been a big accomplishment that could not have happened without everyone who supported me and believed in me. In the first place, I would like to thank my main supervisor David Gally for giving me the opportunity to carry out this PhD. Thank you for guiding me and for being understanding during the turbulent times. Then, to the present members of the lab group (Asim, Emily and Vesa), and the ones who have left (Agata, Amany, Nadejda, Stephen and Zhuneng), but especially the ones that have directly given me guidance and have helped me in so many ways throughout these years: Marianne Keith, Alison Low, Sean McAteer and Annita Chalka: thank you for everything.

I am extremely grateful to the people who has made me feel welcome in a foreign place. Those working in the lab module 2.042, for making it a supportive and fun space with music, dances and good energy: Willow, Amy, Joana, Nicky, Nat and Fiona. And to the people who motivate me with their sheer presence: Holly, Jamie, Ricky, Rose and Spring. Thanks for making the bad moments a bit better, and the good moments great.

The most special acknowledgement goes to my parents because your unconditional love and support have allowed me to become who I am today; and to my sister for walking with me during the early stages of life; and to my partner Pato for the years of unconditional love and support. Thanks to my friends back home who were present in my life despite being far away.

Many thanks to everyone in the LARIF for the hard work and the help in getting the animal experiments for the pilot studies included in this thesis.

Thanks to the people who contributed and helped in the completion of this thesis: Sean and Marianne for carrying out a few experiments whilst I was writing, Alison and David for the ideas on new hypotheses and the feedback, Joana for helping with the statistical analysis and Gavin for reading and giving me feedback on some parts of it.

This work was funded by the National Council of Science and Technology of Mexico, and the College of Medicine and Veterinary Medicine, University of Edinburgh through the University of Edinburgh and University of Glasgow joint PhD studentship in One Health.

Contents

List of Figures

List of Tables

List of abbreviations

Abbreviation	Full description
Abi	Abortive infection
ABR	Antibiotic resistance
amp	Ampicillin
ANOVA	Analysis of variance
AU	Artificial urine
AUC	Area under the curve
bp	Base pairs
BREX	Bacteriophage exclusions
C	Celsius
CC	ClearColi
CCA	Coliform ChromoSelect Agar
CFU	Colony forming units
cm	Chloramphenicol
CRISPR-Cas	Clustered Regularly Interspaced Short Palindromic Repeats-CRISPR-associated protein
DISARM	Defence Island Associated with Restriction-Modification
DNA	Deoxyribonucleic acid
ECL	Enhanced chemiluminescence
EDTA	Ethylenediaminetetraacetic Acid
ESBL	Extended-spectrum Beta Lactamase
EU	Endotoxin Units
FC	Fold Change
GC	Guanine-cytosine

H_2O	Water
HCl	Hydrochloric acid
IBC	Intracellular bacterial communities
IFN	Interferon
IL	Interleukin
INDEL	Insertion/Deletion
IPTG	Isopropyl Beta-D-1-thiogalactopyranoside
kbp	kilo base pairs
kDa	Kilo Daltons
kV	kilo-Volts
LARIF	Large Animal Research and Imaging Facility
LB	Lysogeny Broth
LPS	Lipopolysaccharide
mL	millilitres
MLEE	Multilocus Enzyme Electrophoresis
MLST	Multilocus Sequence Typing
mm	millimetres
MOI	Multiplicity of infection
n	Number of replicates
NaCl	Sodium Chloride
Nal	Nalidixic Acid
NaOH	Sodium hydroxide
OD	Optical Density
OMP	Outer membrane protein
PBS	Phosphate Buffered Saline
PCR	Polymerase Chain Reaction

PFGE	Pulsed Field Gel Electrophoresis
PFU	Plaque forming units
Pgl	Phage growth limitation
PICI	Phage-inducible chromosomal islands
PT	Phage Therapy
PTC	Phage Technology Centre
PU	Pooled canine urine
QS	Quorum Sensing
R(D)SVS	Royal (Dick) School of Veterinary Studies
RFC	Relative Centrifugal Force
RFLP	Restriction Fragment Length Polymorphism
Rif	Rifampicin
RM	Restriction-Modification
RNA	Ribonucleic acid
RPM	Revolutions per minute
s	Seconds
SD	Standard Deviation
SDS	Sodium Dodecyl Sulphate
SDS-PAGE	Sodium dodecyl sulphate–polyacrylamide gel electrophoresis
SG	Specific Gravity
SM	Sodium Magnesium
SNP	Single nucleotide polymorphism
ss	Single stranded
ST	Sequence Type
TA	Toxin-Antitoxin

TEM	Transmission electron microscopy
TNF	Tumour necrosis factor
UPEC	Uropathogenic Escherichia coli
UTI	Urinary tract infection
V	Volts
WGS	Whole genome sequencing
WHO	World Health Organisation
WT	Wild type
µg	micrograms
µL	microliters
µm	micrometres

Chapter 1 Main introduction

1.1 Human and canine urinary tract infections from a One Health perspective

Urinary tract infections (UTIs) are most commonly caused by bacteria and can affect any part of the urinary tract. After respiratory and gastrointestinal infections, UTIs are the third most common type of infection affecting humans worldwide, and the second most common infection presented in the human population in high income countries (Flores-Mireles et al., 2015). It is estimated that almost half of all women experience at least one UTI throughout their lifetime (Foxman, 2003). Worldwide, between 150 and 200 million people are clinically diagnosed with a UTI annually, making the economic burden of UTIs vast. In addition, people with UTIs have a decrease in their quality of life, especially when these are recurrent.

Canine UTIs are also a common cause of morbidity: they are the second most common reason for antibiotic prescription in dogs by veterinarians (De Briyne et al., 2014; Rantala et al., 2004). The incidence of reported canine UTIs is relatively smaller: it is estimated that 14% of dogs will have a UTI throughout their lifetime (Byron, 2019). However, the actual incidence of canine UTIs may be underrated due to absence of clinical signs. It has been estimated that up to 95% of canine UTIs can be silent and up to 50% of patients with recurrent UTIs did not show clinical signs on presentation (Forrester et al., 1999; McGuire et al., 2002; Seguin et al., 2003). There are also concerns over the possibility of cross-species transmission of uropathogens. Different reports have demonstrated the possibility of bacterial exchange between household members, including companion animals, and in professionals with close proximity to pets (Johnson and Clabots, 2006; Sidjabat et al., 2006; Yuri et al., 1998).

1.1.1 Classification of UTIs

There are different ways of classifying UTIs. Depending on the anatomical region that is affected, they can be classified as lower or upper UTIs (Foxman, 2010). Based on the onset of the infection, UTIs can be classified as community-acquired or nosocomial, acute or chronic, and sporadic or recurrent. UTIs can also be classified depending on the severity of the infection into uncomplicated and complicated. Uncomplicated UTIs are those in non-pregnant women that are otherwise healthy and have no known relevant anatomical and functional abnormalities of the urinary tract. Complicated UTIs refer to those cases with a higher chance of complications, such as in men, pregnant women, patients with anatomical or functional abnormalities affecting the urinary tract, patients with urinary catheters or with comorbidities (Ross and Hickling, 2022). These categorisations also apply to dogs, except for the terms ‘complicated’ and ‘uncomplicated’, which are falling out of use in veterinary medicine (Olin and Bartges, 2022).

1.1.2 Diagnosis

Diagnosis of UTIs is based on a positive urine culture, but this can take several days. Clinical signs, a complete urinalysis, and microscopic examination of urine sediment can be useful as an early differential diagnosis. The limit of bacterial counts in urine to diagnose a UTI can range from 10^2 to 10^5 CFU/mL, and is subject to interpretation depending on the presentation of clinical signs and the method of sample collection (Chu and Lowder, 2018; Schmiemann et al., 2010).

Escherichia coli is the bacterial species that is most frequently found causing UTIs. 80 to 90% of community acquired UTIs in humans (Flores-Mireles *et al.*,

2015; Foxman, 2014), and 54% of canine UTIs (Byron, 2019; Hall et al., 2013) are caused by *E. coli*.

1.1.3 Conventional treatment of UTI

Complicated and uncomplicated UTIs are routinely treated with a course of oral antibiotics, and most isolates are susceptible to at least one of the commonly prescribed antibiotics (Seguin *et al.*, 2003). However, increase in rates of resistance have been reported for uropathogens in humans (Blango and Mulvey, 2010; van Driel et al., 2019) and companion animal studies (Ball et al., 2008; Cooke et al., 2002; Normand et al., 2000; Prescott et al., 2002). Some official guidelines are in place to treat UTIs empirically with a lower risk of ineffectiveness due to antibiotic resistance (ABR). Most guidelines for human UTIs recommend nitrofurantoin and trimethoprim-sulfamethoxazole as first-line antimicrobial therapy for uncomplicated UTIs, whilst fosfomycin, pivmecillinam hydrocholride and beta-lactams are alternative options for cases in which first-line antibiotics cannot be used. However, local epidemiological studies need to be taken into consideration when following these guidelines, and the empirical therapy with certain antibiotics must be avoided when high (>10-20%) resistance levels exist locally (Ross and Hickling, 2022). Guidelines to treat UTIs in companion animals suggest amoxicillin, cephalexin or trimethoprim-sulfamethoxazole as first-line antibiotics, whilst fluoroquinolones, nitrofurantoin and cephalexin are usually reserved for cases in which resistance to the first-line antibiotics has been observed (Weese et al., 2019).

With the rising levels or ABR, UTIs are becoming more difficult to treat with conventional therapy, which in turn elevate the chances of recurrent or persistent infections (Schneeberger et al., 2016; Thompson et al., 2011). If UTIs are not resolved, both humans and canine patients can be at risk of further complications like pyelonephritis, urosepsis, and in the most severe

cases septic shock and death (Blango and Mulvey, 2010; Flores-Mireles *et al.*, 2015).

1.2 Escherichia coli

Escherichia coli is a facultative Gram-negative anaerobic bacterium which is commonly present in the gastro-intestinal tract of mammals and some birds (Gordon, 2013). There is a wide genetic diversity within the *E. coli* species due to its high propensity to homologous recombination. In addition, almost all *E. coli* isolates have plasmids, which broadens the diversity even more (Denamur et al., 2021). This diversity has allowed the species to adapt to different environments and occupy different niches. Hence, different *E. coli* strains can colonise different tissues with different levels of pathogenicity (Gordon, 2013).

1.2.1 Classification of *E. coli*

There are different methods of classifying *E. coli* strains which have been useful to identify the relatedness in epidemiological studies, and to distinguish commensal from pathogenic strains. The first substructure of *E. coli* was identified using Multi-locus Enzyme Electrophoresis (MLEE) by Whittam et al. (1983) who initially recognised the existence of four phylogroups. It was observed soon after that the source of the strains was associated with the different groups; and that the strains within the groups shared ecological niches and had similar pathogenicity. As more strains were examined, new groups were added and currently the existence of 8 different phylogroups is recognised: A, B1, B2, C, D, E, F, G and H (Denamur *et al.*, 2021). There is a strong association between the genetic background of *E. coli* isolates and virulence: phylogroups B2 and D are frequently found causing extraintestinal infections, whereas isolates causing intestinal haemorrhagic disease mostly

belong to phylogroups E and B1. PCR-based methods then replaced the MLEE for the classification of phylogroups (Clermont et al., 2000; Clermont et al., 2013) and whole genome sequencing (WGS) is now widely used for this purpose.

Despite the broad diversity of the *E. coli* population, there is a strong association of alleles that is not random, and for this reason, different clonal groups—composed of very closely related isolates that descend from a common ancestor—can be defined that are associated to pathotypes and phylogroups. Serotyping was a common method to classify *E. coli* strains into clonal groups based on the determination of the somatic (O), capsular (K) and/or flagellar (H) antigens. There is a strong association between specific serotypes and certain illnesses (Orskov and Orskov, 1992). These antigens were previously tested by serotyping or by MLEE, and WGS is now substituting these methods.

When studying pathogenic isolates, it is common to find the classification of *E. coli* based on the multi-locus sequence typing (MLST). In this typing method, a region of seven or more housekeeping genes (depending on the origin of the scheme) is sequenced. Different allele numbers are assigned depending on the polymorphic sequences of each gene, and the combination of alleles determines the sequence type (ST) (Maiden et al., 1998). This has proved to be useful to identify related strains for epidemiological studies. WGS allows the classification of *E. coli* isolates on this and the different basis mentioned above.

A more informal classification of the pathogenic strains of *E. coli* is by pathotypes. These are named based on different criteria, such as the affected system or organ, the host species, the pathology caused by the strains or the presence of relevant genes (Denamur *et al.*, 2021). The different pathotypes have acronyms; for instance, strains that cause diarrhoea and intestinal infections belong to the intestinal pathogenic *E. coli* (InPEC) pathotype, whereas those that are not pathogenic in the digestive tract, but can cause disease outside of it belong to the extraintestinal pathogenic *E. coli* pathotype

(ExPEC). Within the ExPEC group, there is the *E. coli* strains that can cause UTI, these are known as uropathogenic *E. coli* (UPEC). ExPEC and UPEC are the pathogroups of interest in this work, with further focus on the clonal group O25:H4-ST131 due to its relevance (1.2.2.3).

1.2.2 Uropathogenic *E. coli* (UPEC)

Uropathogenic *E. coli* (UPEC) is the most frequently isolated bacterial species in both, human (Tandogdu and Wagenlehner, 2016) and canine UTIs (Byron, 2019; Hall *et al.*, 2013). UPEC can inhabit the mammalian gut without causing disturbance, but becomes an opportunistic pathogen in the urinary tract. In ascending infections, the distal gut acts as reservoir of UPEC (Kaper et al., 2004), which can then colonise periurethral and vaginal areas, and ascend to the bladder by the urethra. Once in the bladder, UPEC can grow in urine as a planktonic culture. Bacteria that are in close contact with the bladder epithelium cells can adhere and produce biofilm-like structures, which can serve as a strategy to escape antibacterial compounds (Goller and Seed, 2010). Some UPEC strains are able to invade the bladder cells and replicate within them forming intracellular bacterial communities (IBC), protecting them from antibiotics (Duncan et al., 2004). These can remain as quiescent reservoirs, and are a common cause of persistence. If the immune defences and/or antimicrobial therapy fail to stop the ascension of the UTI, bacteria can migrate through the ureters and colonise the kidneys causing tissue damage and an increased risk of urosepsis (Terlizzi et al., 2017).

1.2.2.1 Virulence factors of UPEC

UPEC must also deal with the innate immune responses of the urinary tract. Structural components of UPEC have an important role in attachment and

invasion of the urothelium. These include lipopolysaccharide (LPS), polysaccharide capsule, flagella, pili, curli, afimbiral adhesins and outer membrane proteins (OMPs). PapG (found at the tip of the Pap-pili) and FimH (located at the tip of type 1 fimbriae) are present in most UPECs (Arafi et al., 2023; Terlizzi *et al.*, 2017). These adhesins have an important role in ascending infections and renal colonisation (Kadry et al., 2020), and the latter has been found essential for the formation of UPEC intracellular bacterial communities (Subashchandrabose and Mobley, 2015). Afimbrial adhesins may include TosA, which is found in ~30% of all UPEC isolates, (Vigil et al., 2011; Xicohtencatl-Cortes et al., 2019), FdeC which has a role in colonisation (Nesta et al., 2012) and Iha (iron regulated adhesin) which facilitates attachment to urothelial cells (Johnson et al., 2015). UPEC's flagellum not only has the role of motility, but also of adherence.

UPEC can also secrete proteins that mediate its virulence. For instance, toxins, such as alpha-haemolysin, can cause renal damage and scarring. Expression of siderophores—such as yersiniabactin, salmochelin and aerobactin—are important for UPEC to be able to survive in an iron-limited environment such as the urinary tract (Reigstad et al., 2007).

1.2.2.2 Microbial metabolism of UPEC

In addition to the virulence factors of UPEC, the metabolic adaptability of UPEC allows its survival and growth in urine, which is hypertonic and has high concentrations of urea and inorganic salts, which make it a hostile environment for most bacteria (Ipe and Ulett, 2016).

In contrast with other pathotypes, UPEC has an extraordinary capacity to rapidly regulate its metabolism in response to nutrient availability; this allows UPEC to colonise different systems (Mann et al., 2017). In the gut, UPEC uses glycoproteins and carbohydrates from the intestinal mucus layer, such as N-

acetylglucosamine and N-acetylneuraminic acid, to grow (Katouli, 2010; Severi et al., 2008); whereas in the urinary tract, these sugars are in very limited concentration. In this sense, glycolysis and other pathways closely related to it, are not an essential pathway for UPEC to grow in urine and the urinary tract (Chan and Lewis, 2022; Reitzer and Zimmern, 2019). UPEC has two-component signalling systems that serve as sensors and regulators for a rapid adaptation to changes in the environment. The BarA/UvrY system serves as a switch between glycolytic (Figure 1.1) and gluconeogenic (Figure 1.2) pathways (Tomenius et al., 2006);

In contrast, urine has very low levels of carbohydrate but consistently contains amino acids and small peptides at a relatively high concentration, for which UPEC has adapted to use as the main energy source. Despite the consistent presence of these macro molecules in urine, some amino acids can be absent or be quickly depleted from urine in the presence of bacteria. For this reason, UPEC heavily relies in metabolic pathways to synthesise amino acids (Chan and Lewis, 2022). UPEC strains unable to synthesise glutamine, leucine, methionine, serine phenylalaline, proline, and arginine, show lower fitness in urine, which indicates that biosynthesis of these amino acid is important. Additionally, the methionine and branched-chain amino acids biosynthesis pathways appear to be essential for UPEC for planktonic growth in urine (Ma et al., 2018; Vejborg et al., 2012).

Catabolism of L-serine, one of the most abundant amino acids in urine, results in ammonium and pyruvate, which can then be used in central metabolic pathways including gluconeogenesis and the tri-carboxilic acid cycle to generate energy and synthesise essential amino acids when these are not available in the medium.

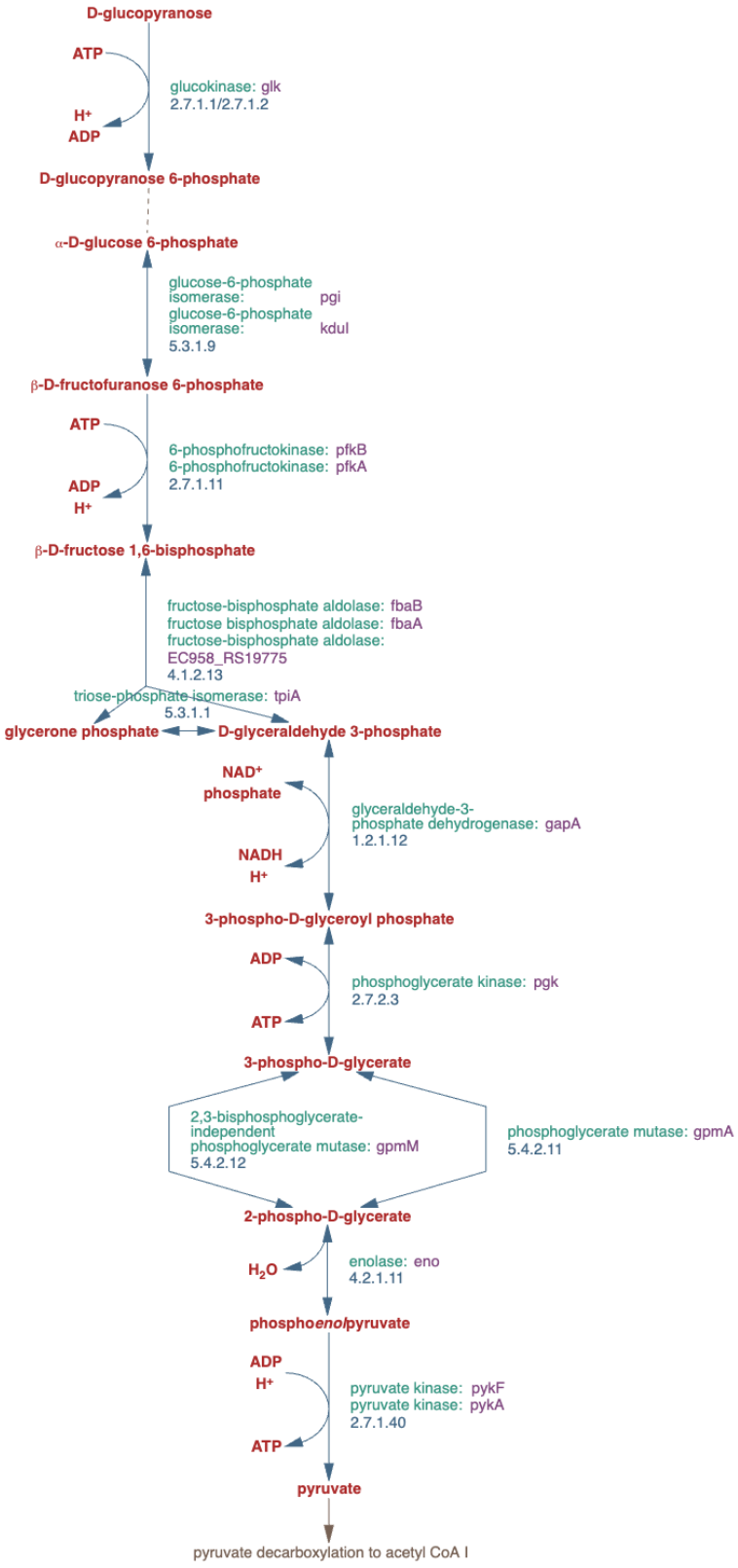

Figure 1.1 Glycolytic pathway of UPEC. UPEC utilises carbohydrates and glycoproteins in the gastrointestinal tract as substrates to grow, for which the glycolytic pathway is of high importance for energy generation and central carbon metabolism. Diagram extracted from biocyc.org (Karp et al., 2019)

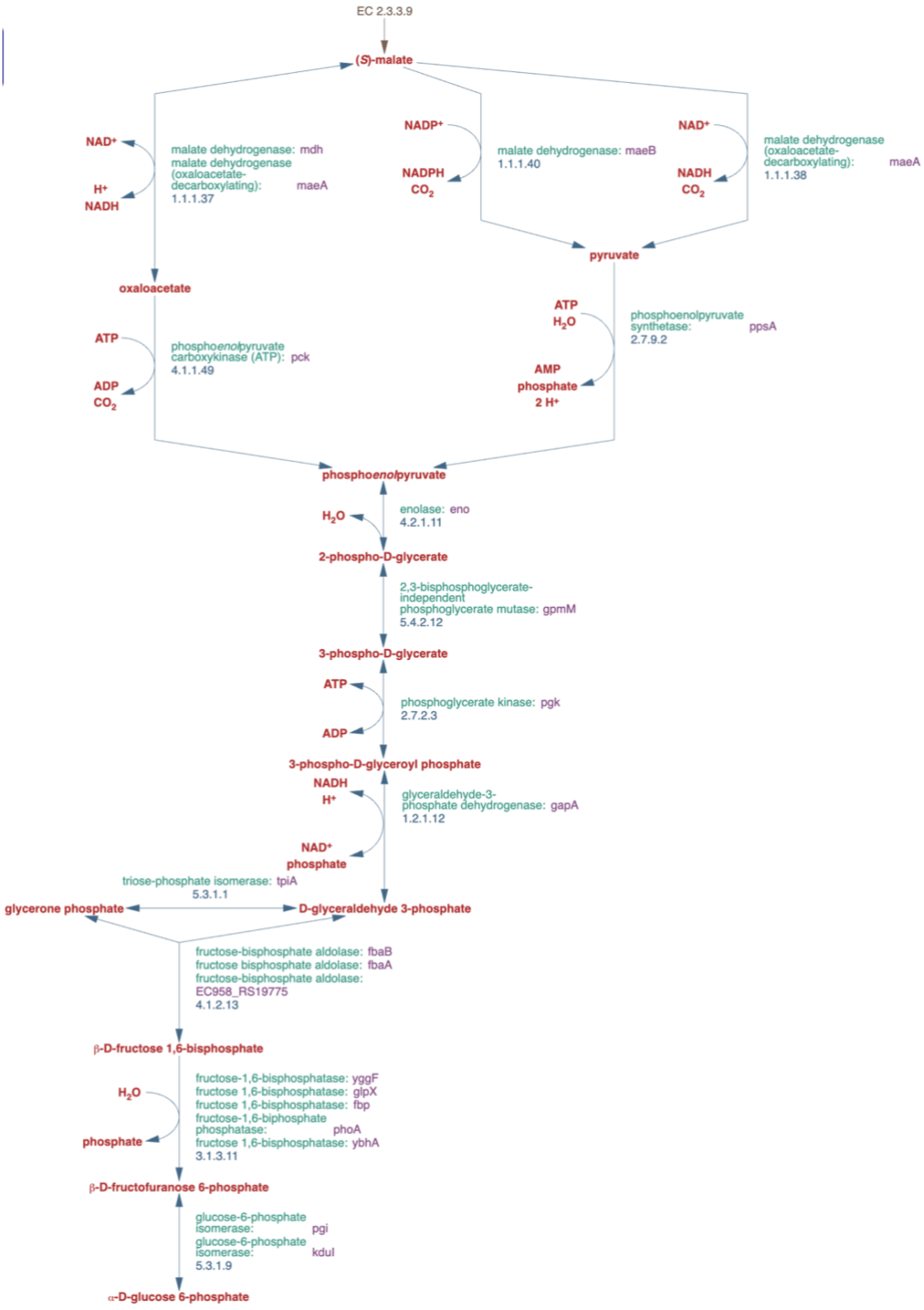

Figure 1.2 Gluconeogenic pathway of UPEC. UPEC has an extraordinary ability to adapt its metabolism to replicate in the urinary tract, where carbohydrates are not readily available and the main carbon source for UPEC are amino acids and small peptides, for which the gluconeogenic pathway is of importance for the survival of UPEC. Diagram extracted from biocyc.org (Karp *et al.*, 2019)

1.2.2.3 Uropathogenic *E. coli* ST131

Within the ExPEC pathotype, some clonal groups are isolated from clinical cases at a higher frequency. Several epidemiological studies have found that four STs represent the majority of all ExPEC isolates: ST131, ST73, ST95 and ST69 (Adams-Sapper et al., 2013; Clermont et al., 2017; Day et al., 2016; Kallonen et al., 2017; Yoon et al., 2018). From these, the emergence of the ST131 has been of particular concern due to its rapid global dissemination, which has allowed it to establish as the current most prevalent clonal group among ExPEC (Manges et al., 2019; Nicolas-Chanoine et al., 2014). Some characteristics of this clonal group that have driven its emergence are the acquisition of resistance to multiple antibiotics without significant fitness cost or loss of pathogenicity, its ability to grow in different environments including urine and serum, and to colonise and persist in the mammalian gut (Sarkar et al., 2018; Vimont et al., 2012).

E. coli ST131 belongs to the phylogenetic group B2, and has two subclades: the serotypes O25:H4 and O16:H5. Most ST131 isolates produce extended-spectrum beta-lactamases and are resistant to fluoroquinolones (Coque et al., 2008; Nicolas-Chanoine et al., 2008). As well as the multidrug-resistant traits, strains within this group are highly pathogenic due to their acquisition of virulence factors (Nicolas-Chanoine *et al.*, 2014). Isolates frequently present Secreted Autotransporter toxin (*sat*), type 1 fimbriae (*fimH*), yersiniabactin receptor (*fyuA*), group 2 capsule (*kpsM II*), uropathogen specific protein (*usp*), pathogenicity island marker (*malX*), adhesin siderophore receptor (*iha*), outer membrane receptor (*ompT*), aerobactin (*iucD*), aerobactin receptor (*iutA*) and serum resistance associated gene (*tratT*). In contrast, they lack P fimbria *pap* genes and cytotoxic necrotizing factor (*cnf1*).

Although ST131 strains seem to have a preference for human hosts, there is evidence that they can be shared between humans and companion animals

(Ewers et al., 2010; Johnson et al., 2016; Johnson et al., 2009; LeCuyer et al., 2018; Platell et al., 2010; Zogg et al., 2018). ST131 *E. coli* has also been isolated from animals in close proximity to urban areas (Mukerji et al., 2019) and poultry meat (Liu et al., 2018). This has raised concerns regarding the potential reservoirs of ST131 strains, and highlights the need to study this clonal group with a One Health perspective.

1.3 Phage therapy as an alternative intervention to treat UTIs

The alarming rise of antibiotic resistance is motivating a search for alternative strategies to prevent and treat bacterial infections (Czaplewski et al., 2016; Rello et al., 2019). Probiotics, oestrogens, methenamine, and Vitamin D have been suggested as supplements for the prevention of recurrent UTIs; whilst adhesins and siderophores have been studied as vaccine candidates (O'Brien et al., 2016). In addition, pillicides and curlicides, D-mannose and FimH antagonists, phenols, bacteriophages and phage lysins have been proposed as an alternative or complementary to antibiotics (Terlizzi *et al.*, 2017).

Bacteriophages (or phages) are viruses that exclusively infect and can kill bacteria. It is estimated that there are 10^{31} phages on the planet, making them the most diverse and abundant biological entities (Suttle, 2005). Within this enormous diversity, tailed phages (from the class *Caudoviricetes*) are the most commonly used for PT and the most represented in databases, thus these phages will be the focus of this work. These are composed of a proteinaceous capsid surrounding and protecting the phage genome, which is most commonly double-stranded DNA (Dion et al., 2020), and a tail, which is joined to the capsid by the connector complex (Nobrega et al., 2018).

The taxonomy of phages, like other viruses, used to be based on morphologic and phenotypic characteristics, but as genomic characterisation of viruses is

becoming the default, a new basis for viral taxonomic classification is being created. These new policies enable the categorisation of viruses without the need to isolate the virus, therefore, characterisation based on the pathogenicity or host range or phenotypical features are not required either (Simmonds et al., 2023; Walker et al., 2022). Nonetheless, for historical reasons phages are commonly still classified based on their morphology (Figure 1.3). Within the tailed viruses, Siphoviruses are characterised by having long and flexible tails which end in a terminator protein (Arnaud et al., 2017). Myoviruses have a tail with a similar structure, but with an additional layer surrounding it called the protein sheath. These form a contractile structure for the injection of the phage genome into the host cell. Phages within these groups have a baseplate at the end of the tail with receptor binding proteins (Nobrega *et al.*, 2018). Podoviruses have short and non-contractile tails with an extension used to deliver the phage genome into the host (Wang et al., 2019).

Depending on their life cycle, phages can be classified as strictly lytic/virulent or temperate/lysogenic. Both begin infection by attaching to the surface of their host and injecting their genetic material into the cytoplasm. Virulent phages take over the replication machinery to construct new virions within the host cell and then lyse it to release the progeny, whereas temperate phages can alternatively induce lysogeny by integrating into the host's DNA in the form of a prophage and remain in a latent state until a stressor compromises the host cell. The phage can then induce the lytic life cycle to release new virions into the environment (Figure 1.4). Other life cycles—such as chronic infections of filamentous phages and pseudolysogeny—have also been described (Clokie et al., 2011), but PT mainly relies on phages with a strict lytic life cycle, as temperate phages could lead to unwanted effects such as general transduction, transfer of antimicrobial resistance, toxins and virulence genes and superinfection immunity from other phages (Drulis-Kawa et al., 2012; Goh, 2016).

Phage therapy (PT)—the use of bacterial viruses to treat bacterial infections—has been a promising option to treat bacterial infections since phage discovery more than a century ago, before antibiotics were discovered. After a brief period of research, phages started losing popularity in western countries partly due to a lack of understanding of phage biology leading to inconsistent clinical outcomes (Cisek et al., 2017). The subsequent discovery of antibiotics eclipsed the interest in PT (Summers, 2001) because they offered a broad spectrum treatment and ease of production, making them a perfect fit for the western commercialization model. Nevertheless, the research on phage biology and PT continued in the former Soviet Union and other Eastern Bloc countries like Poland (Kutateladze and Adamia, 2008; Myelnikov, 2018). The Eliava Institute in Georgia and the Ludvik Hirszfeld Institute of Immunology and Experimental Therapy in Poland have shown the power of phage therapy by safely treating patients for decades. With the increasing levels of antibiotic resistance as well as a greater understanding of phage biology, scientists and clinicians worldwide are now re-exploring the potential of phage therapy.

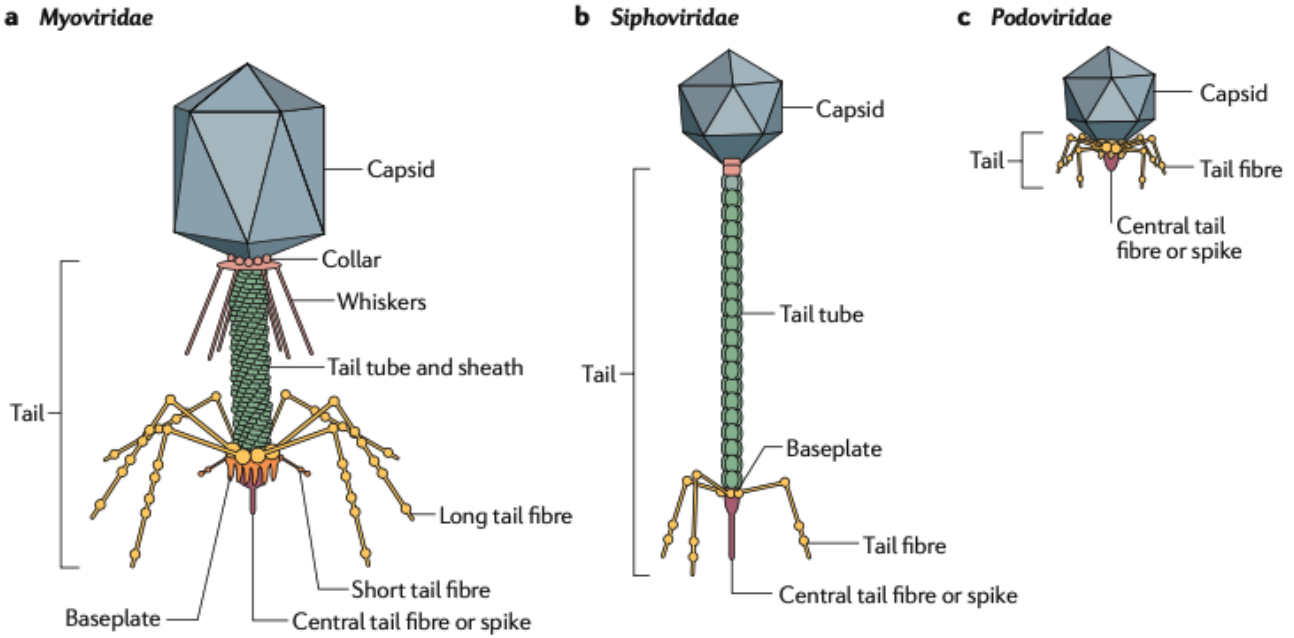

Figure 1.3 Classification of tailed phages by their morphology. Schematic representation of the different morphological phage groups. Extracted from Nobrega *et al.* (2018).

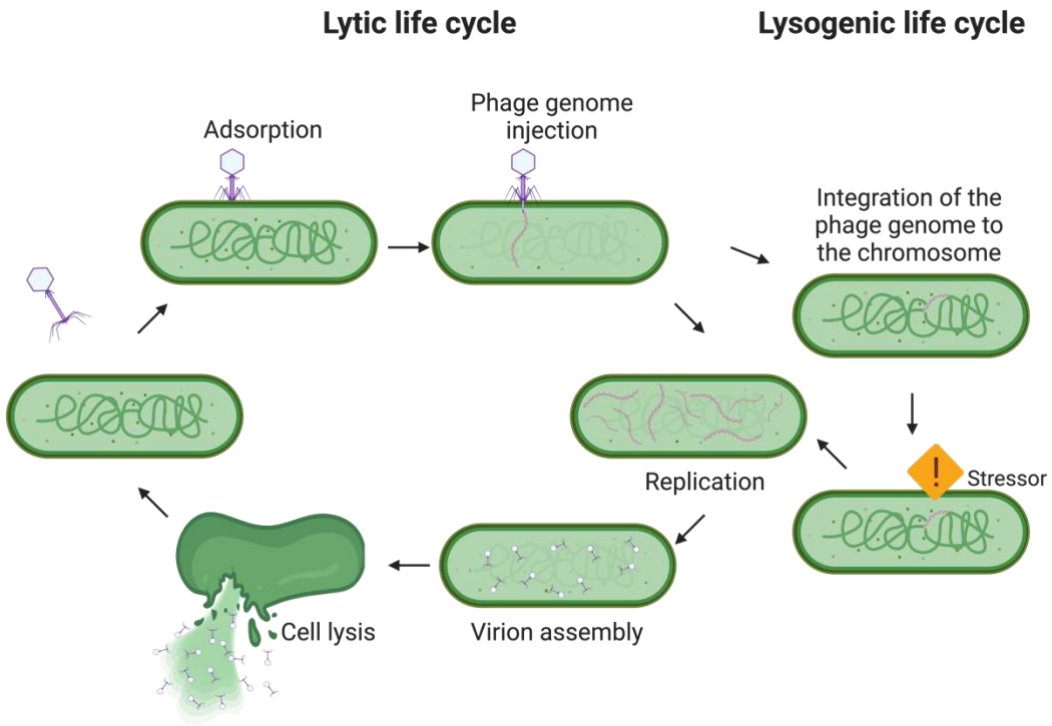

Figure 1.4 Life cycle of tailed phages. To infect their hosts, phages adsorb to the surface of the bacterial cell, they eject of the genome into the cytoplasm of the host, hijack the replication machinery of the bacterium to replicate, transcribe, synthesise and assemble new virions. To release the progeny, the cell is lysed. In the lysogenic life cycle, temperate phages can integrate into the bacterial chromosome and remain latent until a stressor compromises the host cell, in which case, the phage can induce the lytic cycle to search for new potential hosts. Figure created with BioRender.com

1.3.1 Advantages of phage therapy

Phage therapy has some advantages when compared with antibiotics. The narrow spectrum of phages maintains the patient's microbiome relatively unaltered (Cieplak et al., 2018; Mu et al., 2021). They are self-replicating in the presence of their host, which means that high doses are usually not required; but also self-limiting in its absence. As mentioned above, phages can be found in every part of the biosphere, and their isolation is relatively inexpensive (Gordillo Altamirano and Barr, 2019), which could potentially benefit low-income countries to mitigate the most devastating consequences of ABR. In addition, with the enormous diversity of phages it is theoretically possible to exploit different features of phages for difficult-to-treat bacteria. For instance, some phages can degrade biofilms with their enzyme activity (Fong et al., 2017; Lin et al., 2017), others may carry counter-defence systems (Samson et al., 2013). Finally, phages appear to be clinically safe, with almost no documented cases of anaphylaxis (Speck and Smithyman, 2016; Ujmajuridze et al., 2018) and very few reports of adverse consequences, most of them associated to factors other than the phage, such as the adjuvant or inadequate decontamination (Gorski et al., 2020; Sulakvelidze, 2011).

1.3.2 Limitations and issues of phage therapy

Some of the features that make phages advantageous can also create issues for applying PT. The following section briefly describes some of the issues of phage therapy that are preventing implementation as a routine clinical intervention. It is followed by some methods that can be used to address them.

1.3.2.1 Selection of phages to treat infections

Choosing the right phage to effectively treat a particular infection has been one of the main hurdles of PT. Due to their natural narrow host range, phages that are prescribed blindly have a high risk of failure.

The first requirement for phage infection is adsorption onto the surface of the host cell. This generally consist of 1) initial contact, 2) reversible binding and 3) irreversible binding (Bertozzi Silva et al., 2016). The latter occurs when the receptor binding protein of the phage finds a compatible receptor on the bacterial cell. Therefore, the breadth of hosts that a phage can infect is determined first by its receptor binding protein, with which they initiate the infection. The host cell structures that the phage can use as receptors can range from peptides to polysaccharide moieties. Outer membrane proteins, lipopolysaccharide (LPS), antibiotic efflux pumps, flagellum and other appendages have been identified as phage receptors (Bertozzi Silva *et al.*, 2016). In general, receptor binding proteins that target highly conserved motifs tend to be more generalists and have a broader host range, while those targeting variable structures are more specialized. Other features can also influence the spectrum of phages: monovalent phages only have capacity to bind to a single receptor, whilst polyvalent phages can target multiple different receptors, and therefore their host range is usually wider (de Jonge et al., 2019). In addition, mutations in genes encoding the receptor binding protein of phages can lead to change or broadening of the host range (Meyer et al., 2016; Meyer et al., 2012) and some phages are specialised at this by having a hypervariable domain and allowing diverse changes in host range (Liu et al., 2002). Still, most therapeutic phages, even those with a wider host range can target just a subset of closely related bacteria (Weinbauer, 2004).

1.3.2.2 Phage-resistance mechanisms of bacteria

Phages and bacteria have been putting a constant selective pressure on each other for billions of years, leading to an arms race in which bacteria have evolved a wide range of defence tools to avoid being extinguished by their predators (Hampton et al., 2020; Labrie et al., 2010; Rostol and Marraffini, 2019), and phages have evolved counter-attack strategies to circumvent them (Samson *et al.*, 2013; Torres-Barcelo, 2018). Thus, even under the assumption that the binding protein and its receptor are compatible, there are a number of defence tactics that bacteria can use to survive. Different defence strategies have been described for each stage of infection (Figure 1.5), and some of these systems are widely distributed among different bacteria. For instance, 90% of all sequenced bacteria have restriction-modification systems and 50% of all sequenced bacterial genomes contain a CRISPR- Cas system (Makarova et al., 2011).

1.3.2.2.1 Blocking phage adsorption and entry

To escape from phage infection, bacteria can prevent the phage adsorption by altering the surface structure that acts as the phage receptor. Genetic mutations leading to loss or alteration of the phage receptor are commonly reported, but it often comes with a fitness trade-off (Capparelli et al., 2010a; Capparelli et al., 2010b; Duerkop et al., 2016; Evans et al., 2010; Gomez and Buckling, 2011; Leon and Bastias, 2015; van Houte et al., 2016). Consequently, other mechanisms of protein alteration or under-expression have also been reported such as phase variation (Moxon et al., 2006; Scott et al., 2007). Phage receptors can also be modified by glycosylation (Harvey et al., 2018), or masked by polysaccharide capsules (Ohshima et al., 1988; Scanlan and Buckling, 2012), and biofilms can protect bacterial populations by blocking the access of phages to the receptors in the inner layers (Simmons et al., 2018; Vidakovic et al., 2018).

Gram-negative bacteria can produce outer membrane vesicles displaying the phage receptor, which can act as decoys for phages to adsorb, and therefore

reducing the proportion of phage infections (Manning and Kuehn, 2011; Reyes-Robles et al., 2018).

Phage infection can also be prevented at the DNA injection stage. It has been reported that a prophage-encoded transmembrane protein can inhibit the translocation of the phage DNA into the host's cytoplasm (Cumby et al., 2012).

1.3.2.2.2 Cleaving the phage DNA/RNA

Restriction modification (RM) systems are present in approximately 90% of sequenced bacterial genomes (Makarova *et al.*, 2011; Oliveira et al., 2014). There is a wide diversity of these systems, but they are typically comprised of a methyltransferase and a restriction endonuclease, both being able to recognise specific motifs. The methyltransferase modifies the bacterial DNA to distinguish it from foreign DNA and protect it against the cleaving action of the endonuclease. The endonuclease then cleaves only the foreign unmethylated DNA at specific sites (Loenen et al., 2014). In some RM systems, the endonuclease will target the modified viral DNA, whereas the host genome remains unmethylated (Oliveira *et al.*, 2014). In a related way, some defence systems, such as Pgl (phage growth limitation), methylate foreign DNA, which is then cleaved by the restriction endonuclease, but it is only when the phage progeny infects the subsequent cells in a second cycle of infection that the phage DNA is cleaved (Chinenova et al., 1982; Hoskisson et al., 2015; Sumby and Smith, 2002). BREX (bacteriophage exclusion) (Goldfarb et al., 2015; Gordeeva et al., 2019) and DISARM (defence island associated with restriction-modification) (Ofir et al., 2018) systems also include a methyltransferase and an endonuclease, but the mechanisms of protection differ from the classic RM systems in complexity. In addition, it is speculated that the endonuclease is not the effector component in these systems, but the complete mechanism is still not fully understood.

RM and RM-like systems are frequently referred to as the 'innate immune systems' of bacteria, as these can protect without prior exposure to the phage. The bacterial 'adaptive immunity' is conferred by clustered regularly interspaced short palindromic repeats (CRISPR) and CRISPR-associated

protein (Cas) systems. In these, phage DNA sequences are used to create a memory that will guide the defence upon subsequent infections.

CRISPR-Cas systems are present in approximately 50% of genome sequenced bacteria (Makarova *et al.*, 2011), and they are classified into two classes and six types depending on the mechanism (Koonin et al., 2017; Makarova et al., 2018). In types I, II and V a CRISPR RNA-guide can recognise a target sequence in the foreign DNA (or protospacer) and a protospacer adjacent motif (PAM) next to it and cleave it (Zetsche et al., 2015). In contrast, the effector protein-complex in type III systems does not recognise the phage DNA. Instead, it binds to the nascent RNA during phage transcription which activates the ssDNAse (Goldberg et al., 2014; Kazlauskiene et al., 2016; Samai et al., 2015). These systems have an additional level of protection, thanks to the non-specific accessory RNAse, which can cleave poorly recognised sequences, defending the cell from phages that have acquired mutations and that would otherwise be unrecognisable (Deveau et al., 2008; Semenova et al., 2011). This non-specific RNAse activity can also cleave host RNA, inducing a dormant state similar to that seen with some of the abortive systems (see 1.3.2.2.3). Type VI systems are similar to type III in that they target transcribed RNA and can pause bacterial growth (Abudayyeh et al., 2016; Meeske and Marraffini, 2018), but whether they protect against phage invasion is still to be proved (Rostol and Marraffini, 2019).

Prokaryotic Argonautes are guide-dependent nucleases that have been proved to have a role in plasmid and phage defence. They are present in 9% of sequenced bacteria (Makarova *et al.*, 2011). Prokaryotic argonaute proteins can cleave foreign DNA in a non-specific way and then use the DNA fragments as guides for specific interference. The DNA-guides (usually single stranded) or RNA-guides are then recognised by the endonuclease, which generates double strand DNA breaks in the invading DNA (Kuzmenko et al., 2020; Kuzmenko et al., 2019).

1.3.2.2.3 Altruistic defence systems to protect the bacterial population

Abortive infection (Abi) systems and toxin-antitoxin (TA) systems are characterised for triggering a stress response upon phage entry. This drives the infected cell to trigger self-programmed death or enter a dormant state, preventing the escape of newly formed phages, and protecting the bacterial population. For this reason, they are sometimes described as 'altruistic' (Hampton *et al.*, 2020). Abi or TA systems share some features and Abi systems can sometimes be explained by a TA mechanism. The mechanism of each system depends on which essential cellular structures or processes is affected. For example, in the Rex system the bacterial cell membrane can be compromised allowing the leakage of ATP (Parma et al., 1992). Other systems may target proteins involved in replication, transcription or translation (Dy et al., 2014b), and depending on the mechanism, the system can induce cell death or growth arrest. Furthermore, some of the non-lethal TA systems are reversible (Fineran et al., 2009; Pedersen et al., 2002).

Retrons are composed of a reverse transcriptase (RT), a non-coding RNA and an effector protein. Part of the non-coding RNA, which is recognised and transcribed by the RT remains bound to the newly transcribed DNA, forming a DNA-RNA complex. This complex presumably acts as a sensor of the integrity of defence proteins, or other phage structures, or phage-induced changes. They protect via an abortive infection system, but the mechanism depends on the effector protein that each system carries. The most common effector proteins in retron systems are ribosyltransferases, but cold-shock proteins, transmembrane domains and nucleases are also found as effector proteins in the system (Millman et al., 2020).

Cyclic oligonucleotide-based anti-phage signalling system (CBASS) is present in approximately 10% of bacterial genomes. It relies on the production of cyclic oligonucleotides which activates an effector protein that leads to cell death (Cohen et al., 2019).

1.3.2.2.4 Inhibiting phage assembly

In an indirect way, phage-inducible chromosomal islands (PICIs) can interfere with a phage infection lifecycle. PICIs are mobile genetic elements that can use an infecting phage (called helper phage) as a vector for their transference to new hosts. The new phages will contain parts of the PICI that will be carried to the next host. As a consequence of the extra genetic baggage, some of the released phages may lack essential genes, making them incapable to continue the infecting cycle (Penades et al., 2015).

1.3.2.2.5 Other defence systems

A chemical defence system has been reported in *Streptomyces spp*. Doxorubicin and daunorubicin are small molecules that are abundantly produced in these bacterial species. These molecules are inserted into phage DNA, intercalating it and blocking its replication (Kronheim et al., 2018).

It is predicted that many more anti-phage systems are yet to be discovered and many that have been discovered are still to be characterised. Anti-phage defence systems can often be found clustered in the bacterial genome (Makarova *et al.*, 2011), which are referred to as defence islands. This discovery enabled the identification of new candidate defence systems through 'guilt by association'. Doron et al. (2018) used a systematic method to identify anti-phage systems in bacterial genomes. They found 26 candidate systems and verified the anti-phage function of nine of them (Thoeris, Zorya, Hachiman, Shedu, Gabija, Septu, Lamassu, Kiwa and Druantia), but the mechanisms of these systems are still under investigation. Finding a way of preventing failure of the treatment due to resistance mechanisms is hence a challenge for phage therapy.

The emergence of up to 82% of phage resistant variants have been documented in phage-therapy trials and laboratory experiments (Oechslin, 2018). However, phages—in the arms race against bacteria—have also developed strategies to overcome the defence mechanisms of their hosts. Some phages have retroelements which randomly mutate and recombine, leading to variations in the proteins at the tips of the tails which can increase

the targets they can adsorb to (Doulatov et al., 2004; Lampson et al., 2005; Liu *et al.*, 2002). Phages can carry anti-CRISPR proteins, which can interact with the Cas protein to inactivate it (Bondy-Denomy et al., 2013; Hwang and Maxwell, 2019; Pawluk et al., 2016); or proteins capable of disabling RM systems (Rifat et al., 2008). In addition, it has been documented that some phages can overcome TA systems by encoding an antitoxin (Otsuka and Yonesaki, 2012).

In summary, the suitability of a therapeutic phage (or combination of phages) to inhibit a bacterial strain for long periods continues to be one of the main challenges for phage therapy. As more studies of phage-host interactions are published, it is clear that achieving effective therapeutic action without the development of phage resistance is more complicated than simply finding a phage with a compatible receptor-binding protein. In nature it is not to the phage's advantage to completely wipe out its host and so the continual arms race is beneficial both to host and virus. The challenge of PT is to overcome the resistance and therefore survival of bacterial subpopulations to effectively treat an infection.

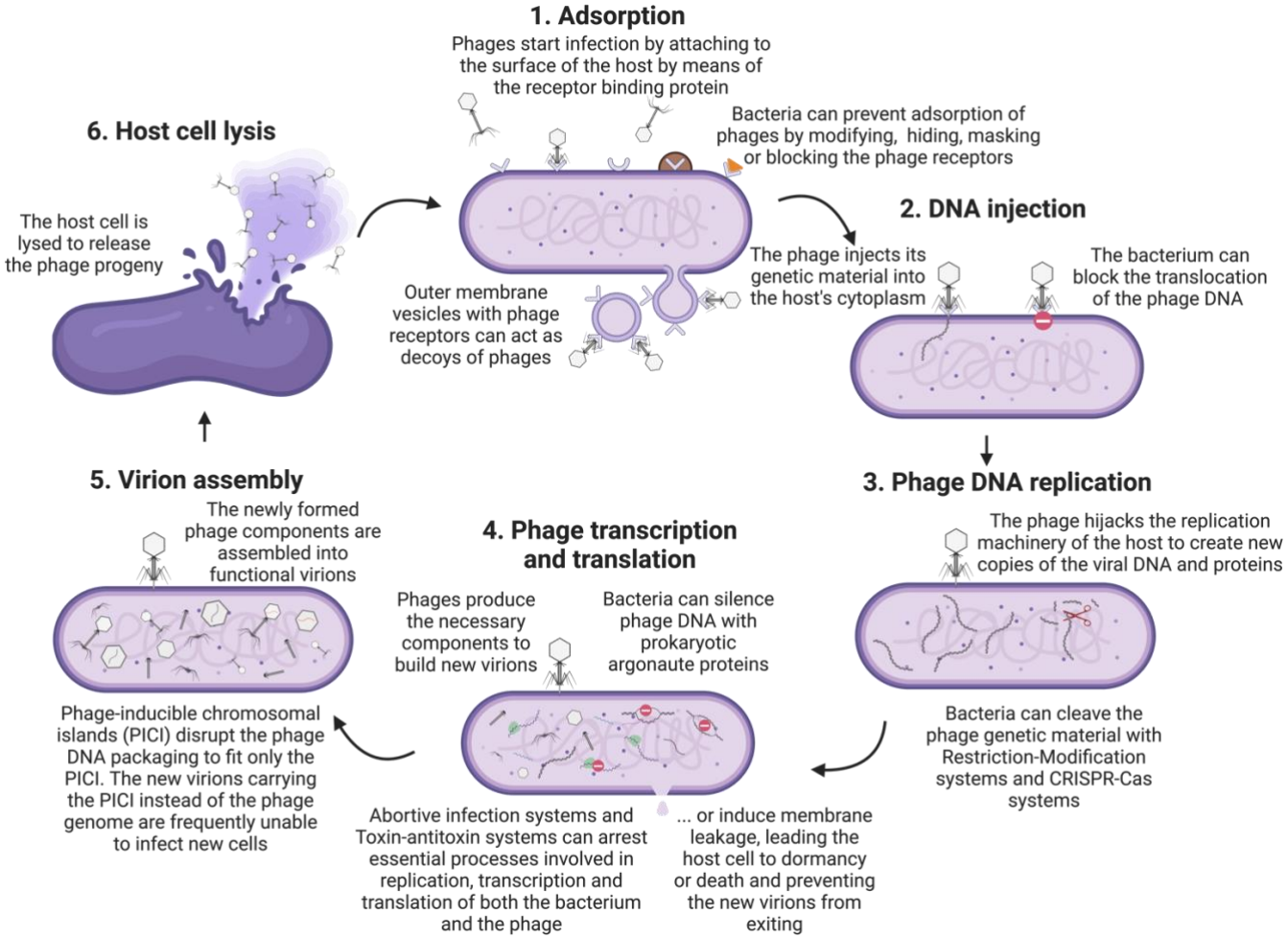

Figure 1.5 Phage resistance mechanisms. Schematic summary of the lytic life cycle of phages and some of the phage-resistance mechanisms of bacteria in each stage of the phage-infection cycle. Figure created with BioRender.com

1.3.2.3 Safety, efficacy and regulatory barriers to the use of PT

Despite the historical and contemporary evidence of their safety and efficacy, phages are still not routinely used in human and veterinary clinics in most parts of the world. Some aspects of phage biology, phage-host interaction and the immune response to PT are still not completely understood (Brix et al., 2020), and the immense diversity of phages makes it difficult to draw confident conclusions on the general safety and effectiveness of all phages. For these reasons, phages may still be perceived as unsafe by the general public and by some clinicians.

The absence of regulatory frameworks for phage use is one of the limiting factors of PT (Furfaro et al., 2018), and there are multiple reasons for this void. In many countries, phages are not suitable to be included as other antimicrobial products due to major differences in their mode of action, diversity, production and stability as well as intellectual property aspects. Therefore, a new regulatory framework for therapeutic phages should be created. Additionally, even though the clinical use of phages is increasing, the demand is not yet sufficient to attract investments to carry out large randomised double-blind clinical trials. Moreover, since ‘tailored’ PT is one of the most attractive formats for phage formulation, the standard methods of testing medical products, such as randomised double-blinded clinical trials, are not easy to carry out (Brix *et al.*, 2020).

Multiple anecdotal or observational studies have been conducted on PT, but many do not comply with the current quality standards or they lack power to draw confident conclusions due to the small number of patients involved. The clinical use of phages has mostly been limited to compassionate use, which refers to the use of unapproved treatments for patients in which all approved options have failed (McCallin et al., 2019). Successful compassionate PT cases have been reported, including those describing the treatment of diabetic

foot ulcers (Fish et al., 2018a; Fish et al., 2018b), pancreatitis (Schooley et al., 2017) and septicaemia (Jennes et al., 2017).

Compassionate phage therapy reports have been useful in the advancement of the use of PT. Very few adverse effects have been detected and mild reactions can be linked to components other than phage; thus, a regulation milestone was achieved based on these observations in compassionate PT cases in Belgium. Nonetheless, for the wider acceptance and adoption of PT, standardised clinical studies are required. Clinical trials have been carried out in humans for topical treatment of vascular ulcers (Markoishvili et al., 2002; Rhoads et al., 2009), chronic otitis (Wright et al., 2009) burn wound infections (Jault et al., 2019) and gastrointestinal infections (Bruttin and Brussow, 2005; Gindin et al., 2019; Sarker et al., 2017; Sarker et al., 2012). A two-phase study preceding a placebo-controlled, double-blind randomised clinical trial was carried out by Ujmajuridze *et al.* (2018) to treat patients with urinary tract infections via transurethral catheter. They first isolated the bacterium causing the infection in each patient and carried out phage-sensitivity tests with the over-the-counter phage cocktail Pyophage (from the Eliavia Institute). The phages were further adapted to the isolated strains of the patient, which led to the increase of phage sensitivity from 41 to 75%. The intravesical phage treatment caused a significant reduction in bacterial counts in 67% of the patients involved, and no adverse effects were observed.

As the demand for phages increases and small clinical trials and case reports are published, the evidence of phage safety increases. But in order to accelerate the acceptance of PT, other resources can be used to further our understanding of the clinical use of phages, and the risks that come with it. Animal models of infection and phage treatment represent a valuable tool to build this body of knowledge on PT. In addition, the establishment of animal models of infection might be of use for pre-screening of therapeutic phages prior to the administration in humans (Melo et al., 2020).

1.3.3 Addressing the issues of phage therapy

1.3.3.1 Phage cocktails

Phage cocktails are a mixture of phages that are put together with the purpose of 1) expanding the target spectrum of the preparation for blind prescription, or 2) preventing the emergence of phage-resistance. An example of the former comes from the Eliava Institute. They adopted a system based on a constant screening of the circulating bacteria and designing their preparations according to their findings (Kutateladze and Adamia, 2008). These cocktails were normally composed of phages against multiple bacterial species. For example, Pyophage is a popular preparation for infected wounds. It contains lytic phages against *Staphylococcus aureus*, *Streptococcus spp*., *E. coli*, *Proteus spp*. and *Pseudomonas aeruginosa*. By targeting the main strains of each species that caused an ailment, they could blindly prescribe these cocktails without susceptibility tests. However, this approach can still lead to treatment failure as they are not effective against all isolates within one species, especially pleiotropic and rapid-evolving bacteria that can easily acquire resistance genes. Bernasconi et al. (2017) tested the Pyophage cocktail against a wide range of *E. coli* isolates (including MDR) and found that 61% of them were susceptible to the cocktail.

It is generally accepted that cocktails will give better lysis, and that resistance is less likely to arise when more than one phage is in play, but the overall performance of phage cocktails depends on the phages that are being combined (Bourdin et al., 2014; Watanabe et al., 2007). Some phage combinations can result in a lower lytic activity than those of the single phages (Niu et al., 2021). Additionally, some authors reject that phage cocktails are more efficient than monovalent phage preparations, and actually consider that using single-phage therapy could prevent a hyper immune reaction, given that phage cocktails generate higher antibody titres (Miedzybrodzki et al., 2009). It is also argued that multiple phages make the pharmacokinetics and

pharmacodynamics less predictable and difficult to study (Chan et al., 2013), as well as the inflammatory response of the recipient, the gene transfer and phage-resistance development (Parracho et al., 2012).

The methodology of phage cocktail preparations should therefore be based on the expected results, and the selection of phages should be guided by the biological features of each individual phage. Effective cocktails should ideally be composed of phages that target different receptors to decrease the chances of resistance by receptor mutation, and to avoid antagonism of the different phages (Gordillo Altamirano and Barr, 2021). In addition, based on the premise that different phages are equipped with different infecting and counter-defence mechanisms, cocktails can serve to reduce the chances of resistance due to mechanisms other than impaired adsorption. For instance, a 6-phage cocktail prepared by Forti et al. (2018) not only had a broader spectrum, but also outperformed the single-phage preparations due to the biofilm degradation properties of some phages, allowing better penetration to the site of infection.

1.3.3.2 Tailored phage therapy

In vitro susceptibility tests are another useful way of demonstrating the effectiveness of phages against a particular clinical isolate before this is administered to the patient. These tests are routinely carried out by spotting phage on soft agar inoculated with the bacterium (Mazzocco et al., 2009) or by measuring the turbidity or respiration of the bacterium in liquid media to detect bacterial growth inhibition. However, these assays are time consuming which makes them unsuitable for urgent cases. It has repeatedly been observed that delays in phage administration correlate with decreased survival of the recipient (Penziner et al., 2021; Pouillot et al., 2012). A further issue is that *in vitro* results not always reflect the outcome *in vivo* (Casey et al., 2018). Whilst these approaches have been helpful in guiding the selection of

therapeutic phages, they still have limitations, especially when it comes to accuracy and speed.

1.3.3.3 Animal models of infection for the study of PT

To avoid failure or adverse effects of PT, it is important to further our understanding of the phage-bacteria-animal interaction. Animal models of infection and PT are of paramount value in the study of these interactions. The species selection for the animal model depends on the best representation of the particular infection, but other important aspects, such as the aim of the study and the budget available, are also important factors.

Different models of infections have been used in the past years to study the safety, efficacy, pharmacokinetics and the interaction with the animal immune system of PT (Brix *et al.*, 2020; Penziner *et al.*, 2021). Trials with invertebrate animal models, such as the nematode *Caenorhabditis elegans* (Augustine et al., 2014; Glowacka-Rutkowska et al., 2018), fruit fly *Drosophila melanogaster* (Heo et al., 2009; Lindberg et al., 2014) and wax moth *Galleria mellonella* (Forti *et al.*, 2018; Nale et al., 2016; Seed and Dennis, 2009), commonly measure the efficacy with survival rates. Moreover, the toxicity of phages, their ability to survive in the gastrointestinal tract, and synergy with the immune system can also be studied in these models to a certain extent. Zebrafish embryos have also proved to be useful models to demonstrate the efficacy of phage. Some advantages of this model are the relatively low cost, transparency, and the developed innate immune system and genetic tractability (Al-Zubidi et al., 2019; Cafora et al., 2019).

Nonetheless, for translational studies and pre-clinical trials, mammals are preferred as models of infection. Unsurprisingly, mice (*Mus musculus*) have been the most popular mammalian model to test the safety and efficacy of phage therapy due to the small size, relative low cost and ease to handle. This

model has also been widely used to study the influence of the animal immune system in phage-bacterium interactions. Murine strains with specific immunodeficiencies have been essential in studying the extent to which each immune component create synergism or interferes with the phage treatment. This unsolved question is controversial, and depends largely on the phage, dose, route and time of administration. Abd El-Aziz et al. (2019) saw that phages and the innate immune system can synergise and achieve a better killing of the bacteria. Other groups have demonstrated that the presence of anti-phage antibodies did not reduce their lysing activity (Capparelli et al., 2007). In contrast, studies have seen a clearance of phages by component of the innate immune system –such as the complement and phagocytic cells— and the adaptive immune system—mainly by neutralising antibodies (Dabrowska, 2019; Hodyra-Stefaniak et al., 2019). However, mice are not suitable models for all bacterial infections and study objectives. For example, the natural resistance of mice to *S. aureus* makes them an unsuitable model; whereas rabbits (*Oryxtolagus cuniculus*), due to their natural susceptibility, have been used to test subcutaneous administration of phage treatment for *S. aureus* infections (Wills et al., 2005).

For extraintestinal *E. coli* infections, different models of infection have been used. Antoine et al. (2021) and Sanmukh et al. (2023) have used *G. mellonella* larvae as animal models of infection to assess the effect of PT in terms of survival. In addition to the low cost, the Greater wax moth larvae has an innate immune system similar to the human one (Casanova-Torres and Goodrich-Blair, 2013; Lavine and Strand, 2002). These studies concluded that their coliphages were able to replicate in the model and increased the survival rate of the experimental group.

One of the early studies of phage safety and efficacy of phages to treat multidrug-resistant UPEC infections was reported by Nishikawa et al. (2008). They saw that intraperitoneal administration of a T4-like phage was safe and significantly reduced the mortality of mice inoculated by transurethral catheter with UPEC.

Pouillot *et al.* (2012) used a rat pup model of sepsis and meningitis to assess the therapeutic action of a lytic phage against an O25:H4-ST131 *E. coli* strain. This model enabled the study of the phage pharmacokinetics, which showed that phage accumulated in the spleen and kidney, but did not reach high concentrations in urine and central nervous system. Despite having previously observed neutralisation of the phage by human serum *in vitro*, 100% of the treated animals survived with a single dose of 10^8 PFU when this was administered timely; whereas delaying the treatment 24 hours reduced the survival rate to 50%.

Dufour et al. (2016) used a murine model of pneumonia, sepsis and UTI to demonstrate the efficacy of a T7-like phage that specifically targets O25b *E. coli* strains. The significant reduction in bacterial load in different organs indicated that this phage has therapeutic potential as a tool to combat the O25b:H4-ST131 clonal group. Other reports on the use of PT in murine models of sepsis by Green et al. (2017) saw that in vitro phage-host interactions were not always mirrored in the animal model. In the intraperitoneal administration of phage HP3 significantly reduced the *E. coli* ST131 load in different organs which was reflected in an overall clinical improvement of the treated mice. The authors also report the *in vitro* assay not always corelated to the observed lytic activity of phage HP3 *in vivo*. This suggests that some *in vitro* models may need further optimisation to better mimic the expected result *in vivo*.

Two studies have isolated the escape variants from animal models that received PT and investigated the cause. Salazar et al. (2021) treated a murine model of sepsis with phage and found that an ST131 *E. coli* strain quickly develops resistance. They studied the cause of phage-resistance by sequencing the population that escaped predation in the animal model. They saw that genetic mutations in genes involved in adsorption were causing the survival of these mutants, but that they had a reduced fitness and virulence. Finally, they exposed the phages to the resistant variants to stimulate evolutionary adaptation of the phages (a method known as phage training) to obtain a cocktail capable of overcoming the observed resistance. Similarly,

Zulk et al. (2022) used two phages to treat clinical UPEC isolates *in vitro* and *in vivo*. The in vitro assays consisted of bacterial cultures in bacteriological medium and human urine with and without phage. They observed phage-resistance arising a few hours after the phage addition. Further investigation revealed the cause of resistance: genetic mutations in genes involved in the biosynthesis of LPS were causing impaired phage adsorption. They saw that the phage-resistant variants had a compromised fitness for growth in urine, and reduced virulence in a mouse model of UTI. These studies are amongst the few animal and clinical trials that investigate the cause of resistance *in vivo*.

Due to major differences in size, physiology and immune response, mice are increasingly being considered as not-ideal for pre-clinical studies of PT for UTI in humans (Andersen et al., 2012; Subashchandrabose and Mobley, 2015). For safety studies, mice are also being questioned as good models, as there is evidence of differences in mice response to toxicity of therapeutic compounds compared to humans (Perrin, 2014). These differences could lead to assumption of safety result and could result in unexpected adverse outcomes in the patient.

In the search for animal models that better represent the urinary tract of humans, domestic and mini pigs are proving to be of use. The similarities of the porcine and human urinary tract in size, dynamics, anatomy and physiology make it a relevant and useful model to study diseases of the urinary tract, as well as other systems and organs (Lunney et al., 2021). Furthermore, the natural susceptibility of pigs to *E. coli* UTIs has been exploited by Nielsen et al. (2019) to successfully establish the first large animal model of cystitis. By instilling UPEC strain UTI89 in the bladder, they found that pigs support the establishment of persistent, non-ascending infection that lasted for 23 days. The bladder size of the pigs allowed the researchers to follow the infection with cystoscopy and bladder biopsies. Moreover, the welfare of the animals was not compromised. Jamalludeen et al. (2009) reported the oral administration of phages in pigs to observe the effect in reducing diarrheal symptoms. But the study of phages as therapy to treat UTI has not been reported in a porcine

model of UTI. A porcine model of UTI can serve to trial the safety and efficacy of phages, and to study the resistance mechanisms that bacteria commonly acquire *in vivo*. In this way, the animal model could bridge the knowledge that has been acquired *in vitro* to the clinical application of phage therapy.

1.4 Aims of the project

The work presented in this thesis aimed to study phage-UPEC interactions to identify and understand the issues that need addressing for safe and reliable phage therapy. For this, the main objectives of the different stages of the project were:

- To establish the foundations of phage-UPEC interaction studies by optimising a synthetic medium that can mimic urine.
- To explore and expand a phage library with enough diversity to target most *E. coli* strains causing UTIs by screening individual phages against a diverse cohort of UPECs.
- To screen individual phages and phage-cocktails for the long-term inhibition of a multidrug-resistant ST131 UPEC.
- To identify and explore the main causes of phage-resistance that could result in ineffective phage therapy.
- To carry out pilot studies for the assessment of the safety and efficacy of phage products in a porcine model.

Chapter 2 Foundations of the study: An artificial urine medium and a phage library to treat urinary tract infections with phage therapy

2.1 Introduction

The majority of *E. coli* strains that cause UTIs belong to the phylogenetic group B2 and group D (Clermont *et al.*, 2000). Groups A and B1, are more commonly associated with commensal and intestinal *E. coli*, and are less commonly associated with extraintestinal infections, as they lack some virulence factors to help them thrive in environments like the urinary tract. Nonetheless, they can also cause UTIs, especially in hosts with a compromised immune system (Gibson et al., 2008; Sidjabat et al., 2009). The epidemiology of canine UTIs in Edinburgh also follows this trend as defined in an unpublished previous thesis of our group (Park de la Torriente, 2018), which examined the phylogeny of locally isolated *E. coli* strains causing UTIs in dogs (Figure 2.1). As expected, most of the canine UPECs (coloured in pink and yellow in the outer ring) were within phylogroups B2 and D, but some others belong to groups A, B1, C and E. Being aware of this diversity is key in building a broad and diverse phage library with potential to treat most of the *E. coli* UTIs that may be encountered at the Small Animal Hospital, in the Royal (Dick) School of Veterinary Studies, University of Edinburgh (R(D)SVS).

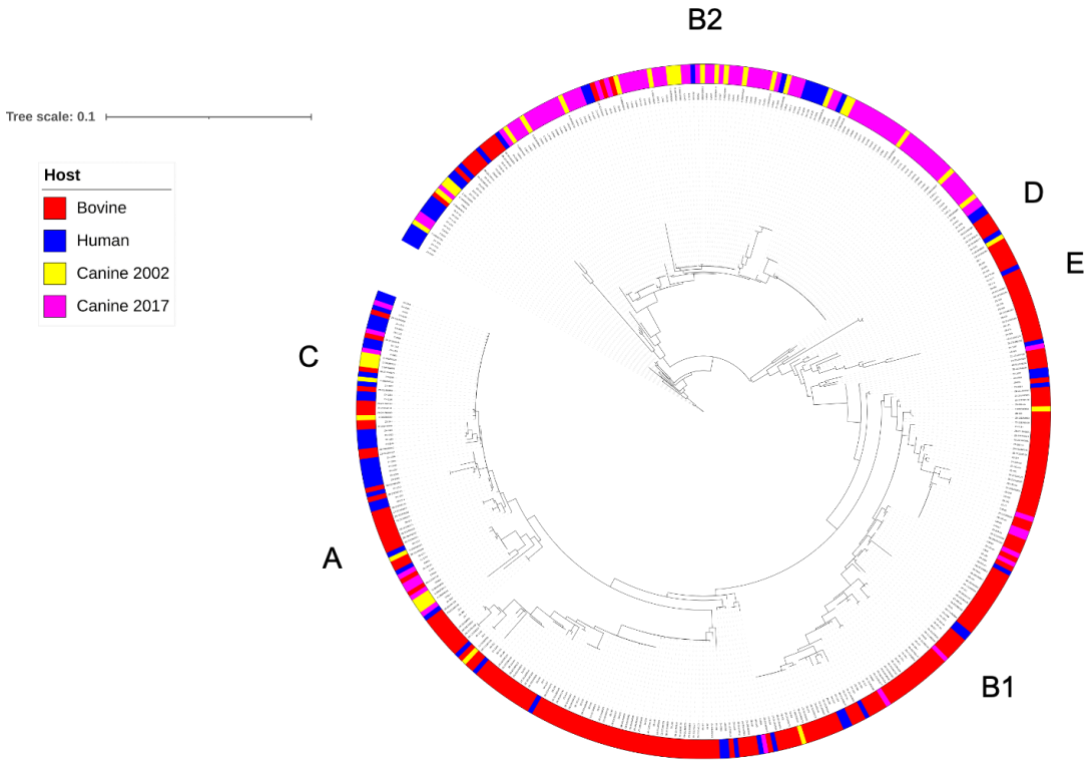

Figure 2.1 MLST-based phylogenetic tree of canine (magenta and yellow), human (blue) and bovine (red) E. coli isolates. Majortity of uropathogenic *E. coli* isolates belong to the phylogroup B2 and D, but a few isolates from canine UTIs can be found in the other groups. Dendrogram generated with iTOL (Letunic and Bork, 2007)

UPECs have a remarkable metabolic adaptability and versatility which allow them to cope with the nutrient restrictions in the urinary tract, so they can survive, multiply and colonise (Ipe et al., 2016). Compared to other environments in which nutrients are abundant, UPECs utilise pathways that allow the metabolism of amino acids and peptides, nucleotide biosynthesis, nutrient transport mechanisms and osmoadaptive systems. 84 cytoplasmic proteins of UPECs have been identified as significantly induced in human urine compared with standard laboratory media (Alteri et al., 2009). Studying phage-UPEC interactions in LB or other rich media might result in outcomes that are difficult to interpret and extrapolate to clinical settings. It is therefore important to study UPEC-phage interactions in a medium in which bacterial metabolism and physiology are likely to be similar to that found in the urinary tract of patients.

Urine is a complex fluid generated by the kidneys to excrete waste and excess compounds from the bloodstream (Bouatra et al., 2013). Its high concentrations of urea and inorganic salts make it hypertonic and naturally antiseptic (Ipe and Ulett, 2016). Its composition is highly variable depending on age, gender, diet, health status, exercise, medication and water intake. Even urine from the same individual may change throughout the day (Barr et al., 2005; Robinson-Cohen et al., 2014; Taylor and Curhan, 2007). In addition, urine is complex: over 3,000 metabolites have been identified in urine; 90 of those compounds are present in human urine with 100% occurrence (Bouatra *et al.*, 2013). The complexity and variability of urine represent a disadvantage in research, which relies on standardised and reproducible media. Some methods to normalise the urine between experiments have been used, such as the use of pooled samples from different individuals and adjusting the concentration to a specific gravity or to creatinine levels (Barr *et al.*, 2005). Nonetheless, the possibility of finding differences between batches of normalised urine is still a limitation.

Different artificial urine formulations have been developed for different research purposes, such as mineral crystallization (Brown et al., 1989;

Christmas et al., 2002; Grases and Llobera, 1998), skin irritation (Mayrovitz and Sims, 2001), and 'multipurpose' (Chutipongtanate and Thongboonkerd, 2010; Sarigul et al., 2019). Some research groups have developed AU media for the study of uropathogens (Brooks and Keevil, 1997; Ipe and Ulett, 2016), but to the best of my knowledge, there are no reports of an AU assessed to study phage interactions with their bacterial hosts.

The initial stage of the project aimed to establish the foundations for phage-canine uropathogenic *E. coli* research by testing and optimising an AU medium to study uropathogenic *Escherichia coli* (UPEC) strains and their interaction with therapeutic phages. For this, two published protocols of human synthetic urine were tested and further modified (Brooks and Keevil, 1997; Sarigul *et al.*, 2019). The growth of a selection of UPEC strains in the two modified urines was assessed based on the 'area under the curve' (AUC), and compared to pooled urine from healthy dogs.

In addition, while the AU was being optimised, phages with therapeutic potential were isolated to build a phage library to treat UTIs caused by *E. coli*. To assess the phage library's potential to target local UPECs, a number of phage-host interaction assays were carried out. For this, 30 phages from the library were tested with 38 sequenced UPEC strains, which were selected based on their phylogeny to ensure that the cohort was representative of the diversity. The effect of the phage on bacterial growth was scored by calculating the ratio of the phage infected culture's AUC to the control culture's AUC. The graphical representation of the dataset with the interaction scores was useful to gain awareness of the library's limitations in order to work towards improving it. Once the final AU protocol had been established, the interactions were also measured in AU and both datasets could be compared for a better assessment of the library.

2.2 Material and methods

2.2.1 Plaque assays

100 µL of phage suspension and 100 µL of a single bacterial strain cultured to Optical Density at 600 nm wavelength (OD_{600}) ~1 was added to 3 ml of molten top agar stabilised at 50°C. The top agar was then distributed on an LB agar plate. The plates were incubated overnight at 37˚C.

2.2.2 Spot assays

3 mL of molten top agar stabilised at 50˚C was gently mixed with 100 µL of an overnight LB culture of the host strain, then poured and distributed on a LB agar plate. After approximately 15 minutes, when the top agar had solidified, 10 µL drops of phage suspension were spotted on it. The plates were left on the benchtop until the plates were dry. They were then closed, inverted and incubated at 37°C overnight.

2.2.3 Bacterial isolates

2.2.3.1 Canine UTI isolates

The *E. coli* isolates that were used for the isolation of phages, the assessment of the AU, and the phage-UPEC interaction assays were kindly provided by Doctor Gavin Paterson (Easter Bush Microbiology Diagnostics) in 2018. A collection of 100 *E. coli* strains were isolated from dogs assessed at the Small Animal Hospital of the R(D)SVS. Freezer stocks were prepared by suspending

a single colony in 500 µl of lysogeny broth (LB) in cryotubes and incubating them at 37˚C with shaking at 170 RPM overnight. On the following day 500 µl of 50% sterile glycerol was added to each cryotube and stored at -75˚C. Prior to their use, a small quantity was taken from the surface of the frozen culture and streaked on LB agar plates and incubated overnight at 37˚C.

In order to represent the UPEC diversity, the isolates used for phage isolation, AU assessment and phage-UPEC interaction assays were selected based on the phylogeny of the strains using dendrograms from a previous project (Figure 2.1) by selecting strains from each cluster.

2.2.3.2 *Escherichia coli* O25:H4-ST131 Strain EC958

Escherichia coli O25b:H4-ST131 strain EC958 was kindly provided by Professor Mathew Upton (Plymouth University). Freezer stocks were prepared by mixing one volume of an overnight culture with one volume of sterile 50% glycerol. The strain was streaked out on LB agar plates from the freezer stock, and overnight cultures were prepared by suspending a single colony in 5 mL of LB or artificial urine (AU).

2.2.4 Bacteriophages

2.2.4.1 Phage technology centre (PTC) phages

Some of the phages used here were acquired from the start-up venture, Phage Therapy Centre (PTC, Bonen, Germany) in 2016. PTC phages included in the phage-host interaction dataset were selected based on the broadest host range shown in spot assays (2.2.2) using 15 diverse UPEC isolates. These

phages were propagated using the same method as the phages isolated in-house (2.2.4.3).

2.2.4.2 Phage isolation

Enrichment. Three UPECs were co-cultured by suspending 500 µL of the overnight cultures in 50 mL of LB and incubating them at 37˚C with shaking for two hours. 500 µL of raw wastewater was added to the flask. The flask was incubated overnight under the same conditions. The following day, 10 mL of the culture was transferred to 15 mL Falcon tubes and centrifuged at 4,863 RFC for 10 minutes. The supernatant was filtered using 0.2 µm Milipore filters and the filtrate was used as a neat suspension of phages for the following steps. This enrichment step was bypassed in the isolation of some of the phages, in which case the plaque assays were carried out using 100 µl of filtered waste water as the neat suspension of phages.

Phage isolation with plaque assays. 1:10 serial dilutions of the lysate were made with SM buffer. The 10^{-4} and 10^{-5} dilutions (or neat filtered waste water) were used in plaque assays (2.2.1). Visible single plaques were cut out using the tip of a syringe. The piece of agar with the plaque was incubated in 1 mL of SM buffer at room temperature for approximately 20 minutes to elute the phage. The eluate was filtered with a 0.22 µm Milipore filter and used as a new neat suspension of phage for the purification steps.

Phage purification. To make sure that the preparations contained a single type of phage, at least three passages of plaque assays with the propagating host were carried out for each phage.

2.2.4.3 Phage propagation

To propagate the phages, 500 µL of the propagating host was cultured in 50 mL of LB for 1 hour 37˚C with shaking. 500 µl of the purified phage neat solution was then added to the culture and this was incubated overnight under the same conditions. On the next morning, 15 mL of the culture was centrifuged at 5000 RPM (4,863 RFC) for 10 minutes, and the supernatant was filtered. The filtrate was the final phage preparation, it was titrated and stored at 4°C until its use.

2.2.4.4 Phage stock solutions

The purified phages were propagated as described above (2.2.4.3). The final phage preparation was titrated by counting the number of single plaques from a suitable dilution in plaque assays and multiplying by the dilution factor. Phage stocks were stored at 4˚C until their use.

2.2.5 Restriction fragment length polymorphism

To identify replicated phages, Restriction Fragment Length Polymorphism (RFLP) was carried out. The DNA of the isolated phages was extracted with the Phage DNA Isolation Kit (Norgen Biotek) following the manufacturer's instructions. 10 µl of phage DNA was digested with 1 µl of restriction enzyme Eco32I (Thermo Scientific) for 30 minutes at 37˚C. The DNA was loaded in a 1.2% agarose gel and run at 100 V for 60 minutes. The gel was visualised and documented with a LI-COR Odyssey Fc Imaging System. Phages with an identical restriction pattern were considered as replicated and the replicas were discarded.

2.2.6 Urine media

2.2.6.1 Pooled canine urine (PU)

Urine samples from healthy adult dogs were kindly sourced by Susan Campbell and Federico Diez. They were collected by the nurses in the Small Animal Hospital (University of Edinburgh, Easter Bush Campus) and stored at -20°C. The frozen samples were then transported to the Roslin Institute Building, where they were thawed and centrifuged at 5000 RPM (4,863 RFC) for 10 minutes to pellet most of the solids. The liquid fraction of the samples was pooled and adjusted with sterile water to a specific gravity (SG) of 1.031. The dilute urine was then sterilised by passing it through a 0.22 µm bottle top filter (Thermo Fisher Scientific). It was aliquoted in 50 mL Falcon tubes and stored at -20°C until its use.

2.2.6.2 Brooks' artificial urine

This protocol was adjusted to obtain the required pH, specific gravity and to avoid precipitation. The list of components and the final concentrations are shown in **Table 2.1**. To prepare the solution, the components (except for the uric acid and the phosphate buffers) were added to 250 mL of distilled water one by one and mixed until fully dissolved. 0.044 g of uric acid sodium salt (Sigma) was dissolved in 1.76 mL of 1M NaOH, as indicated by the manufacturer. The di-potassium hydrogen phosphate and the potassium dihydrogen phosphate were mixed together in 10 mL of distilled water. The phosphate buffer solution and the uric acid were incorporated to the main solution and the final solution was sterilised using a 0.22 µm filter.

Table 2.1 Brooks' Artificial Urine

Component	Concentration (g/100 mL)
Peptone	0.4
Yeast extract	0.001
Lactic acid	0.01
Citric acid	0.04
Urea	1
Uric acid sodium salt	0.104
Creatinine	0.08
Calcium chloride	0.52
Sodium chloride	178
Iron II sulphate 7H2O	0.00012
Magnesium sulphate	0.049
Sodium sulphate $10H_20$	0.32
Potassium dihydrogen phosphate	0.095
Di-potassium hydrogen phosphate	0.12
Ammonium chloride	0.13

2.2.6.3 Sarigul's artificial urine

The original recipe Sarigul *et al.* (2019) was modified in order to avoid precipitation (no uric acid was added) and to enhance the growth of bacteria (peptone and yeast extract were added as an amino acid and nucleic acid sources). The final list of components and their concentration is listed in **Table 2.2**.

Table 2.2 Sarigul's Artificial Urine

Component	Concentration (g/100 mL)
Sodium sulphate	0.17
Tri-sodium citrate	0.072
Creatinine	0.081
Urea	1.5
Potassium chloride	0.2308
Sodium chloride	0.1756
Calcium chloride anhydrous	0.0185
Ammonium chloride	0.1266
Potassium oxalate	0.0035
Magnesium sulphate heptahydrate	0.1082
Sodium dihydrogen orthophosphate dihydrate	0.2912
Sodium phosphate monobasic dihydrate	0.0831
Bacteriological Peptone	0.2
Yeast Extract	0.0018
Ultrapure autoclaved water	To 100 ml

2.2.6.4 Assessment of the artificial urine

A single colony of each strain was suspended in 10 mL of LB and incubated overnight at 37˚C with shaking at 170 RPM. The next day, the cultures were centrifuged at 4863 RFC, the supernatant was discarded and the pellet was resuspended in 10 ml PBS. The spin, wash and resuspension steps were repeated to ensure that no LB medium remained. Using 96-well plates, 5 µL

of bacterial suspension (at an OD_{600} ~ 1) and 5 µL phage or SM buffer (as control) were inoculated in 190 µL of either ACU or pooled canine urine (PCU) as a control. The OD_{620} of each culture was measured with a Multiskan plate reader (Thermo Fisher Scientific) every 20 minutes for 50 cycles. The mean of three technical replicates of each culture was calculated and growth curves of each isolate were plotted using the packages tidyverse, ggplot2, reshape2 and gridExtra in R studio. The assays were repeated at least three times as biological replicates; the results of one representative assay are shown here.

2.2.7 Phage-*E. coli* interaction assays in microtiter plate formats

LB cultures: Overnight cultures were sub-cultured in 5 mL of LB to an OD_{600}~1. 10 µL was added to the wells of microtiter plates containing 180 µL of LB. Phages were added in 10 µL volumes of phage suspension adjusted to titre 10^6 PFU/mL (MOI ~ 0.1). Growth curves of the bacterial culture, in the presence and absence of phage, were generated by measuring the OD_{620} periodically for a total of 18 hours with 10 second-shaking before each reading.

Urine cultures: Artificial urine (AU) and pooled canine urine (PU) cultures in microtiter plates were set as follows: 10 µL of overnight bacterial cultures in AU were added to the wells of microtiter plates containing 180 µL of urine (AU or PU). Phages were added in 10 µL volumes of phage suspension adjusted to titre 3 x 105 PFU/ml (MOI ~ 0.1). Growth curves of the bacterial culture, in the presence and absence of phage, were generated by measuring the OD_{620} periodically for a total of 18 hours with constant shaking between readings.

2.2.8 Phage-UPEC interaction dataset

Overnight cultures of the UPEC isolates were subcultured in 5 ml of LB to an OD_{600}~1. 10 µl was added to the wells containing 180 µl of LB in microtiter plates. 10 µl of phage suspension adjusted to titre 1 x 10^7 PFU/mL (MOI ~ 0.1) was added. Growth curves of the bacterial culture, in the presence and absence of phage, were generated by measuring the OD_{620} periodically for a total of 18 hours in a Multiskan plate reader (Thermo Fisher Scientific). The mean of three technical replicates was used to calculate the area under the curve (AUC) in R for each interaction and for the no-phage control using the function of auc in the package MESS. Each phage-host pair was given a score by calculating the ratio of the AUC to the no-phage control AUC. A matrix with all the scores from the interaction data was built and was displayed as a heat map using the function heatmap.2 in the package gplots in R studio.

2.3 Results and discussion

2.3.1 Evaluating two Artificial Urine (AU) protocols as growth media for UPECs

The medium to study the phage-bacterium interactions should ideally reflect the conditions found in the urinary tract. Two published protocols of human synthetic urine (Brooks and Keevil, 1997; Sarigul *et al.*, 2019) were used as a foundation to develop an artificial urine (AU) medium. Modifications had to be implemented to both recipes to avoid precipitation and to obtain acceptable bacterial growth.

To assess the performance of the AUs as growth media, three canine (CAN10, CAN32 and CAN74) and one human UPEC isolate (EC958) were cultured in them and in pooled canine urine (PU). Figure 2.2 shows representative examples of the four UPECs growing in the different modified AU media in the presence and absence of phage. The area under the curve (AUC) was calculated for each growth curve and is shown after the last timepoint. When cultured in Sarigul's AU, the strains achieve a better growth and a higher AUC (mean AUC=12.57, SD=0.9) than in Brooks' AU (mean AUC=10.8, SD=1.19), which is also more similar to those generated in PCU (mean AUC=16.3, SD=3.9). However, there is no significant difference between any of them in a one-way ANOVA paired test.

The AU protocol by Brooks and Keevil (1997) was specifically developed with the objective of studying urinary pathogens, and it contains peptone as the main carbon source for bacterial growth. On the other hand, Sarigul *et al.* (2019) describe their AU formula as 'multipurpose', but it lacks amino acids and trace amounts of nucleic acids. Human urine contains D-serine, arginine, glutamate, glycine and leucine amongst other amino acids (Bouatra *et al.*,

2013; Cosloy and McFall, 1973), and these are the main carbon sources for UPEC growing in urine (Alteri *et al.*, 2009; Alteri and Mobley, 2015). In this study, peptone and yeast extract were added to Sarigul's AU recipe to allow the growth of bacteria. Specific amino acids could alternatively be added individually in different proportions to imitate real urine more rigorously, but the preparation of the medium would be more laborious. For the purposes of our studies, the addition of peptone as a source of amino acids has been shown to be sufficient.

Brooks and Keevil report experiencing some precipitation problems, which they solved by adjusting the pH with the addition of hydrochloric acid. Here, I adjusted the pH of Brooks' AU by modifying the ratio of the potassium buffers. However, this did not solve the precipitation problems, mainly caused by the uric acid, for which uric acid sodium salt was used. Similar precipitation problems were faced when preparing Sarigul's AU, but they were not entirely solved with the sodium salt of uric acid, for which the component was removed from the recipe.

After urea and creatinine, uric acid is one of the most abundant components of urine (Bouatra *et al.*, 2013), however, its absence in Sarigul's AU did not show any detrimental effect on bacterial growth in the assays we have carried out so far. In contrast, precipitation could affect the readings and interpretation of bacterial cultures, as we often rely on turbidity levels to indirectly measure the bacterial growth. There have been reports of optical density measurements being affected by secondary scattering like precipitates (Bernardez and de Andrade Lima, 2015). An AU assessment reported unusually high absorbance measurements in the blank controls which were confirmed to be sterile by culturing on solid media and could be caused by precipitation (Ipe and Ulett, 2016). For this reason, it was decided that for our purposes, it was essential to avoid precipitation at the cost of eliminating uric acid from the formula.

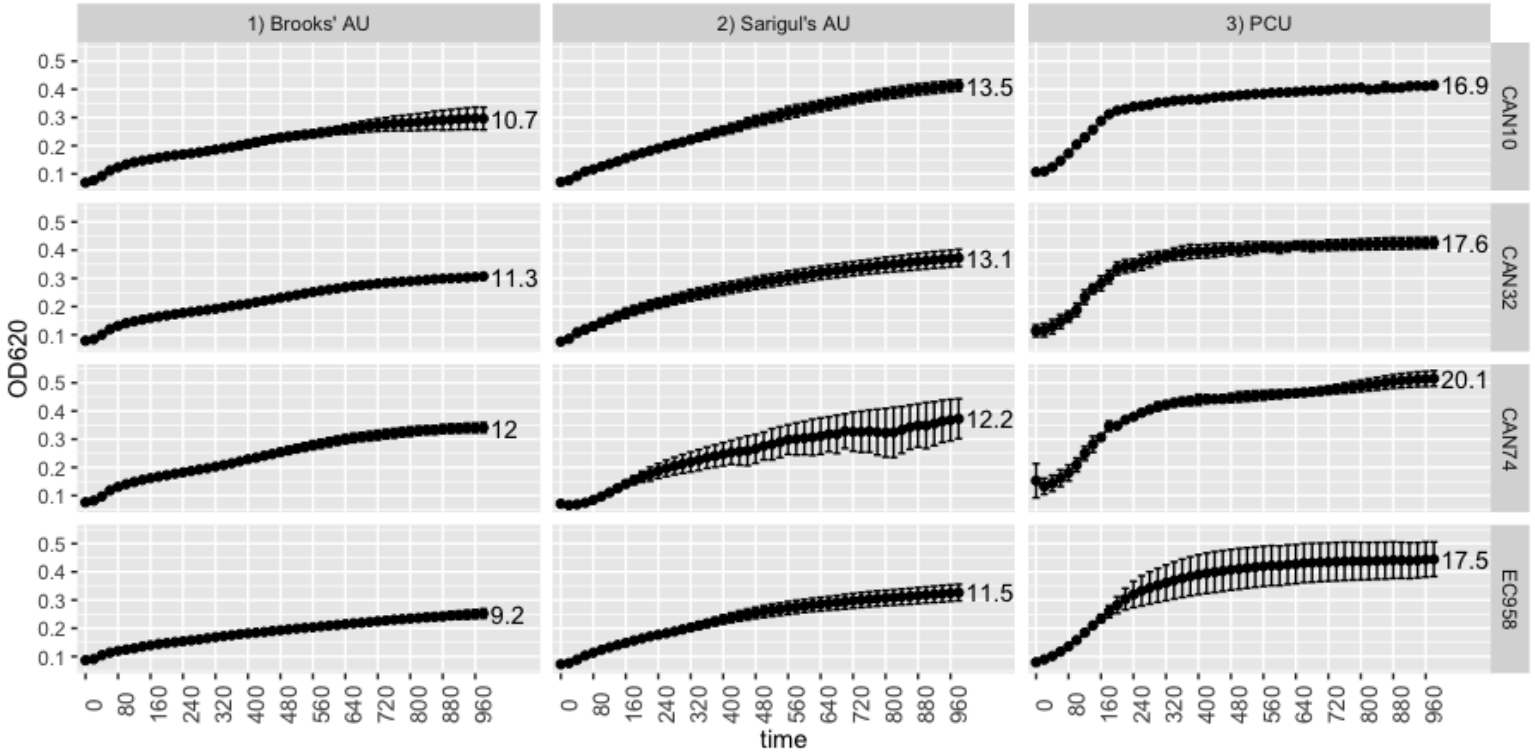

Figure 2.2 Assessment of the Artificial Urine (AU) protocols. Two published protocols of AU were modified and used to grow four UPEC strains. The strains were also cultured in pooled canine urine (PCU) as a reference. Graphs show the mean of three technical replicates and standard deviation shown as error bars. The calculated area under the curve is specified after the final timepoint in each curve

2.3.2 Evaluation of the AU recipes for the study of phage-UPEC interactions

In line with our objectives, the AU should ideally give similar results for phage-bacterium interactions as real urine. Therefore, three UPECs were assayed with phages in the candidate AUs and compared to PU as part of the AU assessment. The AUC was calculated for the cultures and a score was determined for each phage-bacterium interaction which indicates the percentage of the control AUC that is covered by the AUC from the infected culture (Figure 2.3). Thus, the lowest scores represent interactions in which the phage is highly virulent and inhibits the growth of its host, whereas scores closer to 100 represent strains that are more resistant to the phage and grow similarly to the uninfected culture.

Although the scores obtained from the different media were not significantly different from each other using a one-way paired ANOVA test, a trend is visible in that scores obtained with Sarigul's AU were lower than those in the PCU reference (mean=40, SD=13.2 and mean=56.7, SD=19.4, respectively), whereas scores obtained from Brooks' AU assays (mean=70.7, SD=14.4) were generally higher than the PCU reference. This means that the effect caused by the phage is more noticeable in Sarigul's AU.

With the corresponding modifications, Sarigul's AU showed a slightly better performance as an AU medium to allow the growth of UPECs, though not significantly different from Brooks'. The lysing effect of phages is also more evident in this AU. In their publication, Sarigul *et al.* (2019) evaluate a few AUs –including their formula and Brooks'—with attenuated total reflection-Fourier transform infrared spectroscopy and compared them to pooled urine of 28 healthy humans. They concluded that the chemical composition of their AU is more similar to human urine than the other tested AUs. With a few modifications, this AU fulfilled the expectations of a medium to study UPECs and phages interactions for UTIs. This AU protocol has been routinely used by

myself and other laboratory members now for three years. Although the formulation has not changed, new developments by Marianne Keith in how to prepare and store this AU have further optimised its use. The final protocol is now documented as a Standardised Operational Procedure (Appendix 1).

Ideally, the AU media would have been assessed with more UPEC strains and phages, but some limitations prevented this. A finite amount of pooled canine urine was available. In addition, the variation between batches of pooled urine also represented a problem in the reproducibility of the results. Second, the evaluation of the AU was interrupted by the COVID lockdown, delaying the work and putting pressure on generating results going forward. Therefore, Sarigul's AU was selected as the medium of choice for the next stages of the project. Although Brooks' AU was no longer being included for comparison, the use of Sarigul's AU remained under evaluation, by comparing it to PU with phage combinations (See next chapter).

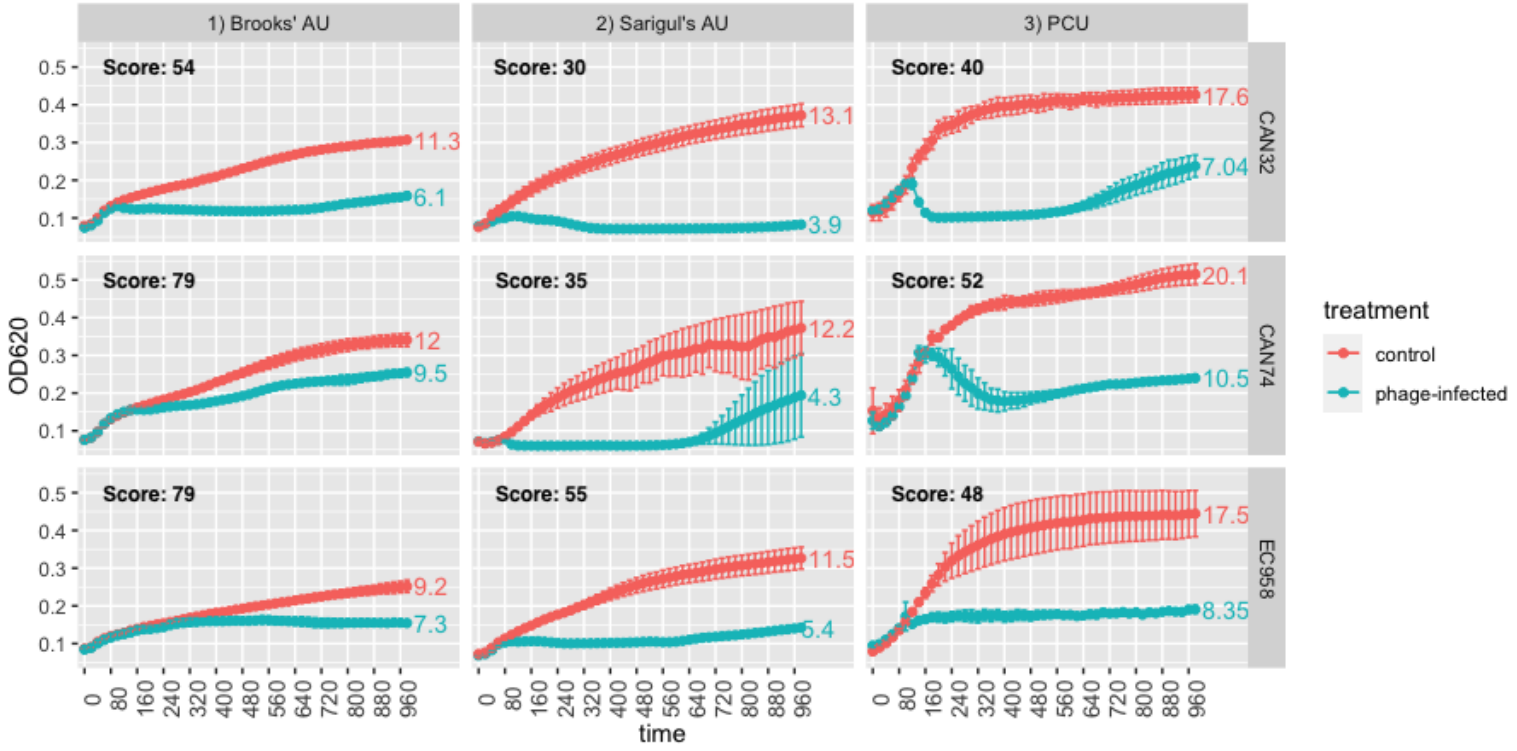

Figure 2.3 Assessment of the Artificial Urine (AU) protocols for phage-bacterium interactions. Representative examples of clinical UPEC cultured in different AU media and in pooled canine urine (PCU). The calculated area under the curve is specified after the final timepoint in each curve. The scores shown at the top left of each panel represent the percentage of the control AUC that is covered by the AUC of the infected culture.

2.3.3 Isolation and selection of phages with potential to lyse UPECs

Our library began with over 100 *E. coli* phages supplied by a start-up company (PTC, Bonen, Germany). We aimed to complement it with phages isolated from environmental samples using representative strains from the local canine UPECs. 26 phages were initially isolated, purified and propagated. The DNA of each phage was extracted (yields ranged from 2 to 24.5 ng/µl) to carry out an RFLP assay to take forward only distinct phages. Restriction profiles showed that many of these phages were replicas of the same phage, and therefore the 14 unique phages were selected for the phage-host interaction assays (Figure 2.4). In order to increase the number and diversity of phages used in the interaction assays, the phage cohort was completed by including phages from the PTC collection, which were known to be distinct and had different host ranges.

The selection of PTC phages was based on the host range demonstrated in spot assays using 15 UPEC, which were selected based on the phylogeny of the cohort to include representative strains of each cluster. Figure 2.5 shows the results of the spot assays. The interactions were classified as complete lysis, shown in black; incomplete lysis or cloudy plaques, shown in grey; and no lysis, shown in white. A list of all the phages used during this research project, their isolation host and the origin of the phage can be found in Appendix 2. Phages included in the interaction assays are marked with a star.

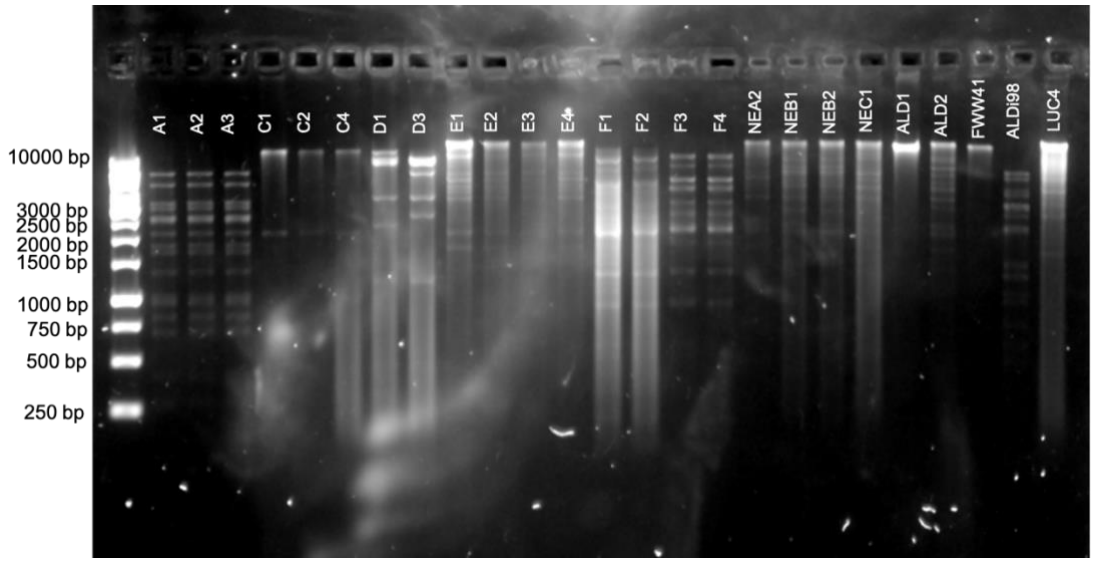

Figure 2.4 Restriction Fragment Length Polymorphism (RFLP) of isolated phages. Phages were isolated and purified from waste water samples. In order to avoid using repeated phages, RFLP was carried out with the DNA of the isolated phages to identify unique phages. Phages with the same restriction pattern were assumed to be closely related and only one of each pattern was used in further studies.

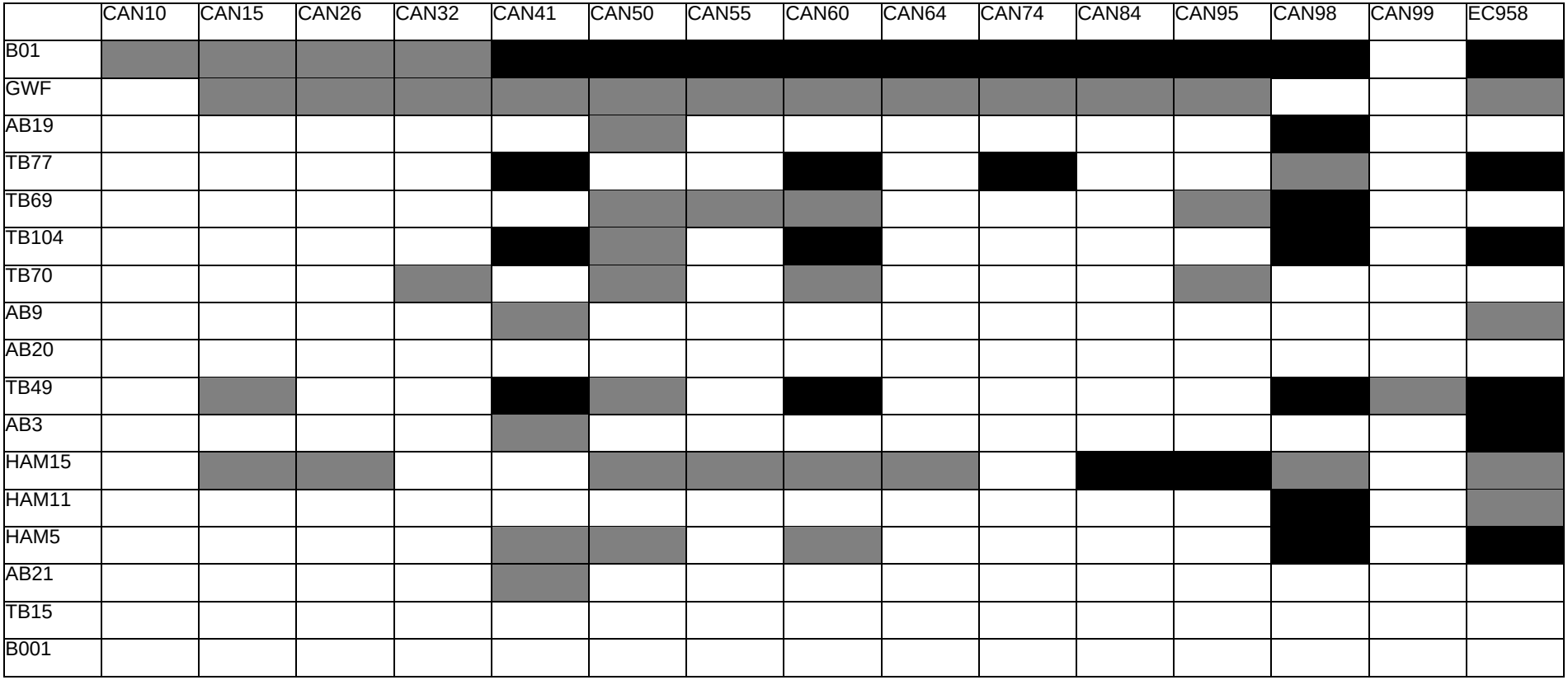

Figure 2.5 Spot assay results of PTC phages. To complement the group of phages isolated for the phage-host interaction assays, phages acquired from the PTC were included. The selection of PTC phages to be used in the interaction assays was guided by spot assay results using 15 clinical UPECs. Interactions resulting in complete inhibition (clear plaques) are shown in black; incomplete lysis or cloudy plaques are represented in grey; white represents no lysis.

2.3.4 Phage-host interaction assays

The interaction of 38 UPEC strains and 30 phages was scored by calculating the ratio of the AUC of the phage-infected culture to the AUC of the control culture. The scores ranged from 16 to 145. A matrix of all the interaction scores was used to create a heatmap (Figure 2.6) in which the most virulent interactions have a low score, reflecting no or poor bacterial growth and are shown in light yellow; the resistant cultures grow similarly to the control and therefore their score is close to 100 and are represented in dark red. Bacteria that grow better in the presence of the phage exceed the 100 score and are also represented in black.

The heatmap shows a general overview of the composition of the phage library. It was clear that some strains are particularly resistant to phages: some are inhibited by only one (n=2, cut-off value = 70) or two phages (n=2), a few more show resistance to all 30 phages (n=3). The same dataset was built by Marianne Keith with interactions measured in the modified Sarigul's AU that I developed (Figure 2.7). The phage-resistance appears to be more marked in this dataset, as there are more isolates that can only be targeted by one (n=5) or two (n=4) phages; and 5 UPECs were resistant to all 30 phages.

When comparing the bacterium-phage interaction scores of individual strains in both media, it is possible to note that phage-susceptibility of an isolate can change when assayed in a different media. Figure 2.8 shows pairwise comparisons of four UPEC isolates with the 30 phages. Some phages lose the ability to lyse some of their hosts in AU, for which the host range is reduced. EC958 for instance, is susceptible to 9 out of 30 phages in LB, whereas only two of the same set of phages are active against the strain in AU. In LB, CAN10 and CAN32 are affected by 6 and 8 phages, respectively; whereas 3 phages, that did not show activity in LB, can inhibit their growth in AU. In contrast, CAN74 is affected by a similar group of phages in both media, except for two

phages that show activity in LB and not in AU, and one phage that is active in AU but not in LB. These differences show the importance of medium selection to investigate agents, such as phages, with therapeutic potential. The use of rich laboratory media to assess therapeutic phages could result in misleading findings that make it difficult to translate to the clinical practice. More importantly, when susceptibility tests for personalised phage therapy are carried out using standard laboratory media, the difference in phage activity could lead to failure of the phage treatment.

In conclusion, the outcomes of this initial part of the project have been pivotal in the advancement of different phage-related projects in the group. The interaction datasets were useful to gain awareness of the limitations of our initial phage collection. Additional steps in the phage isolation protocol improved the recovery of phages that could target the difficult-to-lyse strains or phage-resistant mutants, and that did not lose infectivity in urine. In addition, the interaction datasets also served as preliminary figures for a dataset generated by Marianne Keith that includes 314 *E. coli* strains and 31 phages (Appendix 3). This extended dataset is now being analysed by Antonia Chalka to train a machine learning model that can predict the susceptibility of an *E. coli* isolate to these 31 phages based on the genome sequence of the *E. coli*.

The AU continued to be the main medium used throughout my PhD project, and the phage-host interaction datasets were used as a guide to search for phage combinations that could completely inhibit a UPEC of special concern: *Escherichia coli* O25:H4-ST131, which was the main focus of the rest of my PhD.

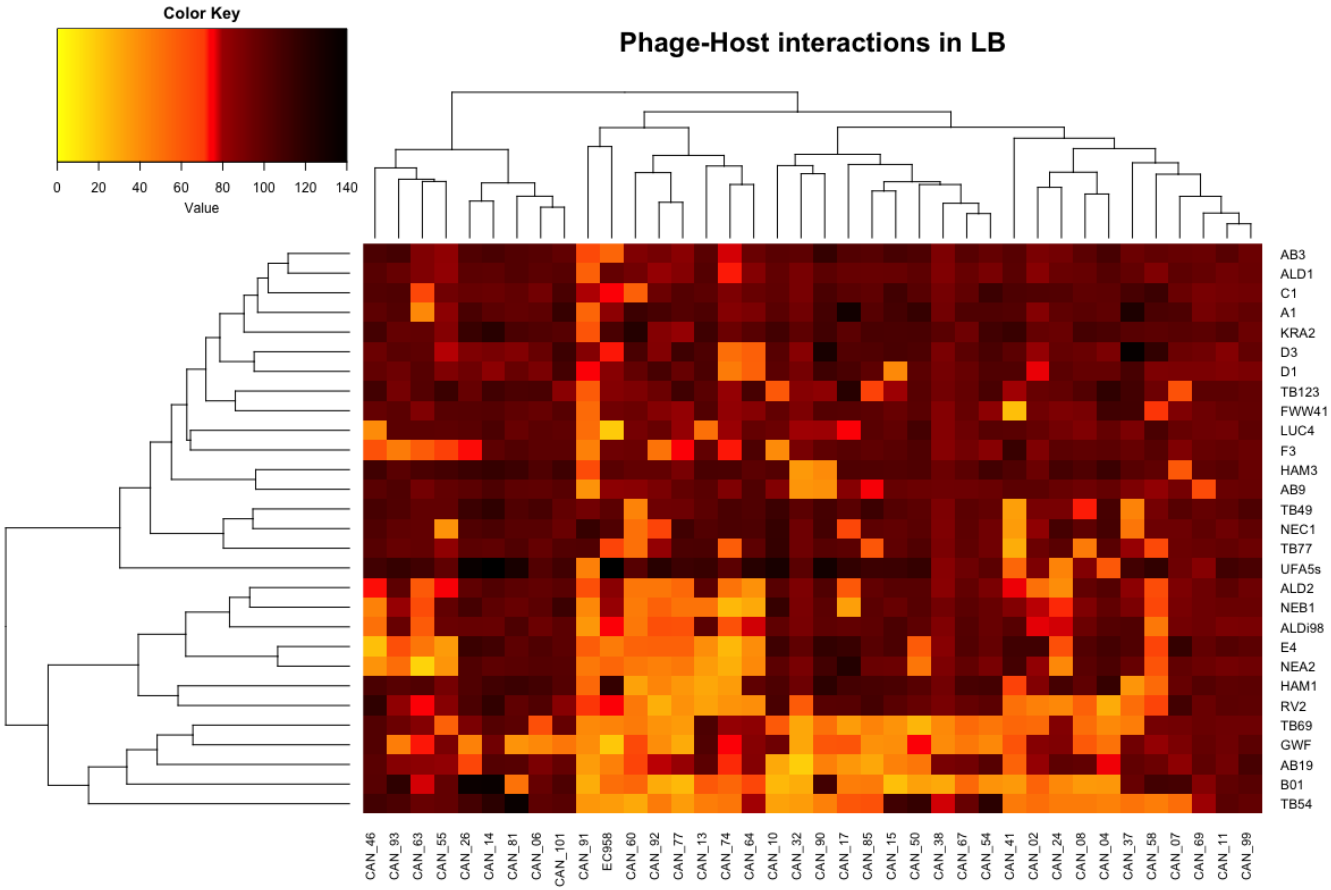

Figure 2.6 LB Phage-host interaction heatmap. 30 UPEC isolates and 30 phages were cultured to measure their interaction, which was scored by calculating the ratio of the AUC of the infected culture to the AUC of the control culture in LB. A strong inhibition of bacterial growth would score low and is represented in yellow; dark red represents a bacterium that grows similarly in the presence and absence of phage. The darkest shades of red represent those interactions in which the presence of phage is conferring some advantage to the bacteria and allow a better growth than with no phage.

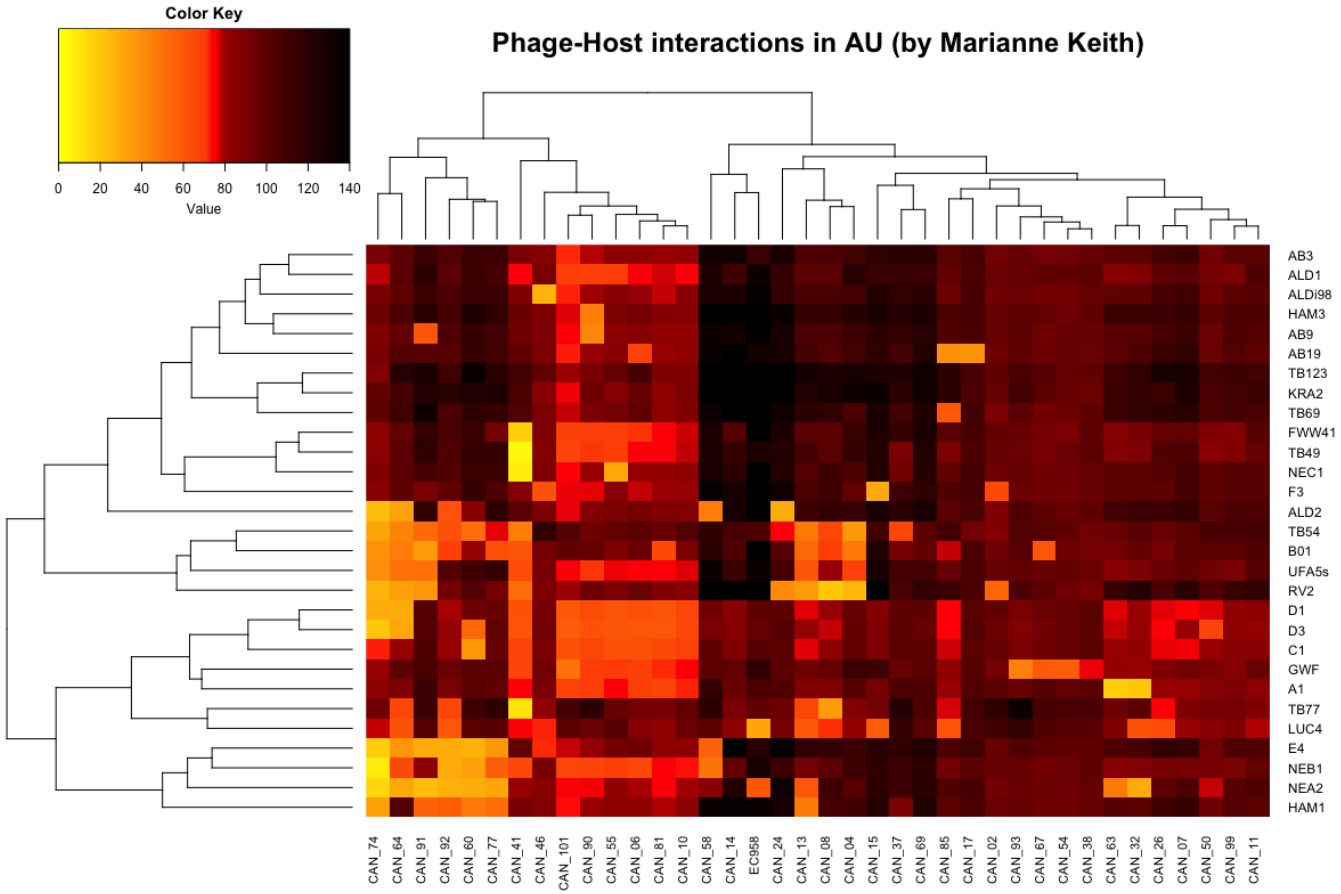

Figure 2.7 AU phage-host interaction heatmap – Work done by Marianne Keith. Each phage-bacterium interaction was scored by calculating the ratio of the AUC of the infected culture to the AUC of the control culture in LB. A strong inhibition of bacterial growth would score low and is represented in yellow; dark red represents a bacterium that grows similarly in the presence and absence of phage. The darkest shades of red represent those interactions in which the presence of phage is conferring some advantage to the bacteria and allow a better growth than with no phage.

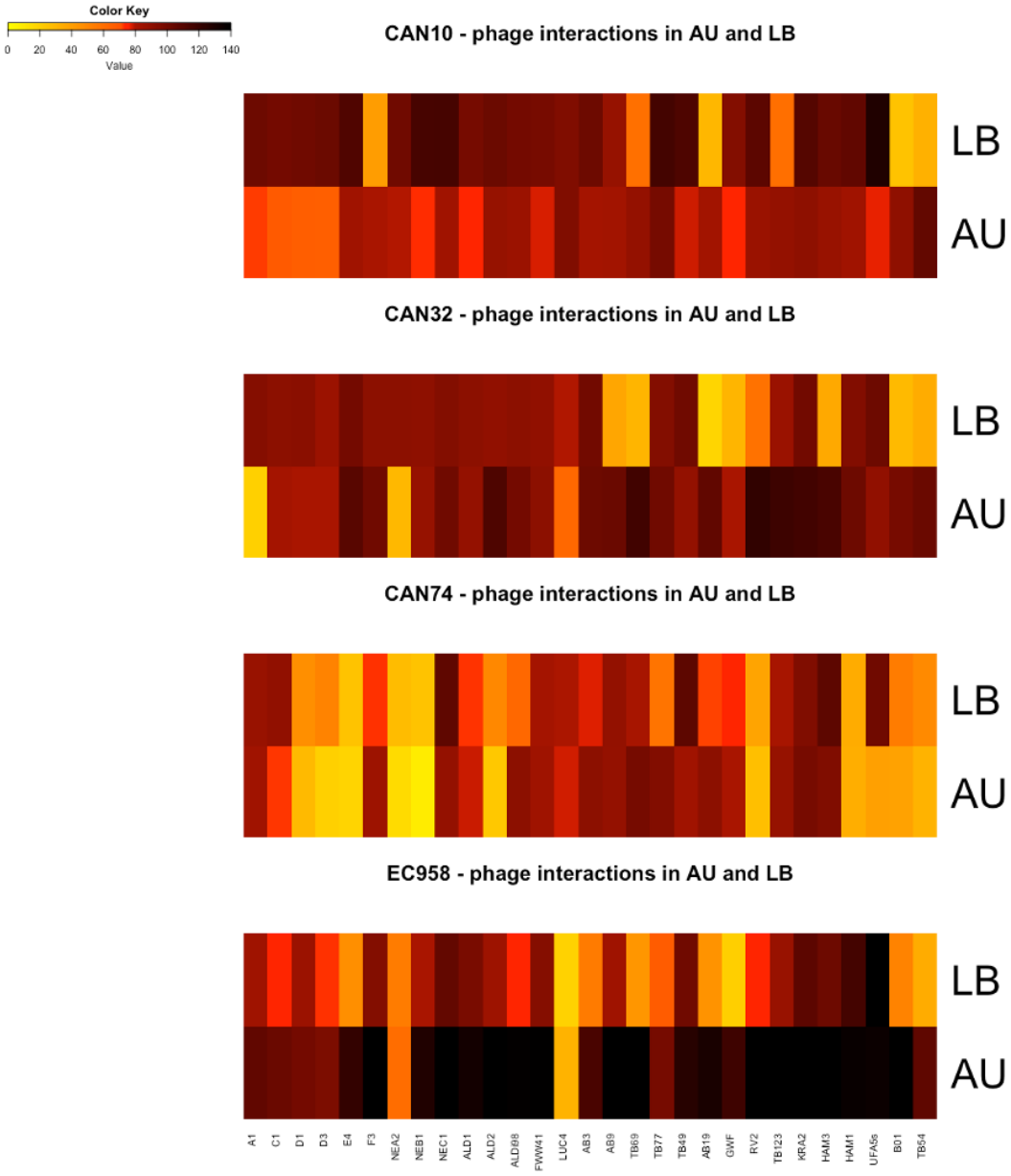

Figure 2.8 Pairwise comparison of four UPEC interactions with 30 phages in LB and AU. The colour represents the score of the interaction: light yellow indicates a low score and therefore a strong inhibition of bacterial growth, whereas dark red represents high scores and no effect on bacterial growth.

Chapter 3 Phage combinations for *in vitro* treatment of *Escherichia coli* O25:H4-ST131 strain EC958

3.1 Introduction

Escherichia coli O25:H4-ST131 is the leading cause of urinary tract and blood infections. It belongs to the phylogenetic group B2, which is the largest group of *E. coli* that are associated with extraintestinal infections. Accordingly, strains within this group are characterised by higher levels of virulence factors that allow them to colonise and potentially cause disease in their hosts, such as fimbriae, curli, autotransporters and siderophores (Forde et al., 2014; Johnson et al., 2013). Most ST131 strains produce the CTX-M-15 type extended-spectrum beta-lactamase (ESBL) and are resistant to fluoroquinolones (Johnson *et al.*, 2013); there have also been reports of ST131 strains showing resistance to last-line carbapenems (Accogli et al., 2014; Cai et al., 2014; Johnson *et al.*, 2013; Naas et al., 2011). The ST131 group has challenged the idea that multidrug-resistance comes with a fitness cost that is usually translated into lower virulence. Moreover, it has demonstrated great capacity to rapidly disseminate across the world (Nicolas-Chanoine *et al.*, 2014). For this reason, it is urgent to find new strategies to prevent and treat *E. coli* ST131 infections, and PT is a promising alternative for this.

Previous studies have reported promising results with phages to treat ST131 *E. coli* strains *in vitro* and in animal models (Dufour *et al.*, 2016; Green *et al.*, 2017; Pouillot *et al.*, 2012). Despite these promising results, failure of PT is relatively common (Jault *et al.*, 2019; Rhoads *et al.*, 2009; Sarker *et al.*, 2017). Bacteria have numerous ways of evading phage predation which can lead to an unsuccessful treatment.

Phage cocktails are a mixture of phages commonly put together with the purpose of avoiding phage resistance and/or expanding the target spectrum of the preparation. It is generally assumed that resistance is less likely to arise when more than one phage is in play. Nevertheless, combining individually active phages against a strain not always results in better lysis than single phages (Bourdin *et al.*, 2014; Watanabe *et al.*, 2007). When phages are

combined into cocktails, they may create antagonism, resulting in a lower lytic activity than those of the single phages; or they can create synergy, resulting in a more pronounced lytic effect than the best single phage in the cocktail. Alternatively, the phages can neither interfere with each other's activity nor facilitate it, creating a neutral combination. The outcome of phage therapy with cocktails not only depends on the phages that are being combined, but also on other factors such as the host strain and the conditions in which they are interacting (Niu *et al.*, 2021).

New methods to design 'intelligent' cocktails have been proposed, in such way that the combination is guided by the biological features of the different phages. In an opinion article, Gordillo Altamirano and Barr (2021) argue that to create effective cocktails one must be aware of the receptors that each phage targets to decrease the chances of resistance by receptor mutation, and to avoid antagonism of the different phages. Different high-throughput approaches for this task have been proposed: using bacterial collections with genome-wide screens such as the Keio collection (Qimron et al., 2006), transposon mutant libraries (Cowley et al., 2018; Mutalik et al., 2020), and epigenetic biosensors (Olivenza et al., 2020), but these platforms can be difficult and expensive to establish, optimise and run.

In this part of the project, I aimed to test phage combinations to find an effective *in vitro* treatment for an ST131 *E. coli* strain EC958, which was originally isolated in 2005 from an 8-year-old girl with a community acquired UTI in the UK. This strain is a representative and well characterised member of the ST131 clonal group. To put together the phage cocktails, the interaction heatmap generated for the previous chapter was used to group the phages based on their infecting activity (Figure 3.1). Phages from different activity groups were then combined in two- and three-phage cocktails. We hypothesised that these combinations of different phages would be able to outmanoeuvre the anti-phage defence systems by combining multiple infection mechanisms. Using EC958 as a model strain, these cocktails were assessed by comparing their lysis level against the best single phage in LB, AU and PU.

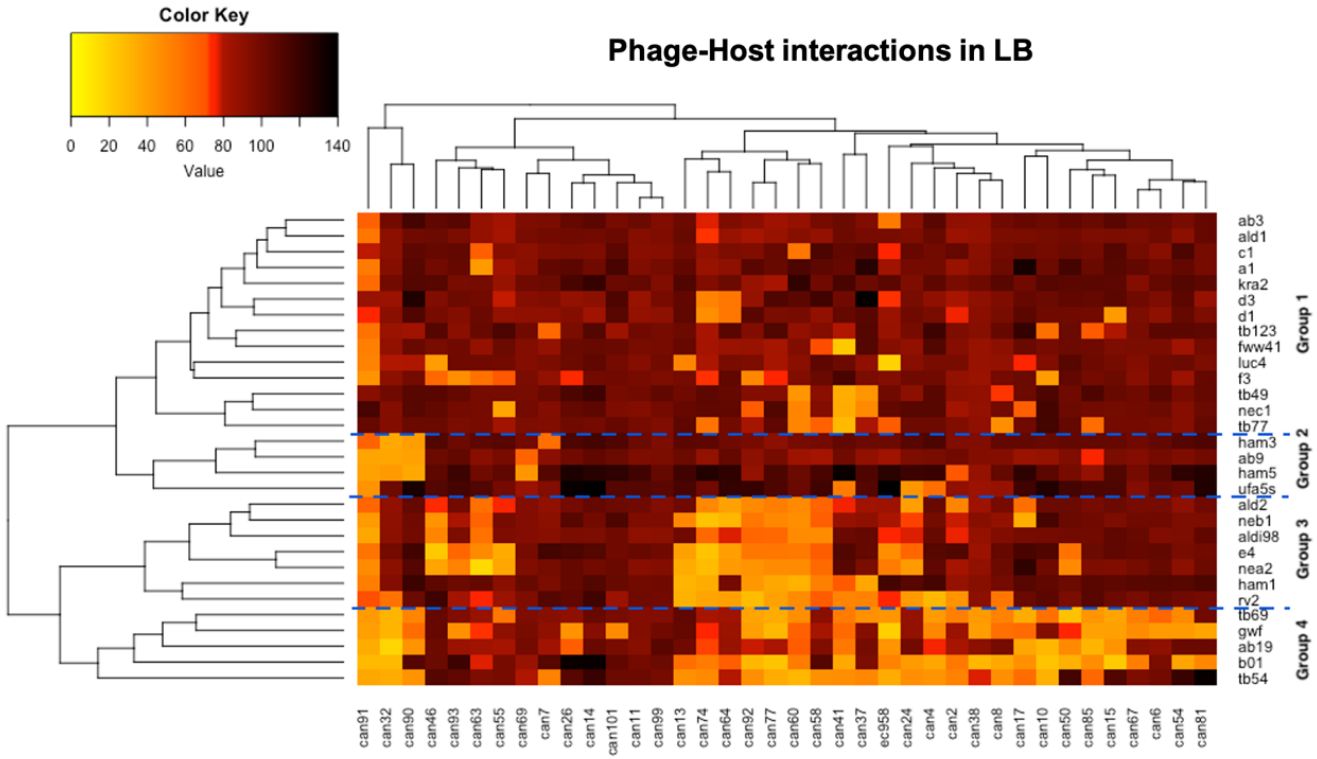

Figure 3.1 Phage-host interaction heatmap with phages grouped by infecting activity. The scores of the phage-bacterium interactions were used to generate a heatmap, in which a strong inhibition of bacterial growth would score low and is represented in yellow; dark red represents a bacterium that grows similarly in the presence and absence of phage. The heatmap was used to cluster the phages into activity groups to be combined into cocktails.

3.2 Material and methods

3.2.1 Characterisation of phage LUC4

3.2.1.1 Phage infection assays

The EC958-LUC4 interaction assays were carried out in microtiter plate format as described above (2.2.7), using different MOIs (~ 0.05, 0.1, 0.5, 1, 5 and 10), and different media: LB, AU and PU. The infection was also assayed in 100 mL AU cultures: A single colony was suspended in 5 mL of AU and cultured overnight at 37°C with shaking. The next morning, 100 mL AU flasks were prewarmed to 37°C in a water bath for ~10 minutes. The overnight culture was sub-cultured by diluting 1 mL in the prewarmed AU flasks. The cultures were incubated for 60 minutes at 37°C with shaking in the water bath. 2 mL of phage suspension, at a concentration of 3 x 10^9 PFU/mL, was then added to the infection flask, whereas 2 mL of SM buffer + LB (9 parts of SM to 1 part of LB) was added to the control flask.

Sampling of the cultures was done every two hours after the addition of phage or SM + LB. 1 mL of each culture was transferred to a cuvette to measure the OD_{600} with a spectrophotometer (Amersham Biosciences). 100 µL was transferred to a 96-well plate, which was then used to make 1:10 serial dilutions of the samples. 5 or 10 µL of each serial dilution were plated on LB agar plates for CFU counting; and on LB top agar with 100 µL of an overnight LB culture of EC958 for PFU counts.

On timepoints T180 and T240, 10 µL of the neat sample was not enough to confidently calculate the concentration of bacteria in the infected culture. For these cases, 5 mL was transferred to a 15 mL Falcon tube and centrifuged at 5000 RPM (4863 RFC) during 10 minutes. 4.5 mL of the supernatant was

carefully discarded and the pelleted cells were resuspended in the remaining supernatant by pipetting up and down. The total volume was spread on an LB agar plate.

The concentration was calculated with the following formula:

$$\text{Bacterial count} = \frac{\text{number of colonies}}{(\text{dilution} * \text{volume})}$$

3.2.1.2 Transmission electron microscopy (TEM)

With the support of the Wellcome Trust Multi User Equipment Grant (WT104915MA), imaging of phage LUC4 was done with transmission electron microscopy in the Electron Microscope Facilities in King's Buildings, University of Edinburgh. Phage LUC4 was propagated in LB as described above (2.2.4.3). 20 mL of the neat phage suspension was concentrated using 10,000 MWCO centrifugal concentrator membrane filters (Vivaspin 20, Sartorius Stedim). One volume of the concentrated suspension was diluted in 9 parts of PBS. The preparation of the sample was done by Stephen Mitchell (Electron Microscope Facilities, King's Buildings) by allowing a droplet of suspension to settle on a Carbon 200 mesh Copper grid for 10 minutes and removing the excess solution with filter paper. A drop of 1% aqueous uranyl acetate was applied for 1 minute, the excess was then removed with filter paper. The grids were air dried. Samples were viewed in a JEOL JEM-1400 Plus TEM. Representative images were collected on a GATAN OneView camera.

3.2.1.3 One-step growth curve

The interaction of phage LUC4 with its host EC958 was characterised with a one-step growth experiment based on the protocol by Kropinski (2018) with minor modifications. A single colony of EC958 was cultured in 5 mL of AU overnight. On the next morning, it was sub-cultured in fresh AU and incubated

at 37°C with shaking for 1 hour. 9.9 mL was transferred to a fresh flask and incubated at 37°C for 5 minutes, after which, 0.1 mL of phage suspension (10^6 PFUs) was added to the flask and left for 10 minutes to adsorb. To synchronise the infected cells, the culture was transferred to a falcon tube and centrifuged at 5000 RPM (4863 RFC) for 10 minutes at 4°C. The supernatant was discarded and the pellet was resuspended in warm AU. In order to avoid having to make serial dilutions before plating, the infected culture was serially diluted at the beginning of the assay in prelabelled flasks: 0.1 mL was diluted in 9.9 mL of AU in flask A; 1 mL was transferred from flask A to 9 mL of prewarmed AU in flask B, and 1 mL was transferred from flask B to 9 mL of prewarmed AU in flask C. A 100 µL sample was taken every 5 minutes, mixed with 3 mL of molten top agar and 100 µL of overnight EC958 culture, and poured on bottom LB agar. Flask A was used for the initial samples, the middle samples were taken from flask B and the final samples were from flask C. Once the top agar had solidified, the plates were incubated at 37°C overnight. The number of PFUs/mL were calculated for each timepoint, depending on the flask that it was taken from, by multiplying by the corresponding factor. The mean values of three biological replicates were plotted using the package ggplot2 in RStudio.

3.2.1.4 End-point adsorption assays

The proportion of virus that can adsorb to EC958 was measured with adsorption assays which were carried out in LB and AU media. For this, overnight cultures were sub-cultured in a 1:100 concentration with fresh media and incubated for 1 hour at 37°C in a shaking water bath. The cultures were infected to an MOI of 0.001. Two samples were taken from the LB culture 5 minutes after infection: one of them was serially diluted and the dilutions were spotted on soft-overlay agar with EC958 to count the total number of phages; the other sample was centrifuged at 12,500 RPM (14,848 RFC) for 3 minutes and the supernatant was serially diluted and spotted on EC958 to count the

free (unadsorbed) phage. The sampling of the AU culture was carried out 20 minutes after the initial infection.

3.2.1.5 Stability at different temperatures and pH

The effects of different environmental conditions on the stability and infectivity of phage LUC4 were explored. 1 mL vials of LUC4 suspensions were titrated at time zero and then stored at -20°C, 4°C, room temperature, 37°C and 50°C in SM buffer, LB, AU and PU.

The stability and infectivity of the phage with different pHs were measured by storing the phage suspended in LB with different pHs –which were modified with the addition of HCl or NaOH.

The titre of the phage at different temperatures was measured after 3 months by making serial dilutions of the phage suspension and plating 10 µL of the different serial dilutions on top agar with EC958. The decrease in PFU/mL numbers from the original titre indicated loss of stability or infectivity.

3.2.1.6 Genetic characterisation of phage LUC4

The genomic DNA of phage LUC4 was extracted using the Phage DNA Isolation Kit (Norgen Biotek). The DNA was sent to Microbes NG (Birmingham, UK) for Illumina sequencing. The reads from the sequencing were assembled and annotated with Prokka using the Phrogs database. The genes were classified according to their predicted function. The software Geneious Prime (v2023.0) was used to represent the genome. In addition, an analysis using PATRIC (Wattam et al., 2014; Wattam et al., 2017) was carried out to identify potential AMR genes and virulence factors. The lifecycle of phage LUC4 was predicted with Phage AI (Tynecki et al., 2020).

3.2.2 Phage cocktails

The lytic activity of phage cocktails was tested and compared to the individual phage LUC4 in microtiter plates as described above (2.2.7), using LB, AU and PU media. Phage suspensions were adjusted to the same titre and combined in equal volumes. EC958 was infected at an MOI of 0.1 with either the individual phage or the phage cocktail. Growth curves were generated with the mean of three technical replicates and the standard deviation is represented with error bars. The interaction scores were calculated as described above (2.2.8). The scores of single phage LUC4, 2-phage cocktails and 3-phage cocktails in each medium were compared with a 2 way ANOVA test.

3.2.3 Isolation of new phages from EC958 variants

New phages were isolated as described above (2.2.4.2) with the difference that the enrichment step was carried out in AU to select for phages that would be active in this media. The isolating hosts used were EC958 or LUC4-resistant mutants that were isolated from EC958-LUC4 interaction assays.

3.3 Results and discussion

3.3.1 Characterisation of phage LUC4

From our library, the most virulent phage against EC958 is LUC4, which is predicted to have a strictly lytic life cycle and morphology of a myovirus (Figure 3.2). LUC4 belongs to the *Straboviridae* family and the *Tequatrovirus* genus. Its 163,861 bp genome encodes for 40 genes involved in DNA, RNA and nucleotide metabolism, 11 tRNA genes, 10 transcriptional regulation genes, 29 genes encoding the tail, 3 genes encoding the connector proteins, 10 genes involved in the structure of the head and the packaging of the genome, 10 genes involved in the host takeover and auxiliary metabolism, and 8 genes involved in lysis (Figure 3.3). In addition, 4 antimicrobial genes and 6 virulence genes were found (Appendix 4).

LUC4 is stable and retains infectivity for at least 3 months when stored between 4 and 37°C, but it cannot survive at freezing (-20°C) temperatures and at 50°C. It also retains infectivity for at least 3 months at pHs between 4.7 and 8.8. When EC958 and LUC4 interact in LB, 98.7% of the phage adsorbs to the host in LB after 10 minutes. In contrast, the rate of adsorption in AU is reduced, as only 73% of the virus adsorbs to the host after 20 minutes (Figure 3.4B). In AU, LUC4 has a latent period of approximately 25 minutes and a burst size of ~78 plaque forming units (PFU) per infected cell (Figure 3.4A).

In 200 µL AU and PU microcultures, EC958 can develop resistance to LUC4 at low and high MOIs. In contrast, in LB this resistance is not observed in all the replicates, which results in growth curves with large error bars (Figure 3.5). EC958 can also resist the LUC4 infection in 100 mL AU culture flasks at an MOI of 10 (Figure 3.6). Phage counts throughout the infection time course show a peak in the early timepoints of the assay –which represent the first

cycle of bursts—followed by a decrease in the number of infectious virus (Figure 3.6C). This could suggest that in the middle and late timepoints of the assay, the resistance is already in place and no new infectious particles are being produced.

Since EC958 can recurrently generate resistance to the single phage LUC4, phage cocktails were tested in search for an antibacterial treatment with long lasting effect.

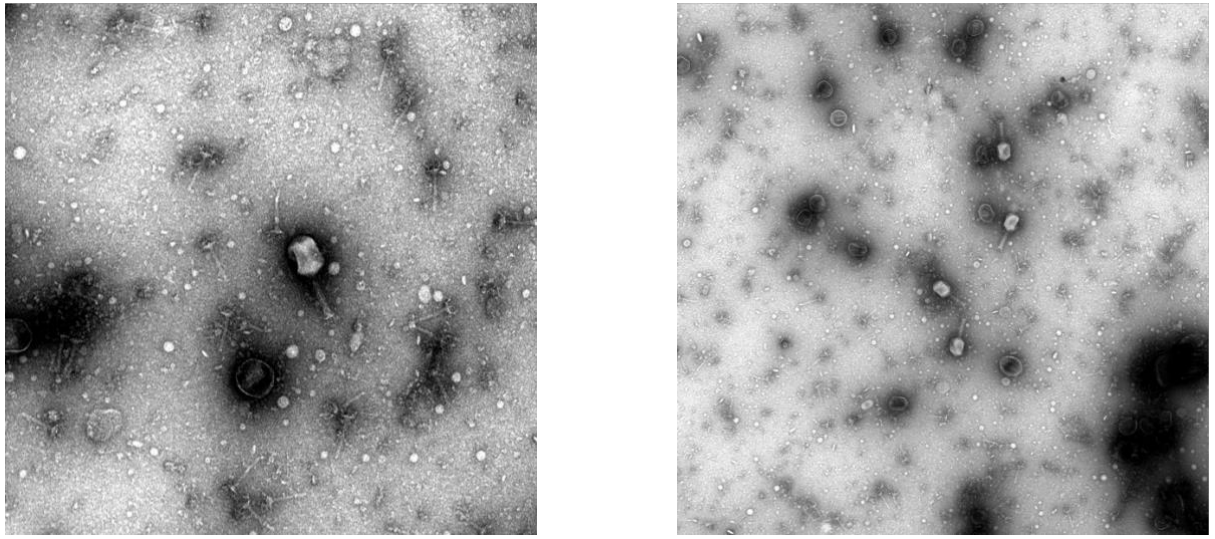

Figure 3.2 Characterisation of phage LUC4. LUC4 is the most virulent phage in our collection that can target EC958. Transmission electron microscopy reveals that LUC4 has the morphology of a myovirus.

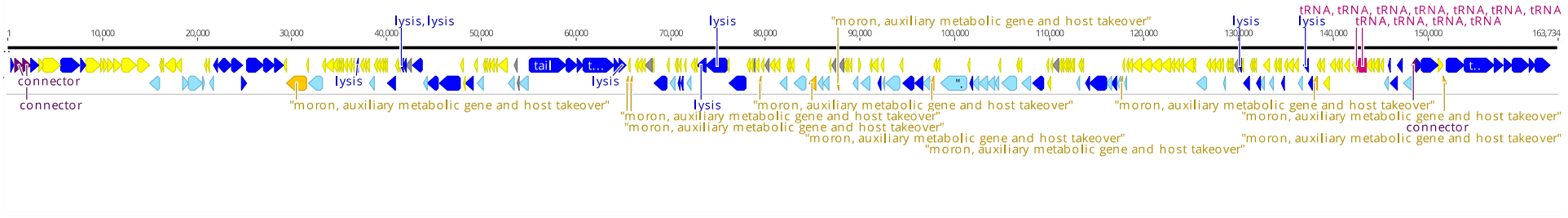

	DNA, RNA and nucleotide metabolism
	moron, auxiliary metabolic gene and host takeover
	Connector
	Head and packaging
	Lysis
	Other
	Tail
	Transcriptional regulation
	tRNA
	Unknown function

Figure 3.3 Genetic characterisation of phage LUC4. LUC4 is the most virulent phage in our collection that can target EC958. The genome of phage LUC4 was annotated with Prokka using the Phrogs database. The annotated genes were classified according to their function and colour-coded using the software Geneious Prime (v2023.0).

A

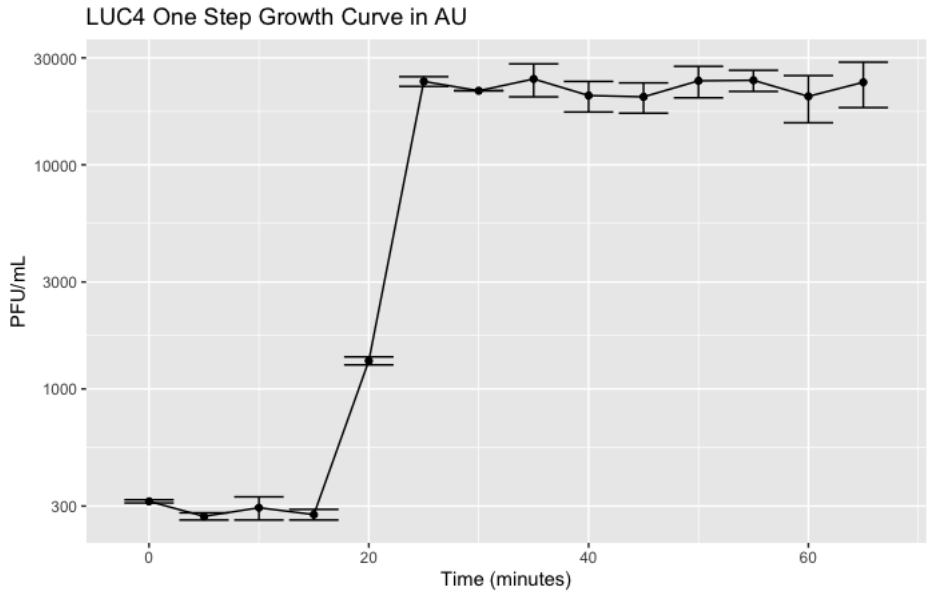

B

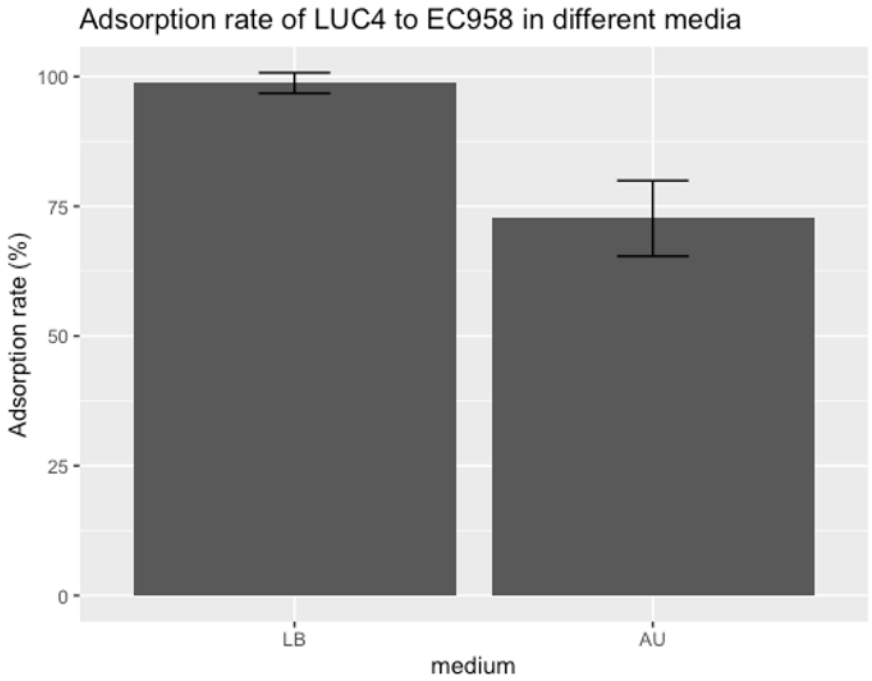

Figure 3.4 Characterisation of LUC4. A) A latent period of approximately 25 minutes and a burst size of 78 viral particles per infected cell were measured with a one-step growth curve of LUC4 with EC958 in AU. B) End-point adsorption assays show a difference in adsorption ratios in different media: 98% of the phages adsorb to EC958 after 10 minutes in LB, whereas 73% adsorb in AU after 20 minutes.

A

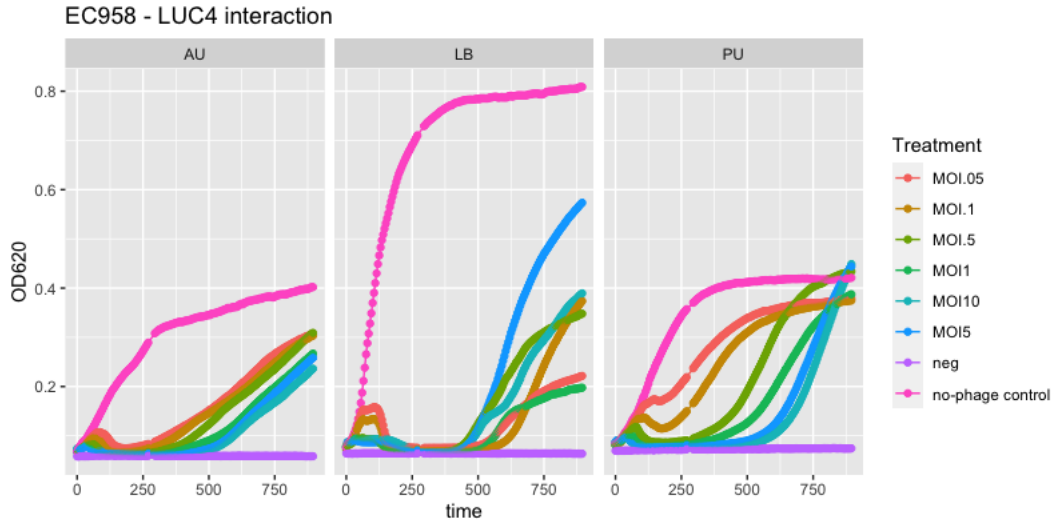

B

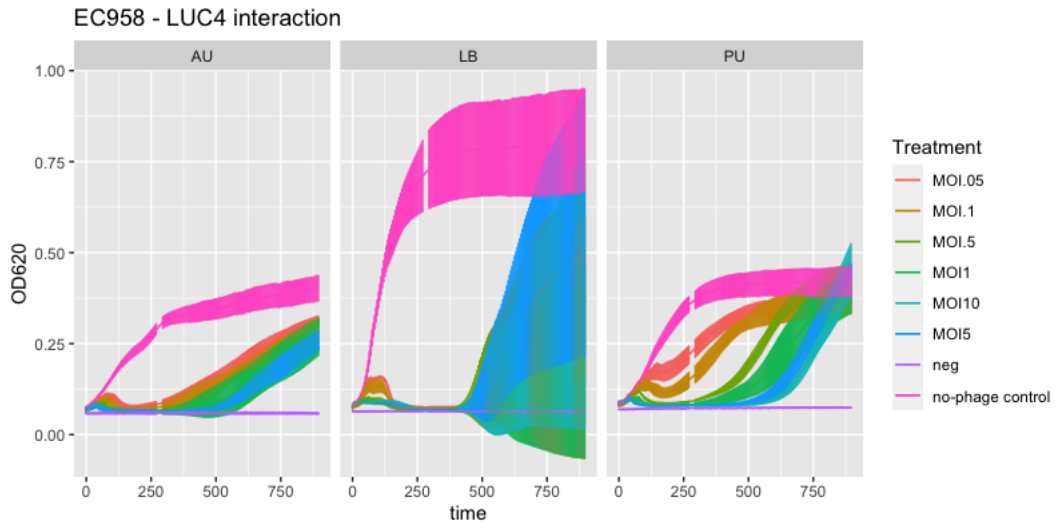

Figure 3.5 EC958-LUC4 interaction in 96-well-plate format (200 µL cultures). OD_{620} of the uninfected and LUC4-infected EC958 cultures at different MOIs for a total of 18 hours. Results are shown A) with and B) without error bars to demonstrate that in LB medium the resistance may not arise in all replicates, causing large variability between replicates.

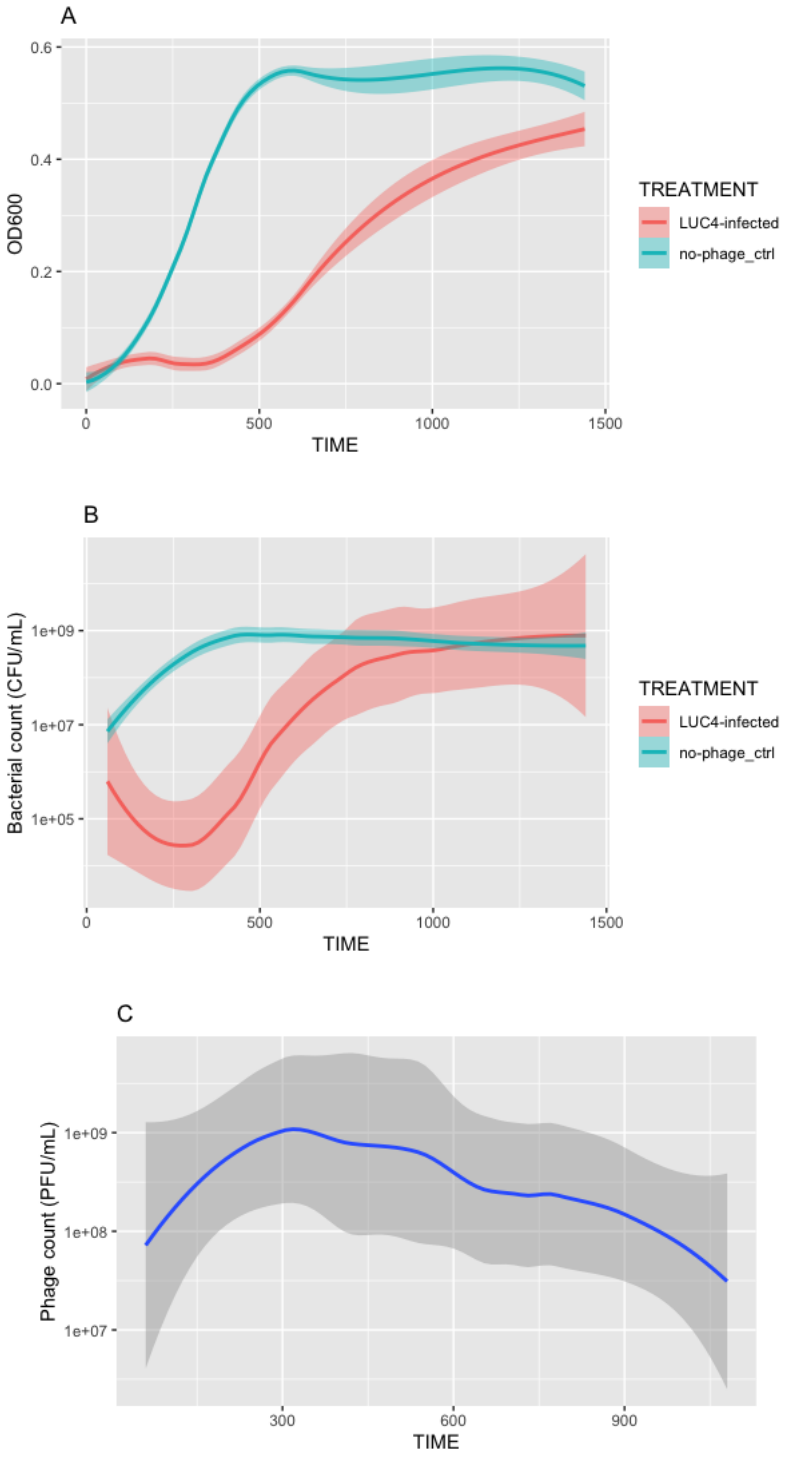

Figure 3.6 EC958-LUC4 interaction in 100 mL flask format. Growth curves of the uninfected (teal) and LUC4-infected (red) EC958 cultures generated by A) measuring the OD_{600}, B) calculating the bacterial density (CFU/ml), and the C) Phage density (PFU/mL) throughout the time course. Data presented as the mean of 5 biological replicates ± SD.

3.3.2 Phage combinations

3.3.2.1 Pairwise combinations

Combining phages into cocktails is one of the most commonly used strategies to reduce the probability of phage resistance. It was hypothesised that the combination of phages from different activity groups would prevent resistance, for which different phage combinations were tested. To test phage combinations in a systematic way, phage LUC4, was first combined with the phages from group 3, which is composed of active (score<60), and inactive (score>60) phages.

Figure 3.7A shows representative examples of EC958 cultured with the single phage LUC4, and in combination with phages ALD2 and NEB1 from group 3, which had shown no activity against EC958 (score>80). In the different media, the EC958 culture can re-emerge after a period of inhibition when LUC4 is added alone, and in combination with the inactive phages. However, only in LB this seems to happen randomly and not in all replicates; this variability between replicates results in large error bars. When LUC4 is combined with phages with low activity (score >60<80), such as ALDi98 and RV2, the inhibition period can be extended but does not avoid it completely in all replicates, as can be seen with the recovery of the culture on the final timepoints of the assay (Figure 3.7B). In combination with an active phage, such as E4 and NEA2 (score <60), LUC4 completely inhibited the bacterial culture in LB (Figure 3.8A). However, when assayed in AU and PU, the additive effect of phages is not seen. Phage combinations show a very similar growth curve as with the single phage LUC4, with resistance emerging at a similar timepoint. In general, none of the pairwise combinations in AU (mean score=49.2, SD=12.3) and in PU (mean score=69.1, SD=7.61) outperformed the single phage LUC4 (mean score=41.2, SD= 12.3 and mean score=58.8, SD= 7.7 in AU and PU, respectively). They did not interfere with the lytic activity of the single phage either, resulting in neutral combinations. In LB, adding an

active phage to LUC4 improved the lysis effect (mean score=40.5, SD=14.7 vs. mean score=23, SD=13.7), but the difference was not statistically significant with Tukey's multiple comparison test (Figure 3.8B).

A

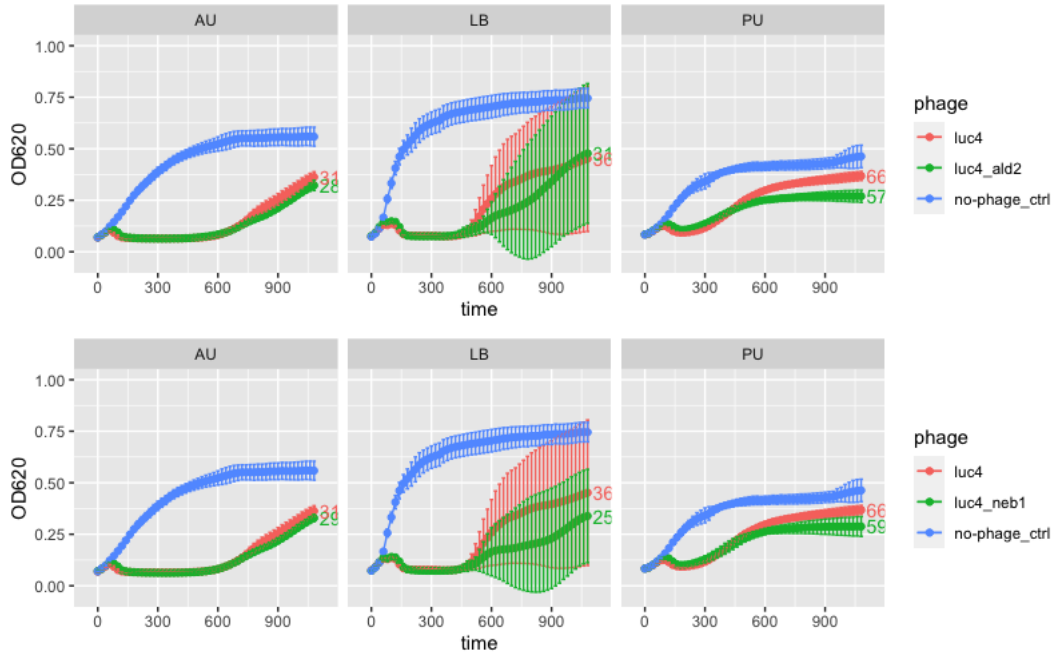

B

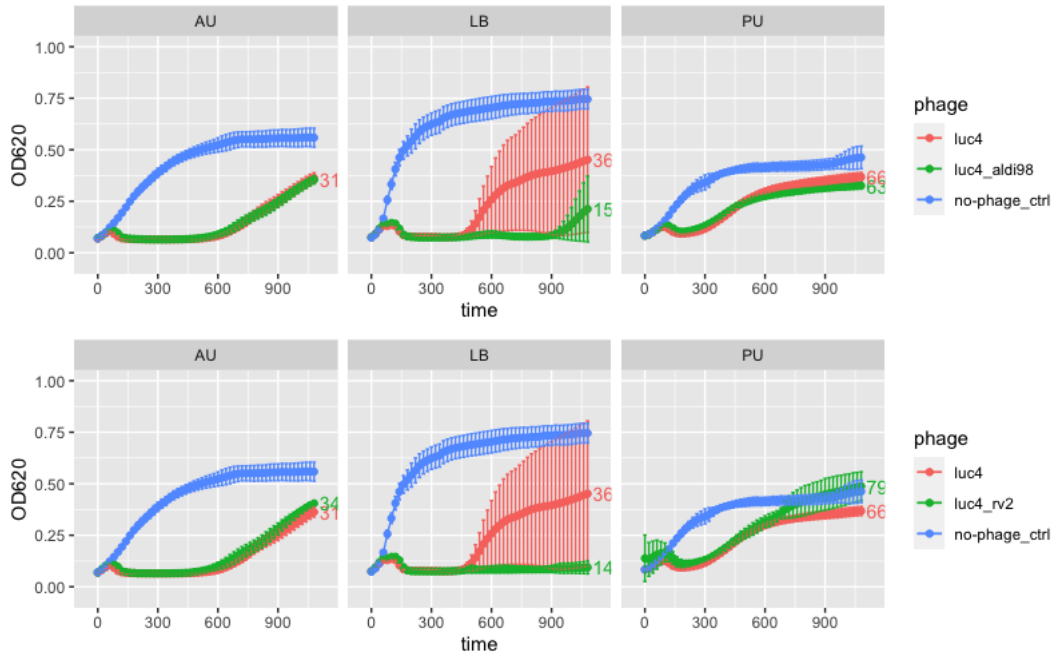

Figure 3.7 Pairwise phage combinations against EC958: LUC4 and Group 3 phages. EC958 was assayed with the single lowest scoring phage –LUC4—and in combination with A) inactive phages (score >80) and slightly active phages (score >60<80) from group 3 in artificial urine (AU), lysogeny broth (LB) and pooled canine urine (PU).

A

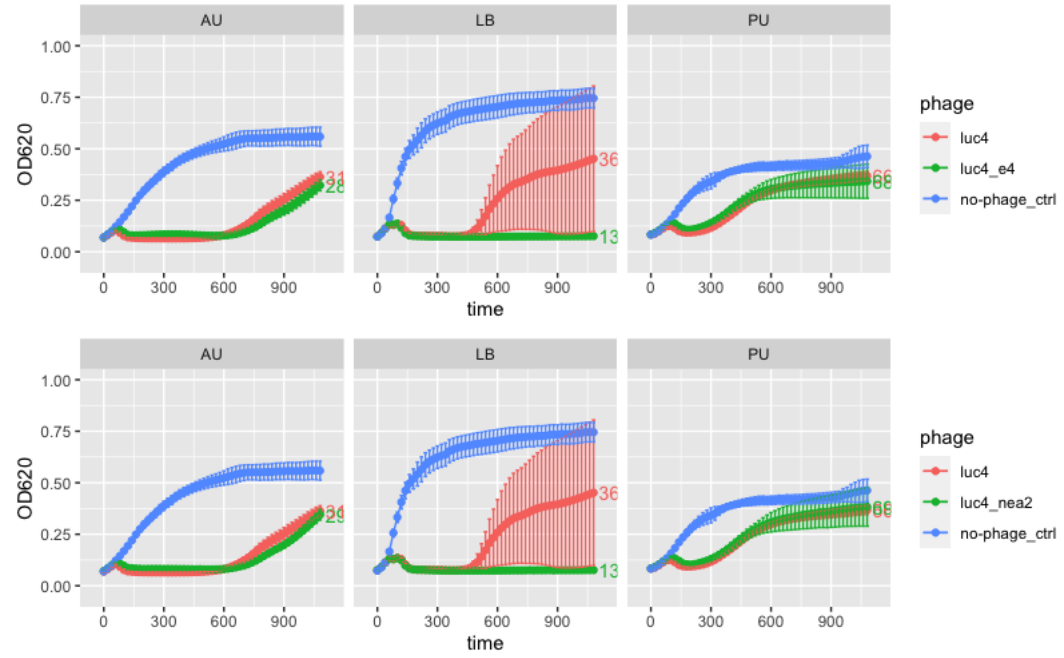

B

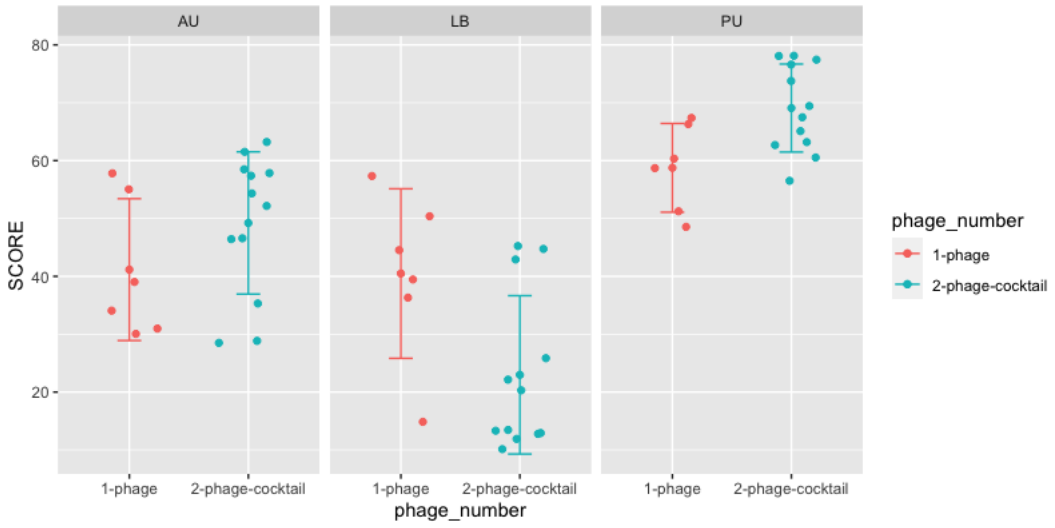

Figure 3.8 Pairwise phage combinations against EC958: LUC4 and Group 3 phages. A) EC958 was assayed with the single lowest scoring phage –LUC4—and in combination with active phages (Score < 55) from group 3 in artificial urine (AU), lysogeny broth (LB) and pooled canine urine (PU). B) Distribution and summary statistics of the single phage LUC4 and pairwise combinations in different media show no statistical difference between groups.

3.3.2.2 Three-phage combinations

The next step in the search for a cocktail that could significantly supress bacterial growth in all media was to include a third phage. The pairwise combinations that performed best in LB (LUC4+E4 and LUC4+NEA2) were used as a base to which the phages from group 4 (all active against EC958 in LB) were added.

In LB, almost all three-phage combinations outperformed the single phage and the pairwise combinations completely inhibited bacterial growth for the 18 hours (Figure 3.10 and Figure 3.11, middle panels). The three-phage cocktails significantly score lower than the single phage LUC4 ($p=0.0056$, Tukey's multiple test) (Figure 3.9).

In AU and PU however, the addition of a third phage is still insufficient to avoid resistance and bacterial regrowth, or to significantly improve the performance of the single best phage and two-phage combinations (Figure 3.9, Figure 3.10, Figure 3.11). These results may not come as a surprise given that the majority of the phages are not active in urine. However, there have been reports in which individual phages with moderate or low lytic activity synergise with other phages to create a cocktail with a better lytic activity (Niu *et al.*, 2021). This was not the case for the phage cocktails tested here, which all resulted in neutral combinations.

To overcome this, new phages were isolated with an enrichment step in AU to select for phages active in this medium.

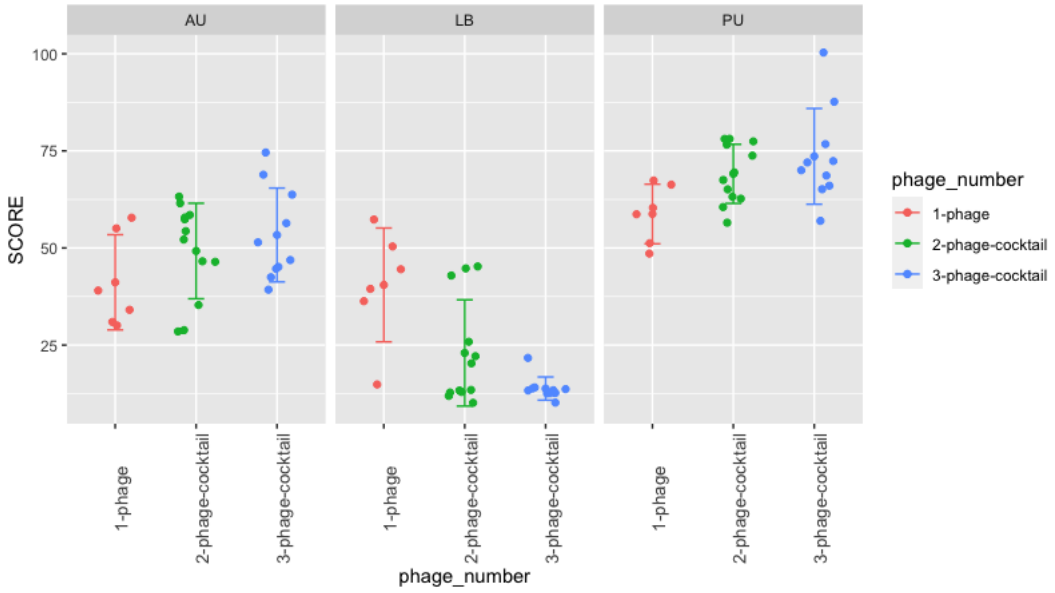

Figure 3.9 Scores of single-phage LUC4, two-phage cocktails and three-phage cocktails by media. Dots represent the interaction scores of independent assays, the mean ±SD are represented with dot and error bars. The scores of three-phage cocktails in LB are significantly different from the single phage (p=0.0056) with a Tukey's multiple test.

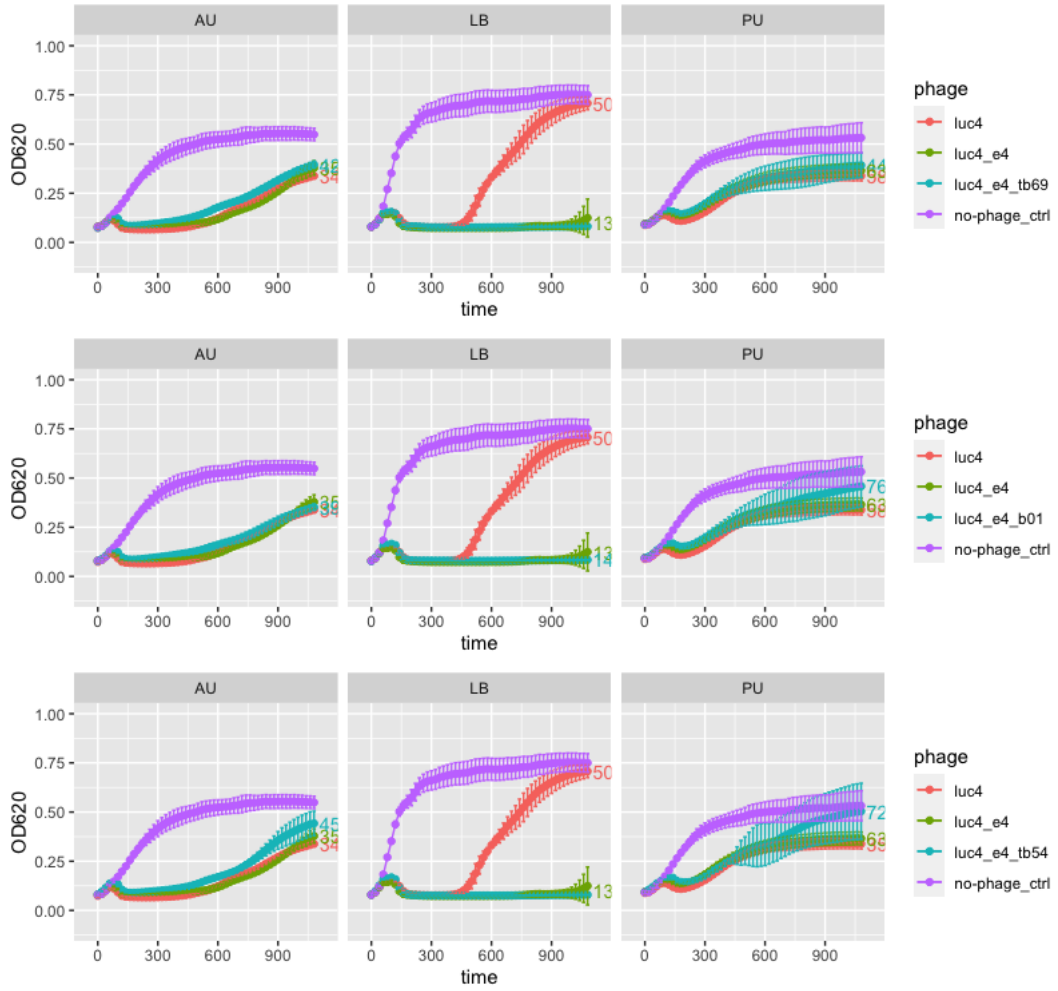

Figure 3.10 Three-phage combinations against EC958: LUC4, E2 and Group 4 phages. EC958 was assayed with the single phage LUC4 and in combination with phage E4 from group 3, and phages from group 4 in artificial urine (AU), lysogeny broth (LB) and pooled canine urine (PU). All individual phages are active against EC958 in LB (Score < 60).

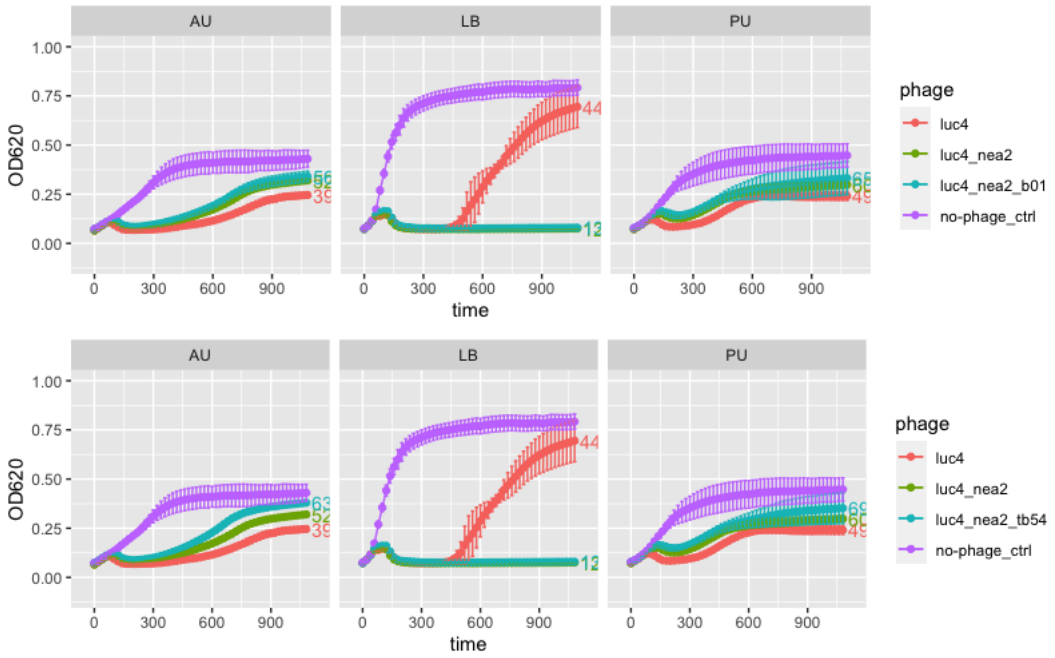

Figure 3.11 Three-phage combinations against EC958: LUC4, NEA2 and Group 4 phages. EC958 was assayed with the single phage LUC4 and in combination with phage NEA2 from group 3, and phages from group 4 in artificial urine (AU), lysogeny broth (LB) and pooled canine urine (PU). All individual phages are active against EC958 in LB (Score < 60).

3.3.3 Phage combinations with newly isolated phages

It has been suggested that isolating from phage-resistant mutants and combining them can be an easy strategy to create phage cocktails with different infection mechanisms (Li et al., 2022). New phages were isolated using EC958 and some of the LUC4-escape mutants as isolating hosts. 4 new phages –CHAP1, BU1, NAM34 and PER3—were isolated, purified, propagated and titrated to be included in the phage cocktail assays. LUC4 was tested in combination with the 4 new phages as before. Unlike with the previous assays only one phage cocktail (LUC4+CHAP1+BU1) managed to inhibit the bacterial growth completely in LB (Figure 3.12, top middle panel), the rest of the combinations of LUC4 with the newly isolated phages did not restrict the growth of EC958 in LB (Figure 3.12). In AU and PU, the combination of phages once again did not have a significantly better effect in preventing the rise of resistance than LUC4. Phage combinations not including LUC4 were also tested but gave no better results (Figure 3.13).

In conclusion, LUC4 is a strictly lytic phage that is highly virulent against EC958 in LB and AU. Nonetheless, after a period of lysis and bacterial growth inhibition, the EC958 is capable of re surging and thriving. Combining three phages from different activity groups significantly improved the effectiveness of the treatment in LB, preventing the resurge of the collapsed bacterial culture for at least 18 hours in most of the assays. However, this synergistic effect was never observed in AU or PU, and all the combinations had a similar activity as the single phage LUC4. The addition of phages did not antagonise the lytic action of LUC4 either, which is a desired feature for a therapeutic phage.

It then became the aim of this PhD project to investigate the cause of phage resistance of EC958 in urine. Since the single phage LUC4 was similarly effective as any phage combination tested, the following parts of the study focused on the interaction of this individual phage with EC958 and the causes of resistance.

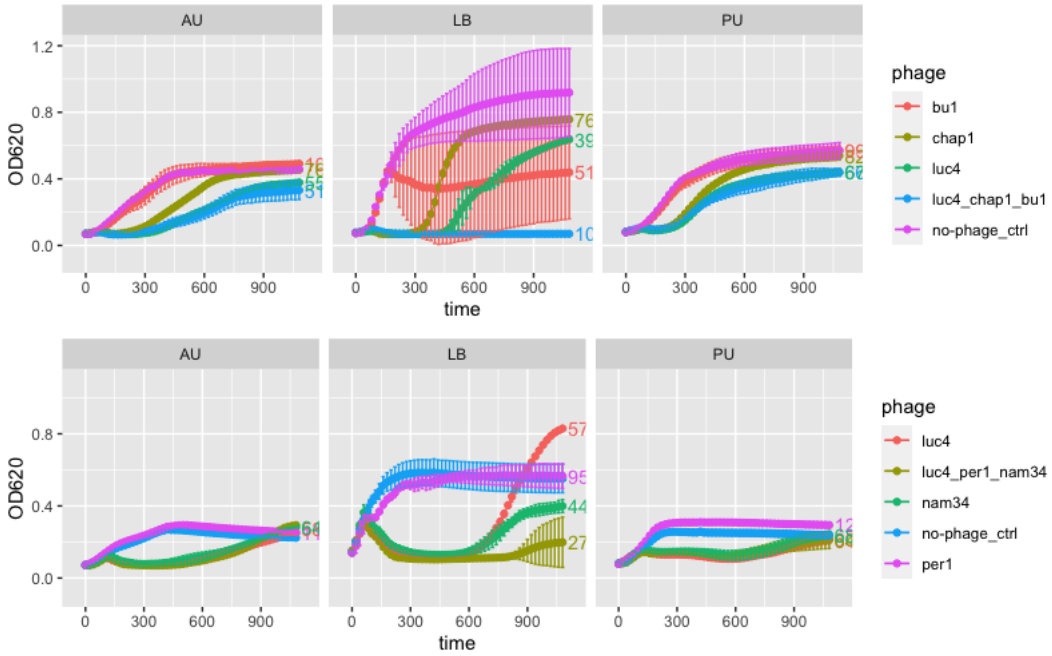

Figure 3.12 Single phages and phage combinations against EC958: LUC4 and newly isolated phages. EC958 was assayed with the single phage LUC4 and in combination with newly isolated phages BU1, CHAP1, NAM34, PER1 in artificial urine (AU), lysogeny broth (LB) and pooled canine urine (PU). The new phages were isolated using LUC4-resistant mutants as hosts.

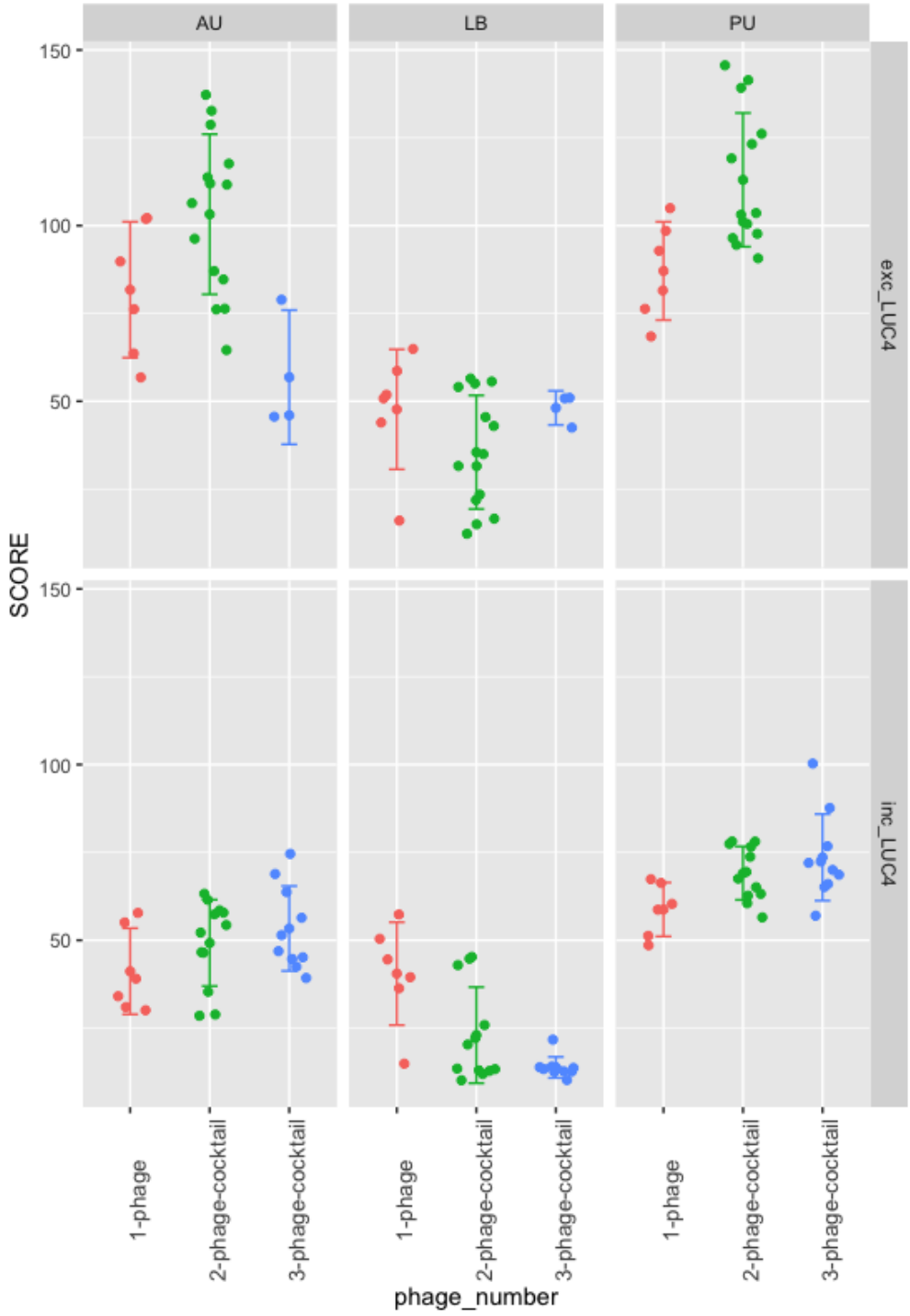

Figure 3.13 Interaction scores of phage cocktails excluding LUC4 (top panels) and including LUC4 (bottom panels). Different single phages, two-phage and three-phage combinations were tested with EC958. To prove that the inefficacy of the phage combinations in AU and PU were not due to phage LUC4 antagonising other phages, the scores of the interactions of cocktails that included LUC4 and the ones that excluded LUC4 were plotted separately.

Chapter 4 *E. coli* strain EC958 can resist the infection of phage LUC4: fixed resistance

4.1 Introduction

As introduced in Chapter 4, *Escherichia coli* strain EC958 is a representative and well characterised member of the ST131 clonal group. It has virulence genes that encode for type 1 fimbriae, curli, the afimbrial adhesin, siderophores and autotransporter proteins (Forde *et al.*, 2014; Schembri et al., 2015; Totsika et al., 2011). It contains a 135.6 kbp IncF plasmid (pEC958—HG941719) with 12 antibiotic resistance genes, and a small high-copy cryptic plasmid (pEC958B) (Phan et al., 2015a). It is CTX-M-15 positive, fluoroquinolone, aminoglycoside and trimethoprim-sulfamethoxazole resistant, which makes it difficult to treat with antibiotics. In addition, the results reported in the previous chapter indicated that the regrowth of EC958 is difficult to inhibit with phages as well, especially in urine media. In this chapter, we aimed to identify the cause of phage-resistance of EC958.

EC958 has been used by several research groups as a model to study the ST131 clonal group. Those studies have focused on understanding its resistance to antibiotics (Phan et al., 2020; Phan et al., 2015b), to human serum (Phan et al., 2013) and other mechanisms of immune evasion (Chamoun et al., 2020; Stocks et al., 2019), as well as virulence traits, such as enhanced motility (Kakkanat et al., 2017), fimbriae regulation (Sarkar et al., 2016a; Totsika *et al.*, 2011) and biofilm formation (Sarkar et al., 2016b). EC958 was used with several other strains to study the effect of quorum sensing inhibitors on antimicrobial susceptibility, biofilm formation and relative pathogenicity (Henly et al., 2021). It has also been characterised in terms of its methylome using PacBio sequencing focusing mainly on the role of the different methyltransferases encoded in EC958 (Forde et al., 2015). To the best of our knowledge though, the phage resistance mechanisms of strain EC958 have not yet been studied.

Phages and bacteria have been putting constant selective pressure on each other for billions of years, leading bacteria to evolve a wide range of defence strategies to avoid being wiped out by their predators (Bernheim and Sorek, 2020; Labrie *et al.*, 2010). Different defence strategies have been described for each stage of infection (Figure 1.5). For instance, one of the most commonly reported mechanisms of resistance involves changes in the phage receptor that lead to impaired adsorption. Additionally, some of these systems are widely distributed among different bacteria: 90% of all sequenced bacteria have restriction-modification systems and 40% of all sequenced bacterial genomes contain a CRISPR- Cas system (Makarova *et al.*, 2011).

Given the urgent need to count on alternative treatment options for *E. coli* strains of concern like this one, this part of the study aimed to understand the phage-resistance mechanisms of EC958 in order to look for potential solutions and prevent failure of phage treatment. To begin understanding the resistance, the infection process of EC958 by phage LUC4 was broken down by timepoints. The resistant populations were classified according to their phenotype: whether they were susceptible or resistant to the phage. Those colonies that were resistant to the phage in subsequent infections were assumed to have acquired a fixed resistance; whereas those who were susceptible were assumed to have gone through a transient resistance.

The fixed resistant variants were analysed with short and long-read sequencing, which provided evidence of the outer membrane protein that is used as receptor for the phage LUC4. This was further confirmed by cloning the receptor into a suitable recipient strain. Transcriptomics methods and protein immuno-blotting served as confirmation of the findings.

4.2 Material and methods

4.2.1 Isolation of escape variants and subsequent challenge to phage LUC4

The population that escaped the phage infection was studied in the first instance by isolating and re-challenging them with phage LUC4. Infections assays were carried out as described before (2.2.7) in microtiter plate format using LB, AU and PU as growth media. The cultures were incubated at 37°C in the plate reader. After 24 hours, a sample of the cultures was serially diluted in PBS and 10 µL of each dilution was plated on LB agar. Single colonies were passaged twice by streaking them out on LB agar plates. Single colonies were then cultured overnight in the appropriate liquid medium to be used in infection assays on the next day.

To explore the composition of the resistant population at different timepoints in AU, infection assays of EC958 were carried out in the 100 mL flask format as described above (**Error! Reference source not found.**). Single colonies were isolated from the serial dilutions plated on LB agar plates, and then purified by passaging them twice on LB agar plates.

The phenotype of the isolated bacteria was verified with infection assays in microtiter plate format as described before (2.2.7). The escape variants were classified as ‘fixed resistant’ when they grew similarly to the uninfected control in the presence of phage, and as ‘transiently resistant’ when they showed phage-driven lysis in the growth curve. The phenotype of the fixed resistant variants was verified by repeating the infection assays twice more.

4.2.2 Short-read sequencing of the permanently resistant variants

32 of the variants that showed a permanent resistant phenotype were sent to Microbes NG (Birmingham, UK) to be Illumina-sequenced. The bacterial samples were prepared following the guidelines of the company.

The quality of the sequencing was assessed with FastQC. The trimmed reads of each sequence were used to search for SNPs or small INDELs using Snippy with the default parameters (Seemann).

4.2.3 Pulse-Field Gel Electrophoresis (PFGE)

To gain evidence on whether the fixed resistant variants with no identified SNPs had any genomic rearrangements, these samples were embedded in agarose and their DNA was extracted using the CHEF Bacterial Genomic DNA Plug Kit (Bio-Rad) following the manufacturer's protocol. Digestion of the genomic DNA was carried out overnight with the enzymes XbaI, BcuI (SpeI) (Thermo Scientific), and BlnI (AvrII) (Takara Bio) at 37°C. The next day, the digested DNA was washed with the kit's wash buffer and then stabilised with 0.5X TBE. A 1.5% agarose gel was made and the agarose plugs containing the digested DNA were loaded into the wells. The gel was run for 20 hours in a Bio-Rad CHEF-DR pulsed electrophoresis chamber with a cooling unit set at 4°C. The initial switch time was programmed for 2.2 s, the final switch time was 54.2 s and the gradient was set to 6 V/cm. The gels were stained by bathing them in Gel Red (BIOTIUM) diluted in 0.5 TBE for 60 minutes, and then visualised and documented in a LI-COR Odyssey Fc Imaging System.

4.2.4 Transcriptomic studies

An RNA-seq experiment was carried out to see the difference between EC958 and four of the permanently resistant variants with putative genomic rearrangements.

Infection assays in flask format were set up as described above (**Error! Reference source not found.**). Cells in mid-exponential phase (OD_{600}~0.2) were harvested and the RNA was extracted following the method by (Stead et al., 2012): ~10^8 cells were transferred to an Eppendorf tube from each culture and centrifuged at 6000 RPM (5000 RFC) for 10 minutes. The supernatant was discarded and the cells were lysed by resuspending the pellet in 100 µL of RNA extraction solution (18 mM EDTA, 0.025% SDS, 1% 2-mercaptoethanol, 95% RNA grade formamide), vortexing and incubating them at 95°C for 7 minutes. The samples were then centrifuged at 13,000 RPM (16,000 RFC) for 5 minutes to pellet the cell debris. The supernatant was transferred to a fresh tube. RNA concentrations were estimated with Nanodrop (Thermo Fisher), and ~50 µg of RNA was purified with the QIAGEN RNeasy MinElute Cleanup Kit following the instructions by the manufacturer.

The concentration and quality of the RNA was measured in a 4200 Tapestation (Agilent Technologies). The RNA samples were sent to Edinburgh Genomics (Edinburgh, UK) where they were prepared for manual Illumina Stranded sequencing with NovaSeq SP 50PE.

The quality of the sequencing data was checked with FastQC. STAR (Dobin and Gingeras, 2015) was used to map the reads in the reference EC958 genome with the following parameters: --outFilterType BySJout, --outFilterMultimapNmax 20, --outSAMunmapped within, --outSAMtype BAM sortredByCoordinates. The quantification of mapped reads in each gene was determined with FeatureCounts (Liao et al., 2013) with the following parameters: -t CDS, -g product, -Q 10, -s 1.

The .bam files with the number of reads confidently mapped to each gene were imported to RStudio. The package EdgeR (Robinson et al., 2009) was used to normalise the data, filter the very lowly expressed genes (with less than 4 counts per sample and less than 20 reads across all samples) and carry out a differential expression analysis. The results from the analysis were plotted using the package ggplot2 (Wickham, 2011).

4.2.5 Long-read sequencing

This part of the project was carried out with the help and close supervision of Natalie Ring; Postdoctoral Fellow in the Roslin Institute. 11 permanently-resistant variants were processed for long-read sequencing. Genomic DNA was extracted with the MagAttract HMW DNA Kit (QIAGEN) and purified with the ProNex Size-Selective Puification System, following the manufacturers' instructions. The DNA concentrations were measured with Qubit dsDNA HS Assay Kit (Invitrogen).

The DNA samples were barcoded with the Oxford Nanopore Rapid Barcoding Kit (SQK-RBK004), pooled and loaded into a MinION flow cell (Chemistry R9.4.1) following the manufacturer's protocol. The sequencing was carried out in a GridION Mk1 for a total of 72 hours. The minimum length threshold was set to 200 bp and the minimum quality score to 10. The pores were scanned every 1.5 hours. The basecalling was carried out with the Super-accurate basecalling model of Guppy.

Porechop (https://github.com/rrwick/Porechop.git) was used to trim the adaptors from the reads. Reads were then filtered by size and quality to a 100x coverage with Filtlong (Wick and Menzel, 2017) and assembled using Unicycler (Wick et al., 2017) in the hybrid mode using the Illumina sequence reads described above (4.2.2). Prokka (Seemann, 2014) was used for the annotation and Easyfig (Sullivan et al., 2011) was used to align and visualise the sequences.

4.2.6 Cloning and expression of EC958's OmpC in ClearColi™

To clone EC958's ompC, the genomic DNA of EC958 was first extracted with the QIAGEN DNeasy Blood & Tissue Kit following the manufacturer's protocol. It was then used as the template in a PCR to amplify the *ompC* sequence with primers containing the target sequence for restriction enzymes SalI and BamHI (Appendix 5). A 50 mL reaction was made using the Q5 High-Fidelity DNA Polymerase (New England Biolabs), following the recommendations by the manufacturer. The PCR was run in a Thermo Hybaid PCR Express Thermal cycler with an initial denaturation step at 94°C for 4 minutes, 30 cycles of 94°C for 30 s, 63°C for 30 s and 72°C for 1.5 min; and a final elongation step at 72°C for 4 minutes.

The PCR product was run in a 1.2% agarose gel –stained with Gel Red (BIOTIUM)—at 100 V for 60 minutes. The band with the expected size was excised and the DNA was cleaned up with the Omega Micro Elute Gel Extraction Kit. The clean PCR product and the vector pWKS30 were digested with the restriction FastDigest enzymes SalI and BamH (Thermo Scientific). 30 µL reactions were set as shown in **Table 4.1** and **Table 4.2**; they were incubated at 37°C for 1 hour.

Table 4.1 Digestion reaction of PCR product

10 µL	PCR product
3 µL	10X FastDigest Buffer (Thermo Scientific)
1 µL	FastDigest Enzyme SalI (Thermo Scientific)
1 µL	FastDigesr Enzyme BamHI (Thermo Scientific)
15 µL	Nuclease-free H_20 (NEB)

Table 4.2 Digestion reaction of pWKS30

5 µL	pWKS30
3 µL	10X FastDigest Buffer (Thermo Scientific)
1 µL	Fast Digest Enzyme SalI (Thermo Scientific)
1 µL	FastDigest Enzyme BamHI (Thermo Scientific)
20 µL	Nuclease-free H_20 (NEB)

The reactions were run in a 1.2% agarose gel for 60 minutes at 100 V. The bands of the corresponding size were excised and the DNA was cleaned up with Omega Micro Elute Gel Extraction Kit.

The ligation reaction was set up as shown in **Table 4.3**. A ligation reaction with no insert (vector only) was set up by substituting the volume of insert for nuclease-free H2O.

Table 4.3 Ligation reaction of pWKS30 and *ompC*

10 µL	Digested insert
5 µL	Digested pWKS30
2 µL	10X FastDigest Buffer (Thermo Scientific)
1 µL	T4 DNA Ligase (Thermo Scientific)
2 µL	Nuclease-free H_20 (NEB)

Chemically competent DH5-alpha cells (NEB 5-alpha Competent *E. coli*, New England Biolabs) were transformed with the construct and the vector following

the manufacturer's protocol. The transformed cells were plated on LB plates with 50 µg/mL ampicillin, and incubated overnight at 37°C.

To validate the constructs, the plasmid of the transformed cells was extracted with the Omega Micro Elute Gel Extraction Kit and digested with FastDigest enzymes KpnI and EcoRI (Thermo Scientific). The digestion patterns were compared to the results of an in-silico analysis.

4.2.6.1 Preparation of electrocompetent ClearColi cells

ClearColi cells were made electrocompetent by inoculating 250 µL of an overnight culture in 25 mL of LB and incubating them at 37°C with shaking to an OD_{600}=0.6. Cells were subsequently pelleted by spinning at 5000 RPM (4,863 RFC) for 10 min at 4°C. They were resuspended in an equivalent volume of sterile, ice-cold 10% autoclaved glycerol (Sigma Aldrich). Cells were washed four more times by spinning them down to pellet them, the volume of ice-cold 10% autoclaved glycerol in which the cells were resuspended was halved in each step. In the final wash step, the cells were resuspended in 800 µL of 10% glycerol.

4.2.6.2 Electro-transformation of ClearColi

Electrocompetent ClearColi cells were then transformed with the constructs or the empty plasmid by adding 5 µL of the construct or the empty vector to 50 µL of competent cells, and then mixing them by flicking. The total volume was transferred to an ice-cold 1 mm electroporating cuvette (FLOWGEN). The dry cuvettes were pulsed in a Bio-Rad *E. coli* Pulser at 1.8 kV. 1 mL of LB was added to the cuvette immediately after the shock. The cells were allowed to recover for 90 minutes at 37°C with shaking. 100 µL was spread on LB-

ampicillin (amp) agar plates at a concentration of 50 µg/mL and incubated overnight at 37°C.

4.2.6.3 Restriction digestion for the validation of constructs

Constructs were extracted with the E.Z.N.A. Plasmid DNA Mini Kit (Omega). 6 µL of the plasmid extraction samples was digested with FastDigest enzymes (Thermo Scientific) for 1 hour at 37°C. The digestion products were run in a 1% agarose gel and visualised in a LI-COR Odyssey Fc Imaging System. The samples with the expected restriction profile were selected for the subsequent steps.

4.2.7 Infection assays of transformed ClearColi™

To verify the phenotype of the transformed ClearColi™, 500 µL of overnight cultures were sub-cultured in 50 mL of LB-amp and AU-amp. After 90 minutes of incubation at 37°C with shaking, the cultures were induced by adding IPTG to a final concentration of 1mM, and incubating for one more hour. The induced cultures were used in infection assays in the microtiter plate format at an MOI of 0.1 with phage LUC4. They were also used in spot assays with serial dilutions of phage LUC4 by mixing 100 µL of the induced culture with 3 mL of molten top agar + 1mM IPTG.

4.2.8 Competitive fitness assays

Fitness assays were carried out to prove that the permanently resistant variants are outcompeted by the reversible variants. Two OmpC variants

(ECRA304.8 and ECRA 544.4) were cultured on LB agar plates with 20 µg/mL rifampicin (rif) and incubated at 37°C overnight. Three resistant colonies were passaged twice more on the same medium to purify them. EC958 and the rifampicin-resistant variants were cultured overnight in 5 mL of LB. EC958 and the rifampicin-resistant ECRA304.8 were co-cultured in 50 mL of LB at 37°C with shaking for 24 hours; another flask was co-cultured with EC958 and rif-resistant ECRA544.4. Viable cell counts for EC958 and the competing rif-resistant variants were determined at time zero and after 24 hours of co-culturing by selective plating.

Fitness was calculated using the following formula:

Fitness index (f.i.) = LN (Ni (1)/ Ni (0)) / LN (Nj (1)/ Nj (0))

Where:

Ni (0) = initial colony counts of EC958

Ni (1) = final colony counts of EC958

Nj (0) = initial colony counts of ECRA304.8 or ECRA544.4

Nj (1) = final colony counts of ECRA304.8 or ECRA544.4

To verify that the loss of fitness was not due to the acquisition of the rifampicin resistance, the fitness assays were carried out with ECRA304.8 and ECRA544.4 and their rifampicin-resistant variants in the same way.

4.2.9 Outer membrane protein extraction

500 µL of overnight cultures was diluted in 50 mL of AU and incubated at 37°C to an OD_{600}~0.2. The cells were pelleted by centrifugation at 5000 RPM (4863 RFC) for 10 minutes and resuspended in 50 mL PBS; this wash step was repeated once more. The bacteria were transferred to 1.5 mL Eppendorf tubes

and stored at -20°C overnight. On the next day, the pellet was thawed and sonicated in a XUBA1 ultrasonic bath (Grant) for 10 cycles of 1 minute with 1-minute cooling breaks between each cycle. The samples were then centrifuged at 8,000 RPM (6000 RFC) for 45 seconds to pellet the cell debris. The supernatant was decanted into a fresh tube which was centrifuged at 14,000 RPM (18,000 RFC) for 30 minutes. The supernatant was discarded, the pellet was resuspended in 200 µL of 2% sarkosyl and incubated at room temperature for 30 minutes. The samples were then centrifuged at 14,000 RPM (18,000 RFC) for 30 minutes, washed with PBS, centrifuged again for 10 minutes and resuspended in 50 µL of PBS and 50 µL of 2X Laemmli Sample buffer (SIGMA). The proteins were separated with SDS-PAGE by loading 25 µL of each sample into a 10% Mini-PROTEAN TGX precast gel and running it at 90 V for 120 minutes. The gel was then stained with Instant Blue Coomasie Protein Stain (Abcam) and incubated overnight at RT in a platform shaker. The stained gel was washed twice with PBS before imaging.

4.2.10 Western blots

This part of the work was carried out by the research group's core scientist: Sean McAteer. The permanently resistant variants with no SNPs detected were cultured in 4mL AU at 37ºC overnight (OD_{600}=0.4-0.5). The cells were pelleted by centrifugation and lysed by incubation at 100ºC for 5 minutes in 0.1mL of 2X Laemmli Sample buffer (Sigma). The proteins were separated with SDS-PAGE by loading the samples into two 4-20% Mini-PROTEAN TGX precast gels (Bio-Rad) and running them at 150 V for 60 minutes. The gels were transferred to separate nitrocellulose membranes at 60 V for 60 minutes. The membranes were washed with PBS twice and then blocked with a 5% skimmed milk solution in PBS at 4°C overnight. After the blocking, the membranes were washed with PBS then incubated in a 1:10000 dilution of the OmpC antibody (Invitrogen#PA5-117701) or the RecA antibody (Enzo Life

Sciences#ADI-MSA-205E) in 5% skimmed milk at room temperature with agitation for ~1 hour. The membranes were washed with PBS three times then incubated in a 1:2000 dilution of the species-specific HRP-labelled secondary antibody (NEB#7074 for anti-OmpC, NEB#7076 for anti-RecA) in 5% skimmed milk for ~1 hour at room temperature with agitation. The membranes were then washed three times with PBS.

The visualisation was done by chemiluminescence imaging by adding enhanced chemiluminescence (ECL) solutions. The ECL solution 1 was composed of 1 ml luminol, 440 µL coumaric acid solution and 10 ml 1M Tris-HCl at pH 8.5 diluted in distilled water to 100 ml final volume; ECL solution 2 was made by adding of 64 µL hydrogen peroxide and 10 ml 1M Tris-HCl at pH 8.5 diluted in distilled water to a final volume of 100 ml. The membranes were bathed in a 1:1 solution of ECL 1 and 2, then incubated for 5 min with gentle agitation. The light emitted from the reaction was captured on Hyperfilm ECL in a dark room.

4.3 Results

4.3.1 The composition of the escape population to phage LUC4 infection changes throughout the time course

The first approach to understand the mechanism driving EC958 to escape predation by LUC4 consisted in studying the escape variants of the phage infection. For this, I first recovered single colonies from the resistant population 24 hours after the infection. These single colonies were passaged twice in fresh LB to avoid the carryover of remaining phage. They were then infected with the phage in a new liquid assay to verify whether they had remained resistant or if they had regained susceptibility to the phage. The escape variants that were tested could be classified according to their phenotype: resistant or susceptible. Interestingly, the proportion of each phenotype was different depending on the medium that they had been recovered from. Escape variants recovered from LB were mostly resistant to LUC4 in the subsequent challenges, whereas the ones recovered from pooled urine had mostly reverted to susceptible. The escape variants harvested from the AU cultures after 24 hours were all susceptible to LUC4 (Figure 4.1A).

A time course analysis of the composition of the resistant population in AU was carried out in order to dissect the composition of the resistant population throughout the infection cycles. The results showed that a permanently-resistant population is present and dominant in the early timepoints of the assay, but seems to be outcompeted and eclipsed by the transiently resistant subpopulation that reverts to susceptible when the pressure of the phage is taken off (Figure 4.1B).

A

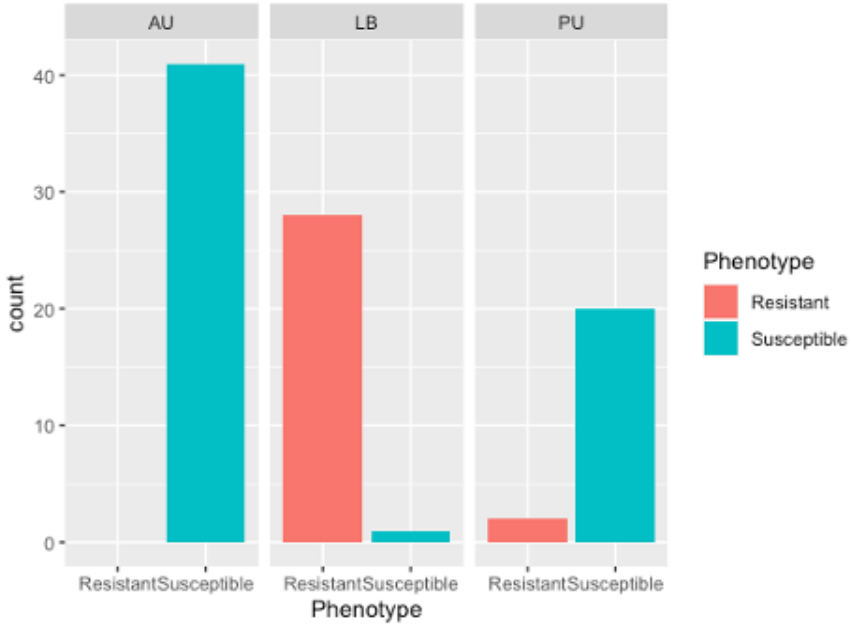

B

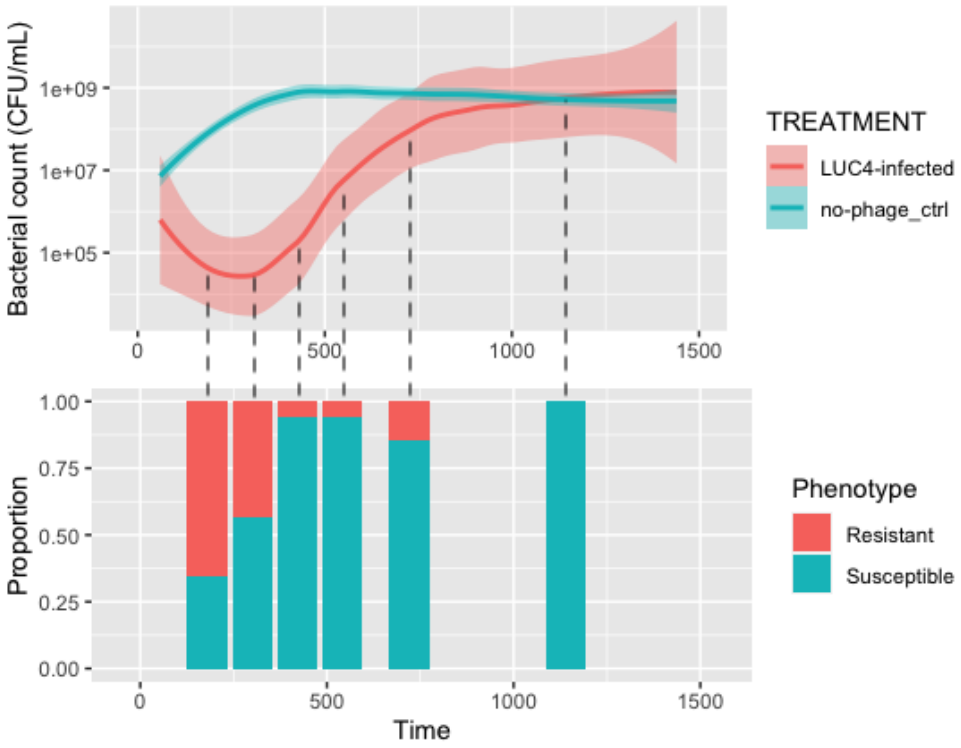

Figure 4.1 The composition of the escape population. The surviving population to the phage infection has a different proportion of permanently resistant and reversibly resistant variants depending on A) the culture media and B) the harvest timepoint. The growth curve of EC958 with and without phage represents the mean of 5 biological replicates ± SD (shaded area). The proportion of resistant and susceptible variants was calculated based on the results of at least 15 isolated single colonies challenged with the phage.

4.3.2 The fixed resistance is mainly caused by changes or loss of function of OmpC

30 of the permanently-resistant variants were Illumina sequenced; the trimmed reads were analysed with Snippy (Seemann). The concatenated output tables can be found in Appendix 6. The results showed that 10 of the variants (33%) had a SNP or small INDEL in *ompC*; two of them (6%) in one of the components of the regulatory system of OmpC (*envZ* and *ompR*) and one (3%) in the intergenic region of *ompC*, suggesting a loss of function or downregulation of this outer membrane protein, which led us to the supposition that this is likely the main receptor for the phage. 16 (50%) of the sequenced samples did not have any mutation detectable with Snippy, and three had mutations in genes that were not very obviously relatable to phage interaction (Figure 4.2).

4.3.3 Long-read sequencing reveals additional variants with loss of OmpC

We hypothesised that some of the variants with no SNP/INDEL detected could have genomic rearrangements that could be difficult to detect with tools such as short-read sequencing and Snippy. To gain evidence of this, the DNA of 12 variants was extracted and then digested with three different enzymes: XbaI, SpeI and Bln. Pulse field gel electrophoresis (PFGE) was carried out with the digested DNA and the restriction profiles were compared to the parent EC958. Differences in at least one of the restriction profiles were found in 7 of the 12 variants (Figure 4.3).

To map the putative rearrangements, 11 variants were long-read sequenced using Oxford Nanopore Technologies. The barcoding adaptors were trimmed

and the reads were filtered by quality and length before they were assembled. Two of the samples did not have reads that could be assembled into a circular chromosome, and they were excluded from the subsequent analysis. The reads from the 9 remaining variants and WT EC958 were assembled into two circular unitigs –one with mean length of 5,098,511 bp (min = 5,069,796 bp, max = 5,114,754), and one 135,600 bp long—and two linear unitigs (4,088 and 1,822 bp). The chromosomal unitigs were aligned and visualised using Easyfig (Sullivan *et al.*, 2011), which showed that there were deletions in 5 of the sequences, insertions in 2 of the sequences and one sequence with an inversion and a deletion. Variant ECRL10 did not show any chromosomal changes compared to the parent EC958 (Figure 4.4).

A zoomed-in and annotated view of the region shows that 4 variants have undergone large deletions that imply the loss of *ompC* (Figure 4.5); whereas one of the variants—ECRA720.15—has a large inversion followed by a deletion (Figure 4.6A), and in variant ECRA304.3 an IS-like element has disrupted *ompC* (Figure 4.6B). Variant ECRA184.8 has an intact *ompC* gene, but a large deletion in the *ompR* region which might be causing the loss of function of *ompC* (Figure 4.7A). Similarly, *ompR* in variant ECRP3 appears to be disrupted by an IS-like element (Figure 4.7B).

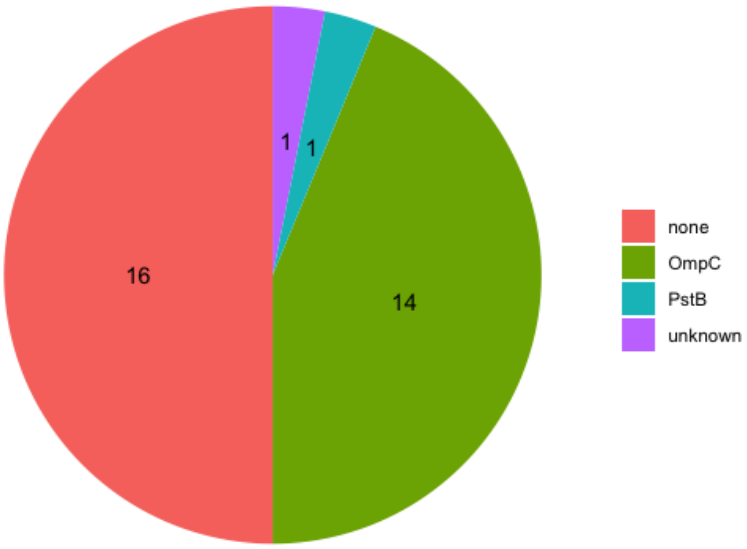

Figure 4.2 Variant calling with Snippy. Fixed-resistant variants were Illumina-sequenced. The genomes were analysed with Snippy, which revealed 14 variants with SNPs or small INDELs disrupting *ompC, ompR, envZ* or the intergenic region immediately upstream from *ompC*, suggesting a loss of function of *ompC* (green section). No SNP or INDEL could be detected with Snippy in 16 of the samples, which led to the hypothesis of large genomic rearrangements. Two variants had SNPs in unknown or unrelated genes (*pstB*).

A

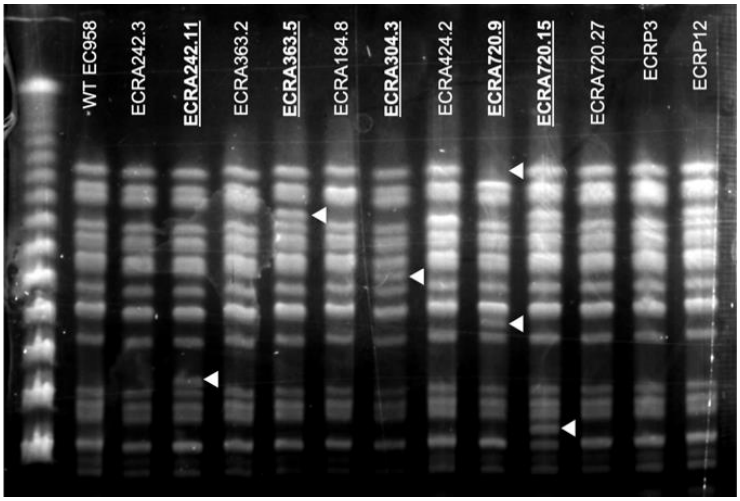

B

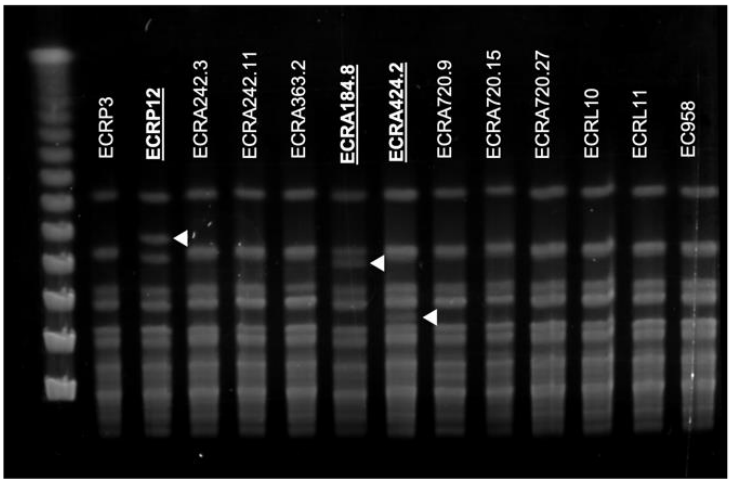

C

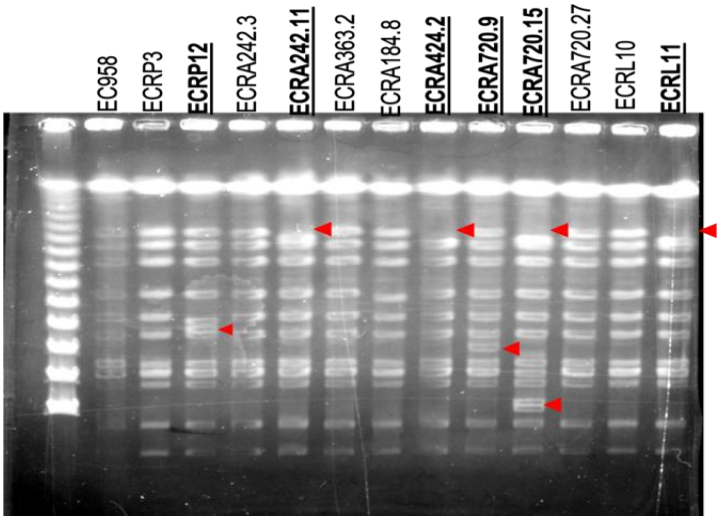

Figure 4.3 Pulse Field Gel Electrophoresis (PFGE). Fixed-resistant variants with no SNP/INDEL detected were processed for PFGE. The genomic DNA was digested with restriction enzymes A) XbaI, B) SpeI and C) Bln and ran with PFGE to search for differences in restriction patterns. Results indicate that some of the permanently resistant variants have gone through chromosomal structural changes.

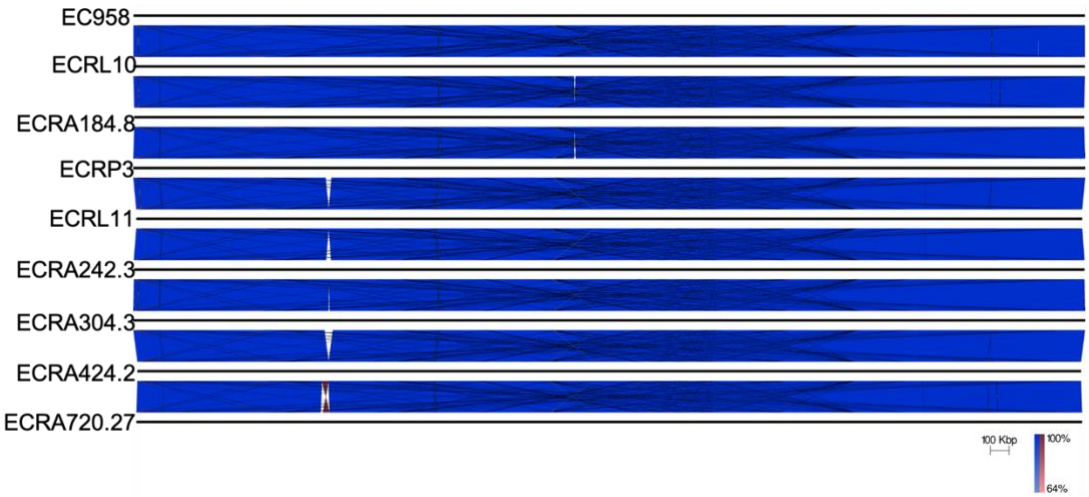

Figure 4.4 Genome sequence alignments show deletions, insertions and inversions. Permanently resistant variants with no SNPs/INDELs were long-read sequenced. Alignments of the genome sequences show differences in two parts of the chromosome

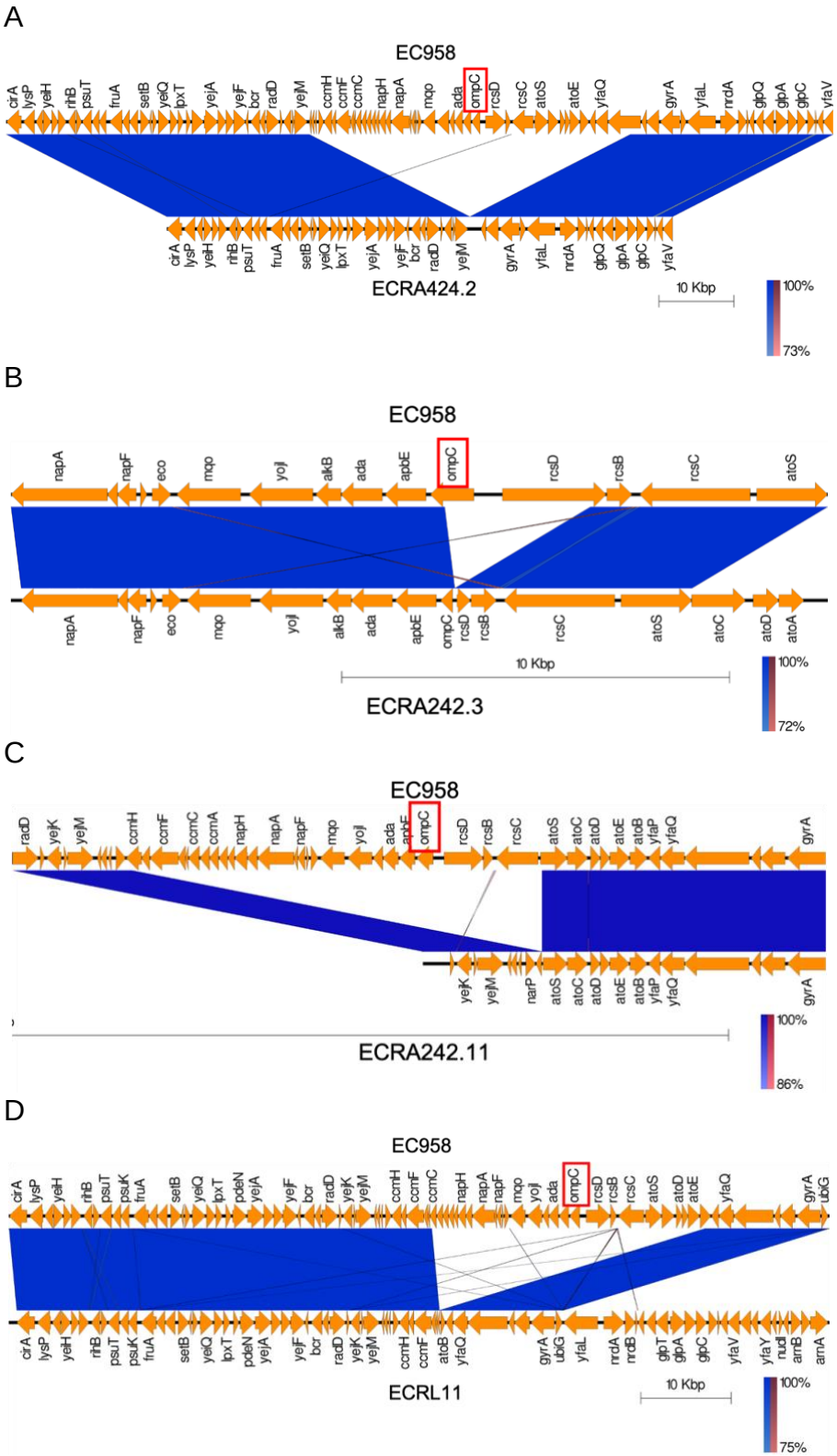

Figure 4.5 Zoomed-in sequence alignment of EC958 to fixed resistant variants. The fixed resistant variants that did not have a SNP/INDEL were long read-sequenced. Alignment of the genome sequences to WT-EC958 shows large deletions causing the loss of *ompC*.

A

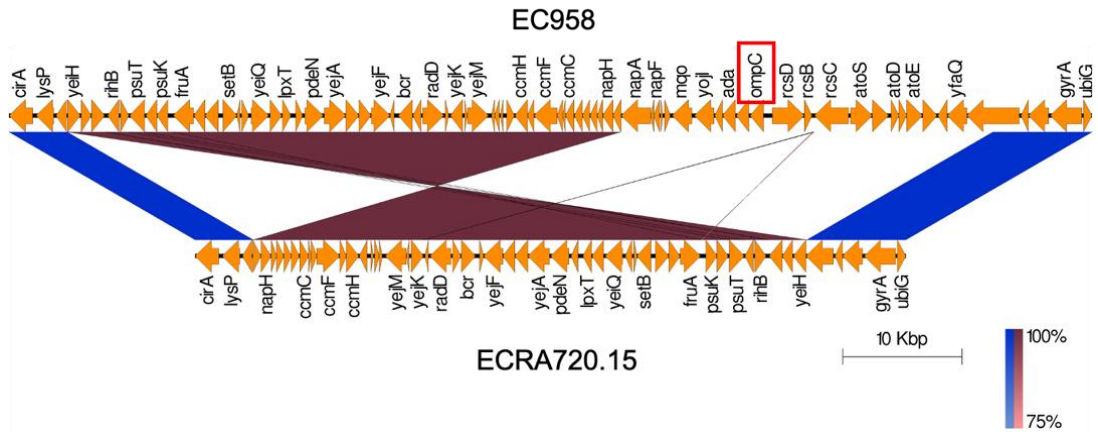

B

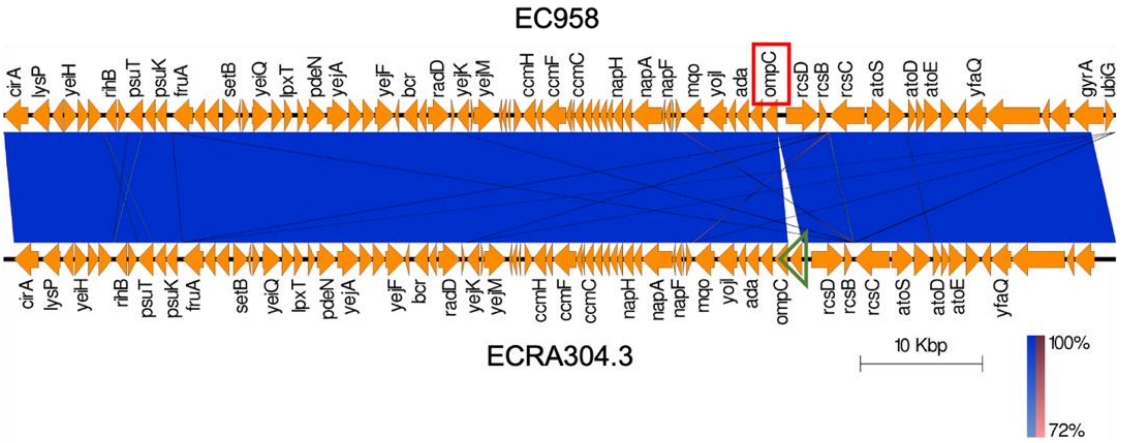

Figure 4.6 Zoomed-in sequence alignment of EC958 to fixed resistant variants. The fixed resistant variants that did not have a SNP/INDEL were long read-sequenced. Alignment of the genome sequences to WT-EC958 shows A) an inversion and a large deletion that include *ompC*, and B) an insertion sequence element disrupting *ompC*.

A

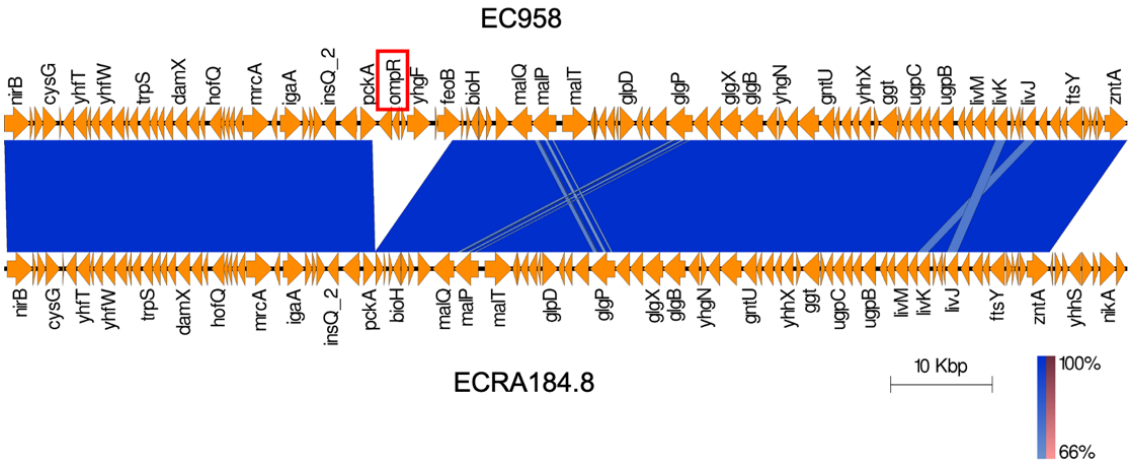

B

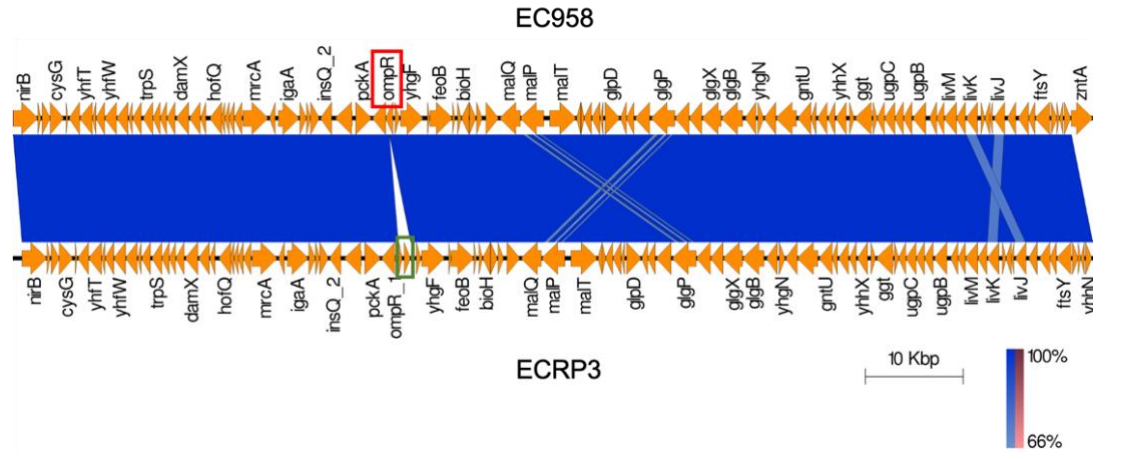

Figure 4.7 Zoomed-in sequence alignment of EC958 to fixed resistant variants. The fixed resistant variants that did not have a SNP/INDEL were long read-sequenced. Alignment of the genome sequences to WT-EC958 shows A) a large deletion that affect *ompR*, and B) an insertion sequence element disrupting *ompR*.

4.3.4 Outer membrane protein gels are not a reliable method to determine the absence and downregulation of the phage receptor

It is known that chromosomal rearrangements can trigger changes in gene expression that can allow bacteria to quickly adapt to hostile environments. A well-known example in *E. coli* is the expression of type 1 fimbriae mediated by an invertible element (Abraham et al., 1985). Since the PFGE results indicated that some of the permanently resistant variants could have genomic rearrangements, we hypothesised that these could be driving changes in gene expression, and that a transcriptomic analysis could reveal the differentially expressed genes.

At this stage of the project, time pressures dictated that both, the long-read sequencing and the differential expression analysis were done simultaneously. Considering that the phage receptor could be a gene being under-expressed by phase variation, the outer membrane proteins of these variants were extracted and run in an SDS-PAGE gel to determine whether these variants were expressing OmpC. The stained gels in Figure 4.8 show a band of ~36kDa corresponding to OmpC in all the samples except ECRL11. This gave us confidence to assume that an RNA-seq experiment would shed light onto the genes causing the resistance.

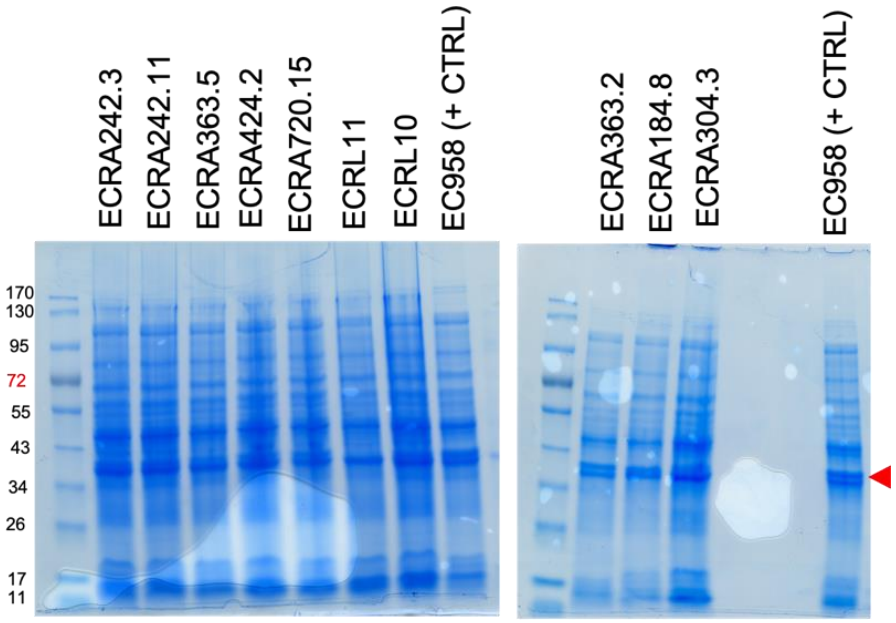

Figure 4.8 SDS-PAGE of the outer membrane proteins of the permanently-resistant variants. With the objective of confirming the expression of OmpC in the variants with fixed-resistance, the outer membrane proteins were extracted and ran in SDS-PAGE. All the variants except one (ECRL11) show a band of approximately the same size of that predicted for OmpC (~36kDa, red arrow).

4.3.5 Differential expression analysis of four variants with fixed resistance and putative chromosomal rearrangements

The RNA of WT EC958 and four of the permanently-resistant variants (ECRA242.3, ECRA304.3, ECRA424.2. and ECRA720.15) was extracted at mid-exponential phase in AU cultures. The RNA samples were sequenced and a differential expression analysis revealed that *ompC* was the most differentially expressed gene in the variants, compared to the WT EC958 (Table **4.4**, Table **4.5**, Table **4.6** and Table **4.7**).

Putting together the results from the differential expression and the long-read sequencing, it is now clear that the reason why *ompC* appears as the most differentially expressed gene is that it is either absent due to large deletions, or disrupted by an insertion element (Figure 4.4).

Table 4.4 Differential expression analysis of ECRA242.3 relative to EC958

	logFC	logCPM	PValue	FDR
porin OmpC	**-18.15**	**12.69**	**0**	**0**
response regulator transcription factor RcsB	-15.97	7.40	0	0
phosphotransferase RcsD	-15.86	7.28	0	0
periplasmic nitrate reductase subunit alpha	-15.62	7.04	0	0
serine protease inhibitor ecotin	-15.12	6.54	0	0
two-component system sensor histidine kinase RcsC	-14.86	6.28	0	0
MgtC/SapB family protein	-7.26	6.26	0	0
acid-activated periplasmic chaperone HdeA	-7.25	11.38	0	0
acid-resistance protein HdeD	-7.07	6.84	0	0
acid resistance gamma-aminobutyrate antiporter GadC	-6.14	9.26	0	0
two-component system sensor histidine kinase AtoS	-5.70	5.91	8.69e-318	3.06e-315
glutamate decarboxylase	-5.74	9.88	8.21e-310	2.66E-307
acid-activated periplasmic chaperone HdeB	-7.58	9.63	1.78E-290	5.31E-288
cytochrome c-type biogenesis heme lyase CcmF	-13.68	5.10	1.34E-256	3.73E-254
acetoacetate metabolism transcriptional regulator AtoC	-4.34	5.87	2.35E-238	6.09E-236
bifunctional DNA-binding transcriptional regulator/O6-methylguanine-DNA methyltransferase Ada	-12.97	4.39	8.79E-226	2.13E-223
microcin J25 efflux ABC transporter YojI	-12.81	4.22	5.76E-196	1.31E-193
cytochrome c biogenesis heme-transporting ATPase CcmA	-12.51	3.93	1.12E-184	2.41E-182
cytochrome c-type protein NapC	-12.80	4.21	3.46E-170	7.07E-168
malate dehydrogenase (quinone)	-11.97	3.38	2.34E-156	4.55E-154

Table 4.5 Differential expression analysis of ECRA304.3 relative to EC958

	logFC	logCPM	PValue	FDR
porin OmpC	**-9.82**	**12.71**	**0**	**0**
autotransporter adhesin Ag43	3.47	8.05	0	0
bifunctional anthranilate synthase glutamate amidotransferase component TrpG/anthranilate phosphoribosyltransferase TrpD	2.56	9.70	4.48E-161	5.79E-158
TIGR04211 family SH3 domain-containing protein	-1.88	7.16	1.30E-149	1.26E-146
RpoE-regulated lipoprotein	-2.21	6.80	2.10E-123	1.63E-120
ATP-independent periplasmic protein-refolding chaperone Spy	1.83	7.93	1.91E-118	1.24E-115
anthranilate synthase component I	2.49	9.53	1.78E-115	9.88E-113
bifunctional indole-3-glycerol-phosphate synthase TrpC/phosphoribosylanthranilate isomerase TrpF	2.03	9.35	4.77E-107	2.31E-104
glycine zipper 2TM domain-containing protein	2.42	4.68	5.10E-99	2.20E-96
DUF2502 domain-containing protein	1.67	5.72	8.98E-89	3.49E-86
cell-envelope stress modulator CpxP	1.39	7.67	5.25E-82	1.85E-79
osmotically-inducible lipoprotein OsmB	1.47	6.77	8.50E-74	2.75E-71
anti-sigma-E factor RseA	-1.45	8.59	4.50E-70	1.34E-67
RNA polymerase sigma factor RpoE	-1.41	8.32	2.84E-64	7.88E-62
general stress protein	2.18	8.58	1.70E-56	4.40E-54
RNA chaperone/antiterminator CspA	-1.52	10.28	5.85E-54	1.42E-51
kdo(2)-lipid IV(A) palmitoleoyltransferase	-1.25	6.40	5.97E-51	1.36E-48
YaiY family protein	1.29	5.48	3.42E-49	7.39E-47
DUF2776 family protein	1.58	4.89	1.26E-48	2.57E-46
outer membrane lipoprotein Slp	1.32	8.80	8.22E-47	1.60E-44

Table 4.6 Differential expression analysis of ECRA424.2 relative to EC958

	logFC	logCPM	PValue	FDR
porin OmpC	**-18.00**	**12.70**	**0**	**0**
response regulator transcription factor RcsB	-15.89	7.41	0	0
phosphotransferase RcsD	-15.78	7.29	0	0
periplasmic nitrate reductase subunit alpha	-15.54	7.06	0	0
serine protease inhibitor ecotin	-15.04	6.56	0	0
two-component system sensor histidine kinase RcsC	-14.78	6.30	0	0
two-component system sensor histidine kinase AtoS	-14.38	5.90	0	0
acetoacetate metabolism transcriptional regulator AtoC	-14.30	5.82	0	0
acid-resistance protein HdeD	-7.75	6.86	0	0
acid-activated periplasmic chaperone HdeB	-7.25	9.64	0	0
MgtC/SapB family protein	-7.23	6.28	0	0
acid-activated periplasmic chaperone HdeA	-7.02	11.40	0	0
cytochrome c-type biogenesis heme lyase CcmF	-13.60	5.12	2.63E-256	7.85E-254
cytochrome c-type biogenesis thiol:disulfide oxidoreductase CcmH	-13.36	4.88	2.86E-256	7.92E-254
nitrate/nitrite response regulator protein NarP	-13.00	4.52	2.59E-242	6.71E-240
bifunctional DNA-binding transcriptional regulator/O6-methylguanine-DNA methyltransferase Ada	-12.89	4.42	8.43E-226	2.04E-223
acid resistance gamma-aminobutyrate antiporter GadC	-5.83	9.28	1.81E-195	4.13E-193
microcin J25 efflux ABC transporter YojI	-12.73	4.25	1.22E-193	2.63E-191
glutamate decarboxylase	-5.57	9.90	8.09E-183	1.65E-180
cytochrome c biogenesis heme-transporting ATPase CcmA	-12.43	3.96	8.53E-182	1.66E-179

Table 4.7 Differential expression analysis of ECRA720.15 relative to EC958

	logFC	logCPM	PValue	FDR
porin OmpC	**-18.29**	**12.69**	**0**	**0**
phosphotransferase RcsD	-15.94	7.27	0	0
serine protease inhibitor ecotin	-15.20	6.54	0	0
two-component system sensor histidine kinase RcsC	-14.94	6.27	0	0
two-component system sensor histidine kinase AtoS	-14.54	5.87	0	0
acetoacetate metabolism transcriptional regulator AtoC	-14.46	5.79	0	0
response regulator transcription factor RcsB	-13.83	7.39	0	0
periplasmic nitrate reductase subunit alpha	-13.48	7.04	0	0
acid-activated periplasmic chaperone HdeB	-7.43	9.63	0	0
acid-resistance protein HdeD	-7.32	6.83	0	0
MgtC/SapB family protein	-7.10	6.25	0	0
acid-activated periplasmic chaperone HdeA	-7.06	11.38	0	0
bifunctional DNA-binding transcriptional regulator/O6-methylguanine-DNA methyltransferase Ada	-13.05	4.36	2.96E-252	8.84E-250
glutamate decarboxylase	-5.37	9.88	1.78E-248	4.95E-246
acid resistance gamma-aminobutyrate antiporter GadC	-5.58	9.27	2.30E-230	5.96E-228
microcin J25 efflux ABC transporter YojI	-12.89	4.20	5.65E-213	1.37E-210
malate dehydrogenase (quinone)	-12.05	3.35	1.29E-170	2.95E-168
autotransporter adhesin Ag43	3.54	8.10	2.57E-163	5.53E-161
ferredoxin-type protein NapF	-10.74	4.27	2.94E-158	6.02E-156
FAD:protein FMN transferase ApbE	-11.85	3.15	1.25E-153	2.42E-151

4.3.6 Western blots confirm the absence or under-expression of OmpC in the permanently-resistant variants with no SNP detected

Even though the long-read sequencing and the RNA-seq results were in accordance with each other, the outer membrane protein gels were inconclusive, as there was a band present on the size anticipated for OmpC (Figure 4.8). To check whether these bands were OmpC or a different protein of similar molecular weight, Sean McAteer –the core scientist in our group— carried out Western Blots with an OmpC antibody. These results showed that the samples have a low expression of the OmpC, compared to WT EC958 (Figure 4.9). A RecA antibody was used in a parallel assay as a control to ensure that any differences were not due to loading variations.

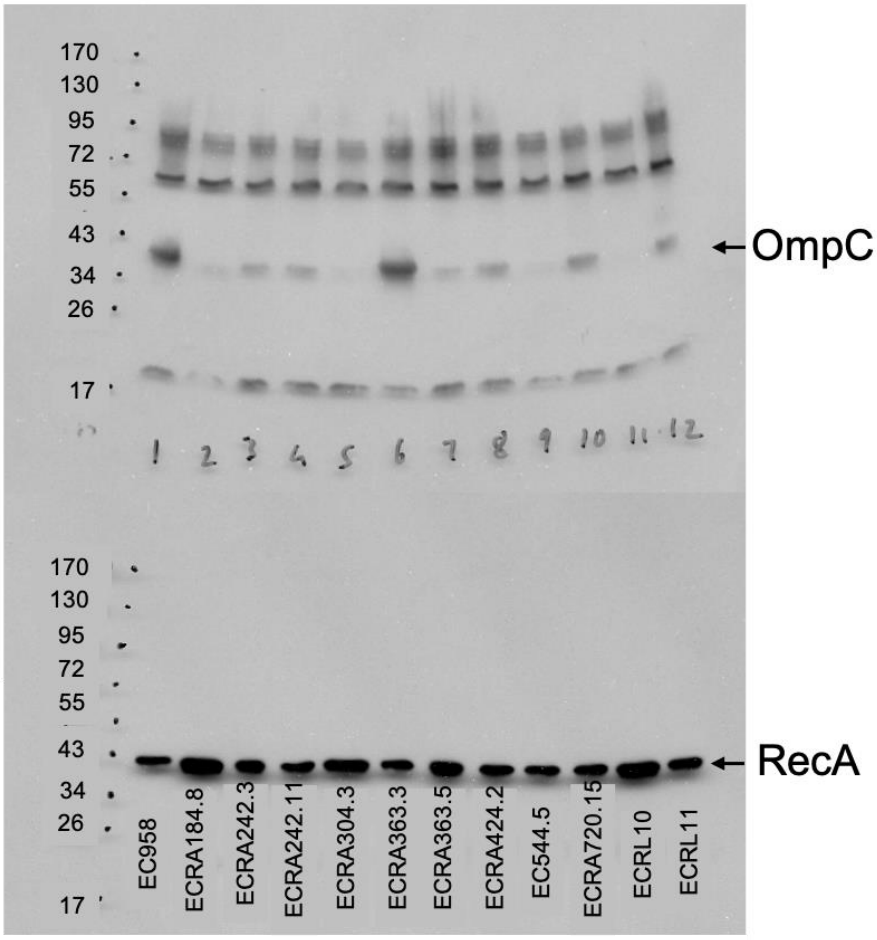

Figure 4.9 Western blot analysis of OmpC (upper panel) in EC958 (lane 1, control) and 11 of the permanently resistant variants with putative genomic rearrangements (lanes 2 to 12). Lower signal of OmpC can be observed in all the resistant variants, except one (ECRA363.5). Lower panel shows a loading control Western blot using a RecA antibody. ***Work carried out by Core Scientist: Sean McAteer.***

4.3.7 OmpC acts as the receptor for phage LUC4

The analysis of the fixed resistant variants provided good evidence to propose that the outer membrane protein OmpC is the main receptor for phage LUC4, with mutations in *ompC* leading to complete phage resistance. To prove this, the *ompC* gene from EC958 was cloned into the vector pWKS30. The commercially available *E. coli* strain ClearColi™ (Mamat et al., 2015), which naturally lacks the protein, and is therefore resistant to LUC4, was transformed with the construct and induced to express EC958's OmpC; it was then challenged with phage LUC4. Results in solid and liquid media show that the transformed and induced ClearColi became sensitive to phage LUC4 (Figure 4.10). These results confirm that the receptor that phage LUC4 uses to adsorb on its host is the outer membrane porin OmpC.

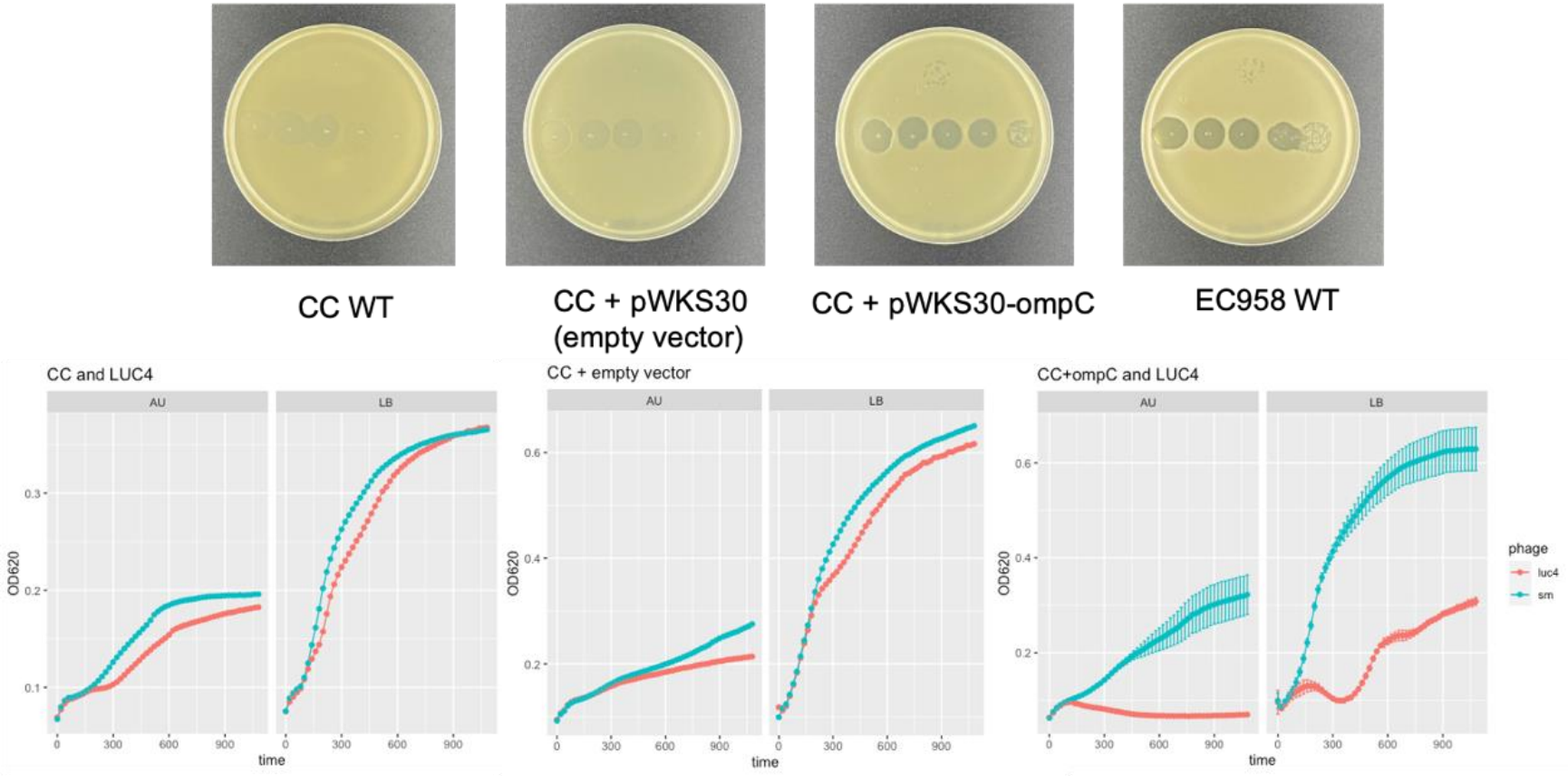

Figure 4.10 OmpC acts as the phage receptor for LUC4. EC958's ompC was cloned into vector pWKS30. *E. coli* strain ClearColi (CC) which does not express OmpC was transformed with the construct, induced and challenged with phage LUC4. ClearColi™+*ompC* becomes susceptible to phage LUC4 in solid and liquid assays.

4.3.8 The loss of function of OmpC has a fitness cost and is outcompeted by the reversibly resistant population

The fixed resistant variants of EC958 are present in a higher proportion than the transiently resistant variants during the early timepoints in the LUC4 infection assays, but as time progresses, the transiently resistant variants become the dominating population to the extent that by the end of the 18-hour culture it is difficult to isolate any permanently resistant variants (Figure 4.1). This suggests that the fixed resistant variants could have compromised fitness due to the loss of function of OmpC compared to WT EC958 and the reversibly resistant variants.

ECRA304.8 and ECRA544.4 are two variants with a fixed LUC4-resistance caused by a SNP in *ompC* that results in an early stop codon (Appendix 6). Their fitness was measured in relation to the WT EC958. For this, spontaneous Rifampicin-resistant mutants of ECRA304.8 and ECRA544.4 were isolated, and cultured in LB with EC958. LB and LB + Rifampicin plates were used to calculate the difference in growth after 24 hours. A reduced fitness is noticeable for both resistant variants (Figure 4.11A and C). There was a small concern over whether the rifampicin resistance was responsible for the reduced fitness. To prove this was not the case, the rifampicin-resistant and the parent (rifampicin-susceptible) OmpC-variant were used in a competition assay in the same way as described before. The acquisition of resistance to rifampicin involves a small loss of fitness (Figure 4.11B and D), which is not enough to attribute to the full fitness loss. Therefore, it can be concluded that the loss of OmpC comes with a fitness cost that puts the fixed-resistant population in disadvantage, allowing the reversibly resistant population to outcompete it.

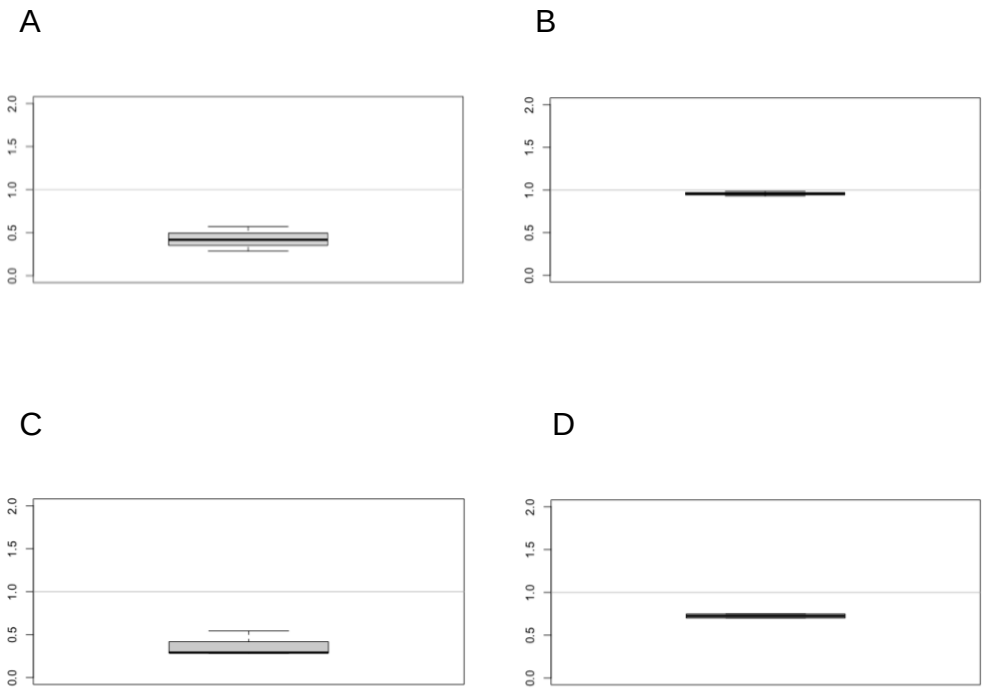

Figure 4.11 Competitive fitness of* OmpC*-variants ECRA304.8 and ECRA544.4 relative to WT EC958. To confirm the hypothesis that the fixed resistance had a fitness cost that was outcompeted by the transiently-resistant variants, competition assays were carried out**.** A) Fitness of ECRA304.8 relative to WT EC958 cultured in LB for 24 hours. B) Fitness of ECRA304.8 relative to WT EC958 cultured in LB for 24 hours. Fitness values above 1.0 indicate greater fitness than the WT EC958; values below 1.0 indicate that the variants are less fit than EC958.

4.4 Discussion

From the results shown in Chapter 4, it was concluded that *E. coli* strain EC958 –a representative member of the ST131 group—is difficult to target and neutralise with phages, especially in urine. In this chapter, this resistance was explored to deeper extent using one lytic phage from our collection: LUC4.

There is an increasing number of reports describing phage-resistance mechanisms, but many of them use standard laboratory media and end-point assays. This commonly selects for resistance mechanisms that lead to a fully resistant population, whereas those that do not prevent bacterial death can be easily overlooked (Hyman and Abedon, 2010). Here, by breaking down the 12-hour interaction assays into different timepoints and exploring the composition of the phage-resistant population we could deduce that at least two mechanisms were involved. The first one, described in this chapter, implicates mutations, loss or under-expression of the phage receptor protein –OmpC— causing a complete and permanent resistant phenotype.

SNPs and small INDELs leading to frameshifts or stop-codons, and subsequent inactivation of OmpC gave an explanation to 40% of the permanently resistant variants. This type of resistance mechanism is well known in *E. coli* and other species and it is commonly described in the literature (Hampton *et al.*, 2020; Labrie *et al.*, 2010; Rostol and Marraffini, 2019). Short read sequencing provides enough depth to identify these small mutations with confidence. However, it is usually not possible to detect genome rearrangements or mobile genetic elements, and therefore a different platform is required in which long reads are generated (Bayliss et al., 2017; Karlsson et al., 2015). Here, 50% of the permanently-resistant variants did not output any SNP or INDEL in the phage receptor using short read sequencing, for which Oxford Nanopore Sequencing Technologies was used to identify these genomic changes.

Genome instability is a strategy that can allow bacteria to adapt quickly to changing environments. A classic example is the expression of type 1 fimbriae, which can be turned on and off with an invertible element (Abraham *et al.*, 1985). Similarly, reversible chromosomal rearrangements have been linked to phase-variable phenotypes that confer resistance to phage infection (Scott *et al.*, 2007). With this mechanism in mind, it was thought that a simple explanation could be that the rearrangements could lead to under-expression of OmpC. SDS-PAGE gels of the outer membrane proteins of the variants showed a band with a similar size to OmpC (Figure 4.8), but results from long-read sequencing and RNA-seq analysis contradicted this, as both indicated the loss and/or under-expressions of OmpC. A Western blot assay using an OmpC antibody was used to confirm the absence or under-expression of the protein (Figure 4.9). This showed that outer membrane protein preparations separated by SDS-PAGE and stained with Coomassie dye are not a reliable method to detect the differences in protein production and expression. As these are not specific, it is likely that another membrane protein of similar size could be causing the ~36 kDa band to appear in the gel.

It is relevant to mention that some of the variants reverted to the susceptible phenotype at some point after several assays in which they were classified as resistant. These variants were dropped out of the subsequent long-read sequencing and RNA-seq due to the limitations in the number of samples that could be processed: only the samples that were confidently categorised as permanently resistant were selected. Nonetheless, it is hypothesised that the rearrangements are unstable and these variants had conformations that reverted to the original phenotype as it implies better fitness in the absence of phage.

Both, the RNA-seq and the long-read sequencing results indicate that most of the samples that were chosen on this basis have their resistance attributable to the loss of *ompC* or its regulatory genes: *envZ* and *ompR*. The exception being one sample in which no difference has been found, and two samples that could not be analysed because assembly of the genome was not possible.

Although the latter could be due to poor quality reads, we are inclined to believe it has a biological explanation. Based on the observations that some of the fixed resistant variants eventually reverted to the original phenotype, it is hypothesised that these samples could have been going through that process, for which different subpopulations were being co-sequenced. Forde *et al.* (2014) encountered a similar event when sequencing EC958 with PacBio RSI platform. They report a discrepancy in the Phi1 prophage region which showed an inverted orientation in approximately 50% of the reads. They conclude that high frequency allele switching had occurred during the propagation of EC958, causing the variability in alleles. The two samples that were found difficult to assemble are planned to be re-sequenced and if the difficulties of assembly persist, a bioinformatics consultation may allow us to discern the reads from the different subpopulations.

The outer membrane protein OmpC has an important role in bacterial osmoregulation. With OmpF, OmpC controls the permeability of solutes such as nutrients and antibiotics across the outer membrane. Their expression is regulated by the EnvZ-OmpR two-component regulatory system at the transcriptional level, depending on external factors such as pH, nutrient availability, temperature etc. (Le Dain et al., 1996; Liu and Ferenci, 2001; Pratt et al., 1996).

Although important, we speculate that the permanent resistance is of minor concern for applied phage therapy. First, the competition assays indicate that the loss of function of OmpC signifies a trade-off in fitness compared to the WT (Figure 4.11). A reduced fitness in phage-resistant mutants has been reported before (Capparelli *et al.*, 2010b; Duerkop *et al.*, 2016; Salazar *et al.*, 2021; Zulk *et al.*, 2022). Additionally, it has been shown that the loss of *ompC* and *ompF* brought significant reduction of virulence in an avian pathogenic *E. coli* (Hejair et al., 2017). In the patient, a loss of fitness as such may allow the immune response to clear the resistant population. Alternatively, other strategies can be implemented to prevent to a certain extent the rise of these mutants; for instance, the use of cocktails or a phage-antibiotic combined

therapy. However, mutations in *ompC* have also been linked to antibiotic resistance (Liu et al., 2012; Sanchez-Romero and Casadesus, 2014; Trampari et al., 2022), which is important to consider when selecting the antibiotic to complement PT in combined therapy.

The transiently resistant population is dominant in the late timepoints of the phage infection. It is less straightforward to address and we speculate, more difficult to prevent. For this reason, the study of this transient resistance became the main focus of the study, and the findings are described in the next chapter.

Chapter 5 *E. coli* strain EC958 can resist the infection of phage LUC4: transient resistance

5.1 Introduction

Results of the previous chapters have shown that *Escherichia coli* strain EC958, in addition to being multidrug-resistant, is also difficult to suppress for long periods with phages or phage-combinations at different MOIs. Understanding how EC958 has the capacity to persist and thrive in the presence of this phage became the main focus of my PhD studies. Although research of phage-resistance mechanisms has dramatically increased in the last few years, to the best of our knowledge, EC958 received little attention with respect to phage resistance, despite repeatedly being used as a model strain to study the ST131 group and other aspects of pathogenesis.

The evidence that fundamental knowledge about gene function may allow the prediction about the phenotype of a bacterium and growing reports on anti-phage systems has enabled the production of bioinformatics tools to identify characterised anti-phage systems. Tools like PADLOC (Payne et al., 2022) and DefenseFinder (Tesson et al., 2022) can aid in the search for genes that are important for phage-resistance. However, as mentioned in the last chapter, the anti-phage system of EC958 being investigated in this work is not straightforward, as it was observed when cultured in urine but not in LB. Most of the defence systems that have been published have been studied and tested in standard laboratory media, such as LB. The fact that this resistance is highly dependable on the growth conditions makes it unlikely that the currently known systems are underpinning it.

Phenotypic differences have been noted in bacteria cultured in urine compared to LB. For example, a number of virulence genes are upregulated when UPEC is cultured in urine and when it is infecting the urinary tract of mice, but not when it is grown in LB (Snyder et al., 2004). Nutrient availability also influences the metabolic pathways used by bacteria (Mann *et al.*, 2017). These factors will likely affect the dynamics of phage infection and host response, enabling different resistance strategies in the different media.

The transient resistance mechanism of EC958 in urine is the main focus of study in this chapter. The exploration began with a bioinformatics search for the known anti-phage systems that are encoded in EC958's genome, and a global analysis of the transcriptional profile of phage-infected and uninfected bacteria. The most differentially expressed genes were studied in more detail with genetic manipulation of EC958, which was challenging due to the multidrug-resistance of the strain. In addition, EC958 was cultured in the supernatant of an infected culture to test whether a signalling molecule could be triggering the resistance.

5.2 Material and methods

5.2.1 Identification and mapping of the anti-phage defence systems in *E. coli* strain EC958

The reference genome of *E. coli* O25:H4-ST131 strain EC958 was retrieved from the NCBI Genbank (Accession numbers: NZ_HG941718.1) (Forde *et al.*, 2014). It was analysed to detect the presence of anti-phage systems using the online tool PADLOC (Payne *et al.*, 2022). The output and the reference sequence files were used to visualise the location of the systems within the chromosome and plasmid using the software Geneious Prime (v2023.0).

5.2.2 Transcriptomic studies

An RNA-seq experiments was carried out to study the difference in gene expression between uninfected and infected EC958. Infection assays in flask format were set up as described above (**Error! Reference source not found.**). Cells in mid-exponential phase (OD_{600}~0.2) were harvested and the RNA was extracted as described above (4.2.4). The RNA samples were sent to Vertis Biotechnologie AG (Friesing, Germany) where they were processed for rRNA depletion, preparation of strand specific cDNA, adapter ligation and Illumina NextSeq 500 sequencing. The results were analysed as described above (4.2.4).

5.2.3 Validation of RNA-seq results with RT-qPCR

The differential expression of three genes –EC958_RS11570, EC958_RS11580 and EC958_RS11585 (predicted to encode for a pigL-family deacetylase, an acetyltransferase and a YaiO-family outer membrane beta-barrel protein, respectively)—between uninfected and phage-infected samples was verified with RT-qPCR. The infection assays, the RNA extraction and purification were repeated as described above (4.2.4). The samples were DNAse-treated with the TURBO DNA-free Kit (Invitrogen) following the manufacturer's instructions. The cDNA of the samples was synthetised with the iScriptTM cDNA Synthesis Kit (Bio-Rad) following the protocol attached in the product. The cDNA was then diluted with 150 µL of nuclease free H_2O. 8 µL of each sample was mixed with 10 µL of iTaq Universal SYBR Green Supermix (BioRad), 0.6 µL of 10 µM primers (Appendix 5) and 1.4 µL of nuclease free H2O. A no-template control reaction was included in each run.

The Bio-Rad CFX96 Real-Time System Thermal cycler was programmed for an initial denaturation step at 95°C for 5 minutes, followed by 40 cycles of 95°C for 10 seconds and 60°C for 1 minute, and a fluorescent reading at the end of each cycle. The results were retrieved with the CFX Manager 3.1 Software. The mean fold change expression of the infected samples in relation to the uninfected samples was calculated with the ΔΔCt method, using gene *hcaT* as the housekeeping gene. The results were plotted with the package ggplot2 in RStudio.

5.2.4 Outer membrane protein gels

Infection assays of EC958 were carried out as described above (**Error! Reference source not found.**) to an OD_{600}~0.2. For the fixed resistant

variants, these were cultured in AU without the phage to an OD_{600}~0.2. Outer membrane proteins were extracted and stained as described above (4.2.9)

5.2.5 Over-expression of the YOMP operon with putative phage-resistance function

The genomic DNA of EC958 was extracted with the QIAGEN DNeasy Blood & Tissue Kit following the manufacturer's protocol. It was then used as the template in a PCR to amplify the 4775 bp operon that we hypothesised had a protective function against phage infection. The primers used in this PCR (oprnFSmaI and oprnRSalI) containing the target sequence for restriction enzymes SmaI and SalI are listed in Appendix 5.

A 50 µL reaction was made using the Q5 High-Fidelity DNA Polymerase (New England Biolabs), following the manufacturer's recommendations. The PCR was run in a Thermo Hybaid PCR Express Thermal cycler with an initial denaturation step at 98°C for 4 minutes, 35 cycles of 98°C for 15 s, 63°C for 30 s and 72°C for 3 min; and a final elongation step at 72°C for 6 minutes.

The PCR product was run in a 1.2% agarose gel –stained with Gel Red (BIOTIUM)—at 100 V for 60 minutes. The band corresponding to ~5 Kbp was excised and the DNA was cleaned up with the Omega Micro Elute Gel Extraction Kit. The clean PCR product and the vector pBAD33 were digested with the FastDigest Enzymes SmaI and SalI (Thermo Scientific). 30 µL reactions were set as shown in Table 5.1 and Table 5.2; they were incubated at 37°C for 1 hour.

Table 5.1 Digestion reaction of PCR product	
5 µL	PCR product
3 µL	10X Fast digest buffer
1 µL	Fast digest enzyme SmaI
1 µL	Fast digest enzyme SalI
20 µL	Nuclease-free H_20

Table 5.2 Digestion reaction of pBAD33	
2 µL	pBAD33
3 µL	10X Fast digest buffer
1 µL	Fast digest enzyme SmaI
1 µL	Fast digest enzyme SalI
23 µL	Nuclease-free H_20

The reactions were run in a 1% agarose gel for 75 minutes at 100 V. The bands of the corresponding size were excised and the DNA was cleaned up with Omega Micro Elute Gel Extraction Kit.

The ligation reaction was set up as shown in Table 5.3 and incubated at room temperature for 1 hour. A control ligation reaction with no insert (vector only) was set up by substituting the volume of insert for nuclease-free H_2O.

Table 5.3 Ligation reaction of pBAD33	
9 µL	Digested insert
5 µL	Digested pWKS30
2 µL	10X FastDigest Buffer (Thermo Scientific)
1 µL	T4 DNA Ligase (Thermo Scientific)
3 µL	Nuclease-free H_20

Chemically competent DH5-alpha cells (NEB 5-alpha Competent *E. coli*, New England Biolabs) were transformed with the construct and the vector following the manufacturer's protocol. The transformed cells were plated on LB with 50 µg/mL ampicillin, and incubated overnight at 37°C.

5.2.5.1 Colony PCR for the validation of constructs and mutants

The colonies that grew on the selective agar plates were picked with a sterile pipet-tip or pick, patch-plated on LB-amp agar and then inoculated into a master mix for colony PCR (Table **5.4**) to verify the presence of the construct or the genetic modification. The thermal cycler was programmed with the following conditions: 94°C for 10 minutes, 30 cycles of (94°C for 30 s, 65°C for 30 s, 68°C for 5 min), and 68°C for 5 minutes.

Table 5.4 Colony PCR on transformed cells	
12.5 µL	One-Taq Quick-Load (New England Biolabs)
0.5 µL	10 µM F primer
0.5 µL	10 µM R primer
11.5 µL	Nuclease-free H_20

The PCR products were run in a 1% agarose gel stained with Gel Red (BIOTIUM) at 100 V for 60 minutes. The gel was documented in a LI-COR Odyssey Fc Imaging System. The colonies that showed a band of the expected size were cultured overnight at 37°C in LB-amp. The next day, freezer stocks were made by transferring 700 µL of the overnight cultures into cryotubes containing 700 µL of 50% glycerol.

The plasmid of was extracted with the E.Z.N.A. Plasmid DNA Mini Kit (Omega).

5.2.5.2 Preparation of electrocompetent *E. coli* EC958 cells

Electrocompetent cells were prepared by inoculating 250 µL of an overnight culture in 25 mL of LB and incubating them at 37°C with shaking to an OD_{600}=0.6. Cells were subsequently pelleted by spinning at 5000 RPM (4,863 RFC) for 10 min at 4°C. They were resuspended in an equivalent volume of sterile, ice-cold 10% autoclaved glycerol (Sigma Aldrich). Cells were washed four more times by spinning them down to pellet them, the volume of ice-cold 10% autoclaved glycerol in which the cells were resuspended was halved in each step. In the final wash step, the cells were resuspended in 800 µL of 10% glycerol.

5.2.5.3 Electro-transformation of competent EC958

Aliquots of 50 µL of competent cells were added with 5 µL of the construct or the empty vector and mixed by flicking. The total volume was transferred to an ice-cold 1 mm electroporating cuvette (FLOWGEN). The dry cuvettes were pulsed in a Bio-Rad *E. coli* Pulser at 1.8 kV. 1 mL of LB was added to the cuvette immediately after the shock. The cells were allowed to recover for 90

minutes at 37°C with shaking. 100 µL was spread on LB-chloramphenicol (cm) agar plates at a concentration of 50 µg/mL and incubated overnight at 37°C.

On the following day, colonies were patch-plated on LB-cm agar and cultured in 5 mL AU-cm (25 µg/mL) at 37°C overnight. The overnight cultures were sub-cultured in AU-cm and incubated for 60 minutes at 37°C, after which L-arabinose was added to final concentration of 1 µM to induce the expression of the operon. After 60 minutes of incubation, the cultures were challenged to LUC4 infections in microtiter plate format (2.2.7). WT EC958 and empty-pBAD33 transformed EC958 were included in the assay as controls.

5.2.6 Construction of knockout mutants

To knockout the genes of interest in EC958, the Lambda red protocol (Datsenko and Wanner, 2000) was used with some modifications. Due to the multidrug-resistance of EC958, using the original Lambda red protocol would make it difficult to select mutants. The group's core scientist –Sean McAteer— modified plasmid pKD46 by inserting a Tellurite resistance gene.

Competent EC958 cells were prepared (5.2.5.2) and transformed (5.2.5.3) with the modified pKD46+TelR as described above. After allowing the transformed cells to recover for ~120 minutes in LB at 30°C, 100 and 200 µL was spread on LB-tellurite agar plates (25 µg/mL) and incubated overnight at 30°C.

A single colony of the transformed EC958 was grown overnight at 30°C with shaking in LB-tellurite (25 µg/mL). On the next morning, 250 µL of the overnight was sub-cultured in 25 mL of LB-tellurite and incubated for 120 minutes at 30°C, after which the culture was induced by adding L-arabinose to a final concentration of 1 µM. The cultures were incubated for further 60 minutes, and made competent as described above (4.2.6.1).

The chloramphenicol resistance cassette of pKD3 was amplified by PCR using primers with the 45-bp regions of the genes to knockout (Appendix 5). 50 µL reactions were prepared using the Q5 High-Fidelity DNA Polymerase (New England Biolabs), following the manufacturer's recommendations. The PCR was run in a Thermo Hybaid PCR Express Thermal cycler with an initial denaturation step at 95°C for 7 minutes, 35 cycles of 94°C for 15 s, 50°C for 30 s and 72°C for 1.5 min. The products were run in a 1% agarose gel with Gel Red (BIOTIUM) at 100 V for 60 minutes. The amplicon bands of the expected size were excised and cleaned-up with the Omega Micro Elute Gel Extraction Kit.

50 µL aliquots of electro-competent and arabinose-induced EC958 + pKD46-TelR were mixed with ~500 ng of clean PCR product, mixed gently and transformed as described above (4.2.6.2). The transformed cells were added with 1 mL of LB and incubated at 37°C for ~120 minutes. 100 and 200 µL were spread on LB-cm (25 µg/mL) agar plates and incubated overnight at 37°C. Colony PCR was carried out to verify that the chloramphenicol cassette had been inserted in the correct site as described above (5.2.5.1).

5.2.7 Infection assays of the knock-out mutants

The verified knockout-mutants were challenged with phage LUC4 in 100 mL AU assays as described above (2.3.4). The phenotype of the resistant population was verified by isolating, purifying and culturing single colonies and challenging them with the phage in microtiter plates (2.2.7).

5.2.8 Supernatant assays

5.2.8.1 Harvesting the supernatant from EC958 cultures

EC958 was cultured in 100 mL liquid media (AU, PU or LB) with and without phage LUC4 (MOI~10). The flasks were incubated until the cultures had reached an OD_{600} between 0.2 and 0.4, after which, the culture was transferred to 50 mL Falcon tubes and centrifuged at 5000 RPM (4863 RFC) for 10 minutes to pellet the cells. The supernatant was first filtered with a 0.22 µm Milipore filter and then transferred to a Vivaspin Centrifugal concentrator membrane of 3,000 MWCO (SARTORIUS). They were centrifuged at 5000 RPM (4863 RFC) for ~60 minutes or until most of the supernatant had passed. The filtrate derived from infected cultures was tested on soft overlay agar with EC958 to verify the absence of phage LUC4. The supernatant was combined in different proportions with fresh media and used in infection assays in microtiter plate format (2.2.7).

5.2.8.2 Adsorption assays with supernatant

The rate of phage adsorption in AU and supernatant was carried out by MSc. Student, Zhuneng Zhou. Briefly, 1 mL of EC958 overnight culture was sub-cultured in 100 mL of fresh AU and incubated at 37°C for 90 minutes. The culture was then divided in two and transferred to 50 mL Falcon tubes, centrifuged at 5000 RPM (4863 RFC) for 10 minutes. The supernatant was discarded and the pelleted cells were resuspended in prewarmed supernatant and in fresh AU for the control. Phage LUC4 was added at an MOI of 0.001. 1 mL samples were taken from each flask every 5 minutes for 35 minutes. The samples were centrifuged at 12,500 RPM (14,848 RFC) for three minutes. The supernatant with the free/unadsorbed phage was serially diluted and spotted

on LB agar with soft overlay agar containing EC958 (2.2.2). The plaques were counted and the percentage of unadsorbed phage was calculated with the following formula:

$$\text{Free phage pecentage} = \frac{\text{Phage titre in Samples}}{\text{Phage titre at t=0}} \times 100\%$$

5.3 Results

5.3.1 The EC958 chromosome encodes for 8 anti-phage systems

Escherichia coli O25b:H4-ST131 strain EC958 is a multidrug-resistant bacterium that has been used as a model strain to study the *E. coli* ST131 group, but there is still a knowledge gap in the way EC958 interacts with phage. The reference genome of *Escherichia coli* O25b:H4-ST131 strain EC958 was retrieved from the NCBI GenBank and analysed with PADLOC (Payne *et al.*, 2022): an online tool to search for phage-defence systems within bacterial genomes. The output showed defence systems in 8 different loci (Appendix 7): Type I restriction-modification (RM) system, Type II RM system, retron, AbiE abortive infection system and BREX. Figure 5.1 shows the different systems distributed in different parts of the chromosome, and not clustered into a defence island as seen in other bacteria (Doron *et al.*, 2018; Makarova *et al.*, 2011).

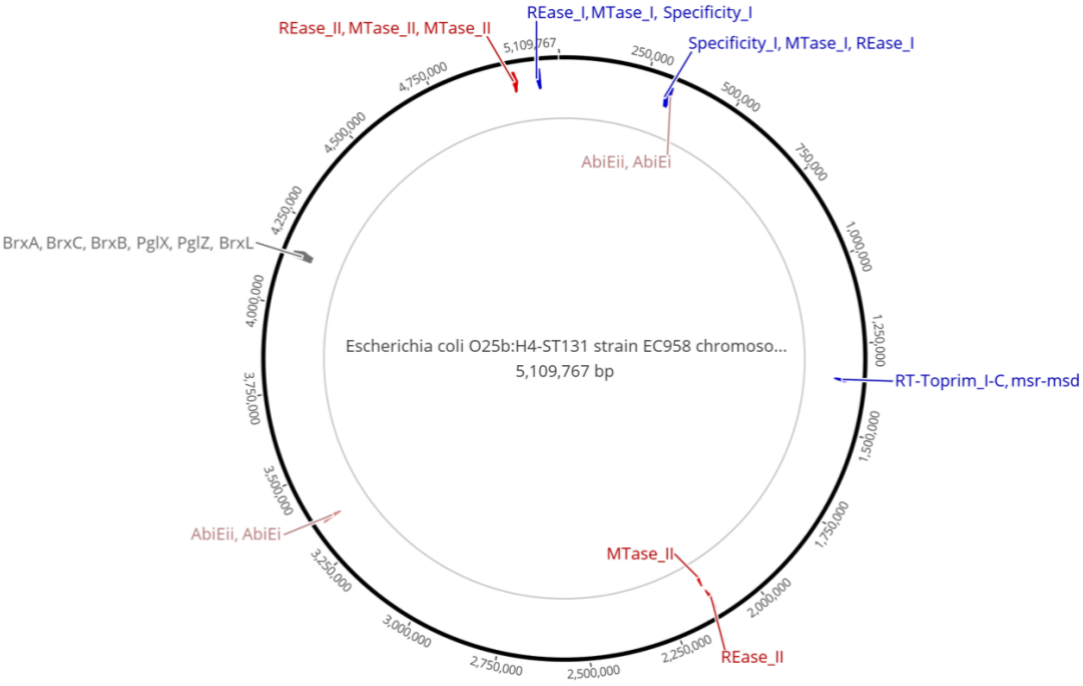

Figure 5.1 **The known antiphage defence systems of *Escherichia coli* O25:H4-ST131 strain EC958.** The reference genome of EC958 was analysed with PADLOC to search for the encoded defence systems. 8 known anti-phage systems were found and mapped on the chromosome of EC958.

5.3.2 Comparative transcriptomic analysis on LUC4-infected and uninfected EC958

To better understand what causes the reversible resistance of EC958, a transcriptomic analysis using RNA-seq was carried out to compare the gene expression profile between the uninfected and the phage-infected EC958 in mid-exponential phase.

788 genes were differentially expressed with statistical significance (FDR<0.05) (Figure 5.3). Three of the top 3 upregulated genes in the infected samples are clustered into an operon of yet unknown function (Figure 5.3). This operon contains genes predicted to have the function of a PIG-L family deacetylase, an acetyltransferase, and a YaiO family outer membrane beta-barrel protein; for which this operon will hereon be referred as the YOMP (YaiO family outer membrane beta-barrel protein) operon. The differential expression of these genes in the uninfected and infected samples was verified with qPCR (Figure 5.4A).

Given that a putative outer membrane beta-barrel protein is being expressed in the infected samples, the outer membrane proteins were extracted separated by SDS-PAGE and stained with Coomasie blue dye. However, the results did not show a difference in outer membrane protein pattern between the uninfected and the infected samples (Figure 5.4B).

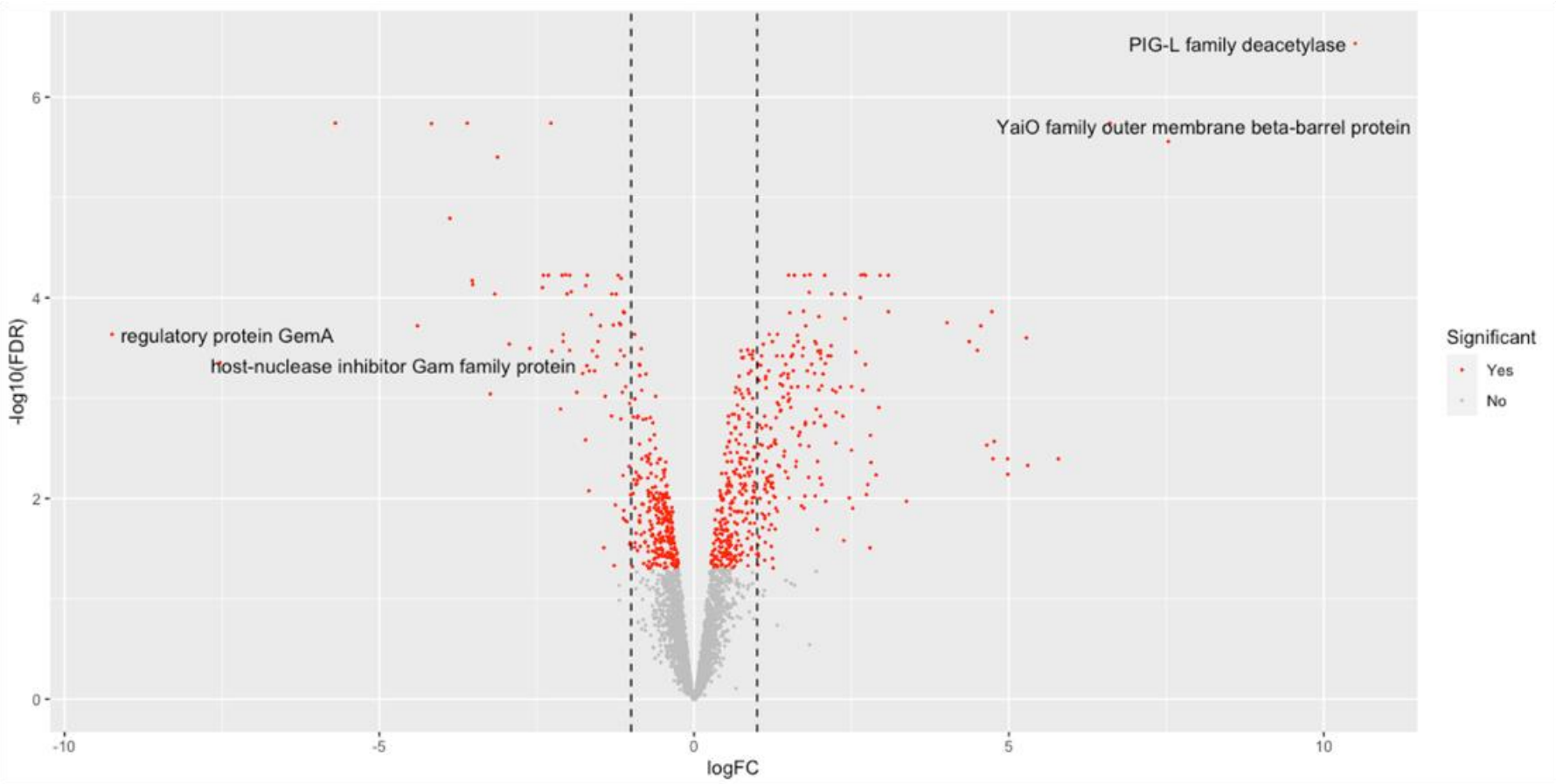

Figure 5.2 Transcriptomic analysis of uninfected and phage-infected cells at similar OD. To gain insight into the resistance mechanism of EC958, an RNA-seq experiment was carried out to compare the transcription profile of uninfected and LUC4-infected cultures. A volcano plot to represent the results of the differential expression analysis shows 788 genes expressed differently with statistical significance (FDR<0.05, red dots).

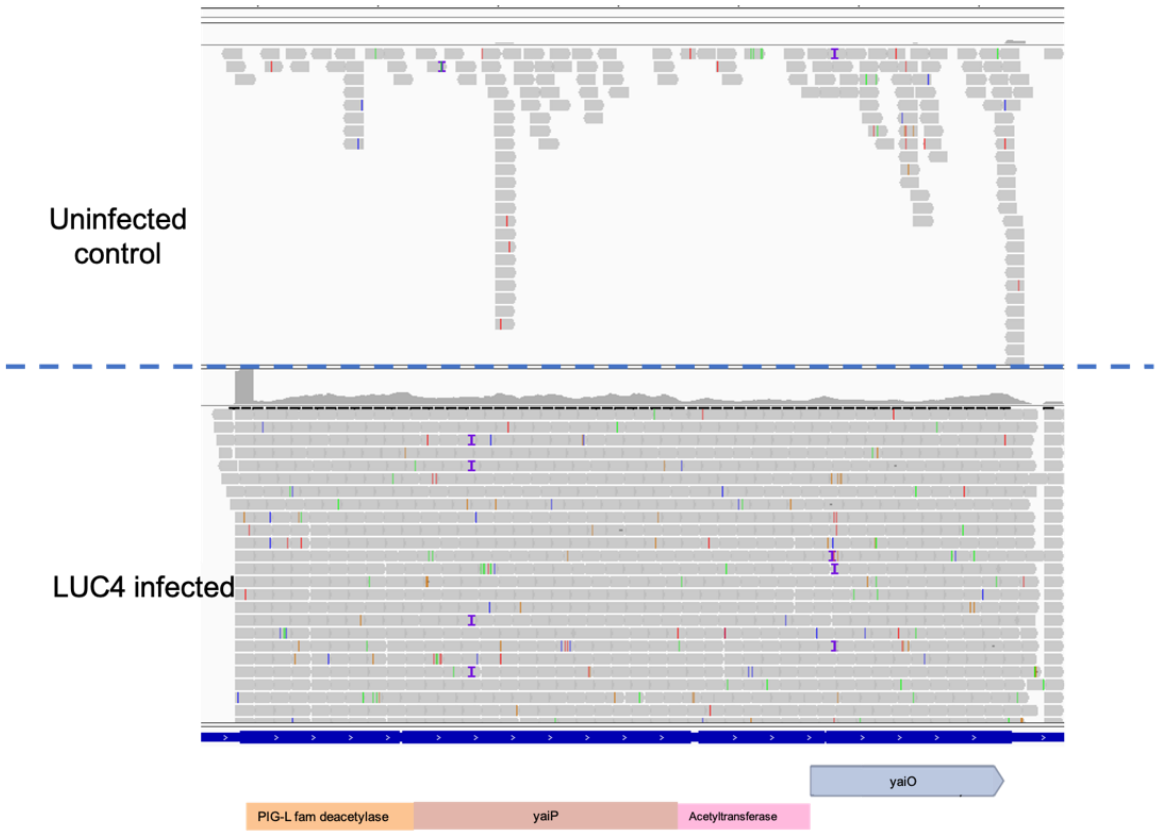

Figure 5.3 RNA-seq results show a highly expressed operon in the infected samples. RNA-seq reads (grey rectangles) mapped to the reference genome show the difference in transcription levels in a 4-gene operon, herein called the YOMP operon, that includes a putative deacetylase, a glycosyltransferase, an acetyltransferase and an outer membrane beta barrel protein.

A

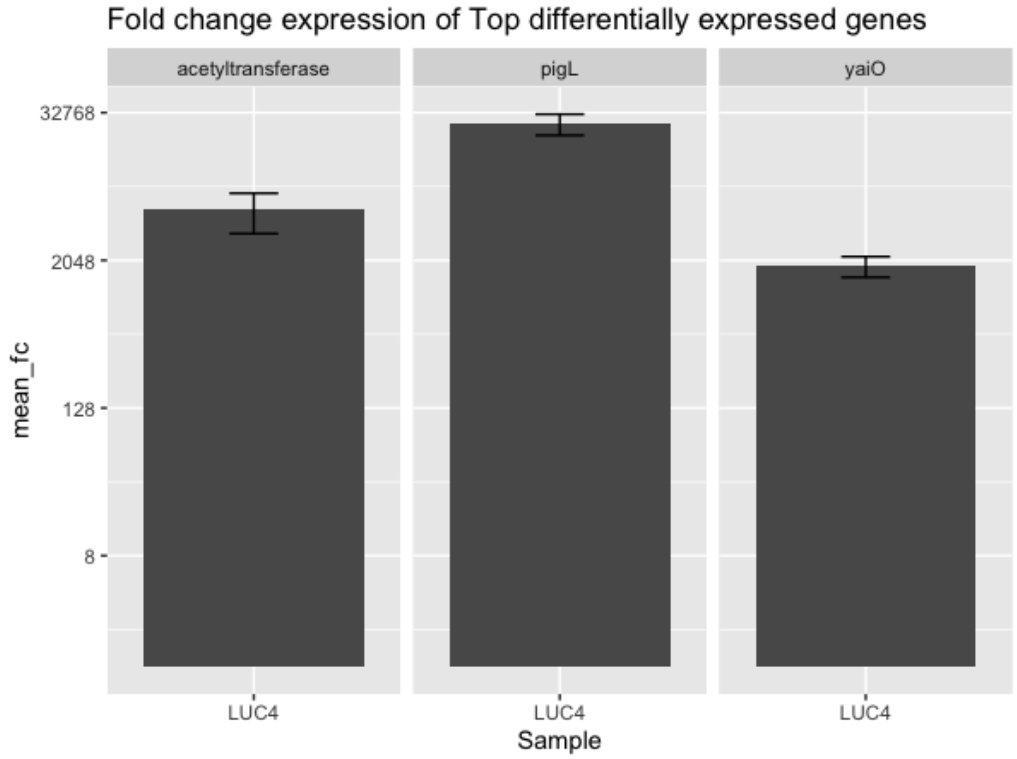

B

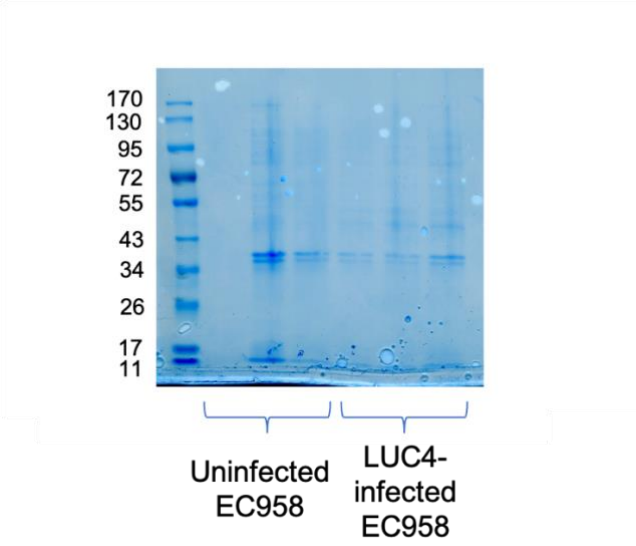

Figure 5.4 Validation of RNA-seq results. The top differentially expressed genes from the RNA-seq experiment were validated with RT-qPCR. The transcription levels of the genes Acetyltransferase, pigL-family deacetylase and *yaiO* were measured in uninfected and phage-infected samples in mid exponential phase. The Mean fold change (mean_fc) in transcription levels were calculated with the ΔΔCT method, using gene *hcat* as the housekeeping gene. The results represent three biological replicates ±SD. B) Outer membrane proteins (OMP) were extracted and run in an SDS-PAGE gel. Coomasie blue staining shows no difference in OMP patterns between uninfected and infected samples.

5.3.3 Cloning the differentially expressed operon into an inducible vector

The RNA-seq results and their confirmation with RT-qPCR brought up the hypothesis that the expression of the YOMP operon could protect the bacteria from phage infection, therefore, if the YOMP operon was over-expressed prior to the phage challenge, the culture would show nearly complete resistance to the phage. To test this, the operon was cloned into the inducible vector pBAD33 (Figure 5.5). EC958 was then transformed with the construct and induced with arabinose. The induced culture was infected with phage LUC4 at an MOI of 0.1. The results of these assays were unexpected, as the addition of arabinose suppresses the susceptibility of all the cultures –including the WT EC958 control—to the phage LUC4 (Figure 5.6). Naturally, we could not draw any conclusions from these assays, and it was therefore decided that another approach should be used to test this hypothesis. Nonetheless, the intriguing result of adding arabinose to the medium was a first indication that metabolism was likely involved.

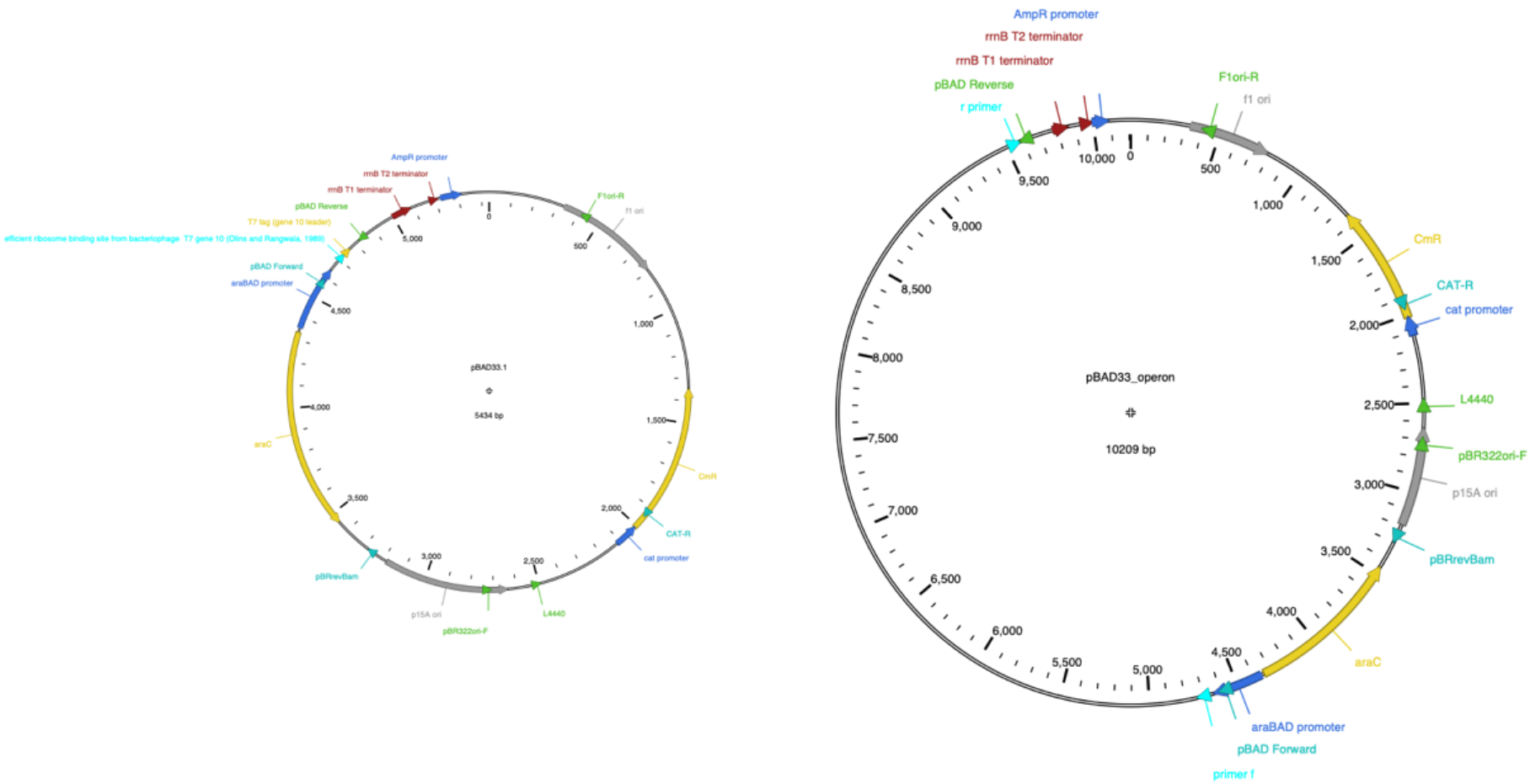

Figure 5.5 Cloning the putative resistance YOMP operon into vector pBAD33. The YOMP operon, which that was found highly overexpressed in the infected samples in the transcriptomic analysis, and that presumably conferrs resistance to the phage, was cloned into the inducible vector pBAD33.

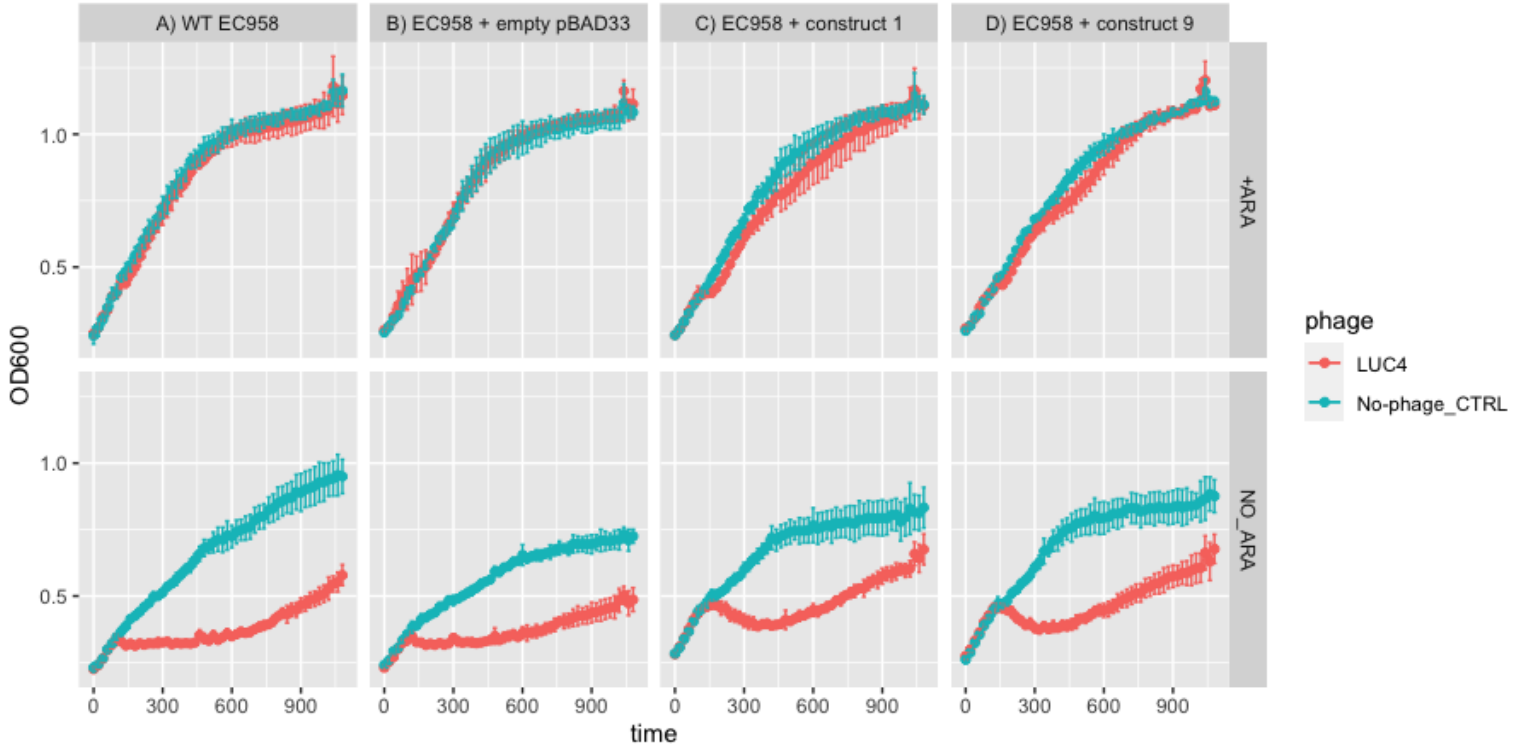

Figure 5.6 Inducing the YOMP operon with arabinose in transformed EC958 inhibits the phage infection. EC958 was transformed with the construct and challenged with the phage alongside WT-EC958 and EC958+empty vector with (+ARA) and without arabinose induction (NO_ARA). Arabinose inhibits the phage infection in all cultures and the effect of the over-expression of the operon is not possible to observe.

5.3.4 Knock-out mutants show no significant difference in phage resistance

In an alternative attempt to demonstrate the role of the YOMP-operon in phage defence, knockout (KO) mutants of two of the genes within the operon –pigL-family deacetylase and acetyltransferase—were made using the lambda red method with some modifications. I could not successfully knock out gene *yaiO* with the same method.

The KO-mutants were assayed with phage LUC4 and compared to the WT EC958. The growth curves in Figure 5.7 show that the KO-mutants can resist the infection of LUC4 similarly to the WT EC958. Escape variants were subsequently rechallenged with LUC4; we found that 38% of the resistant population derived from EC958-ΔpigL was permanently resistant and 62% had reverted to susceptible, whereas 47% of the resistant colonies from the EC958-Δacetyltransferase were permanently resistant and 53% were susceptible. In addition, the initial lysis showed an additional 10-fold reduction for both mutants.

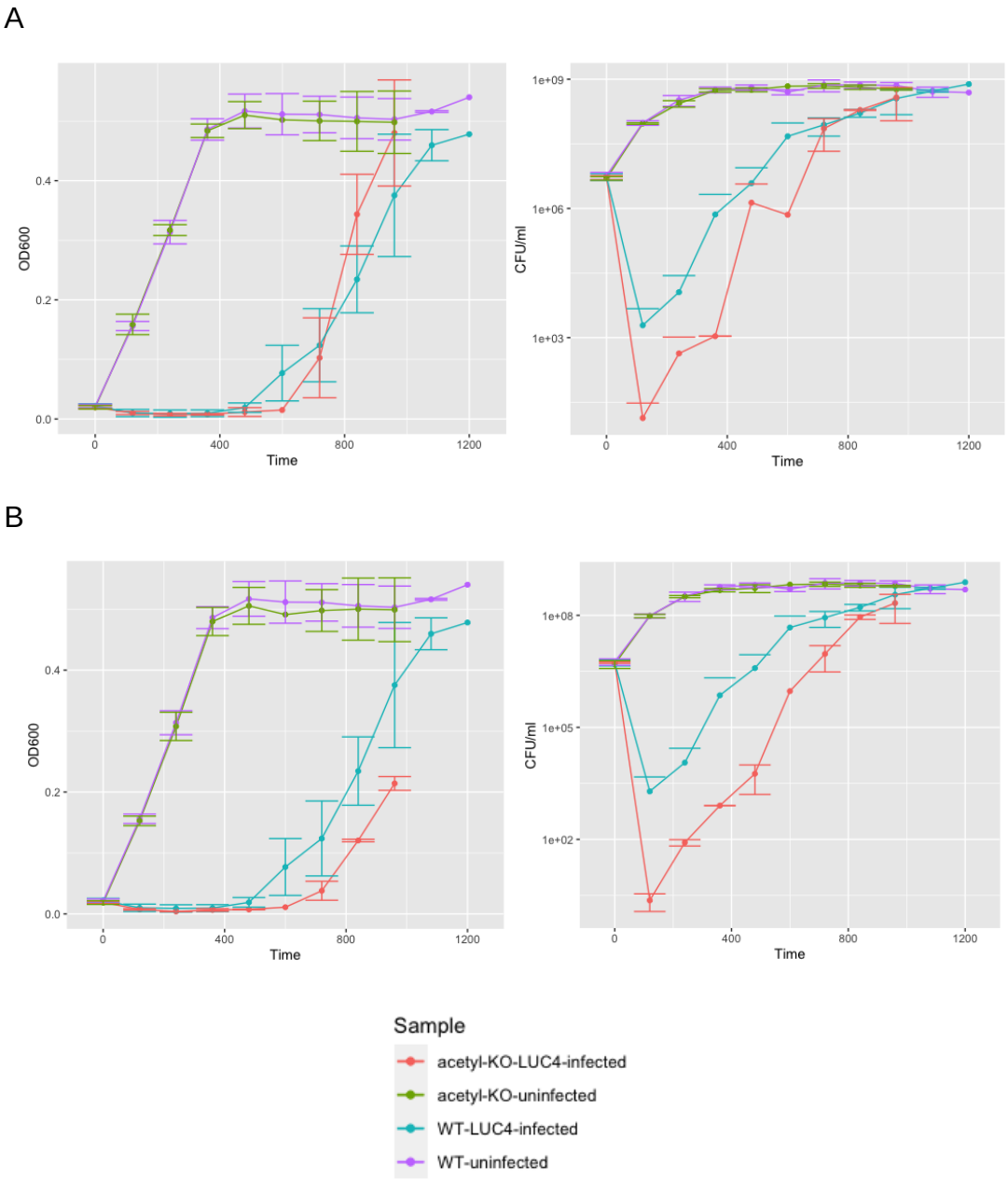

Figure 5.7 Infection assays of knockout-mutants. To test whether the YOMP-operon confers phage-resistance to EC958, knockout mutants were made and these were challenged with the phage. ΔpigL-EC958 and Δacetyl-EC958 can resist LUC4 infection in a similar way that the WT EC958 in AU. The curves represent the results of three biological replicates ±SD

5.3.5 The protective effect of EC958's supernatant against phage infection

While trying to understand how it is possible for EC958 to resist the phage infection at high MOIs, it was postulated that the infected cells could be producing and releasing a signalling molecule causing the activation of a defence system in neighbouring cells. To test this, the lysate of a LUC4-infected EC958 culture was harvested by pelleting the bacteria and filtering the supernatant, it was then passed through a centrifugal concentrator membrane of 3,000 MWCO to have a filtrate free of phage. The supernatant was mixed in increasing proportions with fresh AU, and these were used as growth media for infection assays with naïve EC958. The results show that an increasing proportion of supernatant can accelerate the emergence of phage resistance, to the extent of almost complete resistance when cultured in supernatant only (Figure 5.8). A similar effect can be seen in the PU assays (Figure 5.9A), which provided reassurance around the validity of the AU as a model medium to study UPEC-phage interactions. In contrast, LB supernatant did not confer any protection to the culture (Figure 5.9B), highlighting once again, the importance of using suitable media and representative models to study pathogens and therapeutic interventions. Interestingly though, the supernatant of uninfected EC958 cultures could also confer protection against phage infection (Figure 5.10), which indicated that it was a facet of the 'used' nature of the medium rather than the phage infection.

Three more strains were cultured in EC958's supernatant, but none of them showed any increased resistance to phage LUC4 (Figure 5.11). This indicated that the phage itself does not lose infectivity as a result of the supernatant, and that this resistance mechanism is specific to certain strains of *E. coli*.

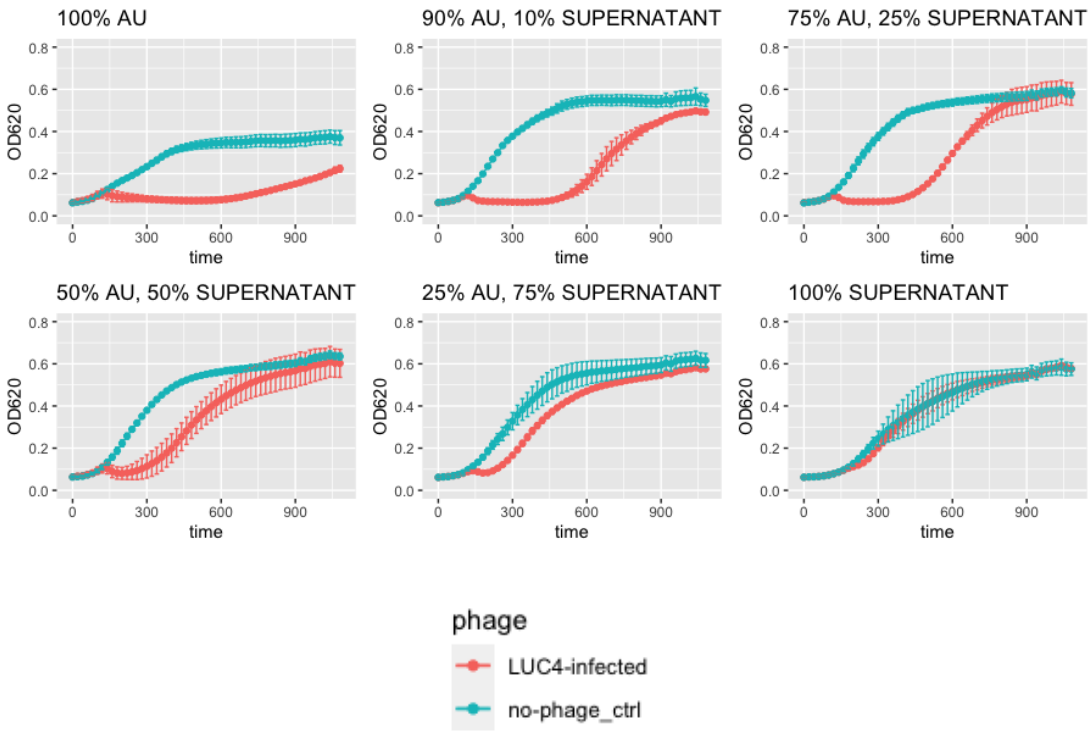

Figure 5.8 The addition of supernatant from a LUC4-infected EC958 culture has a concentration-dependent protective effect against phage infection. The supernatant from a LUC4-infected EC958 culture was harvested and combined with fresh AU in increasing proportions to be used as growth medium for infection assays with naïve EC958 and phage LUC4. Increasing concentrations of supernatant accelerate the resistance response to the phage. Three biological replicates were carried out; the growth curves in this figure are from one representative example with the mean of three technical replicates ±SD.

A

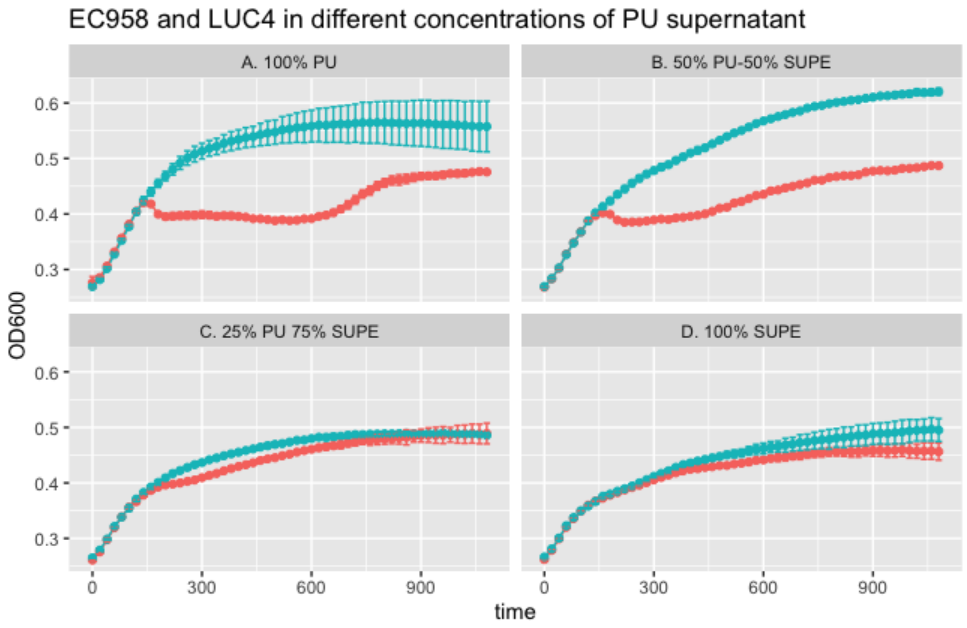

B

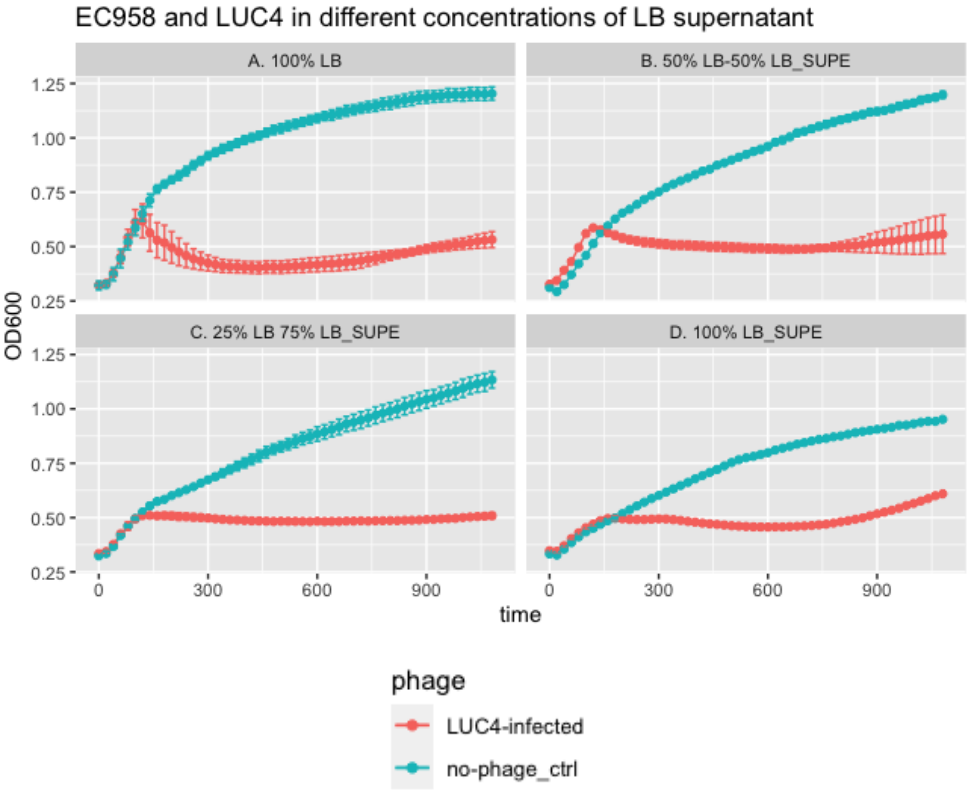

Figure 5.9 The effect of the LUC4-infected EC958 culture supernatant using other media. A) The supernatant of LUC4-infected EC958 culture in PU has a protective effect similar to the one observed in AU (Growth curves represent the mean of one biological and three technical replicates ±SD). B) The supernatant harvested from a LUC4-infected EC958 culture in LB does not confer any protection to the phage infection. (Three biological replicates were carried out; the growth curves in panel B are from one representative example with the mean of three technical replicates ±SD).

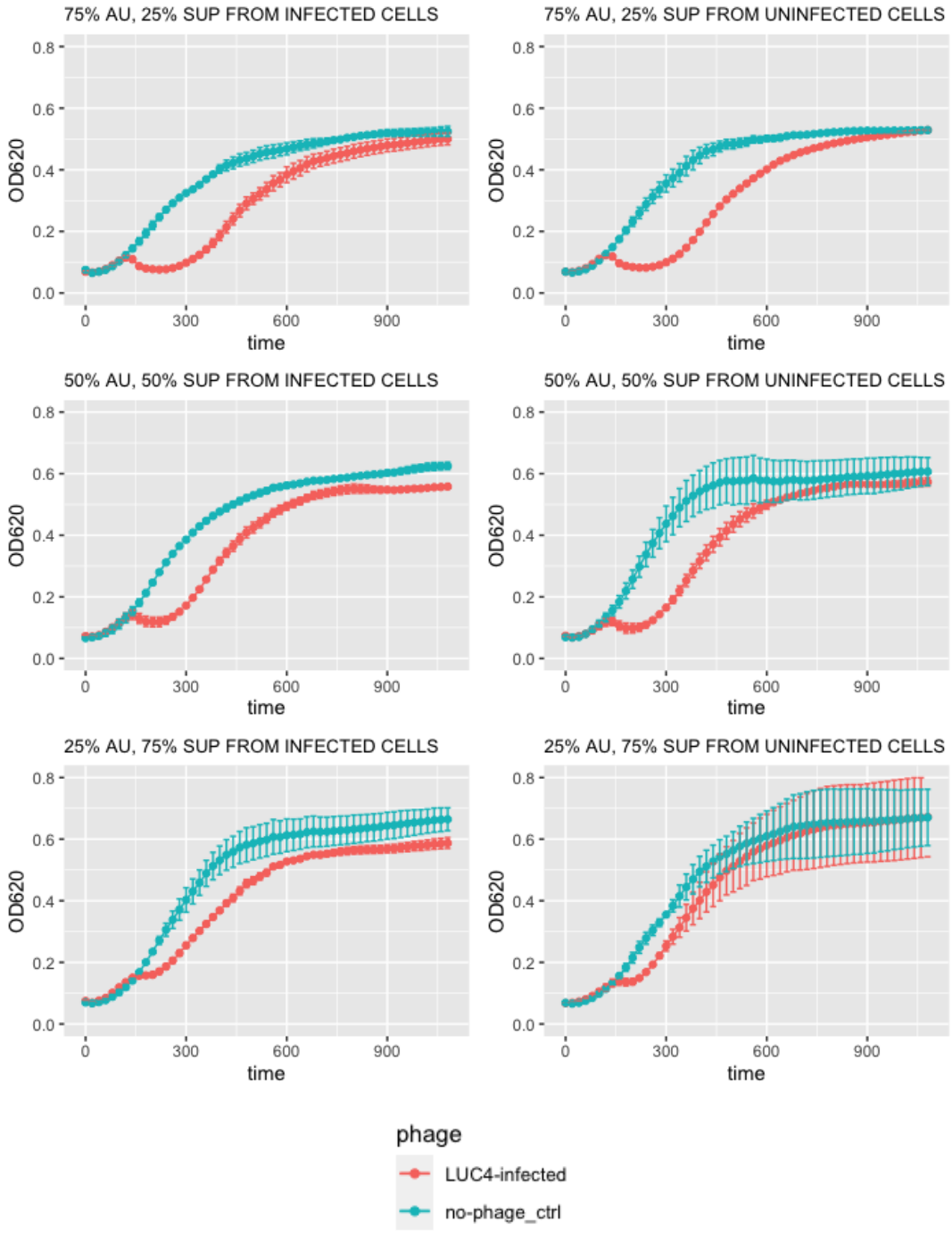

Figure 5.10 Supernatant from uninfected and phage-infected cultures have a similar protective effect against phage predation. When EC958 is cultured in different concentrations of supernatant from an uninfected and infected culture, the same level of protection is observed. A total of three biological replicates were carried out; the growth curves in this figure are from one representative example with the mean of three technical replicates ±SD.

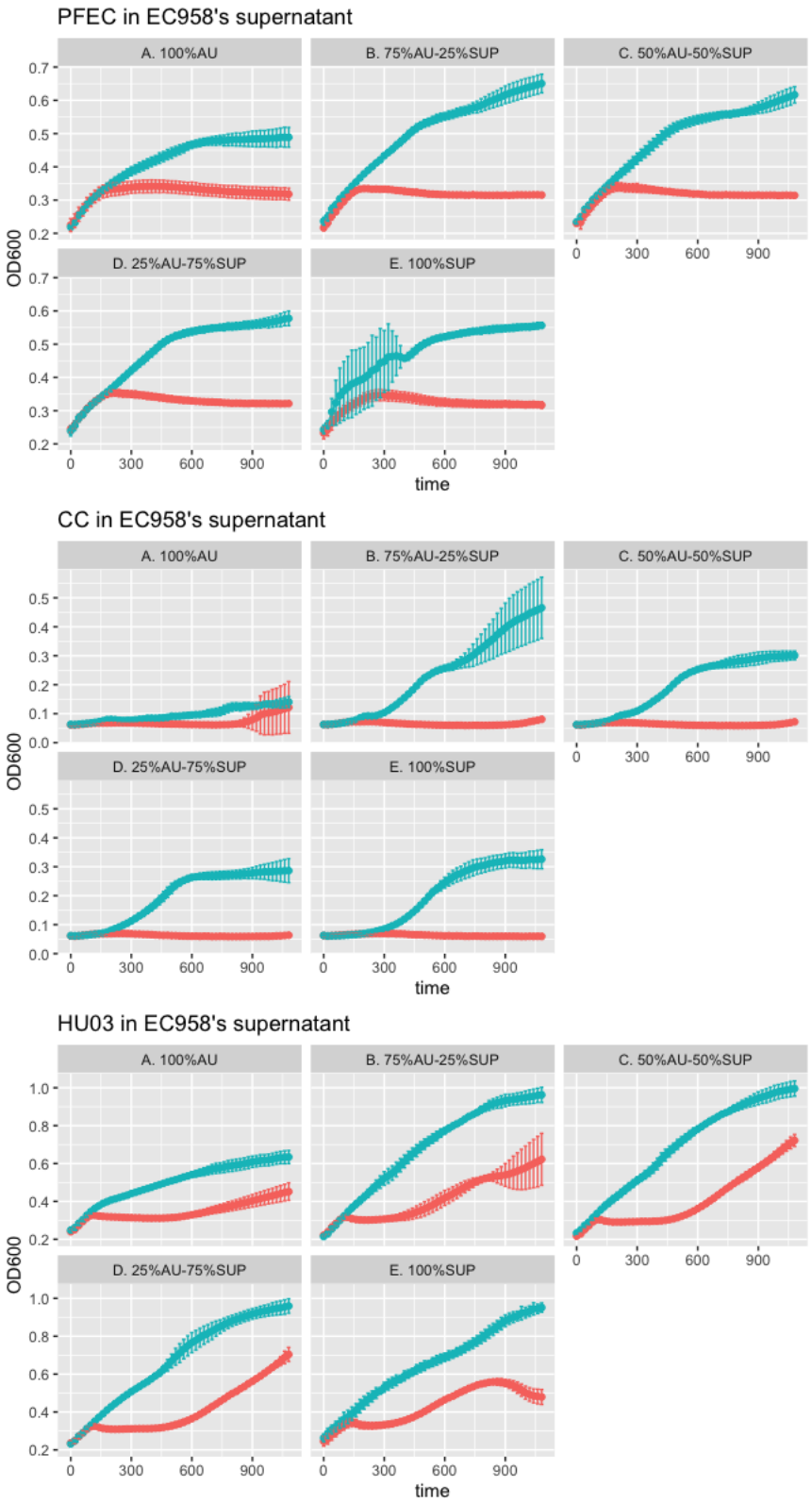

Figure 5.11 The supernatant of EC958 does not confer phage-resistance to other E. coli strains. Three additional strains (PFEC, ClearColi and HU03) were cultured with different concentrations of EC958 supernatant and challenged with phage LUC4, but no protection was conferred to these strains against the phage. These experiments were carried out once with three different strains. The growth curves represent the mean of three technical replicates ±SD.

5.3.6 Phage LUC4 can adsorb to its host EC958 in supernatant but does not produce infective progeny

The protective effect of the supernatant against phage predation may be the answer to the phage resistance that EC958 shows. In order to dissect the mechanism of resistance I was interested in pinpointing the stage of infection in which the phage infection is stalled. Numerous anti-viral defence systems consist in changing, masking, hiding or downregulating phage receptors to avoid phage adsorption.

During his time in our research group, MSc. student Zhuneng Zhou, carried out adsorption assays of phage LUC4 and its host EC958 using supernatant and fresh AU as control. A representative example of the results shown in Figure 5.12 shows that phage LUC4 is still capable of adsorbing to the bacteria in the presence of the supernatant, although at a slower pace compared to fresh AU. In accordance with the previously obtained results, in fresh AU, LUC4-infected EC958 cultures show a dramatic increase in the number of PFU/mL 20 minutes after the start of the infection. This burst is not registered in the supernatant cultures; even after 2 hours of incubation (data not included). The fact that the phage is still adsorbing to the host in the protective supernatant, but unable to generate infecting progeny indicates that the resistance mechanism is not related to the inhibition of adsorption and further studies are needed to identify when the infection is being impeded. However, Zhuneng's work provides evidence that the growth conditions involving the supernatant induce a non-productive state in terms of the capacity of LUC4 to release new virus.

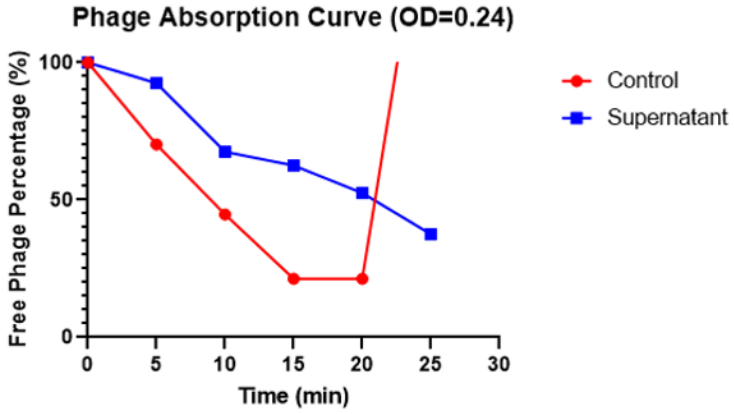

Figure 5.12 Adsorption rates of phage LUC4 to its host EC958 in AU and Supernatant: Work done by Msc. Student Zhuneng Zhou. The rate of adsorption of phage LUC4 to its host in supernatant (blue curve) is slower than the one measured in fresh AU (Red curve, Control). A dramatic increase in free phage counts is seen after 20 minutes of incubation in AU which represents the burst of the first cycle of infection. This burst is not detected in the supernatant assays. Three independent replicates were carried out. This figure shows one representative example with the mean of three technical replicates.

5.4 Discussion

The results of the previous chapters indicate that the reversible resistant population outcompetes the fixed one and becomes the dominant population (4.3.8), which is difficult to target with the addition of different phages or higher MOIs. It comprises a reversible or unstable process that confers resistance to the strain during the middle and late timepoints in the infection assays, but the susceptible phenotype is observed again after being passaged in fresh medium. Since this resistance is recurrently observed in artificial and pooled canine urine, it is considered that this type of resistance may be an issue for any clinical application of phage therapy and therefore it is important to understand.

The exploration of EC958's anti-phage systems began with a search using PADLOC. The output included 4 restriction-modification (R-M) systems, a duplicated abortive infection system, a retron, and the BREX system (Figure 5.1). RNA-seq results show that most of the defence genes were not upregulated in infected samples compared to uninfected controls. In fact, only the genes encoding the toxin and antitoxin in the AbiE system were found slightly up regulated with significance (LogFC= 0.5 and 0.4, FDR=0.006 and 0.036, respectively, Appendix 8). The rest of the genes were down regulated and/or were not differentially expressed with statistical significance. It is unlikely that the AbiE abortive system is the sole player in resisting phage LUC4, given that the resistance emerges even at high MOIs, in which nearly all the cells are targeted by the phage from the first cycle of infection. In addition, the resistance is not observed in LB. For this reason, it is assumed that resistance is not caused only by the characterised anti-phage systems in EC958; although partial involvement is a possibility and defined knock-outs in the different systems would allow this to be tested.

To gain a better understanding of the reversible resistance mechanism, we compared the transcription profiles of uninfected and infected cultures at a similar OD. This means that the RNA of the phage-infected culture was harvested after resistance had emerged and the culture was in mid-exponential phase: approximately 12 hours after the start of the assays. The results from this experiment showed an overwhelming list of differentially expressed genes between conditions. It was decided that the top over-expressed genes in the infected samples would be studied first. These genes were clustered into an operon and encoding a predicted deacetylase, an acetyl-transferase, a glycosyltransferase and a beta-barrel outer membrane protein (Figure 5.3).

The most straight forward method to prove the defensive function of the up-regulated operon was cloning the whole operon into an inducible vector. pBAD33 was used as its chloramphenicol resistance cassette would the selection of transformants. However, induction requires the addition of arabinose; a sugar that is not normally present in urine, and which had an unexpected effect. The results from the phage challenge were impossible to interpret, as the addition of arabinose causes the phage infection to be blocked in both the WT and the transformants (Figure 5.6). Despite not having obtained a straightforward answer with this assay, the unexpected results were a first indication that a metabolic pathway associated with carbon source could be related to phage resistance.

As an alternative approach, the genes were deleted using a modified version of the Lambda-red homologous recombination system. Since antibiotics are used as selection markers, genetic modification of EC958 is problematic due to its multidrug-resistance. Sean McAteer, a core scientist in our group, cloned the Tellurite resistance gene into pKD46, which contains the Lambda-red recombinase. The genes EC958_RS11570 and EC958_RS11580, encoding a predicted pigL-family deacetylase and an acetyltransferase, respectively, were substituted by a chloramphenicol resistance cassette from pKD3; unfortunately, inactivation of gene yaiO was unsuccessful.

According to our initial hypothesis, the inactivation of these genes should result in a more susceptible bacterial culture. This was not the case and the cultures developed resistance to the phage at a similar timepoint as the WT, although the initial level of killing and initial recovery of both knock-out mutants seemed to be slower (Figure 5.7). Furthermore, the recovering population still contained a mixture of fixed and reversibly resistant bacteria which indicated that this operon, whilst relevant to initial phage sensitivity, did not encode the reversible resistance being investigated.

As the experimental design was re-analysed, it became evident that comparing a non-infected and an infected-and-recovering bacterial population at the same OD was confounded by major differences in the growth medium; as the infection flask has gone through a massive lysis event that releases bacterial contents and debris into the medium. When examining the RNA-seq data, a number of the up-regulated genes in the phage surviving population relate to permeases and nutrient transporters, and this led us to speculate that the operon was more likely somehow involved in nutrient scavenging, potentially explaining the expression of an additional beta-barrel outer member protein (YaiO). The role of the YOMP operon for scavenging is beyond the scope of my PhD project, but the research group still has the objective of carrying out metabolomic assays to gain a better understanding of this process. Furthermore, it could also be linked to the phage-resistance, as there was about a ten-fold further reduction in bacterial counts during the initial LUC4 infection cycles (~120 minutes after infection) when one of the genes in the operon were deleted. My earlier idea that somehow YaiO may substitute for OmpC as a major porin and not be a receptor for LUC4 was attractive but incorrect.

Culturing naïve bacteria with phage in the supernatant of EC958 was originally intended to help explain how EC958 can survive and thrive after nearly all cells have been infected by a lytic phage in the first cycle. We hypothesised that a signalling molecule produced by the infected cells could be activating a defence system in the yet uninfected cells. As shown in Figure 5.10, the

protective effect is found in both the supernatant of infected and uninfected EC958 cultures. Unlike some compounds, such as proflavine (Foster, 1947) and arsenite (Spizizen et al., 1951) the supernatant has no direct detrimental effect on the phage, as it is can still complete its infection cycle in other hosts (**Error! Reference source not found.**); and it does not inhibit the phage adsorption to the host (**Error! Reference source not found.**). Due to time constraints, the role of the supernatant in phage resistance could not be fully investigated. However, by summing up the results of different assays, a few new hypotheses have been generated and these will be explored in future research.

It was first thought that a quorum sensing (QS) molecule –or an autoinducer— was preventing the infection cycle of the phage to be completed. Previous research has found that QS systems can influence bacteria-phage interaction, and some of the resistance mechanisms that have been studied are related to these systems. Biofilm production, regulated by QS, could increase phage resistance due to restrictions on phage access to bacteria within the inner layers of the biofilm (Rossmann et al., 2015). *E. coli* QS genes have also been shown to alter expression of phage receptors and therefore impact on susceptibility (Hoyland-Kroghsbo et al., 2013); but these do not explain the resistance that is observed in EC958. First, by culturing EC958 with constant shaking, the formation of biofilms is inhibited (Totsika *et al.*, 2011). Second, while transcription levels of *ompC* are reduced in the infected culture by 0.7 LogFC, (FDR=0.01, Appendix 8), it is still expressed and the reduction at the population level is likely a result of the *ompC*-mutant subpopulations. Finally, Zhuneng's results show that the final adsorption of phage to EC958 is not affected when cultured in supernatant (Figure 5.12).

One of the functions of QS systems is on bacterial metabolism, which can affect the interaction with phage. It is commonly accepted that for most phages to be able to replicate, their host must be in a metabolically active physiological state. In other words, when the host is not actively growing, the phage cannot complete its infecting cycle (Bryan et al., 2016). However, this applies only to

bacteria growing in specific conditions, as it has been shown that depending on the nutrients in the medium, the growth of either the host, the virus or both can be sustained. Ultraviolet light, mustard gas and irradiation inhibit the replication of *E. coli* but can still sustain the virus multiplication (Spizizen, 1943); whereas culturing temperatures above the optimal can limit the phage production or release, while maintaining the host replication (Foster, 1948). Similarly, certain nutritional limitations could affect the phage production, despite the host cell being capable of replicating. Absence of phosphate and magnesium can severely limit the viral multiplication. Based on the observation that the transient resistance is not present in a complex laboratory medium, like LB, a new hypothesis has been formulated:

Nutrient availability in urine is limited, but UPECs can adapt to these hostile environments by changing their expression profile and synthesising the nutrients that they need to replicate (Alteri and Mobley, 2015). In contrast, phages within their host may be unable to adapt to nutrient starvation (Cohen, 1949). The differences in phage production depending on the growth media have been reported when comparing LB to a minimal medium (Fowler and Cohen, 1948). When an *E. coli* B was cultured in minimal medium, the viral production was significantly stimulated when supplemented with specific amino acids, such as isoleucine, phenylalanine, aspartic acid, proline, lysine, valine, arginine, and glutamic acid. Whereas other amino acids, such as tyrosine, histidine and valine inhibited the production of nascent phages. The addition of glycine, alanine, threonine, methionine, and tryptophane did not affect phage production. In this sense, due to the small amount of added peptone in AU, the limited availability of certain amino acids and peptides may initially allow proliferation of phage LUC4, but as certain factors are used up, the conditions change to prohibit the production of new phage particles, even though bacterial growth is able to continue due to the evolved metabolic adaptability of ST131. In conclusion, it may be that the nutritional status could directly impact on phage production or could trigger a resistance mechanism. For either case, it is proposed that the metabolic status of EC958 in AU is

critical for LUC4 infection. This specific relationship will be a focus for the research following on from the work defined in this thesis.

Future work intended to confirm or discard the hypotheses mentioned above includes metabolomic assays with different carbon sources to identify the nutrient requirements for phage replication, Mass Spectrometry analysis to compare the composition of the medium at different timepoints and/or to identify the putative signalling molecule. Finally, we are interested in finding whether the anti-phage systems encoded in EC958 –and especially the AbiE abortive system—is involved in the resistance and to what extent.

A better understanding of a recurring phage-resistance mechanism that is expressed in urine may represent an advancement towards a safe and successful implementation of phage therapy to treat urinary tract infections. Furthermore, in order to determine the importance of tackling this resistance, it is important to confirm the existence and relevance of this type of resistance in an animal model, which would also be essential to test the safety and efficacy of PT in UTI patients.

Chapter 6 A porcine model of UTI and Phage therapy: Pilot study

The work described in this chapter was carried out jointly with Doctor Alison Low and Marianne Keith, and in collaboration with the Large Animal Research and Imaging Facilities (LARIF).

6.1 Introduction

Applied PT is still in its infancy in most of the world with a few exceptions, like the Eliava Institute in Georgia and the Ludvik Hirszfeld Institute of Immunology and Experimental Therapy in Poland, in which patients have been treated safely for decades (Abedon et al., 2011; Kutateladze and Adamia, 2008). The rising levels of antibiotic resistance is causing an increasing interest in scientists and clinicians worldwide to explore the potential of PT. Like any other therapeutic product for humans and/or animals, phage products need to be assessed for safety and efficacy. Animal models of infection are key in translating the data of phage research into human and veterinary clinical practice.

Flies, nematodes, wax moth larvae, zebra fish, mice, hamsters, rats, rabbits, birds, calves, sheep, pigs and dogs have been used as animal models to study phage therapy (Brix *et al.*, 2020; Penziner *et al.*, 2021). A few PT trials have been reported for extraintestinal *E. coli* infections using animal models of infection: Sanmukh *et al.* (2023) and Antoine *et al.* (2021) used *Galleria mellonella* larvae to assess the effect of PT in terms of survival; whereas Nishikawa *et al.* (2008), Salazar *et al.* (2021), Zulk *et al.* (2022), Ali et al. (2021), Dufour *et al.* (2016), Pouillot *et al.* (2012) and Green *et al.* (2017) have used rodent models of urinary, systemic and nervous system infections. The low cost of mice, their relative ease to handle, the vast availability of tools and reagents for research, and the possibility of genetically modifying strains make them the most popular animal model for PT trials.

Mice have been the preferred model to study UTIs as well (Barber et al., 2016). However, the murine model also has several limitations. The size of the murine urogenital organs is substantially smaller, and the urine that mice produce is more concentrated than the urine of larger mammals. This makes mice less susceptible to UTIs, which is reflected in a different pathogenesis and pathophysiology (Andersen *et al.*, 2012; Subashchandrabose and Mobley,

2015). The immune response of mice to bacterial colonisation of the bladder has major differences to the ones observed in larger mammals (Dawson et al., 2017). Furthermore, their use in drug safety trials is being questioned increasingly, as a large proportion of therapeutic compounds that were safe for mice did not have the same outcome in humans (Perrin, 2014). To test the safety of pharmaceuticals produced in *E. coli*, for instance, the murine model may have limited value due to the low susceptibility of mice to endotoxin.

Domestic and mini pigs are increasingly being considered as suitable models to study pathologies and practice surgery of the urinary tract. The porcine urinary tract is anatomically and physiologically similar to the human urinary tract (Swindle et al., 2012); therefore, the urodynamics of the pig are comparable to those of the human. The natural susceptibility of pigs to *E. coli* UTIs makes this species fundamentally suitable to study the progression of the pathology and potential treatments. Previously, Nielsen *et al.* (2019) successfully established a model of cystitis using ~35 kg pigs inoculated with *E. coli* strain UTI89 via transurethral catheter.

This final chapter covers a pilot study that will enable future *in vivo* studies of the bacteria-phage interactions and emergence of phage-resistance that have been described in this work. The low number of animals limits the scope of the study, for which the main objectives were to gain an understanding of the viable methods and challenges of the model. Nonetheless, it was of interest to obtain preliminary results regarding 1) the suitability of pigs as models of *E. coli* ST131 bladder infections and intravesical PT, 2) the safety of phages that were propagated using a detoxified *E. coli* strain (Mamat et al., 2015), and 3) the resistance mechanisms that are employed by bacteria *in vivo*. The latter could further validate the *in vitro* models that are currently being used in our research studies (e.g., the artificial urine medium). Here the results of three pilot studies are presented: a bacteriophage safety trial, the establishment of a UTI model, and then the use of such model to test the efficacy of phage treatment.

The safety pilot study had the objective of determining whether the phage preparation was safe to be instilled in the bladder of the porcine model. The clinical health of the animals was monitored, and blood samples were taken to measure inflammation markers. The pilot study for the development of a porcine model of UTI had the objectives of 1) testing the efficacy of a swabbing method of *E. coli* inoculation, 2) determining whether the pig model can be colonised by the E. coli clinical strain EC958, and 3) observing the clinical signs of the animals with a UTI and the bacterial burden in them. The final pilot study has the objective of determining the efficacy of phage therapy in the pig model of UTI. In addition, with the objective of validating the methods being used in our research group –in particular the artificial urine medium—the resistant bacteria recovered after the treatment were assessed to determine whether these has a fixed resistance, or were susceptible to the phage.

6.2 Material and methods

6.2.1 Experimental design

6.2.1.1 Bacteriophage safety trial

A pilot study to determine the safety of the detoxified phage preparations using ClearColi™ (Mamat *et al.*, 2015) was carried out. Three juvenile pigs were instilled with 100 mL of the phage LUC4 suspension. The pigs were monitored closely for two hours following the instillation, after which it was spaced out to twice daily. Blood samples were taken before the instillation (T=0), as well as 24 and 48 hours after. Inflammation markers (IFN-alpha, IFN-gamma, IL-4, IL6, IL-8, IL10, IL-12/IL23p, IL-beta and TNF-alpha) were measured in the blood of the pigs to determine whether a significant immune response had been triggered by the treatment (Table 6.1).

Table 6.1 Timeline plan for the safety of bacteriophage pilot study

15/08/2022	16/08/2022	17/08/2022	18/08/2022	19/08/2022	20/08/2022	21/08/2022	22/08/2022	23/08/2022	24/08/2022
Acclimatisation							Bladder catheterisation for bacteriophage instillation; blood sampling; health monitoring	Blood sampling; health monitoring	Sedation; blood sampling; euthanasia; urine collection by cystocentesis; post-mortem analysis

6.2.1.2 Pilot study for the development of a porcine model of UTI

With the objective of establishing less invasive and more refined methods of animal experimentation, the swabbing method of bacterial inoculation reported in an online seminar by Fernandez (2020) was tested in this pilot study. This method has not been published and was reported to still be under optimisation by personal communication. Considering that there was a high risk of unsuccessful UTI establishment, the protocol for this pilot study could follow different procedures depending on whether the swabbing method had led to a successful establishment of UTI. For this, a threshold of $>10^5$ CFU/mL with no clinical signs (Scott et al., 2015) or $>10^2$ CFU/mL with clinical signs (Foxman, 2014) was set to consider an established UTI.

After a 7-day acclimatisation period, the pigs were inoculated with *E. coli* strain EC958 via the swabbing method (6.2.5.2). The bacterial burden in the urine of the infected pigs was determined at 24, 48 and 72-hours post infection. **Plan A**: If the bacterial counts of the three pigs at T=72 was above the threshold, the UTI establishment would be considered successful. The pigs would receive the control treatment (0.9% NaCl solution). Their health status would be monitored and the bacterial burden in urine determined every day until termination at T=96. **Plan B**: If at 72-hours post infection one of the pigs had bacterial counts in urine below the threshold, but the other two had levels above it, the individual with low bacterial burden would be sedated and the inoculation by swabbing would be repeated. At T=192, the pigs would receive the control treatment, provided that they had maintained the UTI. Monitoring would continue until termination at T=240. If the pig with the double swabbing remained uninfected, she would not receive the control treatment but would be monitored along with her peers**. Plan C**: If two or three pigs had bacterial counts in urine below the threshold at T=72, these pigs would be anesthetised to be inoculated with EC958 via transurethral catheter. Monitoring and the bacterial counts in urine would be determined until T=192, in which they would all receive the NaCl solution treatment. Clinical monitoring and bacterial counts would continue until termination at T=240 (Table ***6.2***).

Table 6.2 Timeline plan of the pilot study for the development of a porcine model of UTI

	15/08/22	…	21/08/22	22/08/22	23/08/22	24/08/22	25/08/22	26/08/22	27/08/22	28/08/22	29/08/22	30/08/22	31/08/22
	Acclimatisation			Free catch urine sample; sedation; *E. coli* inoculation by swabbing; clinical monitoring	Free catch urine sample; clinical monitoring	Free catch urine sample; clinical monitoring	**DECISION POINT**						
Plan A: all pigs have an established UTI							General anaesthesia; bladder catheterisation; urine sample; control treatment	Free catch urine sample; clinical monitoring	Free catch urine sample; clinical monitoring	Free catch urine sample; clinical monitoring	Sedation; euthanasia; urine collection; post-mortem analysis		
Plan B: Two pigs have an established UTI; one pig with no established UTI				**Positive pigs:**			Free catch urine sample; clinical monitoring	Free catch urine sample; clinical monitoring	Free catch urine sample; clinical monitoring	Free catch urine sample; clinical monitoring	General anaesthesia; bladder catheterisation for control treatment	Free catch urine sample; clinical monitoring	Sedation; euthanasia; urine collection; post-mortem analysis
				Negative pig:			Sedation; second *E. coli* inoculation by swabbing	Free catch urine sample; clinical monitoring	Free catch urine sample; clinical monitoring	Free catch urine sample; clinical monitoring	Free catch urine; clinical monitoring	Free catch urine; clinical monitoring	Sedation; euthanasia; urine collection; post-mortem analysis
Plan C: Two or all pigs are negative to UTI							General anaesthesia; bladder catheterisation for second E. coli inoculation	Free catch urine sample; clinical monitoring	Free catch urine sample; clinical monitoring	Free catch urine sample; clinical monitoring	General anaesthesia; bladder catheterisation fir control treatment	Free catch urine; clinical monitoring	Sedation; euthanasia; urine collection; post-mortem analysis

6.2.1.3 Pilot study of Phage Therapy efficacy

This part of the study was carried out after the UTI model development pilot study (from 12th September 2022 to 22nd September 2022), as the method of inoculation was based on the results obtained with the swabbing and the direct bladder instillation. Given that the swabbing method of inoculation was not successful, the pigs in this group were inoculated by transurethral catheterisation. The health and bacterial burden in the urine of the pigs was monitored for the following days (from T=0 to T=120). At 120 hours after inoculation, the pigs were treated with the phage preparation via transurethral catheterisation. The pigs were monitored at least twice daily for the next days and the bacterial burden in urine determined until the end of the study at T=168. At this point, the pigs were euthanised and a post-mortem analysis was carried out (Table ***6.3***).

Table 6.3 Timeline plan of the pilot study of the efficacy of phage therapy in the porcine model of UTI

05/09/22	…	13/09/22	14/09/22	15/09/22	16/09/22	17/09/22	18/09/22	19/09/22	20/09/22	21/09/22
Acclimatisation			General anaesthesia; bladder catheterisation; transurethral *E. coli* inoculation; free catch urine sample	Free catch urine sample; clinical monitoring	Free catch urine sample; clinical monitoring	Free catch urine sample; clinical monitoring	Free catch urine sample; clinical monitoring	General anaesthesia; bladder catheterisation; phage treatment instillation	Free catch urine sample; clinical monitoring	Sedation; euthanasia; urine collection; post-mortem analysis

6.2.2 Preparation of the therapeutic phage suspension

Phage LUC4 was used in both pilot studies: the phage safety trial and for the phage efficacy trial (experimental group). It was propagated and titrated by Doctor Alison Low as described above (2.2.4.3) using ClearColi+pWKS30-*ompC* (4.2.6) as the host strain. The lysate containing the phage was tested to quantify the amount of endotoxin using the HEK-blueTM LPS detection kit (InvivoGen), a cell-based colorimetric assay for the detection of biologically active endotoxin, following the manufacturer's instructions. Based on the results and the Endotoxin Units (EU) recommended for parenteral administration, one volume of the neat phage suspension was diluted in 50 parts of medical grade 0.9% NaCl solution (Aqupharm, Animal Care). The sterility of the preparation was verified by plating 200 µL samples on LB agar plates and incubating them at 37ºC for 48 hours. The stability of the phage in 0.9% NaCl solution was tested by measuring the titre after 48 hours at 4ºC. The pH was measured with a pH tester (Checker, Hanna Instruments). To ensure that the phage was able to adsorb and infect when suspended in the 0.9% saline solution, an adsorption assay was carried out as described above (3.2.1.4) and compared to the adsorption rate in LB.

6.2.3 Bacterial growth conditions

Escherichia coli O25:H4-ST131 strain EC958 was used in the development of the UTI model and phage therapy efficacy trial. To stimulate type-1 fimbrial expression, static cultures of EC958 were carried out by Marianne Keith as described by Totsika *et al.* (2011) and Nielsen *et al.* (2019). A single colony of EC958 was inoculated in 25 mL of LB broth in a 50 mL falcon tube. The culture was incubated statically at 37ºC overnight. The next day, 25 µL of the culture

was sub-cultured in 25 mL of fresh LB and incubated statically at 37ºC overnight. The subculture was repeated once more. The static culture of EC958 was centrifuged at 2500 RFC for 20 minutes to pellet the cells. They were resuspended in 50 mL of 0.9% NaCl to achieve a concentration of 10^8CFU/mL.

The expression of type-1 fimbriae was verified by Marianne Keith with an agglutination test using yeast cells as described by Kuan and Yeh (2019). For this, 1000 µL of the bacterial inoculum (48-hour static cultures, two subcultures), and EC958 cultures with inhibited expression of type-1 fimbriae (incubated with shaking) were transferred to a 6-well plate and then mixed with 1000 µL of 0.5% *Saccharomyces cerevisiae* suspension. The plate was incubated at 37ºC for 30 minutes and then checked for agglutination.

6.2.4 Animal sourcing, housing and conditions

All the experiments were carried out in the Large Animal Research and Imaging Facilities (LARIF, Easter Bush Campus, University of Edinburgh). All procedures were approved by the Named Veterinary Surgeon Stefano Guido and by the Roslin Institute Animal Welfare and Ethical Review Body (AWERB).

9 juvenile (12-15 weeks, ~40 kg) crossbred (Large White X Landrace X Hampshire) female pigs were purchased from a local farm (Easter Howgate, SRUC). Three pigs were used in the phage safety trial; the other 6 were used in the phage efficacy trial. After being transported to the LARIF, the pigs were allowed to acclimatise in their pens for 7 days before the start of the study. Daily visits from one of the group members were carried out during the acclimatisation period to habituate the pigs to human presence and handling and reduce stress during the study. The pigs were fed *ad libitum* on a commercial grower diet and access to fresh water was available at all times.

The enclosure was bedded with straw and was cleaned daily. Environmental enrichment was provided.

6.2.5 Procedures on animals

The anaesthesia and vital sign monitoring were done by the Anaesthetists: Rachel Gregson and Eddie Clutton. The surgical procedures and blood sampling was done by the Named Veterinary Surgeon Stephen Greenhalgh. Urine sample collection by bladder emptying via transurethral catheter was done by the Named Veterinary Surgeon Stephen Greenhalgh. Urine sample collection by free catch was done by myself, Doctor Alison Low, Peter Tennant (LARIF animal technician) and Adrian Ritchie (LARIF animal technician).

6.2.5.1 Anaesthesia and pre-operative preparation

General anaesthesia for trans-urethral catheterisation: Animals were first sedated with an intramuscular injection of Ketamine (7 mg/kg), Medetomidine (7 µg/kg) and Midazolam (0.2 mg/kg). They were then mask-induced with isoflurane 1-3% in 100% oxygen. The pigs were then cannulated on the auricular vein for intravenous access, a 5 mL blood sample was taken, and Hartmann's solution (4mL/kg/hr) was administered. If necessary, intravenous propofol was administered as additional induction to facilitate intubation. 2% Lidocaine was applied topically onto the larynx before the pigs were intubated with a cuffed endotracheal tube of 8-9 mm of internal diameter. The anaesthesia was maintained with an isoflurane in oxygen:air mixture. Heart rate, oxygen levels, spirometry, arterial blood pressure and temperature were monitored throughout the procedure. The eyes of the animals were periodically lubricated during the procedure.

Sedation for short procedures: The animals were sedated with an intramuscular injection of Ketamine (7 mg/kg) and Medetomidine (10 µg/kg). The vital signs of the animals during these short procedures were monitored by checking their reflexes, the colour of the mucous membranes, and measuring the respiratory rate and the pulse. At the end of the procedure, the medetomidine was reverted with an injection of Atipamezole (10 µg/kg).

6.2.5.2 Bacterial inoculation by urethral swabbing

The peri-vulvar region of the pigs was cleaned with dilute povidone-iodine solution. Long OB/GYN swabs (TX705, Texwipe) were dipped into the bacterial suspension, the bacteria were inoculated by swabbing at the urethral opening. This was repeated three times.

6.2.5.3 Trans urethral instillation of phage or bacteria

After the pre-operative preparation, the anesthetised pigs were placed in dorsal recumbency with the pelvis elevated, and the hindlimbs carefully tied to remain pulled cranially. The peri-vulvar region was cleaned with dilute povidone-iodine solution. With aseptic technique, the tip of a Standard Foley catheter was lubricated and then inserted through the urethral opening with the aid of a vaginal speculum when needed. Successful bladder catheterisation was confirmed by the flow of urine from the catheter, after which the balloon of the Foley catheter was inflated. The bladder was emptied by aspiration with a 50 mL syringe. Approximately 50 mL of the urine was collected in sterile Falcon tubes to be used for analysis.

6.2.5.3.1 Bacteriophage instillation

100 mL of the phage preparation was administered to the bladder for the pigs in the safety trial and the experimental group in the efficacy trial. To minimise the risk of immediate expulsion of the phage, the pigs remained under anaesthesia with the catheter occluded for 30 minutes before the balloon was deflated and the catheter was gently removed. The pigs were closely monitored for two hours after the instillation with clinical observations recorded every 30 minutes.

6.2.5.3.2 Bacterial inoculation via trans-urethral catheter

100 mL of *Escherichia coli* strain EC958 suspension (5 x 10^8 CFU/mL) was slowly instilled into the bladder of the catheterised pigs. The pigs remained under anaesthesia with the catheter occluded for 30 minutes before the balloon was deflated and the catheter was gently removed.

6.2.5.4 Blood sample collection

Blood was collected from the pigs in the safety trial at the timepoints indicated in the experimental design (T=0, 24 and 48h) while under general anaesthesia or sedation. A 5 mL blood sample was taken from the jugular or auricular vein and transferred to a red-capped collection tube (BD Vacutainer). The samples were maintained at room temperature for a maximum of 2 hours, then stored at 4ºC overnight and processed for cytokine level measurements on the next day.

6.2.5.5 Urine sample collection

Urine samples were collected by bladder emptying by catheter at the time of the programmed procedures (as indicated in the experimental plan), or by free

catch on different time points at least once per day. The urine samples were collected in sterile 50 mL Falcon tubes, which were then sealed, labelled and stored for a maximum of 2 hours at room temperature before being processed for analysis.

6.2.6 Clinical monitoring of the animals

The animals in both trials were monitored for clinical signs of disease. Constant monitoring was procured in the two first hours after the procedures to detect any severe adverse reaction caused by the bacterial or phage instillation, the anaesthetics or the clinical procedure. After that, the animals were monitored a minimum of twice each day.

The clinical observations were recorded in each occasion and included the measurement of rectal temperature, bladder inflammation signs, body condition, food consumption, activity, respiration pattern, recumbency and hydration status. The scoring and monitoring sheets that were used can be found in Appendix 9.

6.2.7 Medication for treatment of disease

In case the pigs showed signs of mild or moderate illness, administration of non-steroid anti-inflammatory drugs (NSAIDs), specifically Meloxicam at a dose of 0.4mg/kg via intramuscular injection, was indicated.

6.2.8 Termination and post-mortem sampling and analysis

At the end of the studies the pigs were sedated with an intramuscular injection of ketamine (7 mg/kg) and medetomidine (10 µg/kg). The auricular vein was punctured for intravenous access and euthanasia was achieved with the administration of pentobarbital (80 mg/kg). The death of the animals was confirmed by ensuring the cessation of the heart activity with a stethoscope. A final sample of urine was collected by ultrasound-guided cystocentesis.

The abdominal cavity of the cadavers was examined, the bladder, urethra and kidneys were removed, and dissected to expose the mucosal layer or parenchyma and observe any macroscopical changes.

6.2.9 Processing of the blood samples

This part of the work was carried out by the group's Research Assistant, Marianne Keith. The blood samples were left at room temperature for no more than 2 hours and then stored at 4ºC overnight. The next day, the samples were centrifuged at 717 RPM (100 RFC) for 5 minutes to pellet the red blood cells. The serum was harvested and aliquoted in different tubes to avoid freeze-thawing multiple times. These were stored at -75ºC until their use for the Luminex assays. The levels of IFN-alpha, IFN-gamma, IL-1 beta, IL-10, IL-12/IL-23p40, IL-4, IL-6, IL-8 (CXCL8) and TNF-alpha were measured in the serum with a Cytokine & Chemokine 9-Plex Porcine PorcartaPlexTM in a Magpix System (Luminex) following the assay protocol in the user guide by the manufacturer. Each sample was run in duplicate.

6.2.10 Processing of urine samples

6.2.10.1 *In vitro* phage-infection assays

During the acclimatisation period, urine samples were taken from the pigs and used for phage-infection assays. Two 25 mL flasks of filter-sterilised pig urine were prewarmed at 37ºC for 15 minutes. 250 µL of an overnight AU culture of EC958 was added to each flask and these were incubated at 37ºC with shaking for 60 minutes. Three samples were taken, serially diluted and plated for bacterial counts at T=0. The infection flask was then infected with phage LUC4 at and MOI of ~10, and the control flask was added with an SM-LB solution at a 10 to 1 ratio. After 120 minutes of incubation, three samples were taken, serially diluted and plated on LB agar plates for colony counts.

6.2.10.2 Bacterial counts in urine

Urine samples from the inoculated pigs were collected at least once daily by free catch, or by bladder emptying via transurethral catheter on the days of procedure. The urine samples were serially diluted and plated in triplicate on Coliform ChromoSelect Agar (Sigma-Aldrich) with 20 µ/mL of Nalidixic Acid (CCA+Nal agar). Colonies were counted to determine the bacterial burden in urine.

6.2.10.3 Ex-vivo phage-infection assays of infected urine

The rest of the collected urine sample was divided into two equal volumes, one of them was added with 10^8 PFUs of phage LUC4, the other one was added with SM-LB solution as a control. The samples were incubated for 120 minutes

at 37ºC with shaking, after which a sample was serially diluted and plated on CCA+Nal agar for bacterial counts. Single colonies from these agar plates were purified and then challenged with phage LUC4 in AU as described before (2.2.7) to determine the phenotype of the bacterial populations in the samples collected from the infected pigs (Figure 6.1).

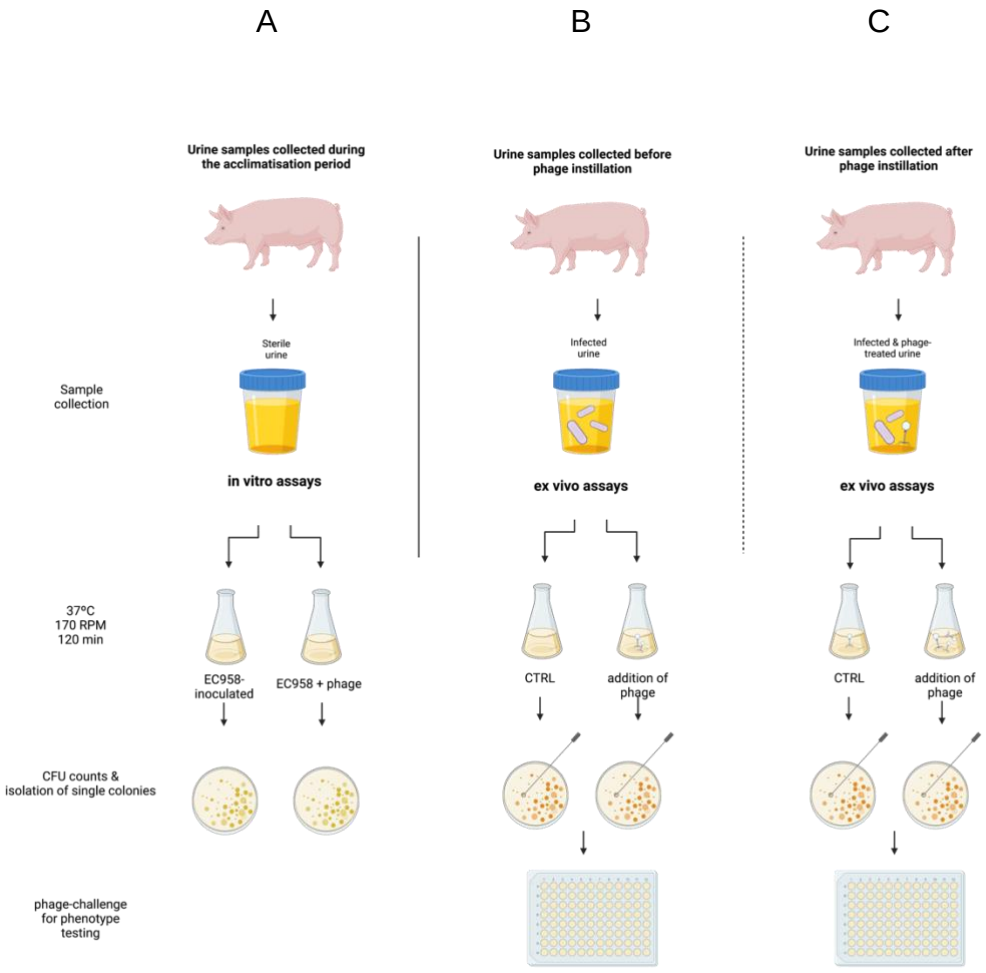

Figure 6.1 Schematic workflow of urine sample processing. Urine samples were collected from the pigs in different stages of the experiment. A) During the acclimatisation process, urine samples were taken, filter-sterilised and used for *in vitro* assays as described above (2.3.4). B) After the bacterial inoculation, but before the phage treatment was instilled in the bladder, and C) after the phage instillation, EC958-infected urine samples were divided in two, one was treated with phage while the other one was left as control, they were cultured at 37ºC for 120 minutes. CFU counts were determined to calculate the mean FC. Finally, single colonies were challenged with the phage to determine the phenotype proportion in each stage of the study.

6.3 Results

6.3.1 Production of detoxified phage using ClearColi™

With the objective of producing phage with low levels of endotoxin, LUC4 was propagated in ClearColi+pWKS30-*ompC*. The neat suspension (titre of 6.85 $x10^{10}$ PFU/mL) was assayed by Doctor Alison Low to measure the endotoxin levels; the results of the assay indicated that the phage suspension contained ~100 EU/mL. Based on the guidelines by the USDA (Brix *et al.*, 2020) the maximum amount of endotoxin recommended for parenteral administration is 5 EU per kg of body weight. The body weight of the pigs ranged between 40 and 45 kg, for which one part of the neat suspension was diluted in 50 parts of medical grade 0.9% NaCl solution. With this a final product was obtained, which complied with the recommended maximum endotoxin concentrations and had still had a high titre. The stability and infectivity of the phage was confirmed after 48 hours at 4ºC. This suspension had a pH of 7.5 and proved to be sterile after 48 hours of incubation at 37ºC.

The adsorption rate of the phage was tested in 0.9% saline solution. 94% of the phage adsorbed to EC958 within 25 minutes. This proportion of the adsorbed phage is similar to what is seen in LB (93%), although at a slightly slower pace (Figure 6.2).

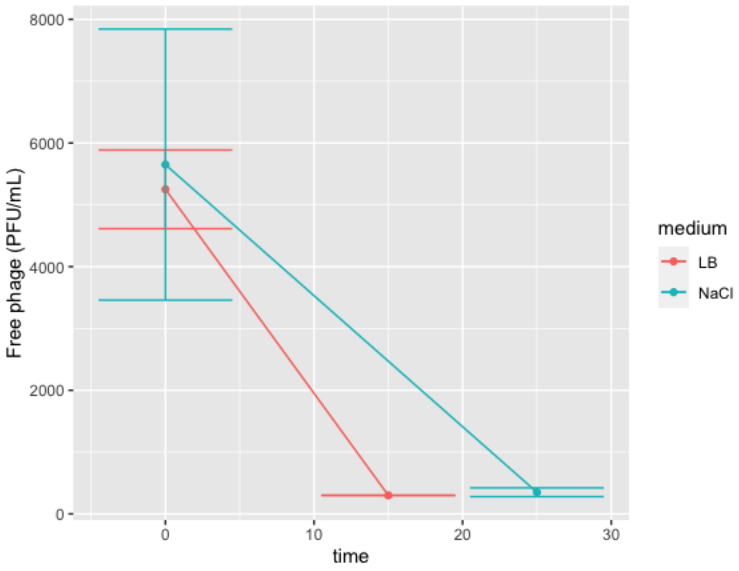

Figure 6.2 Adsorption assays of phage LUC4. To ensure that the phage is able to adsorb to E. coli EC958 when suspended in 0.9% NaCl solution, the adsorption rate was measured in vitro. Results show that >90% of phage LUC4 LB is able to adsorb in 0.9% NaCl solution, and in LB.

6.3.2 Bacteriophage safety trial

6.3.2.1 Transurethral administration of phage suspension does not cause adverse effects or severe inflammation in the pig model

The amount of endotoxin that is released during phage propagation is one of the major concerns for safety of phage products. Macrophages and other immune cells are sensitive to LPS, which respond by producing cytokines such as IL-1, IL-6, IL-8, and TNF-α. The inflammatory response is likely to cause clinical symptoms such as high fever, leukopenia, tachycardia, tachypnoea and hypotension (Schneier et al., 2020). We are interested in proving that therapeutic phage suspensions are safe to be administered into the bladder without further processing. After the phage instillation, the animals in the safety trial were constantly observed during their recovery from anaesthesia and for two hours post instillation. Their breathing rate and pattern, food and water consumption and social behaviour was observed and recorded during this period. No abnormalities in these indicators were observed during these first hours. Thereafter, the monitoring was spaced out to twice a day. There were no abnormalities observed in the health indicators throughout the study.

Likewise, cytokine levels in blood at 24 and 48 hours indicated that no significant effect was created by the administration of phage. TNF-alpha, IFN-gamma, IL-4, IL-6, IL-10 and IL-1 beta levels in all samples of all timepoints were below the detectable level (data not included). IFN-alpha, IL-12/IL-23p40, IL-8 (CXCL8) levels at 24- and 48-hours after the phage instillation were not significantly different to the baseline levels at T=0 (Figure 6.3). With these and the clinical monitoring results, it was concluded that the transurethral instillation of phage produced with ClearColi+pWKS30-*ompC* and adjusted to a concentration of 5 EU/kg is safe in the pig model.

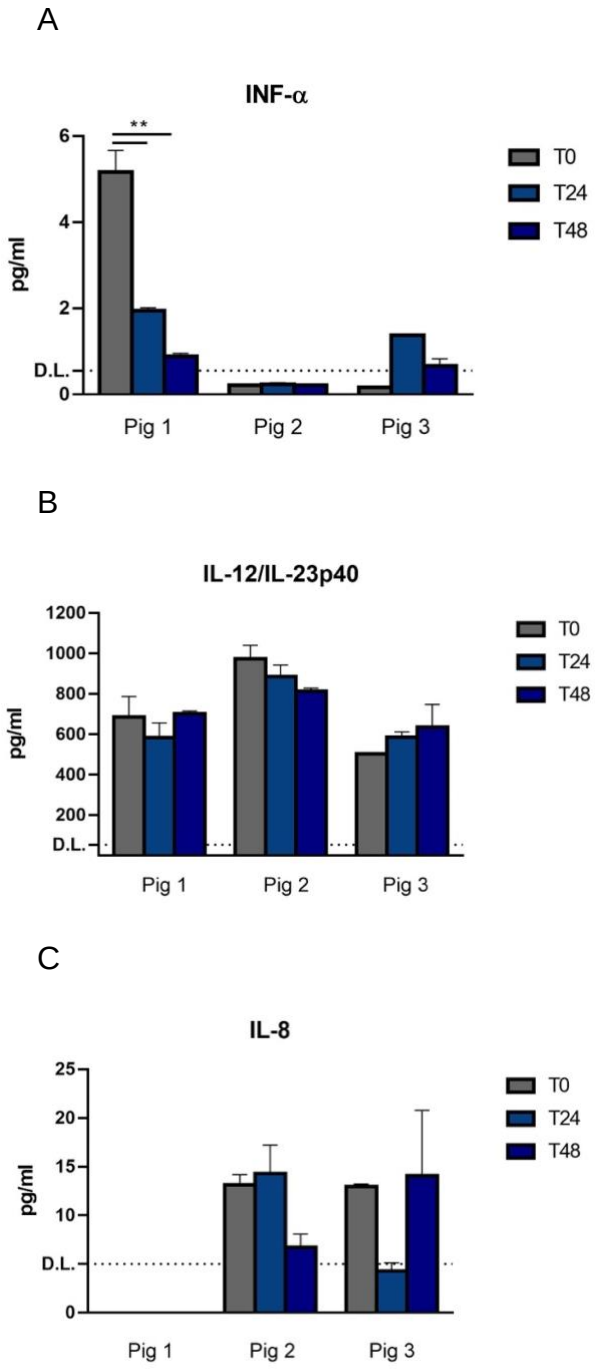

Figure 6.3 Circulating levels of cytokines in the bacteriophage safety trial—Samples were processed by Marianne Keith; data was plotted by Alison Low and statistical analysis was carried out by Joana Alves. Cytokines were measured in blood before (T0) the transurethral administration of phage LUC4, as well as 24- and 48-hours post instillation. The administration of phage did not cause a significant increase in A) IFN-alpha, B) IL-12/IL23p40 and C) IL-8 (One-way ANOVA with multiple comparison tests). Data represents the mean concentration in each animal based at each timepoint on two technical replicates. Dotted lines represent the detection level. All other cytokines were below the detection level.

6.3.3 Pilot study for the development of a porcine model of UTI

6.3.3.1 Bacterial inoculation by transurethral catheterisation is a more reliable method to establish a UTI in the pig model than the swabbing method

With the aim of establishing more refined and less invasive methods in animal experiments, we were keen to replicate the bacterial inoculation by swabbing reported by Jeffrey Fernandez (Senior Scientist, Janssen Research & Development) and Jessica Henn (Associate Scientist, Janssen Research & Development) in an online seminar (Fernandez, 2020). This method was carried out on the control group at the beginning of the trial. Following the inoculation by swabbing, bacterial shedding levels in Pig 1C appeared always low. In addition, no pyrexia or clinical signs of bladder inflammation, were observed. For these reasons, at 72 hours post-swabbing (decision-making point), it was decided that transurethral catheterisation for direct bladder inoculation was needed, as the UTI had not successfully established in this pig (Figure 6.4, red dotted line).

Pigs 2C and 3C had low levels of bacteriuria at 24-, 48- and 72-hours post-swabbing and no pyrexia or changes in food and water consumption had been observed. However, some clinical signs had been observed that suggested bladder inflammation and discomfort, which led us to think that the UTI could still be establishing and the bacterial counts would increase in the following days. In order to establish whether the bacteria needed several days to properly colonise with the swabbing method, the pigs did not get a second inoculation at this point. Unlike what was expected, the bacterial counts in the urine of pigs 2C and 3C decreased to undetectable levels on the next days. At T=168 instead of receiving the control treatment, the pigs were reinoculated with EC958 via transurethral catheter (Figure 6.5, top panel, black dotted line). After the inoculation by catheter, bacterial counts in urine remained above 10^5 CFU/mL for all control pigs.

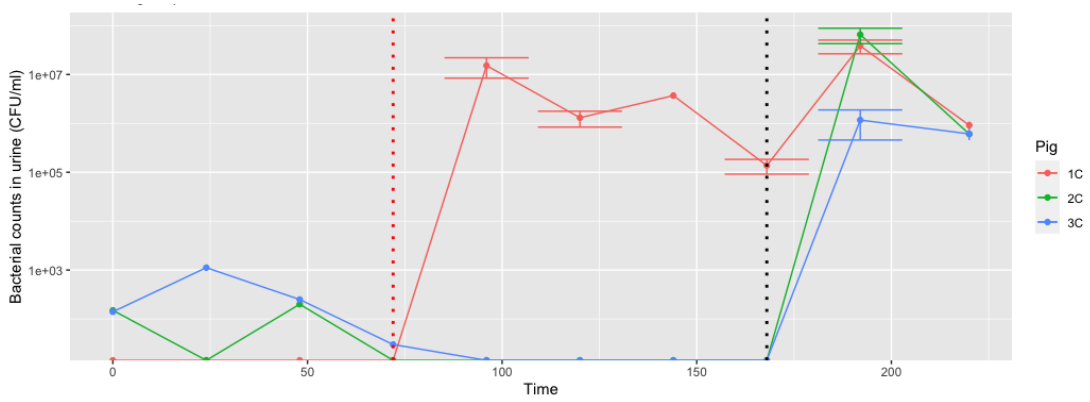

Figure 6.4 Pilot study for the development of a porcine model of UTI: Bacterial shedding in urine. Pigs in the pilot study for the development of a UTI model were inoculated with *E. coli* EC958 by the swabbing method at T=0; Pig1C was inoculated via transurethral catheter at T=48 (red dotted line), after which the bacterial levels increased and remained above 10^5 CFU/mL. Pigs 2C and 3C were inoculated via transurethral catheter at T=168 (black dotted line), after which the bacterial counts in urine increased above 10^5 CFU/mL.

6.3.4 Pilot study of Phage Therapy efficacy

6.3.4.1 A single dose of phage LUC4 has no long-term effects reducing the levels of bacteriuria

Since the swabbing method did not give the expected results in the UTI model development trial, pigs in the PT-experimental group were inoculated with EC958 via transurethral catheter at the beginning. Pigs 1T and 3T showed signs of bladder inflammation approximately 8 hours after the procedure, such as stranguria. Despite this, their overall social behaviour and food consumption remained unaffected, and the signs of inflammation were self-resolved by 24-hours post-infection. Pig 2T, on the other hand, did not show the same initial signs of bladder inflammation, but at 48 hours post-infection, signs of mild illness started to appear: her activity and social engagements were reduced, and her temperature and respiratory rate were above normal. As the protocol indicated, meloxicam was administered, which alleviated the pyrexia and other clinical signs but did not affect the bacterial colonisation of the bladder.

Bacterial counts were generally above 10^4 CFU/mL during the first 48 hours post-infection for all pigs in the experimental group, but could vary substantially from one sample collection to the next (Figure 6.5). Pig 1T remained with high levels of bacteriuria until the time of treatment, whereas Pigs 2T and 3T had more variation in the bacterial counts: bacterial counts in Pig 2T decreased substantially from T=72 to the time of treatment instillation, by which the bacteriuria was at 1.13 X 10^3 CFU/mL; Pig 3T had nearly cleared the UTI, and by the time of the phage instillation the bacteriuria levels were close to the detection limit (33 CFU/mL).

One of the objectives of the porcine model of UTI and PT was to observe the effect of the lytic phage *in vivo*. As mentioned above, one pig (3T) had almost completely cleared the UTI before the time of the treatment, therefore, it cannot be concluded whether the reduction from 33 CFU/ml in urine to undetectable levels was caused by the phage treatment. Both, Pigs 1T and 2T had a reduction of bacterial burden in urine in the first hours after the procedure (Figure 6.5, blue line), but the extent of each one was dramatically different: a 4.7 $\log_{10}$ reduction was observed in Pig 1T three hours after the administration of phage, whereas a more modest fold reduction of 0.64 was detected in Pig 2T. The effect in bacterial inhibition was very short-termed in both cases, as in the following sample collection (4- and 3-hours post treatment for pig 1T and 2T, respectively), the bacterial levels in urine were on the rise again, and remained as such for the rest of the study.

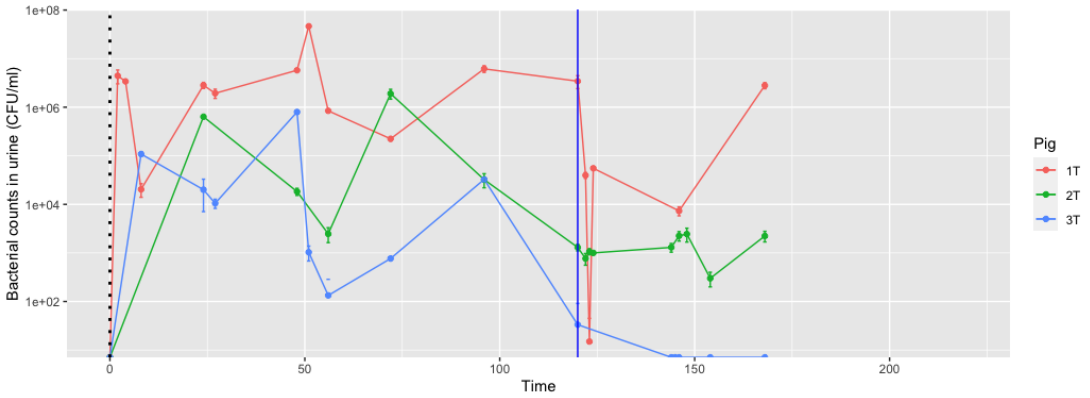

Figure 6.5 Pilot study of the efficacy of PT: Bacterial shedding in urine. Pigs in this pilot study were inoculated with EC958 via transurethral catheter on T=0 (black dotted line), and were bladder-instilled with the phage-treatment at T=120 (blue solid line). A dramatic --but short-lived—drop of bacterial counts in urine could be observed in pig 1T. A more subtle drop was observed in pig 2T. Bacterial counts in urine of pig 3T are not possible to interpret, as this individual seemed to have a self-resolving UTI and was close to clearing the infection by the time of the treatment.

6.3.4.2 Lesions in the bladder mucosa

At the end of the study the pigs were euthanised and their bladders, kidney and urethra were harvested in the post-mortem examination. Figure 6.6 shows the mucosal layer of the bladders. The bladder of the three pigs in the control group show dark red spots, indicative of haemorrhage; whereas from the experimental group, only the bladder from Pig 2T presents such lesions and there are less extensive (Figure 6.6, bottom middle panel). The bladders of Pigs 1T and 3T did not show any macroscopical alterations. Due to the differences in the time of the bacterial inoculation, treatment and harvesting of the organs between both groups, it is not possible to state with confidence that the reduced bladder damage was due to the phage treatment. The kidney and urethra of all pigs had no apparent pathological changes, which may indicate that this model of infection is appropriate to study the localised infection of the bladder without further ascension.

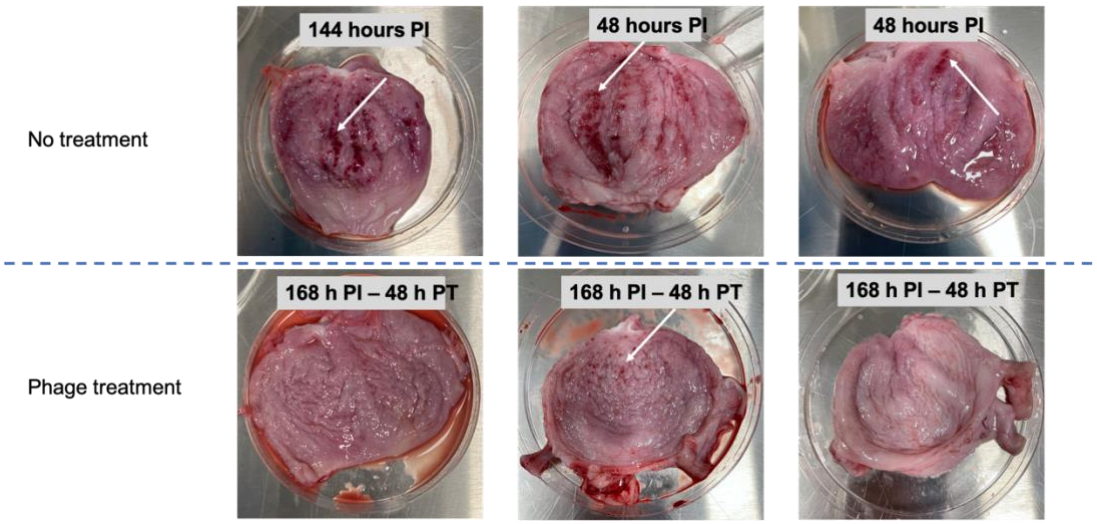

Figure 6.6 Lesions in the mucosal layer of the bladder. Dark red spots, indicative of haemorrhage, were found on the bladder mucosa of the infected pigs. The pigs who received the phage-treatment appear to have less extensive lesions, but the time of organ harvesting was different, for which it is not possible to affirm with confidence that this could be caused by the phage

6.3.4.3 *Ex vivo* assays: phage LUC4 does not lyse EC958 as readily in infected pig urine

In the infection assays with AU a lysis event caused by the phage is reflected as a dramatic drop in bacterial counts (Figure 3.6). In a similar way, a 4.5 $\log_{10}$ reduction is observed 120 minutes after phage infection in an *in vitro* assay carried using uninfected pig urine (Figure 6.7A).

During the trial, the urine samples from the infected pigs in the experimental control were used in *ex vivo* assays with phage LUC4. For this, the infected urine samples were divided into two equal volumes, one was infected with phage and the other one was left as control. Bacterial counts were determined at Times = 0 and 120 to calculate the fold change for each condition.

The results of the assay show that phage LUC4 affects the bacterial population differently when these have been growing in the pig bladder. Several different outcomes could be observed: 1) the phage treatment could have a lysing effect, in which case the bacterial counts would be reduced; 2) or it could lead to a slower bacterial replication rate, and 3) in one sample from pig 2T, the bacteria replicated at a faster rate in the presence of phage than the control. The outcome could vary from sample to sample within the same individual (Figure 6.7B).

On the occasions in which a lysis event was observed, the reduction in bacterial counts was more subtle than what had been seen in the *in vitro* assays: a maximum reduction of 2 $\log_{10}$ was observed in the *ex vivo* only in one of the assays, which suggests that the bacteria growing in the bladder conditions are less susceptible to the phage than *in vitro*.

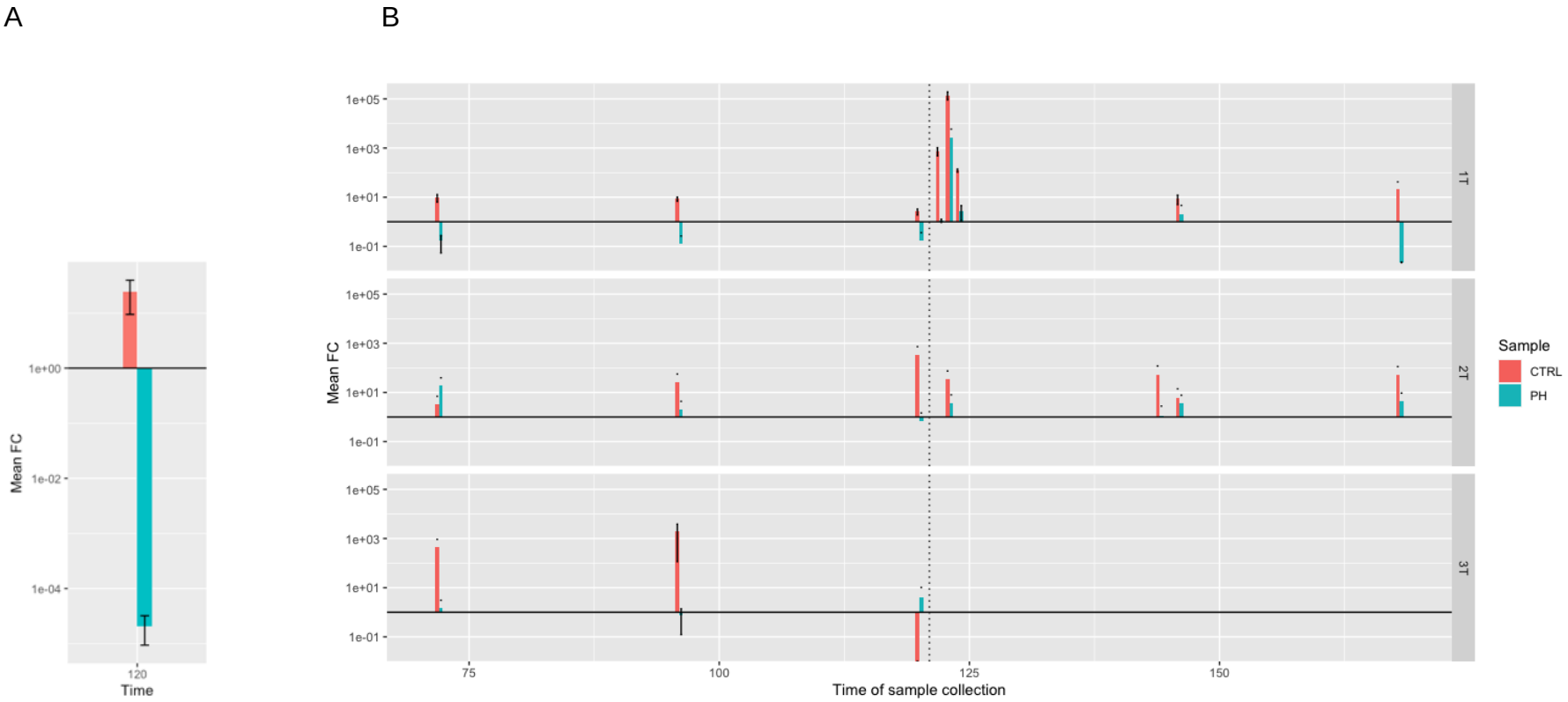

Figure 6.7 Differences of in-vitro and ex-vivo response of EC958 to phage LUC4. A) *In vitro* infection assays in sterile pig urine show a 4.5 $\log_{10}$ reduction of EC958 120 minutes after the addition of phage LUC4. B) *Ex vivo* assays with infected pig urine during the trial show that the addition of phage does not always cause a reduction of bacterial counts; and when it does, it is not as dramatic as the *in vitro* assays had shown.

6.3.4.4 The population of EC958 after the administration of PT, is mostly susceptible to the phage

In the previous chapters it has been demonstrated that the surviving population of EC958 to phage LUC4 infection is heterogeneous: there is a fixed-resistant subpopulation (resistant) and a transiently resistant population (susceptible) (4.3.1). One of the aims of the animal model of UTI and PT was to determine whether the EC958 populations had a similar composition *in vivo* to that of the *in vitro* assays. The relevance of the different resistance mechanisms in the animal host can shed light into the most important issues to be addressed for applied PT.

Single colonies were isolated and phenotype-tested before the administration of the phage treatment in order to observe the composition of the naïve EC958 population in the bladder. As was expected, all the single colonies taken from the control assays (naïve EC958 population) gave rise to phage-susceptible populations, (Figure 6.8, CTRL). After being challenged with the phage *in vitro*, 4 (4.4%) of the 90 single colonies isolated gave rise to phage-resistant populations, but the vast majority (95.6%) had the susceptible phenotype (Figure 6.8, PH).

When the urine samples were collected after the pigs had received the phage treatment (Time>120), all the single colonies that were isolated directly from the pig tested as phage-susceptible (Figure 6.9, PH). Since there was a possibility that some of the bacterial cells might not have been in contact with the phage in the bladder, the urine sample was treated with more phage. When single colonies were isolated, purified and re-challenged with phage, 12 (13%) resistant colonies were isolated. The variants that were resistant to the phage were tested again with the phage but they had reverted to susceptible (Figure 6.9, PHX2).

Figure 6.8 Phenotype of individual colonies isolated from infected pig urine before the administration of phage. To determine the proportion of phenotypic variants in the bacteria colonising the pig bladders, single colonies were isolated and challenged with phage LUC4. All the colonies tested directly from the pig urine were susceptible to the phage (CTRL); when the infected urine was exposed to the phage, and single colonies were isolated 120 minutes after infection (PH), only a 4% of resistant variants were observed.

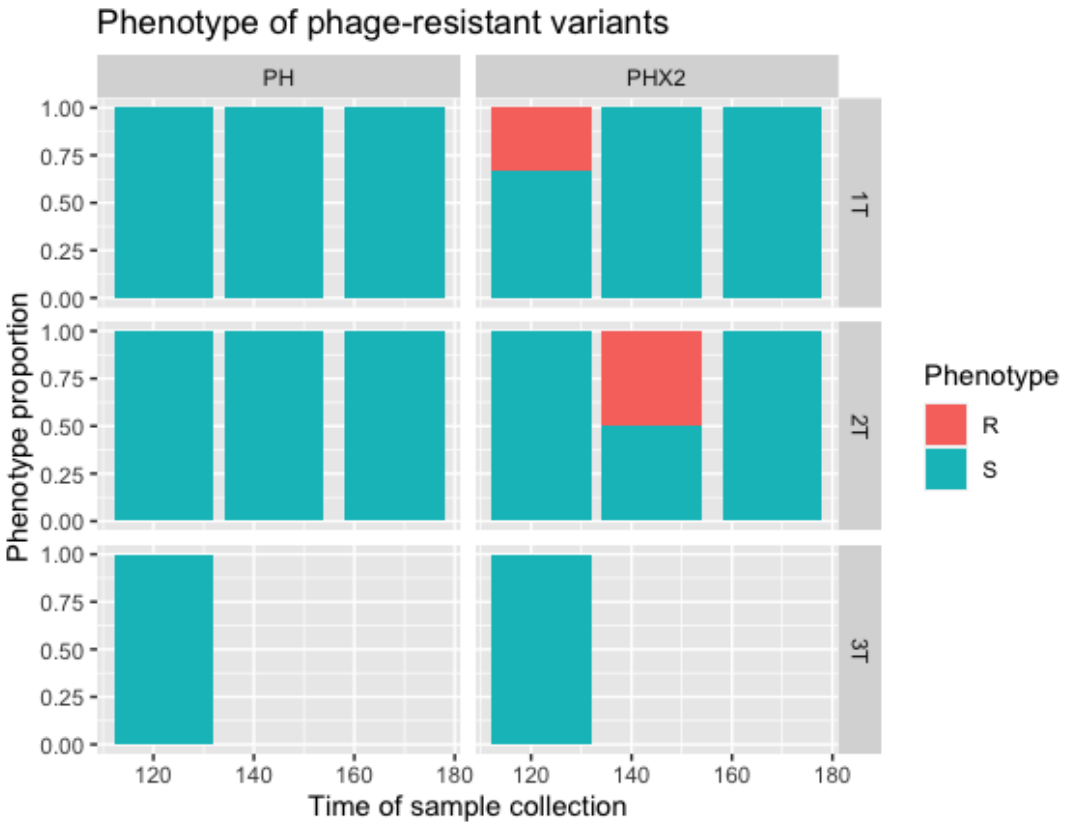

Figure 6.9 Phenotype of individual colonies isolated from infected pig urine after the administration of phage. Single colonies were isolated and challenged with phage LUC4 to determine their phenotype. All the colonies tested directly from the pig urine (PH) were susceptible to the phage, despite having been exposed to the phage in the bladder; when the infected and treated urine was further exposed to the phage *in vitro*, 13% of resistant variants were observed for pig 1T and 2T, respectively.

6.4 Discussion

Domestic pigs and mini pigs have increasingly been proving to be a suitable model to study human diseases. For pathologies of the urinary tract, pigs have similar anatomy, physiology and urodynamics as humans. In addition, pigs are better suited than mice to mimic the production of proinflammatory cytokines seen in humans in response to LPS.

Lipid A in the lipopolysaccharide of Gram-negative bacteria can trigger a strong inflammatory response characterised by the production of proinflammatory cytokines (Daneshian et al., 2006) and activation of the coagulation cascade (Anspach, 2001). Phage therapy relies on bacteria for the production of the therapeutic preparations, which means that large amounts of endotoxin are released when the phages are propagated. To make these phage products safe for animal and humans, the endotoxin has to be removed, which is a major challenge for biopharmaceutical manufacturers and can be expensive, laborious and needs special equipment (Saraswat et al., 2013; Wilding et al., 2019). Thus, a large part of research and development is dedicated to developing effective and low-cost endotoxin removal methods.

Genetically modified *E. coli* strains that produce low endotoxin have been developed with the purpose of bypassing the need of downstream LPS removal. Here, we aimed to use ClearColi™, a detoxified *E. coli* strain, to produce a phage preparation that was ready to be administered without further downstream processing. Levels of endotoxin were measured *in vitro* with the HEK-Blue assays and the phage suspension was adjusted to the recommended concentration for animal use. The safety of the phage product was tested *in vivo* with the pig model, by measuring the levels of inflammatory cytokines and monitoring the overall health of the animals. The results indicated that the phage produced in ClearColi™ can safely be instilled in the bladder of the pig model via transurethral catheter.

The second main objective of the pilot studies was to establish a swine model of UTI. A yet unpublished method of inoculation by swabbing was tested in the control group with the purpose of a) using less invasive and more refined methods and b) establish an ascending bladder infection that better replicates the community acquired UTIs. The pigs that were swabbed were not colonised as expected. While two of the pigs were shedding low levels of bacteria in urine during the first two days post-inoculation, it is likely that this was an effect of the bacteria that were able to colonise the site of inoculation. They nevertheless did not manage to ascend into the bladder, for which it was concluded that the swabbing method needs further optimisation. The bacterial inoculation by transurethral catheter was a more reliable method to ensure the establishment of *E. coli* infection, as has been shown before (Nielsen *et al.*, 2019). Most of the pigs (5/6) kept shedding at $>10^4$ CFUs/mL (average level), and the clinical signs of bladder inflammation and discomfort were resolved by the second day after infection without the need of medication. Only one individual showed further clinical signs of infection like fever and reduced physical activity, but these were easily treated with the administration of NSAIDs. However, one of the pigs (3T) in the experimental group did not manage to retain the infection for a period that was long enough to see the effect of the phage (Figure 6.5, bottom panel, blue curve). It is hypothesised that this effect is due to individual differences that make some animals more resistant to chronic infection. For instance, it has been seen that the host immune response can affect the bladder colonisation: if it is too vigorous, the inflammation in the mucosa can lead to a chronic infection (Flores-Mireles *et al.*, 2015; O'Brien et al., 2015); whereas a weak lymphocytic response can inhibit the development of the UTI, as is seen in immunocompromised mice (Hannan et al., 2012). Optimising the inoculum dose to make it more similar to a natural ascending infection could also lead to better outcomes in the bladder colonisation and persistence of bacteriuria.

The administration of phage LUC4 to treat the EC958 infection caused a reduction of bacterial counts in urine but this was very short-lived. Based on the *in vitro* assays in urine that had been carried out previously, a resurge of

the bacteria was not unexpected. In both, *in vitro* and *in vivo* assays, the onset of resistance was noticeable between 180 and 240 minutes after the administration of phage, but the increase in bacterial numbers was more dramatic in at least one of the pigs; whereas in flasks, the recovery of the bacterial population is slower. An important observation here is that urine sample collection can be problematic in pigs. The animals had different behaviours in water consumption and urine production. For this reason, samples can have different concentrations or some urinations can be missed. A complete picture of the infection dynamics was therefore not always possible. For instance, although the reduction in bacterial numbers after the phage instillation in pig 2T was not as dramatic as the one seen on pig 1T, we are aware that the earliest morning urination could have happened while the team was catheterising, sampling and treating pig 1T. Pig 2T was therefore not completely attended and said sample could have had a higher burden of bacteria.

Most PT efficacy studies do not report and/or investigate, the cause of resistance of bacteria (McCallin *et al.*, 2019). Even studies with unsuccessful outcomes, fail to inquire into the mechanisms. In our group, one of the objectives of establishing an animal model of UTI and PT is to be able to study the cause of resistance *in vivo*. In this pilot study, as had been anticipated, the phage resistance observed was mainly caused by a transient mechanism; whereas the genetic mutations that lead to impaired phage adsorption were not seen. Other research groups have found that the phage resistance that the UPEC had acquired was due to genetic mutations in the phage receptor with a murine model, which came with a fitness cost that impaired the ability to adhere and colonise the bladder tissue (Salazar *et al.*, 2021; Zulk *et al.*, 2022). In contrast, the vast majority of the resistant variants that were isolated here were susceptible to the phage in an *in vitro* challenge, which indicates that the type of resistance is of different nature. The handful of single colonies that appeared to be resistant to the phage reverted to susceptible on the second assay. This is likely due to the unstable phase variation that was described above (4.4) and reported by other research groups (Scott *et al.*, 2007), which

selects for the susceptible phenotype in the purification passages to regain its fitness when the predatory pressure is not present. To rule out that these colonies were not misclassified as resistant in the first infection assay due to human error, the experiment would need to be repeated at least twice more, which was not possible in this case. However, the reiterated observation of this effect makes it likely that a reversible phase variation caused these changes.

Ex vivo phage-infection assays were carried out with the urine samples collected from the pigs. For this, the urine samples were divided into two equal volumes; one was treated with phage and the other one was incubated without phage as a control. The fold change was calculated for both at 120 minutes. Different outcomes were observed with the addition of phage: some would have a decrease in the bacteria count from the initial timepoint; in other occasions the bacterial culture was seen to slow down the replication rate; and a few more were not affected by the phage. It is noticeable that the reduction of bacterial counts caused by the phage is not as pronounced and reproducible in the *ex vivo* assays, which indicates that the population that was growing in the bladder resulted less susceptible to the phage, compared to the *in vitro* assays with fresh pig urine.

The results obtained in this pilot study may suggest that the AU medium and the *in vitro* methods that have been used in the lab are valuable and they can represent the phage-bacterium dynamics in the bladder of mammals to a certain extent. However, the major differences in time of bacterial recovery and susceptibility to the phage indicate that there are still gaps that need to be understood to be able to replicate with more fidelity the *in vivo* conditions.

The power to draw conclusions with confidence from these pilot studies is limited due to the reduced animal numbers. Yet, they were useful to find the most adequate and practical methods to be used, and note which ones need further optimisation for future trials with the swine model of UTI.

Chapter 7 General discussion

Antibiotic resistance (ABR) is a global problem that is projected to cause 10 million deaths by 2050 if not addressed (WHO, 2018). The *E. coli* clonal complex O25:H4-ST131 is associated with ABR urinary and blood infections, it is widely distributed in the world, and it is characterised by being highly pathogenic (Nicolas-Chanoine *et al.*, 2014). Given the health threat they pose and the difficulty of treating these infections with conventional antibiotics, new interventions are desperately needed. An interest in phage therapy has re-emerged amidst the search for alternative ways of preventing and treating bacterial infections, but, arguably, few advances have been made in the implementation of phage therapy in clinical practice, especially as a widespread intervention. This project aimed to address some of the issues of phage therapy by establishing *in vitro* and *in vivo* models for *E. coli*-associated urinary tract infection so that phage-host interactions could be examined under more realistic conditions. The research enabled a study of how clinical *E. coli* isolates respond to phage predation focusing on a well characterised ST131 strain: EC938.

There has recently been extensive phage research to aid a deeper understanding of the genetic basis of phage infection, the bacterial response and counter strategies evolved by phage. Despite this, the actual successful application of phage therapy is less common than wished for. One of the reasons may be related to the infection models and laboratory media that are routinely used, which can differ from the results observed *in vivo* (Casey *et al.*, 2018). For instance, the most common method to test phage-susceptibility of bacteria is by spotting serial dilutions of the phage on the bacterial host growing in soft overlay agar. This method is routinely carried out with laboratory growth media which are rich in nutrients, such as LB. In contrast, the urinary tract is a hostile environment with relatively limited nutrient availability. To survive in the urinary tract, UPEC relies on *de novo* synthesis pathways to acquire nutrients (Vejborg *et al.*, 2012); and to colonise it, virulence factors need to be activated (Blango and Mulvey, 2010). Since the *in*

vitro models are not representative of the natural environment in which phages and their hosts are found, it is not surprising that unexpected outcomes are observed *in vivo (Casey et al., 2018)*. In order to close the gap between the data generated *in vitro* and the phage activity *in vivo*, phage-host interactions should be studied in similar conditions to those found in the required site of phage activity, in this case urine and the lining of the urinary tract. In line with this, an artificial urine (AU) medium was optimised and tested for the study of *E. coli*-phage interactions. The final AU medium proved to be similar to pooled canine urine (PU) in that interactions generally appear to have similar trends in both media. In addition, it greatly reduces the issue of chemical variability seen in natural urine (Bouatra *et al.*, 2013).

When studying the interaction of ST131 UPEC strain EC958 and phage cocktails in different media, there were significant differences in the inhibition achieved by the same cocktails in the different media. Complete inhibition of EC958 was relatively easy to achieve with most of the three-phage cocktails in LB, whereas in AU, a consistent resurgence of the culture was observed in every assay. It then became evident that LB was masking a form of phage-resistance that was present in urine.

By breaking down the infection and analysing the phage-resistant population, using LUC4 as phage 'model' for the observed resistance issue, it was revealed that at least two forms of resistance were in play: one leading to a population with a fixed resistance, and the other one which was a transient event in which the surviving population regained susceptibility to the phage in subsequent assays. The assays carried out in LB, only rendered fixed-resistant variants. The AU, in contrast, succeeded in replicating both, fixed and transient forms of phage-resistance of *E. coli* EC958 observed in pooled canine urine and in the bladder in the pig model.

By analysing the genomes of the fixed resistant variants, it was seen that this was caused mostly by SNPs and other chromosomal changes driving the loss of OmpC. The acquisition of genetic mutations in the gene encoding the phage receptor is a commonly reported mechanisms of phage-resistance (Hampton

et al., 2020; Labrie *et al.*, 2010; Rostol and Marraffini, 2019). Likewise, *ompC* variants frequently appeared in EC958-LUC4 cultures, leading to a fixed resistance. This type of resistance that is important to prevent. Although not many clinical studies determine the cause of phage-resistance *in vivo,* some have proved that genetic mutations in the phage receptor led to resistance.

One of the most common methods used to avoid phage-resistance in PT is the use of cocktails, especially those that are prepared with awareness of the infecting properties of each component (Gordillo Altamirano and Barr, 2021; Li *et al.*, 2022; Molina et al., 2022; Niu *et al.*, 2021). For certain cases, such as in immunocompromised patients, addressing this resistance is of especial importance, as the full clearance of the bacterial infection is preferred. In agreement with other successful reports of phage cocktails, the addition of certain phage combinations prevented the rise of this resistant population in LB (Figure 3.10Figure 3.11). Interestingly, in artificial and natural urine cultures, this was not the case. This suggested that the rise of resistance due to genetic mutants was avoided (or delayed) with three-phage cocktails.

Although using the phages in our current collection will not prevent the transient resistance. Nevertheless, it is possible that diversifying our phage library can make a difference in the potential spectrum of the phage cocktails. So far, nearly all the phages in our library have been isolated from waste water samples. Phage isolation form sources (*e.g.* the ocean) could result in finding phages with different infecting or metabolic characteristics. For instance, studies in *E. coli* have seen that 91% of the nitrogen for phage T6 production was sourced from the medium (Kozloff et al., 1951), whereas marine phages of cyanobacteria acquire 40% of nitrogen from the extracellular medium. The difference in these proportions may lie in the theory that marine bacteriophages have adapted to source most of their nutrients from the host, as the external environment contains low concentration of nutrients. In contrast, phages of enteric bacteria can rely on external sources of nutrients (Waldbauer et al., 2019). This is something to consider when the isolation of

phages with a diverse range of metabolic abilities is of interest for the formulation of cocktails.

The pressure of phage LUC4 also selected for *ompC* variants in AU, but they could mostly be isolated shortly after the bacterial culture had started to collapse (2-4h PI). As the time went on, a transient cause of resistance was seen, which was not possible to prevent with cocktails or higher MOIs. Addressing the transient resistance has proved to be more difficult and, in some ways, more important (Figure 4.11). This transient effect allowed a genetically identical resistant population to thrive and outcompete the fixed-resistant variants due to a fitness advantage, even though the phage was still present in considerable concentrations. Assays carried out in PU echoed the AU results, which gave a further validation of the *in vitro* model, and also highlighted the importance of understanding the transient resistance: the fact that it was consistently observed in urine assays indicates that this barrier to treatment might appear in clinical settings. Accordingly, the UTI pig model confirmed that the transient resistance is more impactful than the fixed variants *in vivo*, and the one that is more urgent to address.

It was presumed that previously characterised anti-phage systems were not the sole cause of this transient resistance, despite some of them being encoded in the EC958 genome. The reasons were twofold: first, this transient resistance is not observable in LB, which is a medium that has commonly been used for the characterisation of many of these systems; second, a differential expression analysis with RNA-seq showed no significant upregulation of these systems, except for one the AbiE system. This abortive infection system is a reversible bacteriostatic system that functions through a Type IV toxin-antitoxin mechanism (Dy et al., 2014a). Even though it is unlikely that the AbiE system is causing the phage resistance on its own, it is possible that it is partially involved. The bacteriostatic effect may come into play during the first cycles of infection, but the predatory pressure needs to be removed before the bacteria resume the growth. In this case, the phage remains present and infective

throughout the time course, thus, it is hypothesised that another mechanism comes into play here.

Based on the observations that 1) this resistance can be transferred with the supernatant of infected and uninfected cultures, 2) but the protective effect is concentration-dependent (it can be delayed when the supernatant is diluted with fresh AU), it was initially speculated that a small signalling molecule that is released and accumulates in the supernatant could be triggering the resistance. Quorum sensing (QS) has been found associated with bacterium-phage interactions in different ways: controlling biofilm production (Hammer and Bassler, 2003), downregulating surface proteins to reduce adsorption (Hoyland-Kroghsbo *et al.*, 2013), phage lysis-lysogeny switching (Duddy et al., 2021; Tan et al., 2020), regulating of CRISPR-Cas systems (Patterson et al., 2016) and altering the metabolic state of the population (Qin et al., 2017). Hoyland-Kroghsbo *et al.* (2013) found that a QS molecule could reduce the levels of expression of the phage receptor in *E. coli* and consequently inhibit the adsorption by half. Similarly, Ding et al. (2021) found an association between the autoinducer-2 (AI-2) and resistance to phage T4 in *E. coli*. It was partly attributable to the under-expression of the phage receptor and to the downregulation of cellular metabolism achieved by reducing the expression of global carbon regulatory genes. In this study though, it was established that there was no significant impact on adsorption of LUC4 to EC958 when cultured in the supernatant—where presumably the QS molecule would be, but the possibility of QS-driven metabolic downregulation was not discarded.

Qin *et al.* (2017) also found that QS is associated with the downregulation of metabolism and the physiological state of bacteria, which in turn reduced the susceptibility to phage. These reports led to another hypothesis along the lines of metabolism, carbon sourcing, the physiological state of bacteria and nutrient availability.

The chemical composition and nutrient availability of LB and urine are quite different. Certain nutrients that are in low concentrations in urine may be depleted quickly because they are the preferred carbon source. Rather than

containing a QS molecule, the supernatant could quickly be depleted of nutrients that are necessary for the phage to multiply but allow the bacteria to still grow.

It is commonly assumed that the rate of virus multiplication is a relative to the host growth rate. In other words, the host needs to be actively replicating for most phages to be able to infect them and produce progeny (Bryan *et al.*, 2016; Cohen, 1949). This is true for models growing in nutrient-rich media: in these cases, phages will have larger burst sizes when infecting a culture in exponential phase, and smaller when the host is in lag phase (Price, 1948); whereas many phages are unable to infect and produce progeny when the host is in stationary phase (Bryan *et al.*, 2016). However, under certain conditions, multiplying bacteria are not essential for virus multiplication (Anderson, 1948; Herriott and Price, 1948; Krueger and Fong, 1937; Rouyer and Latarjet, 1946), and some compounds can be inhibitors of bacterial growth whilst allowing phage multiplication, and vice versa (Cohen, 1949). In addition, some nutrients like Ca++, MG++, tryptophan, can be essential for the production of certain phages, but not for the replication of the host (Wahl, 1946). Phages and their hosts can also differ in their need for external nutrients. Some phages need to source some nutrients, like phosphorous and nitrogen, from the medium to be able to replicate (Fowler and Cohen, 1948; Waldbauer *et al.*, 2019). Hence, if these nutrients are not available in the medium, the phage cannot multiply. Furthermore, when minimal medium is supplemented with certain individual amino acids like L-phenylalanine, L-aspartate, L-proline, L-lysine, L-valine, L-arginine or L-glutamic acid, virus production is enhanced, which resulted in shorter latent periods and larger burst sizes (Spizizen, 1943).

A key experiment to test this hypothesis would be to supply different carbon sources in different concentrations to the EC958-LUC4 cultures in AU and supernatant and observe any differences in susceptibility. Comparing these effects in strains which are not capable of resisting phage LUC4, such as ClearColi+pWKS30-*ompC* and PFEC, may also reveal differences that are

important for this effect. Comparative transcriptomic analysis of the bacteria growing in nutrient-limited and nutrient-rich media could be carried out. Candidate genes that are differentially expressed should allow hypotheses to be formulated and tested about the molecular mechanism of the phage inhibition.

Understanding how the nutrient availability and metabolism can influence the bacterial interaction with phages could lead to the decision of the formulation of phage products to avoid or delay resistance. In other words, awareness of the nutrient requirements for phage multiplication that are in low amount in urine, could lead to formulation of phage products with additives for a more effective treatment. The decision of which diluent or vehicle to use for phage suspension can also be dependent on the metabolic requirements. For instance, in the pilot studies of the UTI model, the phage was suspended in 0.9% NaCl solution. Using Hartmann or other solutions containing glucose could result in unexpected outcomes. Furthermore, this knowledge might also be beneficial for the treatment of UTIs in patients with diabetes mellitus or other metabolic conditions that change the 'normal' composition of urine. As show in Figure 5.6, the addition of sugars, like arabinose, may bring unexpected outcomes in phage susceptibility. The presence of glucose in urine in patients with underlying conditions may have also be problematic. In any case, adequate models of infection will be required to validate these and other finding for clinical translation.

In conclusion, the enormous diversity of bacterial pathogens and phages and the mechanisms used during their interaction can complicate the prediction of PT in clinical settings. The understanding of the different resistance mechanisms that exist, and the conditions in which they are activated is important to achieve a safe and effective phage therapy.

Chapter 8 References

Abd El-Aziz, A.M., Elgaml, A., and Ali, Y.M. (2019). Bacteriophage Therapy Increases Complement-Mediated Lysis of Bacteria and Enhances Bacterial Clearance After Acute Lung Infection With Multidrug-Resistant Pseudomonas aeruginosa. J Infect Dis *219*, 1439-1447. 10.1093/infdis/jiy678.

Abedon, S.T., Kuhl, S.J., Blasdel, B.G., and Kutter, E.M. (2011). Phage treatment of human infections. Bacteriophage *1*, 66-85. 10.4161/bact.1.2.15845.

Abraham, J.M., Freitag, C.S., Clements, J.R., and Eisenstein, B.I. (1985). An invertible element of DNA controls phase variation of type 1 fimbriae of Escherichia coli. Proc Natl Acad Sci U S A *82*, 5724-5727. 10.1073/pnas.82.17.5724.

Abudayyeh, O.O., Gootenberg, J.S., Konermann, S., Joung, J., Slaymaker, I.M., Cox, D.B., Shmakov, S., Makarova, K.S., Semenova, E., Minakhin, L., et al. (2016). C2c2 is a single-component programmable RNA-guided RNA-targeting CRISPR effector. Science *353*, aaf5573. 10.1126/science.aaf5573.

Accogli, M., Giani, T., Monaco, M., Giufre, M., Garcia-Fernandez, A., Conte, V., D'Ancona, F., Pantosti, A., Rossolini, G.M., and Cerquetti, M. (2014). Emergence of Escherichia coli ST131 sub-clone H30 producing VIM-1 and KPC-3 carbapenemases, Italy. J Antimicrob Chemother *69*, 2293-2296. 10.1093/jac/dku132.

Adams-Sapper, S., Diep, B.A., Perdreau-Remington, F., and Riley, L.W. (2013). Clonal composition and community clustering of drug-susceptible and -resistant Escherichia coli isolates from bloodstream infections. Antimicrob Agents Chemother *57*, 490-497. 10.1128/AAC.01025-12.

Al-Zubidi, M., Widziolek, M., Court, E.K., Gains, A.F., Smith, R.E., Ansbro, K., Alrafaie, A., Evans, C., Murdoch, C., Mesnage, S., et al. (2019). Identification of Novel Bacteriophages with Therapeutic Potential That Target Enterococcus faecalis. Infect Immun *87*. 10.1128/IAI.00512-19.

Alteri, C.J., Hagan, E.C., Sivick, K.E., Smith, S.N., and Mobley, H.L. (2009). Mucosal immunization with iron receptor antigens protects against urinary tract infection. PLoS Pathog *5*, e1000586. 10.1371/journal.ppat.1000586.

Alteri, C.J., and Mobley, H.L.T. (2015). Metabolism and Fitness of Urinary Tract Pathogens. Microbiol Spectr *3*. 10.1128/microbiolspec.MBP-0016-2015.

Andersen, T.E., Khandige, S., Madelung, M., Brewer, J., Kolmos, H.J., and Moller-Jensen, J. (2012). Escherichia coli uropathogenesis in vitro: invasion, cellular escape, and secondary infection analyzed in a human bladder cell infection model. Infect Immun *80*, 1858-1867. 10.1128/IAI.06075-11.

Anderson, T.F. (1948). The Growth of T2 Virus on Ultraviolet-killed Host Cells. J Bacteriol *56*, 403-410. 10.1128/jb.56.4.403-410.1948.

Anspach, F.B. (2001). Endotoxin removal by affinity sorbents. J Biochem Biophys Methods *49*, 665-681. 10.1016/s0165-022x(01)00228-7.

Antoine, C., Laforet, F., Blasdel, B., Fall, A., Duprez, J.N., Mainil, J., Delcenserie, V., and Thiry, D. (2021). In Vitro Characterization and In Vivo Efficacy Assessment in Galleria mellonella Larvae of Newly Isolated Bacteriophages against Escherichia coli K1. Viruses *13*. 10.3390/v13102005.

Arafi, V., Hasani, A., Sadeghi, J., Varshochi, M., Poortahmasebi, V., Hasani, A., and Hasani, R. (2023). Uropathogenic Escherichia coli endeavors: an insight into the characteristic features, resistance mechanism, and treatment choice. Arch Microbiol *205*, 226. 10.1007/s00203-023-03553-5.

Arnaud, C.A., Effantin, G., Vives, C., Engilberge, S., Bacia, M., Boulanger, P., Girard, E., Schoehn, G., and Breyton, C. (2017). Bacteriophage T5 tail tube structure suggests a trigger mechanism for Siphoviridae DNA ejection. Nat Commun *8*, 1953. 10.1038/s41467-017-02049-3.

Augustine, J., Gopalakrishnan, M.V., and Bhat, S.G. (2014). Application of PhiSP-1 and PhiSP-3 as a therapeutic strategy against Salmonella Enteritidis infection using Caenorhabditis elegans as model organism. FEMS Microbiol Lett *356*, 113-117. 10.1111/1574-6968.12493.

Ball, K.R., Rubin, J.E., Chirino-Trejo, M., and Dowling, P.M. (2008). Antimicrobial resistance and prevalence of canine uropathogens at the Western College of Veterinary Medicine Veterinary Teaching Hospital, 2002-2007. Can Vet J *49*, 985-990.

Barber, A.E., Norton, J.P., Wiles, T.J., and Mulvey, M.A. (2016). Strengths and Limitations of Model Systems for the Study of Urinary Tract Infections and Related Pathologies. Microbiol Mol Biol Rev *80*, 351-367. 10.1128/MMBR.00067-15.

Barr, D.B., Wilder, L.C., Caudill, S.P., Gonzalez, A.J., Needham, L.L., and Pirkle, J.L. (2005). Urinary creatinine concentrations in the U.S. population: implications for urinary biologic monitoring measurements. Environ Health Perspect *113*, 192-200. 10.1289/ehp.7337.

Bayliss, S.C., Hunt, V.L., Yokoyama, M., Thorpe, H.A., and Feil, E.J. (2017). The use of Oxford Nanopore native barcoding for complete genome assembly. Gigascience *6*, 1-6. 10.1093/gigascience/gix001.

Bernardez, L.A., and de Andrade Lima, L.R. (2015). Improved method for enumerating sulfate-reducing bacteria using optical density. MethodsX *2*, 249-255. 10.1016/j.mex.2015.04.006.

Bernasconi, O.J., Dona, V., Tinguely, R., and Endimiani, A. (2017). In vitro activity of three commercial bacteriophage cocktails against multidrug-resistant Escherichia coli and Proteus spp. strains of human and non-human origin. J Glob Antimicrob Resist *8*, 179-185. 10.1016/j.jgar.2016.12.013.

Bernheim, A., and Sorek, R. (2020). The pan-immune system of bacteria: antiviral defence as a community resource. Nat Rev Microbiol *18*, 113-119. 10.1038/s41579-019-0278-2.

Bertozzi Silva, J., Storms, Z., and Sauvageau, D. (2016). Host receptors for bacteriophage adsorption. FEMS Microbiol Lett *363*. 10.1093/femsle/fnw002.

Blango, M.G., and Mulvey, M.A. (2010). Persistence of uropathogenic Escherichia coli in the face of multiple antibiotics. Antimicrob Agents Chemother *54*, 1855-1863. 10.1128/AAC.00014-10.

Bondy-Denomy, J., Pawluk, A., Maxwell, K.L., and Davidson, A.R. (2013). Bacteriophage genes that inactivate the CRISPR/Cas bacterial immune system. Nature *493*, 429-432. 10.1038/nature11723.

Bouatra, S., Aziat, F., Mandal, R., Guo, A.C., Wilson, M.R., Knox, C., Bjorndahl, T.C., Krishnamurthy, R., Saleem, F., Liu, P., et al. (2013). The human urine metabolome. PLoS One *8*, e73076. 10.1371/journal.pone.0073076.

Bourdin, G., Schmitt, B., Marvin Guy, L., Germond, J.E., Zuber, S., Michot, L., Reuteler, G., and Brussow, H. (2014). Amplification and purification of T4-like escherichia coli phages for phage therapy: from laboratory to pilot scale. Appl Environ Microbiol *80*, 1469-1476. 10.1128/AEM.03357-13.

Brix, A., Cafora, M., Aureli, M., and Pistocchi, A. (2020). Animal Models to Translate Phage Therapy to Human Medicine. Int J Mol Sci *21*. 10.3390/ijms21103715.

Brooks, T., and Keevil, C.W. (1997). A simple artificial urine for the growth of urinary pathogens. Lett Appl Microbiol *24*, 203-206. 10.1046/j.1472-765x.1997.00378.x.

Brown, N.D., Poon, B.T., and Phillips, L.R. (1989). Identification and determination of a carboxylic acid metabolite of chloroquine in human urine by high-performance liquid chromatography. J Chromatogr *487*, 189-196. 10.1016/s0378-4347(00)83024-8.

Bruttin, A., and Brussow, H. (2005). Human volunteers receiving Escherichia coli phage T4 orally: a safety test of phage therapy. Antimicrob Agents Chemother *49*, 2874-2878. 10.1128/AAC.49.7.2874-2878.2005.

Bryan, D., El-Shibiny, A., Hobbs, Z., Porter, J., and Kutter, E.M. (2016). Bacteriophage T4 Infection of Stationary Phase E. coli: Life after Log from a Phage Perspective. Front Microbiol *7*, 1391. 10.3389/fmicb.2016.01391.

Byron, J.K. (2019). Urinary Tract Infection. Vet Clin North Am Small Anim Pract *49*, 211-221. 10.1016/j.cvsm.2018.11.005.

Cafora, M., Deflorian, G., Forti, F., Ferrari, L., Binelli, G., Briani, F., Ghisotti, D., and Pistocchi, A. (2019). Phage therapy against Pseudomonas aeruginosa infections in a cystic fibrosis zebrafish model. Sci Rep *9*, 1527. 10.1038/s41598-018-37636-x.

Cai, J.C., Zhang, R., Hu, Y.Y., Zhou, H.W., and Chen, G.X. (2014). Emergence of Escherichia coli sequence type 131 isolates producing KPC-2 carbapenemase in China. Antimicrob Agents Chemother *58*, 1146-1152. 10.1128/AAC.00912-13.

Capparelli, R., Nocerino, N., Iannaccone, M., Ercolini, D., Parlato, M., Chiara, M., and Iannelli, D. (2010a). Bacteriophage therapy of Salmonella enterica: a fresh appraisal of bacteriophage therapy. J Infect Dis *201*, 52-61. 10.1086/648478.

Capparelli, R., Nocerino, N., Lanzetta, R., Silipo, A., Amoresano, A., Giangrande, C., Becker, K., Blaiotta, G., Evidente, A., Cimmino, A., et al. (2010b). Bacteriophage-resistant Staphylococcus aureus mutant confers broad immunity against staphylococcal infection in mice. PLoS One *5*, e11720. 10.1371/journal.pone.0011720.

Capparelli, R., Parlato, M., Borriello, G., Salvatore, P., and Iannelli, D. (2007). Experimental phage therapy against Staphylococcus aureus in mice. Antimicrob Agents Chemother *51*, 2765-2773. 10.1128/AAC.01513-06.

Casanova-Torres, A.M., and Goodrich-Blair, H. (2013). Immune Signaling and Antimicrobial Peptide Expression in Lepidoptera. Insects *4*, 320-338. 10.3390/insects4030320.

Casey, E., van Sinderen, D., and Mahony, J. (2018). In Vitro Characteristics of Phages to Guide 'Real Life' Phage Therapy Suitability. Viruses *10*. 10.3390/v10040163.

Chamoun, M.N., Sullivan, M.J., Goh, K.G.K., Acharya, D., Ipe, D.S., Katupitiya, L., Gosling, D., Peters, K.M., Sweet, M.J., Sester, D.P., et al. (2020). Restriction of chronic Escherichia coli urinary tract infection depends upon T cell-derived interleukin-17, a deficiency of which predisposes to flagella-driven bacterial persistence. FASEB J *34*, 14572-14587. 10.1096/fj.202000760R.

Chan, B.K., Abedon, S.T., and Loc-Carrillo, C. (2013). Phage cocktails and the future of phage therapy. Future Microbiol *8*, 769-783. 10.2217/fmb.13.47.

Chan, C.C.Y., and Lewis, I.A. (2022). Role of metabolism in uropathogenic Escherichia coli. Trends Microbiol *30*, 1174-1204. 10.1016/j.tim.2022.06.003.

Chinenova, T.A., Mkrtumian, N.M., and Lomovskaia, N.D. (1982). [Genetic characteristics of a new phage resistance trait in Streptomyces coelicolor A3(2)]. Genetika *18*, 1945-1952.

Christmas, K.G., Gower, L.B., Khan, S.R., and El-Shall, H. (2002). Aggregation and dispersion characteristics of calcium oxalate monohydrate: effect of urinary species. J Colloid Interface Sci *256*, 168-174. 10.1006/jcis.2002.8283.

Chu, C.M., and Lowder, J.L. (2018). Diagnosis and treatment of urinary tract infections across age groups. Am J Obstet Gynecol *219*, 40-51. 10.1016/j.ajog.2017.12.231.

Chutipongtanate, S., and Thongboonkerd, V. (2010). Systematic comparisons of artificial urine formulas for in vitro cellular study. Anal Biochem *402*, 110-112. 10.1016/j.ab.2010.03.031.

Cieplak, T., Soffer, N., Sulakvelidze, A., and Nielsen, D.S. (2018). A bacteriophage cocktail targeting Escherichia coli reduces E. coli in simulated gut conditions, while preserving a non-targeted representative commensal normal microbiota. Gut Microbes *9*, 391-399. 10.1080/19490976.2018.1447291.

Cisek, A.A., Dabrowska, I., Gregorczyk, K.P., and Wyzewski, Z. (2017). Phage Therapy in Bacterial Infections Treatment: One Hundred Years After the Discovery of Bacteriophages. Curr Microbiol *74*, 277-283. 10.1007/s00284-016-1166-x.

Clermont, O., Bonacorsi, S., and Bingen, E. (2000). Rapid and simple determination of the Escherichia coli phylogenetic group. Appl Environ Microbiol *66*, 4555-4558. 10.1128/AEM.66.10.4555-4558.2000.

Clermont, O., Christenson, J.K., Denamur, E., and Gordon, D.M. (2013). The Clermont Escherichia coli phylo-typing method revisited: improvement of specificity and detection of new phylo-groups. Environ Microbiol Rep *5*, 58-65. 10.1111/1758-2229.12019.

Clermont, O., Couffignal, C., Blanco, J., Mentre, F., Picard, B., Denamur, E., Coliville, and groups, C. (2017). Two levels of specialization in bacteraemic Escherichia coli strains revealed by their comparison with commensal strains. Epidemiol Infect *145*, 872-882. 10.1017/S0950268816003010.

Clokie, M.R., Millard, A.D., Letarov, A.V., and Heaphy, S. (2011). Phages in nature. Bacteriophage *1*, 31-45. 10.4161/bact.1.1.14942.

Cohen, D., Melamed, S., Millman, A., Shulman, G., Oppenheimer-Shaanan, Y., Kacen, A., Doron, S., Amitai, G., and Sorek, R. (2019). Cyclic GMP-AMP signalling protects bacteria against viral infection. Nature *574*, 691-695. 10.1038/s41586-019-1605-5.

Cohen, S.S. (1949). Growth Requirements of Bacterial Viruses. Bacteriol Rev *13*, 1-24. 10.1128/br.13.1.1-24.1949.

Cooke, C.L., Singer, R.S., Jang, S.S., and Hirsh, D.C. (2002). Enrofloxacin resistance in Escherichia coli isolated from dogs with urinary tract infections. J Am Vet Med Assoc *220*, 190-192. 10.2460/javma.2002.220.190.

Coque, T.M., Novais, A., Carattoli, A., Poirel, L., Pitout, J., Peixe, L., Baquero, F., Canton, R., and Nordmann, P. (2008). Dissemination of clonally related Escherichia coli strains expressing extended-spectrum beta-lactamase CTX-M-15. Emerg Infect Dis *14*, 195-200. 10.3201/eid1402.070350.

Cosloy, S.D., and McFall, E. (1973). Metabolism of D-serine in Escherichia coli K-12: mechanism of growth inhibition. J Bacteriol *114*, 685-694. 10.1128/jb.114.2.685-694.1973.

Cowley, L.A., Low, A.S., Pickard, D., Boinett, C.J., Dallman, T.J., Day, M., Perry, N., Gally, D.L., Parkhill, J., Jenkins, C., and Cain, A.K. (2018). Transposon Insertion Sequencing Elucidates Novel Gene Involvement in Susceptibility and Resistance to Phages T4 and T7 in Escherichia coli O157. mBio *9*. 10.1128/mBio.00705-18.

Cumby, N., Edwards, A.M., Davidson, A.R., and Maxwell, K.L. (2012). The bacteriophage HK97 gp15 moron element encodes a novel superinfection exclusion protein. J Bacteriol *194*, 5012-5019. 10.1128/JB.00843-12.

Czaplewski, L., Bax, R., Clokie, M., Dawson, M., Fairhead, H., Fischetti, V.A., Foster, S., Gilmore, B.F., Hancock, R.E., Harper, D., et al. (2016). Alternatives to antibiotics-a pipeline portfolio review. Lancet Infect Dis *16*, 239-251. 10.1016/S1473-3099(15)00466-1.

Dabrowska, K. (2019). Phage therapy: What factors shape phage pharmacokinetics and bioavailability? Systematic and critical review. Med Res Rev *39*, 2000-2025. 10.1002/med.21572.

Daneshian, M., Guenther, A., Wendel, A., Hartung, T., and von Aulock, S. (2006). In vitro pyrogen test for toxic or immunomodulatory drugs. J Immunol Methods *313*, 169-175. 10.1016/j.jim.2006.04.009.

Datsenko, K.A., and Wanner, B.L. (2000). One-step inactivation of chromosomal genes in Escherichia coli K-12 using PCR products. Proceedings of the National Academy of Sciences *97*, 6640-6645. doi:10.1073/pnas.120163297.

Dawson, H.D., Smith, A.D., Chen, C., and Urban, J.F., Jr. (2017). An in-depth comparison of the porcine, murine and human inflammasomes; lessons from the porcine genome and transcriptome. Vet Microbiol *202*, 2-15. 10.1016/j.vetmic.2016.05.013.

Day, M.J., Doumith, M., Abernethy, J., Hope, R., Reynolds, R., Wain, J., Livermore, D.M., and Woodford, N. (2016). Population structure of Escherichia coli causing bacteraemia in the UK and Ireland between 2001 and 2010. J Antimicrob Chemother *71*, 2139-2142. 10.1093/jac/dkw145.

De Briyne, N., Atkinson, J., Pokludova, L., and Borriello, S.P. (2014). Antibiotics used most commonly to treat animals in Europe. Vet Rec *175*, 325. 10.1136/vr.102462.

de Jonge, P.A., Nobrega, F.L., Brouns, S.J.J., and Dutilh, B.E. (2019). Molecular and Evolutionary Determinants of Bacteriophage Host Range. Trends Microbiol *27*, 51-63. 10.1016/j.tim.2018.08.006.

Denamur, E., Clermont, O., Bonacorsi, S., and Gordon, D. (2021). The population genetics of pathogenic Escherichia coli. Nat Rev Microbiol *19*, 37-54. 10.1038/s41579-020-0416-x.

Deveau, H., Barrangou, R., Garneau, J.E., Labonte, J., Fremaux, C., Boyaval, P., Romero, D.A., Horvath, P., and Moineau, S. (2008). Phage response to CRISPR-encoded resistance in Streptococcus thermophilus. J Bacteriol *190*, 1390-1400. 10.1128/JB.01412-07.

Ding, Y., Zhang, D., Zhao, X., Tan, W., Zheng, X., Zhang, Q., Ji, X., and Wei, Y. (2021). Autoinducer-2-mediated quorum-sensing system resists T4 phage infection in Escherichia coli. J Basic Microbiol *61*, 1113-1123. 10.1002/jobm.202100344.

Dion, M.B., Oechslin, F., and Moineau, S. (2020). Phage diversity, genomics and phylogeny. Nat Rev Microbiol *18*, 125-138. 10.1038/s41579-019-0311-5.

Dobin, A., and Gingeras, T.R. (2015). Mapping RNA-seq Reads with STAR. Curr Protoc Bioinformatics *51*, 11.14.11-11.14.19. 10.1002/0471250953.bi1114s51.

Doron, S., Melamed, S., Ofir, G., Leavitt, A., Lopatina, A., Keren, M., Amitai, G., and Sorek, R. (2018). Systematic discovery of antiphage defense systems in the microbial pangenome. Science *359*. 10.1126/science.aar4120.

Doulatov, S., Hodes, A., Dai, L., Mandhana, N., Liu, M., Deora, R., Simons, R.W., Zimmerly, S., and Miller, J.F. (2004). Tropism switching in Bordetella bacteriophage defines a family of diversity-generating retroelements. Nature *431*, 476-481. 10.1038/nature02833.

Drulis-Kawa, Z., Majkowska-Skrobek, G., Maciejewska, B., Delattre, A.S., and Lavigne, R. (2012). Learning from bacteriophages - advantages and limitations of phage and phage-encoded protein applications. Curr Protein Pept Sci *13*, 699-722. 10.2174/138920312804871193.

Duddy, O.P., Huang, X., Silpe, J.E., and Bassler, B.L. (2021). Mechanism underlying the DNA-binding preferences of the Vibrio cholerae and

vibriophage VP882 VqmA quorum-sensing receptors. PLoS Genet *17*, e1009550. 10.1371/journal.pgen.1009550.

Duerkop, B.A., Huo, W., Bhardwaj, P., Palmer, K.L., and Hooper, L.V. (2016). Molecular Basis for Lytic Bacteriophage Resistance in Enterococci. mBio *7*. 10.1128/mBio.01304-16.

Dufour, N., Clermont, O., La Combe, B., Messika, J., Dion, S., Khanna, V., Denamur, E., Ricard, J.D., Debarbieux, L., and ColoColi, g. (2016). Bacteriophage LM33_P1, a fast-acting weapon against the pandemic ST131-O25b:H4 Escherichia coli clonal complex. J Antimicrob Chemother *71*, 3072-3080. 10.1093/jac/dkw253.

Duncan, M.J., Li, G., Shin, J.S., Carson, J.L., and Abraham, S.N. (2004). Bacterial penetration of bladder epithelium through lipid rafts. J Biol Chem *279*, 18944-18951. 10.1074/jbc.M400769200.

Dy, R.L., Przybilski, R., Semeijn, K., Salmond, G.P., and Fineran, P.C. (2014a). A widespread bacteriophage abortive infection system functions through a Type IV toxin-antitoxin mechanism. Nucleic Acids Res *42*, 4590-4605. 10.1093/nar/gkt1419.

Dy, R.L., Richter, C., Salmond, G.P., and Fineran, P.C. (2014b). Remarkable Mechanisms in Microbes to Resist Phage Infections. Annu Rev Virol *1*, 307-331. 10.1146/annurev-virology-031413-085500.

Evans, T.J., Trauner, A., Komitopoulou, E., and Salmond, G.P. (2010). Exploitation of a new flagellatropic phage of Erwinia for positive selection of bacterial mutants attenuated in plant virulence: towards phage therapy. J Appl Microbiol *108*, 676-685. 10.1111/j.1365-2672.2009.04462.x.

Ewers, C., Grobbel, M., Stamm, I., Kopp, P.A., Diehl, I., Semmler, T., Fruth, A., Beutlich, J., Guerra, B., Wieler, L.H., and Guenther, S. (2010). Emergence of human pandemic O25:H4-ST131 CTX-M-15 extended-spectrum-beta-lactamase-producing Escherichia coli among companion animals. J Antimicrob Chemother *65*, 651-660. 10.1093/jac/dkq004.

Fernandez, J.a.H., Jessica (2020). Development of a urinary tract infection animal model in Göttingen Minipigs Webinar. held in www.minipigs.dk.

Fineran, P.C., Blower, T.R., Foulds, I.J., Humphreys, D.P., Lilley, K.S., and Salmond, G.P. (2009). The phage abortive infection system, ToxIN, functions as a protein-RNA toxin-antitoxin pair. Proc Natl Acad Sci U S A *106*, 894-899. 10.1073/pnas.0808832106.

Fish, R., Kutter, E., Bryan, D., Wheat, G., and Kuhl, S. (2018a). Resolving Digital Staphylococcal Osteomyelitis Using Bacteriophage-A Case Report. Antibiotics (Basel) *7*. 10.3390/antibiotics7040087.

Fish, R., Kutter, E., Wheat, G., Blasdel, B., Kutateladze, M., and Kuhl, S. (2018b). Compassionate Use of Bacteriophage Therapy for Foot Ulcer Treatment as an Effective Step for Moving Toward Clinical Trials. Methods Mol Biol *1693*, 159-170. 10.1007/978-1-4939-7395-8_14.

Flores-Mireles, A.L., Walker, J.N., Caparon, M., and Hultgren, S.J. (2015). Urinary tract infections: epidemiology, mechanisms of infection and treatment options. Nat Rev Microbiol *13*, 269-284. 10.1038/nrmicro3432.

Fong, S.A., Drilling, A., Morales, S., Cornet, M.E., Woodworth, B.A., Fokkens, W.J., Psaltis, A.J., Vreugde, S., and Wormald, P.J. (2017). Activity of Bacteriophages in Removing Biofilms of Pseudomonas aeruginosa Isolates from Chronic Rhinosinusitis Patients. Front Cell Infect Microbiol *7*, 418. 10.3389/fcimb.2017.00418.

Forde, B.M., Ben Zakour, N.L., Stanton-Cook, M., Phan, M.D., Totsika, M., Peters, K.M., Chan, K.G., Schembri, M.A., Upton, M., and Beatson, S.A. (2014). The complete genome sequence of Escherichia coli EC958: a high quality reference sequence for the globally disseminated multidrug resistant E. coli O25b:H4-ST131 clone. PLoS One *9*, e104400. 10.1371/journal.pone.0104400.

Forde, B.M., Phan, M.D., Gawthorne, J.A., Ashcroft, M.M., Stanton-Cook, M., Sarkar, S., Peters, K.M., Chan, K.G., Chong, T.M., Yin, W.F., et al. (2015). Lineage-Specific Methyltransferases Define the Methylome of the Globally Disseminated Escherichia coli ST131 Clone. mBio *6*, e01602-01615. 10.1128/mBio.01602-15.

Forrester, S.D., Troy, G.C., Dalton, M.N., Huffman, J.W., and Holtzman, G. (1999). Retrospective evaluation of urinary tract infection in 42 dogs with hyperadrenocorticism or diabetes mellitus or both. J Vet Intern Med *13*, 557-560. 10.1892/0891-6640(1999)013<0557:reouti>2.3.co;2.

Forti, F., Roach, D.R., Cafora, M., Pasini, M.E., Horner, D.S., Fiscarelli, E.V., Rossitto, M., Cariani, L., Briani, F., Debarbieux, L., and Ghisotti, D. (2018). Design of a Broad-Range Bacteriophage Cocktail That Reduces Pseudomonas aeruginosa Biofilms and Treats Acute Infections in Two Animal Models. Antimicrob Agents Chemother *62*. 10.1128/AAC.02573-17.

Foster, R.A. (1947). The action of proflavine on bacteriophage multiplication; a method for the study of inhibitors of virus growth. J Bacteriol *53*, 801. 10.1128/JB.53.6.801-803.1947.

Foster, R.A. (1948). An Analysis of the Action of Proflavine on Bacteriophage Growth. J Bacteriol *56*, 795-809. 10.1128/jb.56.6.795-809.1948.

Fowler, C.B., and Cohen, S.S. (1948). Chemical studies in host-virus interactions; a method of determining nutritional requirements for bacterial virus multiplication. J Exp Med *87*, 259-274. 10.1084/jem.87.4.259.

Foxman, B. (2003). Epidemiology of urinary tract infections: incidence, morbidity, and economic costs. Dis Mon *49*, 53-70. 10.1067/mda.2003.7.

Foxman, B. (2010). The epidemiology of urinary tract infection. Nat Rev Urol *7*, 653-660. 10.1038/nrurol.2010.190.

Foxman, B. (2014). Urinary tract infection syndromes: occurrence, recurrence, bacteriology, risk factors, and disease burden. Infect Dis Clin North Am *28*, 1-13. 10.1016/j.idc.2013.09.003.

Furfaro, L.L., Payne, M.S., and Chang, B.J. (2018). Bacteriophage Therapy: Clinical Trials and Regulatory Hurdles. Front Cell Infect Microbiol *8*, 376. 10.3389/fcimb.2018.00376.

Gibson, J.S., Morton, J.M., Cobbold, R.N., Sidjabat, H.E., Filippich, L.J., and Trott, D.J. (2008). Multidrug-resistant E. coli and enterobacter extraintestinal infection in 37 dogs. J Vet Intern Med *22*, 844-850. 10.1111/j.1939-1676.2008.00124.x.

Gindin, M., Febvre, H.P., Rao, S., Wallace, T.C., and Weir, T.L. (2019). Bacteriophage for Gastrointestinal Health (PHAGE) Study: Evaluating the Safety and Tolerability of Supplemental Bacteriophage Consumption. J Am Coll Nutr *38*, 68-75. 10.1080/07315724.2018.1483783.

Glowacka-Rutkowska, A., Gozdek, A., Empel, J., Gawor, J., Zuchniewicz, K., Kozinska, A., Debski, J., Gromadka, R., and Lobocka, M. (2018). The Ability of Lytic Staphylococcal Podovirus vB_SauP_phiAGO1.3 to Coexist in Equilibrium With Its Host Facilitates the Selection of Host Mutants of Attenuated Virulence but Does Not Preclude the Phage Antistaphylococcal Activity in a Nematode Infection Model. Front Microbiol *9*, 3227. 10.3389/fmicb.2018.03227.

Goh, S. (2016). Phage Transduction. Methods Mol Biol *1476*, 177-185. 10.1007/978-1-4939-6361-4_13.

Goldberg, G.W., Jiang, W., Bikard, D., and Marraffini, L.A. (2014). Conditional tolerance of temperate phages via transcription-dependent CRISPR-Cas targeting. Nature *514*, 633-637. 10.1038/nature13637.

Goldfarb, T., Sberro, H., Weinstock, E., Cohen, O., Doron, S., Charpak-Amikam, Y., Afik, S., Ofir, G., and Sorek, R. (2015). BREX is a novel phage resistance system widespread in microbial genomes. EMBO J *34*, 169-183. 10.15252/embj.201489455.

Goller, C.C., and Seed, P.C. (2010). Revisiting the Escherichia coli polysaccharide capsule as a virulence factor during urinary tract infection: contribution to intracellular biofilm development. Virulence *1*, 333-337. 10.4161/viru.1.4.12388.

Gomez, P., and Buckling, A. (2011). Bacteria-phage antagonistic coevolution in soil. Science *332*, 106-109. 10.1126/science.1198767.

Gordeeva, J., Morozova, N., Sierro, N., Isaev, A., Sinkunas, T., Tsvetkova, K., Matlashov, M., Truncaite, L., Morgan, R.D., Ivanov, N.V., et al. (2019). BREX system of Escherichia coli distinguishes self from non-self by methylation of a specific DNA site. Nucleic Acids Res *47*, 253-265. 10.1093/nar/gky1125.

Gordillo Altamirano, F.L., and Barr, J.J. (2019). Phage Therapy in the Postantibiotic Era. Clin Microbiol Rev *32*. 10.1128/CMR.00066-18.

Gordillo Altamirano, F.L., and Barr, J.J. (2021). Unlocking the next generation of phage therapy: the key is in the receptors. Curr Opin Biotechnol *68*, 115-123. 10.1016/j.copbio.2020.10.002.

Gordon, D.M. (2013). The ecology of Escherichia coli. In Escherichia coli, pp. 3-20. 10.1016/b978-0-12-397048-0.00001-2.

Gorski, A., Borysowski, J., and Miedzybrodzki, R. (2020). Phage Therapy: Towards a Successful Clinical Trial. Antibiotics (Basel) *9*. 10.3390/antibiotics9110827.

Grases, F., and Llobera, A. (1998). Experimental model to study sedimentary kidney stones. Micron *29*, 105-111. 10.1016/s0968-4328(98)00006-7.

Green, S.I., Kaelber, J.T., Ma, L., Trautner, B.W., Ramig, R.F., and Maresso, A.W. (2017). Bacteriophages from ExPEC Reservoirs Kill Pandemic Multidrug-Resistant Strains of Clonal Group ST131 in Animal Models of Bacteremia. Sci Rep *7*, 46151. 10.1038/srep46151.

Hall, J.L., Holmes, M.A., and Baines, S.J. (2013). Prevalence and antimicrobial resistance of canine urinary tract pathogens. Vet Rec *173*, 549. 10.1136/vr.101482.

Hammer, B.K., and Bassler, B.L. (2003). Quorum sensing controls biofilm formation in Vibrio cholerae. Mol Microbiol *50*, 101-104. 10.1046/j.1365-2958.2003.03688.x.

Hampton, H.G., Watson, B.N.J., and Fineran, P.C. (2020). The arms race between bacteria and their phage foes. Nature *577*, 327-336. 10.1038/s41586-019-1894-8.

Hannan, T.J., Totsika, M., Mansfield, K.J., Moore, K.H., Schembri, M.A., and Hultgren, S.J. (2012). Host-pathogen checkpoints and population bottlenecks in persistent and intracellular uropathogenic Escherichia coli bladder infection. FEMS Microbiol Rev *36*, 616-648. 10.1111/j.1574-6976.2012.00339.x.

Harvey, H., Bondy-Denomy, J., Marquis, H., Sztanko, K.M., Davidson, A.R., and Burrows, L.L. (2018). Pseudomonas aeruginosa defends against phages

through type IV pilus glycosylation. Nat Microbiol *3*, 47-52. 10.1038/s41564-017-0061-y.

Hejair, H.M.A., Zhu, Y., Ma, J., Zhang, Y., Pan, Z., Zhang, W., and Yao, H. (2017). Functional role of ompF and ompC porins in pathogenesis of avian pathogenic Escherichia coli. Microb Pathog *107*, 29-37. 10.1016/j.micpath.2017.02.033.

Henly, E.L., Norris, K., Rawson, K., Zoulias, N., Jaques, L., Chirila, P.G., Parkin, K.L., Kadirvel, M., Whiteoak, C., Lacey, M.M., et al. (2021). Impact of long-term quorum sensing inhibition on uropathogenic Escherichia coli. J Antimicrob Chemother *76*, 909-919. 10.1093/jac/dkaa517.

Heo, Y.J., Lee, Y.R., Jung, H.H., Lee, J., Ko, G., and Cho, Y.H. (2009). Antibacterial efficacy of phages against Pseudomonas aeruginosa infections in mice and Drosophila melanogaster. Antimicrob Agents Chemother *53*, 2469-2474. 10.1128/AAC.01646-08.

Herriott, R.M., and Price, W.H. (1948). The formation of bacterial viruses in bacteria rendered nonviable by mustard gas. J Gen Physiol *32*, 63-68. 10.1085/jgp.32.1.63.

Hodyra-Stefaniak, K., Lahutta, K., Majewska, J., Kazmierczak, Z., Lecion, D., Harhala, M., Keska, W., Owczarek, B., Jonczyk-Matysiak, E., Klopot, A., et al. (2019). Bacteriophages engineered to display foreign peptides may become short-circulating phages. Microb Biotechnol *12*, 730-741. 10.1111/1751-7915.13414.

Hoskisson, P.A., Sumby, P., and Smith, M.C.M. (2015). The phage growth limitation system in Streptomyces coelicolor A(3)2 is a toxin/antitoxin system, comprising enzymes with DNA methyltransferase, protein kinase and ATPase activity. Virology *477*, 100-109. 10.1016/j.virol.2014.12.036.

Hoyland-Kroghsbo, N.M., Maerkedahl, R.B., and Svenningsen, S.L. (2013). A quorum-sensing-induced bacteriophage defense mechanism. mBio *4*, e00362-00312. 10.1128/mBio.00362-12.

Hwang, S., and Maxwell, K.L. (2019). Meet the Anti-CRISPRs: Widespread Protein Inhibitors of CRISPR-Cas Systems. CRISPR J *2*, 23-30. 10.1089/crispr.2018.0052.

Hyman, P., and Abedon, S.T. (2010). Bacteriophage host range and bacterial resistance. Adv Appl Microbiol *70*, 217-248. 10.1016/S0065-2164(10)70007-1.

Ipe, D.S., Horton, E., and Ulett, G.C. (2016). The Basics of Bacteriuria: Strategies of Microbes for Persistence in Urine. Front Cell Infect Microbiol *6*, 14. 10.3389/fcimb.2016.00014.

Ipe, D.S., and Ulett, G.C. (2016). Evaluation of the in vitro growth of urinary tract infection-causing gram-negative and gram-positive bacteria in a proposed synthetic human urine (SHU) medium. J Microbiol Methods *127*, 164-171. 10.1016/j.mimet.2016.06.013.

Jamalludeen, N., Johnson, R.P., Shewen, P.E., and Gyles, C.L. (2009). Evaluation of bacteriophages for prevention and treatment of diarrhea due to experimental enterotoxigenic Escherichia coli O149 infection of pigs. Vet Microbiol *136*, 135-141. 10.1016/j.vetmic.2008.10.021.

Jault, P., Leclerc, T., Jennes, S., Pirnay, J.P., Que, Y.A., Resch, G., Rousseau, A.F., Ravat, F., Carsin, H., Le Floch, R., et al. (2019). Efficacy and tolerability of a cocktail of bacteriophages to treat burn wounds infected by Pseudomonas aeruginosa (PhagoBurn): a randomised, controlled, double-blind phase 1/2 trial. Lancet Infect Dis *19*, 35-45. 10.1016/S1473-3099(18)30482-1.

Jennes, S., Merabishvili, M., Soentjens, P., Pang, K.W., Rose, T., Keersebilck, E., Soete, O., Francois, P.M., Teodorescu, S., Verween, G., et al. (2017). Use of bacteriophages in the treatment of colistin-only-sensitive Pseudomonas aeruginosa septicaemia in a patient with acute kidney injury-a case report. Crit Care *21*, 129. 10.1186/s13054-017-1709-y.

Johnson, J.R., and Clabots, C. (2006). Sharing of virulent Escherichia coli clones among household members of a woman with acute cystitis. Clin Infect Dis *43*, e101-108. 10.1086/508541.

Johnson, J.R., Davis, G., Clabots, C., Johnston, B.D., Porter, S., DebRoy, C., Pomputius, W., Ender, P.T., Cooperstock, M., Slater, B.S., et al. (2016). Household Clustering of Escherichia coli Sequence Type 131 Clinical and Fecal Isolates According to Whole Genome Sequence Analysis. Open Forum Infect Dis *3*, ofw129. 10.1093/ofid/ofw129.

Johnson, J.R., Drawz, S.M., Porter, S., and Kuskowski, M.A. (2013). Susceptibility to alternative oral antimicrobial agents in relation to sequence type ST131 status and Coresistance phenotype among recent Escherichia coli isolates from U.S. veterans. Antimicrob Agents Chemother *57*, 4856-4860. 10.1128/AAC.00650-13.

Johnson, J.R., Miller, S., Johnston, B., Clabots, C., and Debroy, C. (2009). Sharing of Escherichia coli sequence type ST131 and other multidrug-resistant and Urovirulent E. coli strains among dogs and cats within a household. J Clin Microbiol *47*, 3721-3725. 10.1128/JCM.01581-09.

Johnson, T.J., Hargreaves, M., Shaw, K., Snippes, P., Lynfield, R., Aziz, M., and Price, L.B. (2015). Complete Genome Sequence of a Carbapenem-Resistant Extraintestinal Pathogenic Escherichia coli Strain Belonging to the Sequence Type 131 H30R Subclade. Genome Announc *3*. 10.1128/genomeA.00272-15.

Kadry, A.A., Al-Kashef, N.M., and El-Ganiny, A.M. (2020). Distribution of genes encoding adhesins and biofilm formation capacity among Uropathogenic Escherichia coli isolates in relation to the antimicrobial resistance. Afr Health Sci *20*, 238-247. 10.4314/ahs.v20i1.29.

Kakkanat, A., Phan, M.D., Lo, A.W., Beatson, S.A., and Schembri, M.A. (2017). Novel genes associated with enhanced motility of Escherichia coli ST131. PLoS One *12*, e0176290. 10.1371/journal.pone.0176290.

Kallonen, T., Brodrick, H.J., Harris, S.R., Corander, J., Brown, N.M., Martin, V., Peacock, S.J., and Parkhill, J. (2017). Systematic longitudinal survey of invasive Escherichia coli in England demonstrates a stable population structure only transiently disturbed by the emergence of ST131. Genome Res *27*, 1437-1449. 10.1101/gr.216606.116.

Kaper, J.B., Nataro, J.P., and Mobley, H.L. (2004). Pathogenic Escherichia coli. Nat Rev Microbiol *2*, 123-140. 10.1038/nrmicro818.

Karlsson, E., Larkeryd, A., Sjodin, A., Forsman, M., and Stenberg, P. (2015). Scaffolding of a bacterial genome using MinION nanopore sequencing. Sci Rep *5*, 11996. 10.1038/srep11996.

Karp, P.D., Billington, R., Caspi, R., Fulcher, C.A., Latendresse, M., Kothari, A., Keseler, I.M., Krummenacker, M., Midford, P.E., Ong, Q., et al. (2019). The BioCyc collection of microbial genomes and metabolic pathways. Brief Bioinform *20*, 1085-1093. 10.1093/bib/bbx085.

Katouli, M. (2010). Population structure of gut Escherichia coli and its role in development of extra-intestinal infections. Iran J Microbiol *2*, 59-72.

Kazlauskiene, M., Tamulaitis, G., Kostiuk, G., Venclovas, C., and Siksnys, V. (2016). Spatiotemporal Control of Type III-A CRISPR-Cas Immunity: Coupling DNA Degradation with the Target RNA Recognition. Mol Cell *62*, 295-306. 10.1016/j.molcel.2016.03.024.

Koonin, E.V., Makarova, K.S., and Zhang, F. (2017). Diversity, classification and evolution of CRISPR-Cas systems. Curr Opin Microbiol *37*, 67-78. 10.1016/j.mib.2017.05.008.

Kozloff, L.M., Knowlton, K., Putnam, F.W., and Evans, E.A. (1951). Biochemical Studies of Virus Reproduction. Journal of Biological Chemistry *188*, 101-116. 10.1016/s0021-9258(18)56151-2.

Kronheim, S., Daniel-Ivad, M., Duan, Z., Hwang, S., Wong, A.I., Mantel, I., Nodwell, J.R., and Maxwell, K.L. (2018). A chemical defence against phage infection. Nature *564*, 283-286. 10.1038/s41586-018-0767-x.

Kropinski, A.M. (2018). Practical Advice on the One-Step Growth Curve. Methods Mol Biol *1681*, 41-47. 10.1007/978-1-4939-7343-9_3.

Krueger, A.P., and Fong, J. (1937). The Relationship between Bacterial Growth and Phage Production. J Gen Physiol *21*, 137-150. 10.1085/jgp.21.2.137.

Kuan, N.L., and Yeh, K.S. (2019). Arginine within a specific motif near the N-terminal of FimY is critical for the maximal production of type 1 fimbriae in Salmonella enterica serovar Typhimurium. Microbiologyopen *8*, e00846. 10.1002/mbo3.846.

Kutateladze, M., and Adamia, R. (2008). Phage therapy experience at the Eliava Institute. Med Mal Infect *38*, 426-430. 10.1016/j.medmal.2008.06.023.

Kuzmenko, A., Oguienko, A., Esyunina, D., Yudin, D., Petrova, M., Kudinova, A., Maslova, O., Ninova, M., Ryazansky, S., Leach, D., et al. (2020). DNA targeting and interference by a bacterial Argonaute nuclease. Nature *587*, 632-637. 10.1038/s41586-020-2605-1.

Kuzmenko, A., Yudin, D., Ryazansky, S., Kulbachinskiy, A., and Aravin, A.A. (2019). Programmable DNA cleavage by Ago nucleases from mesophilic bacteria Clostridium butyricum and Limnothrix rosea. Nucleic Acids Res *47*, 5822-5836. 10.1093/nar/gkz379.

Labrie, S.J., Samson, J.E., and Moineau, S. (2010). Bacteriophage resistance mechanisms. Nat Rev Microbiol *8*, 317-327. 10.1038/nrmicro2315.

Lampson, B.C., Inouye, M., and Inouye, S. (2005). Retrons, msDNA, and the bacterial genome. Cytogenet Genome Res *110*, 491-499. 10.1159/000084982.

Lavine, M.D., and Strand, M.R. (2002). Insect hemocytes and their role in immunity. Insect Biochem Mol Biol *32*, 1295-1309. 10.1016/s0965-1748(02)00092-9.

Le Dain, A.C., Hase, C.C., Tommassen, J., and Martinac, B. (1996). Porins of Escherichia coli: unidirectional gating by pressure. EMBO J *15*, 3524-3528.

LeCuyer, T.E., Byrne, B.A., Daniels, J.B., Diaz-Campos, D.V., Hammac, G.K., Miller, C.B., Besser, T.E., and Davis, M.A. (2018). Population Structure and Antimicrobial Resistance of Canine Uropathogenic Escherichia coli. J Clin Microbiol *56*. 10.1128/JCM.00788-18.

Leon, M., and Bastias, R. (2015). Virulence reduction in bacteriophage resistant bacteria. Front Microbiol *6*, 343. 10.3389/fmicb.2015.00343.

Letunic, I., and Bork, P. (2007). Interactive Tree Of Life (iTOL): an online tool for phylogenetic tree display and annotation. Bioinformatics *23*, 127-128. 10.1093/bioinformatics/btl529.

Li, C., Shi, T., Sun, Y., and Zhang, Y. (2022). A Novel Method to Create Efficient Phage Cocktails via Use of Phage-Resistant Bacteria. Appl Environ Microbiol *88*, e0232321. 10.1128/aem.02323-21.

Liao, Y., Smyth, G.K., and Shi, W. (2013). featureCounts: an efficient general purpose program for assigning sequence reads to genomic features. Bioinformatics *30*, 923-930. 10.1093/bioinformatics/btt656.

Lin, H., Paff, M.L., Molineux, I.J., and Bull, J.J. (2017). Therapeutic Application of Phage Capsule Depolymerases against K1, K5, and K30 Capsulated E. coli in Mice. Front Microbiol *8*, 2257. 10.3389/fmicb.2017.02257.

Lindberg, H.M., McKean, K.A., and Wang, I.N. (2014). Phage fitness may help predict phage therapy efficacy. Bacteriophage *4*, e964081. 10.4161/21597073.2014.964081.

Liu, C.M., Stegger, M., Aziz, M., Johnson, T.J., Waits, K., Nordstrom, L., Gauld, L., Weaver, B., Rolland, D., Statham, S., et al. (2018). Escherichia coli ST131-H22 as a Foodborne Uropathogen. mBio *9*. 10.1128/mBio.00470-18.

Liu, M., Deora, R., Doulatov, S.R., Gingery, M., Eiserling, F.A., Preston, A., Maskell, D.J., Simons, R.W., Cotter, P.A., Parkhill, J., and Miller, J.F. (2002). Reverse transcriptase-mediated tropism switching in Bordetella bacteriophage. Science *295*, 2091-2094. 10.1126/science.1067467.

Liu, X., and Ferenci, T. (2001). An analysis of multifactorial influences on the transcriptional control of ompF and ompC porin expression under nutrient limitation. Microbiology (Reading) *147*, 2981-2989. 10.1099/00221287-147-11-2981.

Liu, Y.F., Yan, J.J., Lei, H.Y., Teng, C.H., Wang, M.C., Tseng, C.C., and Wu, J.J. (2012). Loss of outer membrane protein C in Escherichia coli contributes to both antibiotic resistance and escaping antibody-dependent bactericidal activity. Infect Immun *80*, 1815-1822. 10.1128/IAI.06395-11.

Loenen, W.A., Dryden, D.T., Raleigh, E.A., Wilson, G.G., and Murray, N.E. (2014). Highlights of the DNA cutters: a short history of the restriction enzymes. Nucleic Acids Res *42*, 3-19. 10.1093/nar/gkt990.

Lunney, J.K., Van Goor, A., Walker, K.E., Hailstock, T., Franklin, J., and Dai, C. (2021). Importance of the pig as a human biomedical model. Sci Transl Med *13*, eabd5758. 10.1126/scitranslmed.abd5758.

Ma, J., Cai, X., Bao, Y., Yao, H., and Li, G. (2018). Uropathogenic Escherichia coli preferentially utilize metabolites in urine for nucleotide biosynthesis through salvage pathways. International Journal of Medical Microbiology *308*, 990-999. 10.1016/j.ijmm.2018.08.006.

Maiden, M.C., Bygraves, J.A., Feil, E., Morelli, G., Russell, J.E., Urwin, R., Zhang, Q., Zhou, J., Zurth, K., Caugant, D.A., et al. (1998). Multilocus

sequence typing: a portable approach to the identification of clones within populations of pathogenic microorganisms. Proc Natl Acad Sci U S A *95*, 3140-3145. 10.1073/pnas.95.6.3140.

Makarova, K.S., Wolf, Y.I., and Koonin, E.V. (2018). Classification and Nomenclature of CRISPR-Cas Systems: Where from Here? CRISPR J *1*, 325-336. 10.1089/crispr.2018.0033.

Makarova, K.S., Wolf, Y.I., Snir, S., and Koonin, E.V. (2011). Defense islands in bacterial and archaeal genomes and prediction of novel defense systems. J Bacteriol *193*, 6039-6056. 10.1128/JB.05535-11.

Mamat, U., Wilke, K., Bramhill, D., Schromm, A.B., Lindner, B., Kohl, T.A., Corchero, J.L., Villaverde, A., Schaffer, L., Head, S.R., et al. (2015). Detoxifying Escherichia coli for endotoxin-free production of recombinant proteins. Microb Cell Fact *14*, 57. 10.1186/s12934-015-0241-5.

Manges, A.R., Geum, H.M., Guo, A., Edens, T.J., Fibke, C.D., and Pitout, J.D.D. (2019). Global Extraintestinal Pathogenic Escherichia coli (ExPEC) Lineages. Clin Microbiol Rev *32*. 10.1128/CMR.00135-18.

Mann, R., Mediati, D.G., Duggin, I.G., Harry, E.J., and Bottomley, A.L. (2017). Metabolic Adaptations of Uropathogenic E. coli in the Urinary Tract. Front Cell Infect Microbiol *7*, 241. 10.3389/fcimb.2017.00241.

Manning, A.J., and Kuehn, M.J. (2011). Contribution of bacterial outer membrane vesicles to innate bacterial defense. BMC Microbiol *11*, 258. 10.1186/1471-2180-11-258.

Markoishvili, K., Tsitlanadze, G., Katsarava, R., Morris, J.G., Jr., and Sulakvelidze, A. (2002). A novel sustained-release matrix based on biodegradable poly(ester amide)s and impregnated with bacteriophages and an antibiotic shows promise in management of infected venous stasis ulcers and other poorly healing wounds. Int J Dermatol *41*, 453-458. 10.1046/j.1365-4362.2002.01451.x.

Mayrovitz, H.N., and Sims, N. (2001). Biophysical effects of water and synthetic urine on skin. Adv Skin Wound Care *14*, 302-308. 10.1097/00129334-200111000-00013.

Mazzocco, A., Waddell, T.E., Lingohr, E., and Johnson, R.P. (2009). Enumeration of bacteriophages using the small drop plaque assay system. Methods Mol Biol *501*, 81-85. 10.1007/978-1-60327-164-6_9.

McCallin, S., Sacher, J.C., Zheng, J., and Chan, B.K. (2019). Current State of Compassionate Phage Therapy. Viruses *11*. 10.3390/v11040343.

McGuire, N.C., Schulman, R., Ridgway, M.D., and Bollero, G. (2002). Detection of occult urinary tract infections in dogs with diabetes mellitus. J Am Anim Hosp Assoc *38*, 541-544. 10.5326/0380541.

Meeske, A.J., and Marraffini, L.A. (2018). RNA Guide Complementarity Prevents Self-Targeting in Type VI CRISPR Systems. Mol Cell *71*, 791-801 e793. 10.1016/j.molcel.2018.07.013.

Melo, L.D.R., Oliveira, H., Pires, D.P., Dabrowska, K., and Azeredo, J. (2020). Phage therapy efficacy: a review of the last 10 years of preclinical studies. Crit Rev Microbiol *46*, 78-99. 10.1080/1040841X.2020.1729695.

Meyer, J.R., Dobias, D.T., Medina, S.J., Servilio, L., Gupta, A., and Lenski, R.E. (2016). Ecological speciation of bacteriophage lambda in allopatry and sympatry. Science *354*, 1301-1304. 10.1126/science.aai8446.

Meyer, J.R., Dobias, D.T., Weitz, J.S., Barrick, J.E., Quick, R.T., and Lenski, R.E. (2012). Repeatability and contingency in the evolution of a key innovation in phage lambda. Science *335*, 428-432. 10.1126/science.1214449.

Miedzybrodzki, R., Fortuna, W., Weber-Dabrowska, B., and Gorski, A. (2009). A retrospective analysis of changes in inflammatory markers in patients treated with bacterial viruses. Clin Exp Med *9*, 303-312. 10.1007/s10238-009-0044-2.

Millman, A., Bernheim, A., Stokar-Avihail, A., Fedorenko, T., Voichek, M., Leavitt, A., Oppenheimer-Shaanan, Y., and Sorek, R. (2020). Bacterial Retrons Function In Anti-Phage Defense. Cell *183*, 1551-1561 e1512. 10.1016/j.cell.2020.09.065.

Molina, F., Menor-Flores, M., Fernandez, L., Vega-Rodriguez, M.A., and Garcia, P. (2022). Systematic analysis of putative phage-phage interactions on minimum-sized phage cocktails. Sci Rep *12*, 2458. 10.1038/s41598-022-06422-1.

Moxon, R., Bayliss, C., and Hood, D. (2006). Bacterial contingency loci: the role of simple sequence DNA repeats in bacterial adaptation. Annu Rev Genet *40*, 307-333. 10.1146/annurev.genet.40.110405.090442.

Mu, A., McDonald, D., Jarmusch, A.K., Martino, C., Brennan, C., Bryant, M., Humphrey, G.C., Toronczak, J., Schwartz, T., Nguyen, D., et al. (2021). Assessment of the microbiome during bacteriophage therapy in combination with systemic antibiotics to treat a case of staphylococcal device infection. Microbiome *9*, 92. 10.1186/s40168-021-01026-9.

Mukerji, S., Stegger, M., Truswell, A.V., Laird, T., Jordan, D., Abraham, R.J., Harb, A., Barton, M., O'Dea, M., and Abraham, S. (2019). Resistance to critically important antimicrobials in Australian silver gulls (Chroicocephalus novaehollandiae) and evidence of anthropogenic origins. J Antimicrob Chemother *74*, 2566-2574. 10.1093/jac/dkz242.

Mutalik, V.K., Adler, B.A., Rishi, H.S., Piya, D., Zhong, C., Koskella, B., Kutter, E.M., Calendar, R., Novichkov, P.S., Price, M.N., et al. (2020). High-

throughput mapping of the phage resistance landscape in E. coli. PLoS Biol *18*, e3000877. 10.1371/journal.pbio.3000877.

Myelnikov, D. (2018). An Alternative Cure: The Adoption and Survival of Bacteriophage Therapy in the USSR, 1922-1955. J Hist Med Allied Sci *73*, 385-411. 10.1093/jhmas/jry024.

Naas, T., Cuzon, G., Gaillot, O., Courcol, R., and Nordmann, P. (2011). When carbapenem-hydrolyzing beta-lactamase Kpc meets Escherichia coli ST131 in France. Antimicrob Agents Chemother *55*, 4933-4934. 10.1128/AAC.00719-11.

Nale, J.Y., Chutia, M., Carr, P., Hickenbotham, P.T., and Clokie, M.R. (2016). 'Get in Early'; Biofilm and Wax Moth (Galleria mellonella) Models Reveal New Insights into the Therapeutic Potential of Clostridium difficile Bacteriophages. Front Microbiol *7*, 1383. 10.3389/fmicb.2016.01383.

Nesta, B., Spraggon, G., Alteri, C., Moriel, D.G., Rosini, R., Veggi, D., Smith, S., Bertoldi, I., Pastorello, I., Ferlenghi, I., et al. (2012). FdeC, a novel broadly conserved Escherichia coli adhesin eliciting protection against urinary tract infections. mBio *3*. 10.1128/mBio.00010-12.

Nicolas-Chanoine, M.H., Bertrand, X., and Madec, J.Y. (2014). Escherichia coli ST131, an intriguing clonal group. Clin Microbiol Rev *27*, 543-574. 10.1128/CMR.00125-13.

Nicolas-Chanoine, M.H., Blanco, J., Leflon-Guibout, V., Demarty, R., Alonso, M.P., Canica, M.M., Park, Y.J., Lavigne, J.P., Pitout, J., and Johnson, J.R. (2008). Intercontinental emergence of Escherichia coli clone O25:H4-ST131 producing CTX-M-15. J Antimicrob Chemother *61*, 273-281. 10.1093/jac/dkm464.

Nielsen, T.K., Petersen, N.A., Staerk, K., Gronnemose, R.B., Palarasah, Y., Nielsen, L.F., Kolmos, H.J., Andersen, T.E., and Lund, L. (2019). A Porcine Model for Urinary Tract Infection. Front Microbiol *10*, 2564. 10.3389/fmicb.2019.02564.

Nishikawa, H., Yasuda, M., Uchiyama, J., Rashel, M., Maeda, Y., Takemura, I., Sugihara, S., Ujihara, T., Shimizu, Y., Shuin, T., and Matsuzaki, S. (2008). T-even-related bacteriophages as candidates for treatment of Escherichia coli urinary tract infections. Arch Virol *153*, 507-515. 10.1007/s00705-007-0031-4.

Niu, Y.D., Liu, H., Du, H., Meng, R., Sayed Mahmoud, E., Wang, G., McAllister, T.A., and Stanford, K. (2021). Efficacy of Individual Bacteriophages Does Not Predict Efficacy of Bacteriophage Cocktails for Control of Escherichia coli O157. Front Microbiol *12*, 616712. 10.3389/fmicb.2021.616712.

Nobrega, F.L., Vlot, M., de Jonge, P.A., Dreesens, L.L., Beaumont, H.J.E., Lavigne, R., Dutilh, B.E., and Brouns, S.J.J. (2018). Targeting mechanisms of

tailed bacteriophages. Nat Rev Microbiol *16*, 760-773. 10.1038/s41579-018-0070-8.

Normand, E.H., Gibson, N.R., Reid, S.W., Carmichael, S., and Taylor, D.J. (2000). Antimicrobial-resistance trends in bacterial isolates from companion-animal community practice in the UK. Prev Vet Med *46*, 267-278. 10.1016/s0167-5877(00)00149-5.

O'Brien, V.P., Hannan, T.J., Nielsen, H.V., and Hultgren, S.J. (2016). Drug and Vaccine Development for the Treatment and Prevention of Urinary Tract Infections. Microbiol Spectr *4*. 10.1128/microbiolspec.UTI-0013-2012.

O'Brien, V.P., Hannan, T.J., Schaeffer, A.J., and Hultgren, S.J. (2015). Are you experienced? Understanding bladder innate immunity in the context of recurrent urinary tract infection. Curr Opin Infect Dis *28*, 97-105. 10.1097/QCO.0000000000000130.

Oechslin, F. (2018). Resistance Development to Bacteriophages Occurring during Bacteriophage Therapy. Viruses *10*. 10.3390/v10070351.

Ofir, G., Melamed, S., Sberro, H., Mukamel, Z., Silverman, S., Yaakov, G., Doron, S., and Sorek, R. (2018). DISARM is a widespread bacterial defence system with broad anti-phage activities. Nat Microbiol *3*, 90-98. 10.1038/s41564-017-0051-0.

Ohshima, Y., Schumacher-Perdreau, F., Peters, G., and Pulverer, G. (1988). The role of capsule as a barrier to bacteriophage adsorption in an encapsulated Staphylococcus simulans strain. Med Microbiol Immunol *177*, 229-233. 10.1007/BF00211222.

Olin, S.J., and Bartges, J.W. (2022). Urinary Tract Infections Treatment/Comparative Therapeutics. Vet Clin North Am Small Anim Pract *52*, 581-608. 10.1016/j.cvsm.2022.01.002.

Oliveira, P.H., Touchon, M., and Rocha, E.P. (2014). The interplay of restriction-modification systems with mobile genetic elements and their prokaryotic hosts. Nucleic Acids Res *42*, 10618-10631. 10.1093/nar/gku734.

Olivenza, D.R., Casadesus, J., and Ansaldi, M. (2020). Epigenetic biosensors for bacteriophage detection and phage receptor discrimination. Environ Microbiol *22*, 3126-3142. 10.1111/1462-2920.15050.

Orskov, F., and Orskov, I. (1992). Escherichia coli serotyping and disease in man and animals. Can J Microbiol *38*, 699-704.

Otsuka, Y., and Yonesaki, T. (2012). Dmd of bacteriophage T4 functions as an antitoxin against Escherichia coli LsoA and RnlA toxins. Mol Microbiol *83*, 669-681. 10.1111/j.1365-2958.2012.07975.x.

Park de la Torriente, A. (2018). Using a high throughput assay to measure phage interactions with multidrug resistant E. coli isolates from dogs to develop a phage therapy treatment option. Master of Science (University of Edinburgh).

Parma, D.H., Snyder, M., Sobolevski, S., Nawroz, M., Brody, E., and Gold, L. (1992). The Rex system of bacteriophage lambda: tolerance and altruistic cell death. Genes Dev *6*, 497-510. 10.1101/gad.6.3.497.

Parracho, H.M., Burrowes, B.H., Enright, M.C., McConville, M.L., and Harper, D.R. (2012). The role of regulated clinical trials in the development of bacteriophage therapeutics. J Mol Genet Med *6*, 279-286. 10.4172/1747-0862.1000050.

Patterson, A.G., Jackson, S.A., Taylor, C., Evans, G.B., Salmond, G.P.C., Przybilski, R., Staals, R.H.J., and Fineran, P.C. (2016). Quorum Sensing Controls Adaptive Immunity through the Regulation of Multiple CRISPR-Cas Systems. Mol Cell *64*, 1102-1108. 10.1016/j.molcel.2016.11.012.

Pawluk, A., Staals, R.H., Taylor, C., Watson, B.N., Saha, S., Fineran, P.C., Maxwell, K.L., and Davidson, A.R. (2016). Inactivation of CRISPR-Cas systems by anti-CRISPR proteins in diverse bacterial species. Nat Microbiol *1*, 16085. 10.1038/nmicrobiol.2016.85.

Payne, L.J., Meaden, S., Mestre, M.R., Palmer, C., Toro, N., Fineran, P.C., and Jackson, S.A. (2022). PADLOC: a web server for the identification of antiviral defence systems in microbial genomes. Nucleic Acids Res *50*, W541-550. 10.1093/nar/gkac400.

Pedersen, M.B., Jensen, P.R., Janzen, T., and Nilsson, D. (2002). Bacteriophage resistance of a deltathyA mutant of Lactococcus lactis blocked in DNA replication. Appl Environ Microbiol *68*, 3010-3023. 10.1128/AEM.68.6.3010-3023.2002.

Penades, J.R., Chen, J., Quiles-Puchalt, N., Carpena, N., and Novick, R.P. (2015). Bacteriophage-mediated spread of bacterial virulence genes. Curr Opin Microbiol *23*, 171-178. 10.1016/j.mib.2014.11.019.

Penziner, S., Schooley, R.T., and Pride, D.T. (2021). Animal Models of Phage Therapy. Front Microbiol *12*, 631794. 10.3389/fmicb.2021.631794.

Perrin, S. (2014). Preclinical research: Make mouse studies work. Nature *507*, 423-425. 10.1038/507423a.

Phan, M.D., Bottomley, A.L., Peters, K.M., Harry, E.J., and Schembri, M.A. (2020). Uncovering novel susceptibility targets to enhance the efficacy of third-generation cephalosporins against ESBL-producing uropathogenic Escherichia coli. J Antimicrob Chemother *75*, 1415-1423. 10.1093/jac/dkaa023.

Phan, M.D., Forde, B.M., Peters, K.M., Sarkar, S., Hancock, S., Stanton-Cook, M., Ben Zakour, N.L., Upton, M., Beatson, S.A., and Schembri, M.A. (2015a). Molecular characterization of a multidrug resistance IncF plasmid from the globally disseminated Escherichia coli ST131 clone. PLoS One *10*, e0122369. 10.1371/journal.pone.0122369.

Phan, M.D., Peters, K.M., Sarkar, S., Forde, B.M., Lo, A.W., Stanton-Cook, M., Roberts, L.W., Upton, M., Beatson, S.A., and Schembri, M.A. (2015b). Third-generation cephalosporin resistance conferred by a chromosomally encoded blaCMY-23 gene in the Escherichia coli ST131 reference strain EC958. J Antimicrob Chemother *70*, 1969-1972. 10.1093/jac/dkv066.

Phan, M.D., Peters, K.M., Sarkar, S., Lukowski, S.W., Allsopp, L.P., Gomes Moriel, D., Achard, M.E., Totsika, M., Marshall, V.M., Upton, M., et al. (2013). The serum resistome of a globally disseminated multidrug resistant uropathogenic Escherichia coli clone. PLoS Genet *9*, e1003834. 10.1371/journal.pgen.1003834.

Platell, J.L., Cobbold, R.N., Johnson, J.R., and Trott, D.J. (2010). Clonal group distribution of fluoroquinolone-resistant Escherichia coli among humans and companion animals in Australia. J Antimicrob Chemother *65*, 1936-1938. 10.1093/jac/dkq236.

Pouillot, F., Chomton, M., Blois, H., Courroux, C., Noelig, J., Bidet, P., Bingen, E., and Bonacorsi, S. (2012). Efficacy of bacteriophage therapy in experimental sepsis and meningitis caused by a clone O25b:H4-ST131 Escherichia coli strain producing CTX-M-15. Antimicrob Agents Chemother *56*, 3568-3575. 10.1128/AAC.06330-11.

Pratt, L.A., Hsing, W., Gibson, K.E., and Silhavy, T.J. (1996). From acids to osmZ: multiple factors influence synthesis of the OmpF and OmpC porins in Escherichia coli. Mol Microbiol *20*, 911-917. 10.1111/j.1365-2958.1996.tb02532.x.

Prescott, J.F., Hanna, W.J., Reid-Smith, R., and Drost, K. (2002). Antimicrobial drug use and resistance in dogs. Can Vet J *43*, 107-116.

Price, W.H. (1948). The Stimulatory Action of Certain Fractions from Bacteria and Yeast on the Formation of a Bacterial Virus. Proc Natl Acad Sci U S A *34*, 317-323. 10.1073/pnas.34.7.317.

Qimron, U., Marintcheva, B., Tabor, S., and Richardson, C.C. (2006). Genomewide screens for Escherichia coli genes affecting growth of T7 bacteriophage. Proc Natl Acad Sci U S A *103*, 19039-19044. 10.1073/pnas.0609428103.

Qin, X., Sun, Q., Yang, B., Pan, X., He, Y., and Yang, H. (2017). Quorum sensing influences phage infection efficiency via affecting cell population and physiological state. J Basic Microbiol *57*, 162-170. 10.1002/jobm.201600510.

Rantala, M., Holso, K., Lillas, A., Huovinen, P., and Kaartinen, L. (2004). Survey of condition-based prescribing of antimicrobial drugs for dogs at a veterinary teaching hospital. Vet Rec *155*, 259-262. 10.1136/vr.155.9.259.

Reigstad, C.S., Hultgren, S.J., and Gordon, J.I. (2007). Functional genomic studies of uropathogenic Escherichia coli and host urothelial cells when intracellular bacterial communities are assembled. J Biol Chem *282*, 21259-21267. 10.1074/jbc.M611502200.

Reitzer, L., and Zimmern, P. (2019). Rapid Growth and Metabolism of Uropathogenic Escherichia coli in Relation to Urine Composition. Clin Microbiol Rev *33*. 10.1128/CMR.00101-19.

Rello, J., Parisella, F.R., and Perez, A. (2019). Alternatives to antibiotics in an era of difficult-to-treat resistance: new insights. Expert Rev Clin Pharmacol *12*, 635-642. 10.1080/17512433.2019.1619454.

Reyes-Robles, T., Dillard, R.S., Cairns, L.S., Silva-Valenzuela, C.A., Housman, M., Ali, A., Wright, E.R., and Camilli, A. (2018). Vibrio cholerae Outer Membrane Vesicles Inhibit Bacteriophage Infection. J Bacteriol *200*. 10.1128/JB.00792-17.

Rhoads, D.D., Wolcott, R.D., Kuskowski, M.A., Wolcott, B.M., Ward, L.S., and Sulakvelidze, A. (2009). Bacteriophage therapy of venous leg ulcers in humans: results of a phase I safety trial. J Wound Care *18*, 237-238, 240-233. 10.12968/jowc.2009.18.6.42801.

Rifat, D., Wright, N.T., Varney, K.M., Weber, D.J., and Black, L.W. (2008). Restriction endonuclease inhibitor IPI* of bacteriophage T4: a novel structure for a dedicated target. J Mol Biol *375*, 720-734. 10.1016/j.jmb.2007.10.064.

Robinson, M.D., McCarthy, D.J., and Smyth, G.K. (2009). edgeR: a Bioconductor package for differential expression analysis of digital gene expression data. Bioinformatics *26*, 139-140. 10.1093/bioinformatics/btp616.

Robinson-Cohen, C., Ix, J.H., Smits, G., Persky, M., Chertow, G.M., Block, G.A., and Kestenbaum, B.R. (2014). Estimation of 24-hour urine phosphate excretion from spot urine collection: development of a predictive equation. J Ren Nutr *24*, 194-199. 10.1053/j.jrn.2014.02.001.

Ross, J., and Hickling, D. (2022). Medical Treatment for Urinary Tract Infections. Urol Clin North Am *49*, 283-297. 10.1016/j.ucl.2021.12.004.

Rossmann, F.S., Racek, T., Wobser, D., Puchalka, J., Rabener, E.M., Reiger, M., Hendrickx, A.P., Diederich, A.K., Jung, K., Klein, C., and Huebner, J. (2015). Phage-mediated dispersal of biofilm and distribution of bacterial virulence genes is induced by quorum sensing. PLoS Pathog *11*, e1004653. 10.1371/journal.ppat.1004653.

Rostol, J.T., and Marraffini, L. (2019). (Ph)ighting Phages: How Bacteria Resist Their Parasites. Cell Host Microbe *25*, 184-194. 10.1016/j.chom.2019.01.009.

Rouyer, M., and Latarjet, R. (1946). [Increase in the number of bacteriophages in the presence of bacteria sterilized by irradiation]. Ann Inst Pasteur (Paris) *72*, 89-94.

Salazar, K.C., Ma, L., Green, S.I., Zulk, J.J., Trautner, B.W., Ramig, R.F., Clark, J.R., Terwilliger, A.L., and Maresso, A.W. (2021). Antiviral Resistance and Phage Counter Adaptation to Antibiotic-Resistant Extraintestinal Pathogenic Escherichia coli. mBio *12*. 10.1128/mBio.00211-21.

Samai, P., Pyenson, N., Jiang, W., Goldberg, G.W., Hatoum-Aslan, A., and Marraffini, L.A. (2015). Co-transcriptional DNA and RNA Cleavage during Type III CRISPR-Cas Immunity. Cell *161*, 1164-1174. 10.1016/j.cell.2015.04.027.

Samson, J.E., Magadan, A.H., Sabri, M., and Moineau, S. (2013). Revenge of the phages: defeating bacterial defences. Nat Rev Microbiol *11*, 675-687. 10.1038/nrmicro3096.

Sanchez-Romero, M.A., and Casadesus, J. (2014). Contribution of phenotypic heterogeneity to adaptive antibiotic resistance. Proc Natl Acad Sci U S A *111*, 355-360. 10.1073/pnas.1316084111.

Sanmukh, S.G., Admella, J., Moya-Anderico, L., Feher, T., Arevalo-Jaimes, B.V., Blanco-Cabra, N., and Torrents, E. (2023). Accessing the In Vivo Efficiency of Clinically Isolated Phages against Uropathogenic and Invasive Biofilm-Forming Escherichia coli Strains for Phage Therapy. Cells *12*. 10.3390/cells12030344.

Saraswat, M., Musante, L., Ravida, A., Shortt, B., Byrne, B., and Holthofer, H. (2013). Preparative purification of recombinant proteins: current status and future trends. Biomed Res Int *2013*, 312709. 10.1155/2013/312709.

Sarigul, N., Korkmaz, F., and Kurultak, I. (2019). A New Artificial Urine Protocol to Better Imitate Human Urine. Sci Rep *9*, 20159. 10.1038/s41598-019-56693-4.

Sarkar, S., Hutton, M.L., Vagenas, D., Ruter, R., Schuller, S., Lyras, D., Schembri, M.A., and Totsika, M. (2018). Intestinal Colonization Traits of Pandemic Multidrug-Resistant Escherichia coli ST131. J Infect Dis *218*, 979-990. 10.1093/infdis/jiy031.

Sarkar, S., Roberts, L.W., Phan, M.D., Tan, L., Lo, A.W., Peters, K.M., Paterson, D.L., Upton, M., Ulett, G.C., Beatson, S.A., et al. (2016a). Comprehensive analysis of type 1 fimbriae regulation in fimB-null strains from the multidrug resistant Escherichia coli ST131 clone. Mol Microbiol *101*, 1069-1087. 10.1111/mmi.13442.

Sarkar, S., Vagenas, D., Schembri, M.A., and Totsika, M. (2016b). Biofilm formation by multidrug resistant Escherichia coli ST131 is dependent on type 1 fimbriae and assay conditions. Pathog Dis *74*. 10.1093/femspd/ftw013.

Sarker, S.A., Berger, B., Deng, Y., Kieser, S., Foata, F., Moine, D., Descombes, P., Sultana, S., Huq, S., Bardhan, P.K., et al. (2017). Oral application of Escherichia coli bacteriophage: safety tests in healthy and diarrheal children from Bangladesh. Environ Microbiol *19*, 237-250. 10.1111/1462-2920.13574.

Sarker, S.A., McCallin, S., Barretto, C., Berger, B., Pittet, A.C., Sultana, S., Krause, L., Huq, S., Bibiloni, R., Bruttin, A., et al. (2012). Oral T4-like phage cocktail application to healthy adult volunteers from Bangladesh. Virology *434*, 222-232. 10.1016/j.virol.2012.09.002.

Scanlan, P.D., and Buckling, A. (2012). Co-evolution with lytic phage selects for the mucoid phenotype of Pseudomonas fluorescens SBW25. ISME J *6*, 1148-1158. 10.1038/ismej.2011.174.

Schembri, M.A., Zakour, N.L., Phan, M.D., Forde, B.M., Stanton-Cook, M., and Beatson, S.A. (2015). Molecular Characterization of the Multidrug Resistant Escherichia coli ST131 Clone. Pathogens *4*, 422-430. 10.3390/pathogens4030422.

Schmiemann, G., Kniehl, E., Gebhardt, K., Matejczyk, M.M., and Hummers-Pradier, E. (2010). The diagnosis of urinary tract infection: a systematic review. Dtsch Arztebl Int *107*, 361-367. 10.3238/arztebl.2010.0361.

Schneeberger, C., Holleman, F., and Geerlings, S.E. (2016). Febrile urinary tract infections: pyelonephritis and urosepsis. Curr Opin Infect Dis *29*, 80-85. 10.1097/QCO.0000000000000227.

Schneier, M., Razdan, S., Miller, A.M., Briceno, M.E., and Barua, S. (2020). Current technologies to endotoxin detection and removal for biopharmaceutical purification. Biotechnol Bioeng *117*, 2588-2609. 10.1002/bit.27362.

Schooley, R.T., Biswas, B., Gill, J.J., Hernandez-Morales, A., Lancaster, J., Lessor, L., Barr, J.J., Reed, S.L., Rohwer, F., Benler, S., et al. (2017). Development and Use of Personalized Bacteriophage-Based Therapeutic Cocktails To Treat a Patient with a Disseminated Resistant Acinetobacter baumannii Infection. Antimicrob Agents Chemother *61*. 10.1128/AAC.00954-17.

Scott, A.E., Timms, A.R., Connerton, P.L., Loc Carrillo, C., Adzfa Radzum, K., and Connerton, I.F. (2007). Genome dynamics of Campylobacter jejuni in response to bacteriophage predation. PLoS Pathog *3*, e119. 10.1371/journal.ppat.0030119.

Scott, V.C., Haake, D.A., Churchill, B.M., Justice, S.S., and Kim, J.H. (2015). Intracellular Bacterial Communities: A Potential Etiology for Chronic Lower Urinary Tract Symptoms. Urology *86*, 425-431. 10.1016/j.urology.2015.04.002.

Seed, K.D., and Dennis, J.J. (2009). Experimental bacteriophage therapy increases survival of Galleria mellonella larvae infected with clinically relevant strains of the Burkholderia cepacia complex. Antimicrob Agents Chemother *53*, 2205-2208. 10.1128/AAC.01166-08.

Seemann, T. Snippy: fast bacterial variant calling from NGS reads 2015https. github. com/tseemann/snippy.

Seemann, T. (2014). Prokka: rapid prokaryotic genome annotation. Bioinformatics *30*, 2068-2069. 10.1093/bioinformatics/btu153.

Seguin, M.A., Vaden, S.L., Altier, C., Stone, E., and Levine, J.F. (2003). Persistent urinary tract infections and reinfections in 100 dogs (1989-1999). J Vet Intern Med *17*, 622-631. 10.1111/j.1939-1676.2003.tb02492.x.

Semenova, E., Jore, M.M., Datsenko, K.A., Semenova, A., Westra, E.R., Wanner, B., van der Oost, J., Brouns, S.J., and Severinov, K. (2011). Interference by clustered regularly interspaced short palindromic repeat (CRISPR) RNA is governed by a seed sequence. Proc Natl Acad Sci U S A *108*, 10098-10103. 10.1073/pnas.1104144108.

Severi, E., Muller, A., Potts, J.R., Leech, A., Williamson, D., Wilson, K.S., and Thomas, G.H. (2008). Sialic acid mutarotation is catalyzed by the Escherichia coli beta-propeller protein YjhT. J Biol Chem *283*, 4841-4849. 10.1074/jbc.M707822200.

Sidjabat, H.E., Paterson, D.L., Adams-Haduch, J.M., Ewan, L., Pasculle, A.W., Muto, C.A., Tian, G.B., and Doi, Y. (2009). Molecular epidemiology of CTX-M-producing Escherichia coli isolates at a tertiary medical center in western Pennsylvania. Antimicrob Agents Chemother *53*, 4733-4739. 10.1128/AAC.00533-09.

Sidjabat, H.E., Townsend, K.M., Lorentzen, M., Gobius, K.S., Fegan, N., Chin, J.J., Bettelheim, K.A., Hanson, N.D., Bensink, J.C., and Trott, D.J. (2006). Emergence and spread of two distinct clonal groups of multidrug-resistant Escherichia coli in a veterinary teaching hospital in Australia. J Med Microbiol *55*, 1125-1134. 10.1099/jmm.0.46598-0.

Simmonds, P., Adriaenssens, E.M., Zerbini, F.M., Abrescia, N.G.A., Aiewsakun, P., Alfenas-Zerbini, P., Bao, Y., Barylski, J., Drosten, C., Duffy, S., et al. (2023). Four principles to establish a universal virus taxonomy. PLoS Biol *21*, e3001922. 10.1371/journal.pbio.3001922.

Simmons, E.L., Drescher, K., Nadell, C.D., and Bucci, V. (2018). Phage mobility is a core determinant of phage-bacteria coexistence in biofilms. ISME J *12*, 531-543. 10.1038/ismej.2017.190.

Snyder, J.A., Haugen, B.J., Buckles, E.L., Lockatell, C.V., Johnson, D.E., Donnenberg, M.S., Welch, R.A., and Mobley, H.L. (2004). Transcriptome of uropathogenic Escherichia coli during urinary tract infection. Infect Immun *72*, 6373-6381. 10.1128/IAI.72.11.6373-6381.2004.

Speck, P., and Smithyman, A. (2016). Safety and efficacy of phage therapy via the intravenous route. FEMS Microbiol Lett *363*. 10.1093/femsle/fnv242.

Spizizen, J. (1943). Some Preliminary Studies on the Mechanism of Virus Multiplication. Proc Natl Acad Sci U S A *29*, 109-114. 10.1073/pnas.29.3-4.109.

Spizizen, J., Kenney, J.C., and Hampil, B. (1951). Biochemical studies on the phenomenon of virus reproduction. III. The inhibition of coliphage T2r+ multiplication by sodium salicylate and sodium gentisate. J Bacteriol *62*, 323-329. 10.1128/jb.62.3.323-329.1951.

Stocks, C.J., Phan, M.D., Achard, M.E.S., Nhu, N.T.K., Condon, N.D., Gawthorne, J.A., Lo, A.W., Peters, K.M., McEwan, A.G., Kapetanovic, R., et al. (2019). Uropathogenic Escherichia coli employs both evasion and resistance to subvert innate immune-mediated zinc toxicity for dissemination. Proc Natl Acad Sci U S A *116*, 6341-6350. 10.1073/pnas.1820870116.

Subashchandrabose, S., and Mobley, H.L.T. (2015). Virulence and Fitness Determinants of Uropathogenic Escherichia coli. Microbiol Spectr *3*. 10.1128/microbiolspec.UTI-0015-2012.

Sulakvelidze, A. (2011). Bacteriophage: A new journal for the most ubiquitous organisms on Earth. Bacteriophage *1*, 1-2. 10.4161/bact.1.1.15030.

Sullivan, M.J., Petty, N.K., and Beatson, S.A. (2011). Easyfig: a genome comparison visualizer. Bioinformatics *27*, 1009-1010. 10.1093/bioinformatics/btr039.

Sumby, P., and Smith, M.C. (2002). Genetics of the phage growth limitation (Pgl) system of Streptomyces coelicolor A3(2). Mol Microbiol *44*, 489-500. 10.1046/j.1365-2958.2002.02896.x.

Summers, W.C. (2001). Bacteriophage therapy. Annu Rev Microbiol *55*, 437-451. 10.1146/annurev.micro.55.1.437.

Suttle, C.A. (2005). Viruses in the sea. Nature *437*, 356-361. 10.1038/nature04160.

Swindle, M.M., Makin, A., Herron, A.J., Clubb, F.J., Jr., and Frazier, K.S. (2012). Swine as models in biomedical research and toxicology testing. Vet Pathol *49*, 344-356. 10.1177/0300985811402846.

Tan, C.H., Oh, H.S., Sheraton, V.M., Mancini, E., Joachim Loo, S.C., Kjelleberg, S., Sloot, P.M.A., and Rice, S.A. (2020). Convection and the Extracellular Matrix Dictate Inter- and Intra-Biofilm Quorum Sensing Communication in Environmental Systems. Environ Sci Technol *54*, 6730-6740. 10.1021/acs.est.0c00716.

Tandogdu, Z., and Wagenlehner, F.M. (2016). Global epidemiology of urinary tract infections. Curr Opin Infect Dis *29*, 73-79. 10.1097/QCO.0000000000000228.

Taylor, E.N., and Curhan, G.C. (2007). Differences in 24-hour urine composition between black and white women. J Am Soc Nephrol *18*, 654-659. 10.1681/ASN.2006080854.

Terlizzi, M.E., Gribaudo, G., and Maffei, M.E. (2017). UroPathogenic Escherichia coli (UPEC) Infections: Virulence Factors, Bladder Responses, Antibiotic, and Non-antibiotic Antimicrobial Strategies. Front Microbiol *8*, 1566. 10.3389/fmicb.2017.01566.

Tesson, F., Herve, A., Mordret, E., Touchon, M., d'Humieres, C., Cury, J., and Bernheim, A. (2022). Systematic and quantitative view of the antiviral arsenal of prokaryotes. Nat Commun *13*, 2561. 10.1038/s41467-022-30269-9.

Thompson, M.F., Litster, A.L., Platell, J.L., and Trott, D.J. (2011). Canine bacterial urinary tract infections: new developments in old pathogens. Vet J *190*, 22-27. 10.1016/j.tvjl.2010.11.013.

Tomenius, H., Pernestig, A.K., Jonas, K., Georgellis, D., Mollby, R., Normark, S., and Melefors, O. (2006). The Escherichia coli BarA-UvrY two-component system is a virulence determinant in the urinary tract. BMC Microbiol *6*, 27. 10.1186/1471-2180-6-27.

Torres-Barcelo, C. (2018). Phage Therapy Faces Evolutionary Challenges. Viruses *10*. 10.3390/v10060323.

Totsika, M., Beatson, S.A., Sarkar, S., Phan, M.D., Petty, N.K., Bachmann, N., Szubert, M., Sidjabat, H.E., Paterson, D.L., Upton, M., and Schembri, M.A. (2011). Insights into a multidrug resistant Escherichia coli pathogen of the globally disseminated ST131 lineage: genome analysis and virulence mechanisms. PLoS One *6*, e26578. 10.1371/journal.pone.0026578.

Trampari, E., Zhang, C., Gotts, K., Savva, G.M., Bavro, V.N., and Webber, M. (2022). Cefotaxime Exposure Selects Mutations within the CA-Domain of envZ Which Promote Antibiotic Resistance but Repress Biofilm Formation in Salmonella. Microbiol Spectr *10*, e0214521. 10.1128/spectrum.02145-21.

Tynecki, P., Guziński, A., Kazimierczak, J., Jadczuk, M., Dastych, J., and Onisko, A. (2020). PhageAI - Bacteriophage Life Cycle Recognition with Machine Learning and Natural Language Processing. bioRxiv, 2020.2007.2011.198606. 10.1101/2020.07.11.198606.

Ujmajuridze, A., Chanishvili, N., Goderdzishvili, M., Leitner, L., Mehnert, U., Chkhotua, A., Kessler, T.M., and Sybesma, W. (2018). Adapted Bacteriophages for Treating Urinary Tract Infections. Front Microbiol *9*, 1832. 10.3389/fmicb.2018.01832.

van Driel, A.A., Notermans, D.W., Meima, A., Mulder, M., Donker, G.A., Stobberingh, E.E., and Verbon, A. (2019). Antibiotic resistance of Escherichia coli isolated from uncomplicated UTI in general practice patients over a 10-year period. Eur J Clin Microbiol Infect Dis *38*, 2151-2158. 10.1007/s10096-019-03655-3.

van Houte, S., Buckling, A., and Westra, E.R. (2016). Evolutionary Ecology of Prokaryotic Immune Mechanisms. Microbiol Mol Biol Rev *80*, 745-763. 10.1128/MMBR.00011-16.

Vejborg, R.M., de Evgrafov, M.R., Phan, M.D., Totsika, M., Schembri, M.A., and Hancock, V. (2012). Identification of genes important for growth of asymptomatic bacteriuria Escherichia coli in urine. Infect Immun *80*, 3179-3188. 10.1128/IAI.00473-12.

Vidakovic, L., Singh, P.K., Hartmann, R., Nadell, C.D., and Drescher, K. (2018). Dynamic biofilm architecture confers individual and collective mechanisms of viral protection. Nat Microbiol *3*, 26-31. 10.1038/s41564-017-0050-1.

Vigil, P.D., Stapleton, A.E., Johnson, J.R., Hooton, T.M., Hodges, A.P., He, Y., and Mobley, H.L. (2011). Presence of putative repeat-in-toxin gene tosA in Escherichia coli predicts successful colonization of the urinary tract. mBio *2*, e00066-00011. 10.1128/mBio.00066-11.

Vimont, S., Boyd, A., Bleibtreu, A., Bens, M., Goujon, J.M., Garry, L., Clermont, O., Denamur, E., Arlet, G., and Vandewalle, A. (2012). The CTX-M-15-producing Escherichia coli clone O25b: H4-ST131 has high intestine colonization and urinary tract infection abilities. PLoS One *7*, e46547. 10.1371/journal.pone.0046547.

Wahl, R. (1946). [Influence of the composition of the medium on bacteriophagia]. Ann Inst Pasteur (Paris) *72*, 73-80.

Waldbauer, J.R., Coleman, M.L., Rizzo, A.I., Campbell, K.L., Lotus, J., and Zhang, L. (2019). Nitrogen sourcing during viral infection of marine cyanobacteria. Proc Natl Acad Sci U S A *116*, 15590-15595. 10.1073/pnas.1901856116.

Walker, P.J., Siddell, S.G., Lefkowitz, E.J., Mushegian, A.R., Adriaenssens, E.M., Alfenas-Zerbini, P., Dempsey, D.M., Dutilh, B.E., Garcia, M.L., Curtis Hendrickson, R., et al. (2022). Recent changes to virus taxonomy ratified by the International Committee on Taxonomy of Viruses (2022). Arch Virol *167*, 2429-2440. 10.1007/s00705-022-05516-5.

Wang, C., Tu, J., Liu, J., and Molineux, I.J. (2019). Structural dynamics of bacteriophage P22 infection initiation revealed by cryo-electron tomography. Nat Microbiol *4*, 1049-1056. 10.1038/s41564-019-0403-z.

Watanabe, R., Matsumoto, T., Sano, G., Ishii, Y., Tateda, K., Sumiyama, Y., Uchiyama, J., Sakurai, S., Matsuzaki, S., Imai, S., and Yamaguchi, K. (2007). Efficacy of bacteriophage therapy against gut-derived sepsis caused by Pseudomonas aeruginosa in mice. Antimicrob Agents Chemother *51*, 446-452. 10.1128/AAC.00635-06.

Wattam, A.R., Abraham, D., Dalay, O., Disz, T.L., Driscoll, T., Gabbard, J.L., Gillespie, J.J., Gough, R., Hix, D., Kenyon, R., et al. (2014). PATRIC, the bacterial bioinformatics database and analysis resource. Nucleic Acids Res *42*, D581-591. 10.1093/nar/gkt1099.

Wattam, A.R., Davis, J.J., Assaf, R., Boisvert, S., Brettin, T., Bun, C., Conrad, N., Dietrich, E.M., Disz, T., Gabbard, J.L., et al. (2017). Improvements to PATRIC, the all-bacterial Bioinformatics Database and Analysis Resource Center. Nucleic Acids Res *45*, D535-D542. 10.1093/nar/gkw1017.

Weese, J.S., Blondeau, J., Boothe, D., Guardabassi, L.G., Gumley, N., Papich, M., Jessen, L.R., Lappin, M., Rankin, S., Westropp, J.L., and Sykes, J. (2019). International Society for Companion Animal Infectious Diseases (ISCAID) guidelines for the diagnosis and management of bacterial urinary tract infections in dogs and cats. Vet J *247*, 8-25. 10.1016/j.tvjl.2019.02.008.

Weinbauer, M.G. (2004). Ecology of prokaryotic viruses. FEMS Microbiol Rev *28*, 127-181. 10.1016/j.femsre.2003.08.001.

Whittam, T.S., Ochman, H., and Selander, R.K. (1983). Multilocus genetic structure in natural populations of Escherichia coli. Proc Natl Acad Sci U S A *80*, 1751-1755. 10.1073/pnas.80.6.1751.

WHO (2018). High levels of antibiotic resistance found worldwide, new data shows. In C. Lindmeier, ed. World Health Organization.

Wick, R.R., Judd, L.M., Gorrie, C.L., and Holt, K.E. (2017). Unicycler: Resolving bacterial genome assemblies from short and long sequencing reads. PLoS Comput Biol *13*, e1005595. 10.1371/journal.pcbi.1005595.

Wick, R.R., and Menzel, P. (2017). Filtlong. Available online: github. com/rrwick/Filtlong (accessed on 15 August 2021).

Wickham, H. (2011). ggplot2. Wiley interdisciplinary reviews: computational statistics *3*, 180-185.

Wilding, K.M., Hunt, J.P., Wilkerson, J.W., Funk, P.J., Swensen, R.L., Carver, W.C., Christian, M.L., and Bundy, B.C. (2019). Endotoxin-Free E. coli-Based Cell-Free Protein Synthesis: Pre-Expression Endotoxin Removal Approaches for on-Demand Cancer Therapeutic Production. Biotechnol J *14*, e1800271. 10.1002/biot.201800271.

Wills, Q.F., Kerrigan, C., and Soothill, J.S. (2005). Experimental bacteriophage protection against Staphylococcus aureus abscesses in a rabbit model. Antimicrob Agents Chemother *49*, 1220-1221. 10.1128/AAC.49.3.1220-1221.2005.

Wright, A., Hawkins, C.H., Anggard, E.E., and Harper, D.R. (2009). A controlled clinical trial of a therapeutic bacteriophage preparation in chronic otitis due to antibiotic-resistant Pseudomonas aeruginosa; a preliminary report of efficacy. Clin Otolaryngol *34*, 349-357. 10.1111/j.1749-4486.2009.01973.x.

Xicohtencatl-Cortes, J., Cruz-Cordova, A., Cazares-Dominguez, V., Escalona-Venegas, G., Zavala-Vega, S., Arellano-Galindo, J., Romo-Castillo, M., Hernandez-Castro, R., Ochoa, S.A., and Luna-Pineda, V.M. (2019). Uropathogenic Escherichia coli strains harboring tosA gene were associated to high virulence genes and a multidrug-resistant profile. Microb Pathog *134*, 103593. 10.1016/j.micpath.2019.103593.

Yoon, E.J., Choi, M.H., Park, Y.S., Lee, H.S., Kim, D., Lee, H., Shin, K.S., Shin, J.H., Uh, Y., Kim, Y.A., et al. (2018). Impact of host-pathogen-treatment tripartite components on early mortality of patients with Escherichia coli bloodstream infection: Prospective observational study. EBioMedicine *35*, 76-86. 10.1016/j.ebiom.2018.08.029.

Yuri, K., Nakata, K., Katae, H., Yamamoto, S., and Hasegawa, A. (1998). Distribution of uropathogenic virulence factors among Escherichia coli strains isolated from dogs and cats. J Vet Med Sci *60*, 287-290. 10.1292/jvms.60.287.

Zetsche, B., Gootenberg, J.S., Abudayyeh, O.O., Slaymaker, I.M., Makarova, K.S., Essletzbichler, P., Volz, S.E., Joung, J., van der Oost, J., Regev, A., et al. (2015). Cpf1 is a single RNA-guided endonuclease of a class 2 CRISPR-Cas system. Cell *163*, 759-771. 10.1016/j.cell.2015.09.038.

Zogg, A.L., Zurfluh, K., Schmitt, S., Nuesch-Inderbinen, M., and Stephan, R. (2018). Antimicrobial resistance, multilocus sequence types and virulence profiles of ESBL producing and non-ESBL producing uropathogenic Escherichia coli isolated from cats and dogs in Switzerland. Vet Microbiol *216*, 79-84. 10.1016/j.vetmic.2018.02.011.

Zulk, J.J., Clark, J.R., Ottinger, S., Ballard, M.B., Mejia, M.E., Mercado-Evans, V., Heckmann, E.R., Sanchez, B.C., Trautner, B.W., Maresso, A.W., and

Patras, K.A. (2022). Phage Resistance Accompanies Reduced Fitness of Uropathogenic Escherichia coli in the Urinary Environment. mSphere *7*, e0034522. 10.1128/msphere.00345-22.

Chapter 9 Appendices

9.1 Appendix 1

Standard Operating Procedure: Preparation of Artificial Urine (AU)

REAGENTS REQUIRED:					
Formula	Name	Mass (g) per 100 mL	CAS number	Catalogue code	Manufacturer
Na_2SO_4	Sodium sulphate	0.17			
$Na_3C_6H_5O_7.2H_2O$	Tri-sodium citrate	0.072			
$C_4H_7N_3O$	Creatinine	0.081	60-27-5	K5225680	Sigma
CH_4N_2O	Urea	1.5	57-13-6	15604-1Kg	Sigma
KCl	Potassium chloride	0.2308			
NaCl	Sodium chloride	0.1756			
$CaCl_2$	Calcium chloride anhydrous	0.0185	10043-52-4	C1016-500G	Sigma
NH_4Cl	Ammonium chloride	0.1266			
$K_2C_2O_4.H_2O$	Potassium oxalate	0.0035	607-007-00-3	G0425-250G	Honeywell
$MgSO_4.7H_2O$	Magnesium sulphate	0.1082	10034-99-8	M2773-500G	Sigma
$NaH_2PO_4.2H_2O$	Sodium dihydrogen orthophosphate dihydrate	0.2912	13472-35-0		
$Na_2HPO_4.2H_2O$	Sodium phosphate monobasic dihydrate	0.0831	10028-24-7	71645-1Kg	Sigma
	Bacteriological Peptone	0.2		LP0037	Oxoid
	Yeast Extract	0.0018		70161-100g	Fluka

	Ultrapure autoclaved water

METHOD:

Reagent ID	Formula	Name	Recommended Stock Preparation
1	Na_2SO_4	Sodium sulphate	8.5g in 50mL water (X100)
2	$Na_3C_6H_5O_7.2H_2O$	Tri-sodium citrate	3.6g in 50mL water (X100)
3	$C_4H_7N_3O$	Creatinine	4.05g in 50mL water (X100) do not chill
4	CH_4N_2O	Urea	(15g per 100mL) 22.5g in 150mL water (X10) made fresh on the day of combining reagents. Endothermic, warm to 37C to prevent cooling the mixture upon addition and causing other salts to precipitate *Calculate how much required on the day.*
5	KCl	Potassium chloride	11.54g in 50mL water (X100)
6	NaCl	Sodium chloride	8.78g in 50mL water (X100)
7	$CaCl_2$	Calcium chloride anhydrous	0.925g in 50mL water (X100) caution - alkali
8	NH_4Cl	Ammonium chloride	6.33g in 50mL water (X100)
9	$K_2C_2O_4.H_2O$	Potassium oxalate	2 steps: dissolve 1.75g in 50mL water (X1000) then transfer 5mL to a new tube and make up to 50mL with water for X100
10	$MgSO_4.7H_2O$	Magnesium sulphate	5.41g in 50mL water (X100)
11	$NaH_2PO_4.2H_2O$	Sodium dihydrogen orthophosphate dihydrate	14.56g in 50mL water (X100)

12	$Na_2HPO_4.2H_2O$	Sodium phosphate monobasic dihydrate	4.155g in 50mL water (X100)
13		Bacteriological Peptone	(2g per 100mL) 9g in 450mL water in a glass bottle (X10) and autoclaved.
14		Yeast Extract	0.18g in 100mL water (X100) autoclave

Method for preparing 1L:

1. Take twelve 50 mL tubes and label with sufficient information. There are 12 reagents which require plastic tube storage so you can label these 1 to 12 but missing out number 4 for Urea. You will need two tubes for reagent 9, Potassium oxalate.
2. Weight out the chemical powders to the labelled tubes as described in the table above.
3. Add 40-45 mL ultrapure water to the powders and give them time to go fully into solution. It may be necessary to warm some chemicals.
4. Depending upon what volume of AU you want to prepare, you will need to calculate how much of reagent 4 (Urea) to make. For 1L AU, you need 100 mL of the 10X reagents so you may want to prepare 1.5 times the volumes in order to be able to accurately transfer 100 mL. Urea should be prepared in a glass bottle of sufficient size for the volume being made. After dissolving the powder and making up to the final volume with ultrapure water, warm up the urea, or use pre-warmed water to dissolve. ***Due to the endothermic nature of urea dissolving, the liquid becomes sufficiently cold such that it also cools down the mixture of reagents after it is added and will cause reagent 9 to precipitate. Once reagent 9 precipitates out of solution, it is very difficult to reverse the reaction so you will not get a true AU solution and you will need to begin mixing again! However, urea also breaks down with heat to form isocyanates which may be detrimental to bacteria/phages so it is recommended to avoid unnecessary heating.***
5. The media components, reagents 13 and 14, can be prepared in glass bottles and autoclaved.
   Note, the final AU will be filter sterilized since not all reagents are sufficiently heat stable to be sterilized by autoclaving. It is therefore not essential to autoclave the Peptone or YE but if you plan to keep these media components more than the working day, you should autoclave them and prepare them in glass bottles.

6. Top up the 12 plastic tubes to exactly 50 mL each with more ultrapure water.
7. For reagent 9, Potassium oxalate, transfer 5 mL of the now ready 1000X into a new 50 mL tube and top up to 50 mL to produce the 100X stock.
8. Take ten 10mL stripettes (which can be labelled and reused if the packaging is retained).
9. Being transferring each of the reagents into a 1L beaker or 1L measuring cylinder, one at a time in the order that they appear in the list. (It should work in any order but it can help to prevent precipitation if the order is followed.) Use a stripette to transfer 10 mL for the 100X reagents. Add reagent 9, Potassium oxalate DROPWISE to help avoid precipitation. It will also help to prevent any precipitation if you add in 100-200 mL ultrapure water at the start.
10. Transfer 100 mL of the 10X reagents.
11. Use a Bunsen with the media components (reagents 13 and 14) to maintain sterility of the stocks.
12. After addition of all 14 reagents, top up to 1L with ultrapure water and mix well.
13. Aliquot the AU as desired and freeze for storage longer than 2 days, otherwise keep at 4ºC when not in use.
14. AU contains some reagents which cannot be autoclaved, so the final solution must be filter sterilized using a 0.2 um filter before being used in an experiment.

Disposal: AU can be flushed down the sink with plenty water. AU that has been used to grow bacteria or harbours phages must be collected into an autoclavable container.

9.2 Appendix 2

Phages isolated and used throughout the study

Phage	Host	Stock Titre (PFU/ml)	Source
A1*	CAN32	9.20E+10	Waste water
A2	CAN32	8.93E+10	Waste water
A3	CAN32	7.87E+10	Waste water
C1*	CAN60	3.10E+10	Waste water
C2	CAN60	3.13E+09	Waste water
C4	CAN60	3.67E+09	Waste water
D1*	CAN74	3.33E+09	Waste water
D3*	CAN74	9.90E+09	Waste water
E1	CAN50	1.33E+10	Waste water
E2	CAN50	3.27E+09	Waste water
E3	CAN50	1.31E+09	Waste water
E4*	CAN50	5.50E+09	Waste water
F1	CAN15	1.23E+10	Waste water
F2	CAN15	5.97E+09	Waste water
F3*	CAN15	3.65E+10	Waste water
F4	CAN15	2.80E+10	Waste water
G1	CAN55	1.48E+07	Waste water
H1	CAN95	6.63E+10	Waste water
NEA2*	CAN95	1.86E+11	Waste water
NEB1*	CAN74	1.29E+09	Waste water
NEB2	CAN74	1.26E+09	Waste water
NEC1*	CAN55	1.02E+09	Waste water
ALD1*	CAN98	6.83E+10	Waste water
ALD2*	CAN64	2.07E+10	Waste water
ALDi64	CAN64	7.27E+09	Waste water
ALDi98*	CAN98	1.88E+11	Waste water
FWW41*	CAN41	1.15E+10	Waste water
LUC4*	EC958	2.36E+10	Waste water
AB3	EC9	2.87E+10	Phage Technology Centre
AB9	EC9	1.09E+10	Phage Technology Centre

TB69	EC76	1.27E+10	Phage Technology Centre
TB77	EC70	1.83E+09	Phage Technology Centre
TB49	EC13	9.67E+09	Phage Technology Centre
AB19	EC72	1.04E+10	Phage Technology Centre
GWF	EC2	3.63E+09	Phage Technology Centre
TB70	EC67	6.67E+07	Phage Technology Centre
RV2	E45	1.40E+10	Phage Technology Centre
KRA2	E45	4.24E+11	Phage Technology Centre
TB123	E45	3.57E+10	Phage Technology Centre
HAM53	E45	6.30E+08	Phage Technology Centre
CUCA1	ECRA362.1	6.7E+6	Waste water
CHAP1	ECRA242.9	2.6E+7	Waste water
BU1	ECRA242.2	1.2E+7	Waste water
PER1	ECRA363.9	1.2E+7	Waste water
RIT02	EC958	2.1E+6	Waste water
NAM34	EC958	7.2E+8	Waste water

9.3 Appendix 3

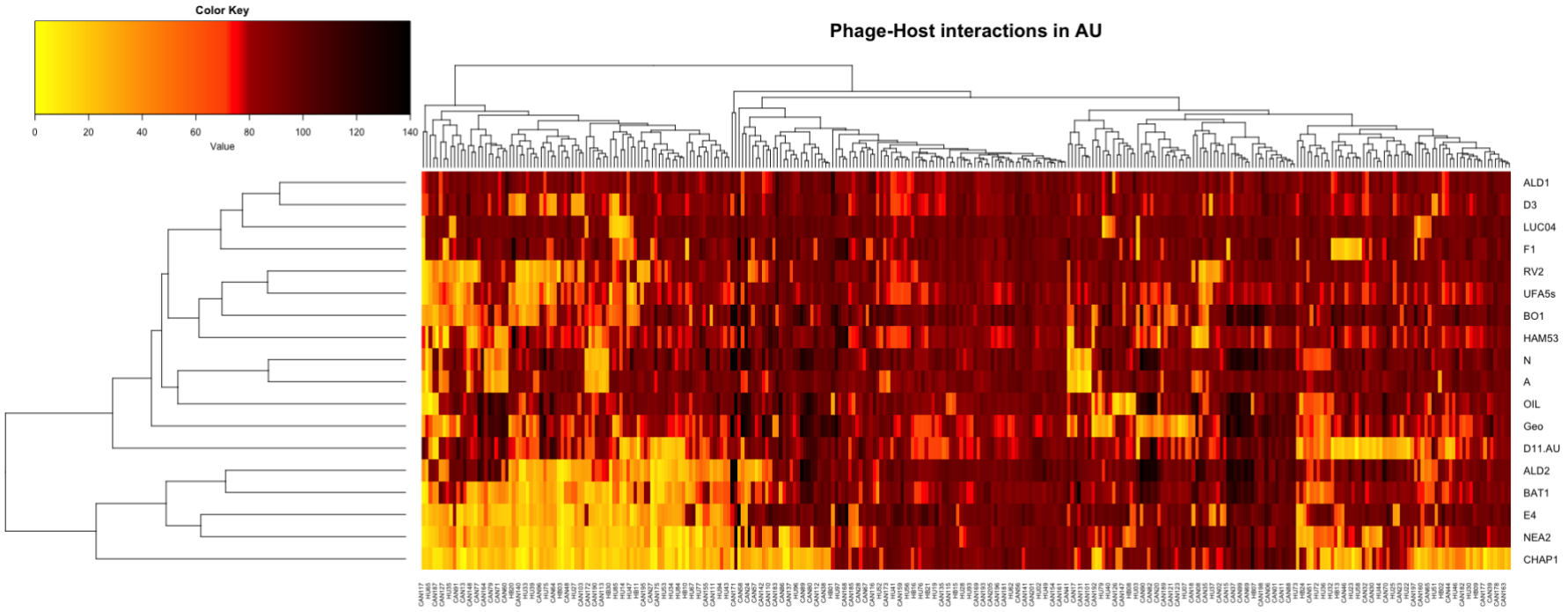

Figure 9.1 Extended phage-host interaction heatmap – work done by Marianne Keith. 300 clinical *E. coli* isolates were assayed in AU with 18 phages. Each interaction was scored by calculating the ratio of the AUC of the infected culture to the AUC of the control culture in LB. Low-scoring interactions (strong inhibition) are represented in yellow and light orange; red marks the ineffective interactions; dark red to black represent those interactions in which the presence of phage is conferring some advantage to the bacteria and allow a better growth than with no phage.

9.4 Appendix 4

Virulence factors and Antibiotic resistance genes encoded in LUC4

Virulence factors encoded in LUC4		
Source Organism	Gene	Product
Salmonella enterica subsp. enterica serovar Typhimurium str. LT2	gyrA	DNA gyrase subunit A (EC 5.99.1.3)
Shigella sonnei Ss046	yhiE	Transcriptional activator GadE
Shigella flexneri 5 str. 8401	vacB	3'-to-5' exoribonuclease RNase R
Escherichia coli O157:H7 str. EDL933	mglA	Galactose/methyl galactoside ABC transporter, ATP-binding protein MglA (EC 3.6.3.17)
Vibrio cholerae O1 biovar El Tor str. N16961	VC0647	Polyribonucleotide nucleotidyltransferase (EC 2.7.7.8)
Escherichia coli O157:H7 str. EDL933	ilvG	Acetolactate synthase large subunit (EC 2.2.1.6)

Antibiotic Resistane Genes encoded in LUC4			
Gene	Product	Function	Classification
GadE	Transcriptional activator GadE	Transcriptional activator GadE	regulator modulating expression of antibiotic resistance genes
gyrA	DNA gyrase subunit A (EC 5.99.1.3)	DNA gyrase subunit A (EC 5.99.1.3)	antibiotic target in susceptible species
AcrEF-TolC	Multidrug efflux system AcrEF-TolC, membrane fusion component AcrE	Multidrug efflux system AcrEF-TolC, membrane fusion component AcrE	efflux pump conferring antibiotic resistance
Ddl	D-alanine--D-alanine ligase (EC 6.3.2.4)	D-alanine--D-alanine ligase (EC 6.3.2.4)	antibiotic target in susceptible species

9.5 Appendix 5

Primers used throughout the project

Use	Primer name	Sequence
OmpC cloning in pWKS30	ompCFSal	CCAAGTCGACAGGGTTAATCAGTATGCAGTGG
OmpC cloning in pWKS31	ompCRBam	AAGGATCCGCAGGCCCTTTGTTCGATAT
RTqPCR	AcetylF3	TTGATGAAAGTGCCGGTGAGGTTG
RTqPCR	AcetylR3	CTATCAGGCAGTTTGCGCCAATCA
RTqPCR	PigL-F-3	GGTGCCCATCCTGATGATATAG
RTqPCR	PigL-R-3	CCACAGCAACCAGGTGT
RTqPCR	YaiO-F-1	TGCTTACACCTACGACTGGACG
RTqPCR	YaiO-R-2	CCTGCCGTCAACCCGAGATTAA
Operon cloning in pBAD33	oprnFSmaI	TGCACCCGGGTCTCCGTCACATCCCGATACATCTCCCTC
Operon cloning in pBAD33	oprnRSalI	TGCAGTCGACCAGCGTGGTGCGTCGTTTGCATTT
Lambda-red knockouts	pigL-KO-R	CTCTGAAAAAGTAAATATAAAGTATATTTAATAAGATTAATTTTTGTGTAGGCTGGAGCTGCTTC
Lambda-red knockouts	pigL-KO-F	ATGGTCATGAAGATAAATAACAAAGTTTTCATTTCTATTACTCCGATGGGAATTAGCCATGGTCC
Lambda-red knockouts	acetyl-KO-F	TTTCCGTTGTGTATGTATTATTAGCTTATGCCATCTGGATTATTTGTGTAGGCTGGAGCTGCTTC
Lambda-red knockouts	acetyl-KO-R	TTTTCTCTGAAAACTACCGAATAAAATATACTGATAGACTGCTGCATGGGAATTAGCCATGGTCC
Lambda-red knockouts	YaiO-KO-F	GAACTTACTCACTCCGACAAGAACTTATCCGTACAGGAGATTAAAGTGTAGGCTGGAGCTGCTTC
Lambda-red knockouts	YaiO-KO-R	TGCTAAAGAGAAAAATGTTCAGATTGCAGACCAGGTGATTATTGAATGGGAATTAGCCATGGTCC
Knockout verification	pigL-KO-check-F	AAGATGGAGCAGCACAGTAGAGTC
Knockout verification	pigL-KO-check-R	TCGTTGCTGGTTGTTGGTGC
Knockout verification	acetyl-KO-check-F	CAAGCCAAATTCCGAGGACAACAG
Knockout verification	YaiO-KO-check-R	CAGGCTTGGCTATCTGACTCGATG
Knockout verification	C1-R	TTATACGCAAGGCGACAAGG
Knockout verification	C1-F	GATCTTCCGTCACAGGTAGG

9.6 Appendix 6

Variant calling with SNIPPY: OUTPUT

Strain	Position	Type	REF	ALT	EVIDENCE	FTYPE	STRAND	NT POS	AA POS	EFFECT	GENE	PRODUCT
ECRP3												
ECRL7	844942	snp	C	T	T:67 C:0	CDS	+	840/2151	280/716	synonymous_variant c.840C>T p.Thr280Thr	dinG	ATP-dependent DNA helicase DinG
ECRL7	2509653	snp	G	A	A:79 G:0	CDS	-	226/1122	76/373	stop_gained c.226C>T p.Gln76*	ompC	porin OmpC
ECRP12	844942	snp	C	T	T:50 C:0	CDS	+	840/2151	280/716	synonymous_variant c.840C>T p.Thr280Thr	dinG	ATP-dependent DNA helicase DinG
ECRA3601	2509264	del	GTAATCATAAGT	G	G:40 GTAATCATAAGT:0	CDS	-	614/1122	202/373	frameshift_variant c.604_614delACTTATGATTA p.Thr202fs	ompC	porin OmpC
ECRA2422	2509264	del	GTAATCATAAGT	G	G:40 GTAATCATAAGT:0	CDS	-	614/1122	202/373	frameshift_variant c.604_614delACTTATGATTA p.Thr202fs	ompC	porin OmpC
ECRA2423												

ECRA2427	2509860	del	ACAGTACTTTAAC	A	A:17 ACAGTACTTTAAC:0	CDS	-	18/1122	3/373	conservative_inframe_deletion c.7_18delGTTAAAGTACTG p.Val3_Leu6del	ompC	porin OmpC
ECRA5444	2509368	snp	G	A	A:36 G:0	CDS	-	511/1122	171/373	stop_gained c.511C>T p.Gln171*	ompC	porin OmpC
ECRA24211												
ECRA3621	2509660	del	ACCGGTCAG	A	A:19 ACCGGTCAG:0	CDS	-	218/1122	71/373	frameshift_variant c.211_218delCTGACCGG p.Thr72fs	ompC	porin OmpC
ECRA36212	2509869	del	TA	T	T:71 TA:1	CDS	-	9/1122	3/373	frameshift_variant c.9delT p.Val5fs	ompC	porin OmpC
ECRA3632	1999003	del	GCGT	G	G:21 GCGT:0							
ECRA3633												
ECRA3635												
ECRA5445	2510215	snp	T	C	C:51 T:0							
ECRA1841	3827140	snp	A	G	G:35 A:0	CDS	-	598/720	200/239	missense_variant c.598T>C p.Ser200Pro	ompR	two-component system response regulator OmpR
ECRA1846	2509099	del	CTGAGCAGCCAGGTAGA	C	C:24 CTGAGCAGCCAGGTAGA:0	CDS	-	779/1122	255/373	frameshift_variant c.764_779delTCTACCTGGCTGCTCA p.Ile255fs	ompC	porin OmpC
ECRA1847	2509877	del	AT	A	A:33 AT:0	CDS	-	1/1122	1/373	frameshift_variant&start_lost c.1delA p.Met1fs	ompC	porin OmpC
ECRA1848	1005559	complex	GGGG	AGGA	AGGA:38 GGGG:4	CDS	+	15/441	5/146	synonymous_variant c.15_18delGGGGinsAGGA p.7	phage tail protein	

ECRA1848	4266751	ins	T	TATCC	TATCC:35 T:2	CDS	-	96/774	32/257	frameshift_variant c.93_96dupGGAT p.Ile33fs	pstB	phosphate ABC transporter ATP-binding protein PstB
ECRA18413												
ECRA3042	3826208	ins	T	TA	TA:28 T:0	CDS	-	813/1353	271/450	frameshift_variant c.813dupT p.Lys272fs	envZ	two-component system sensor histidine kinase EnvZ
ECRA3043												
ECRA3048	2508766	snp	G	C	C:45 G:0	CDS	-	1113/1122	371/373	stop_gained c.1113C>G p.Tyr371*	ompC	porin OmpC
ECRA3049	2509838	snp	A	C	C:59 A:0	CDS	-	41/112	14/373	missense_variant c.41T>G p.Leu14Arg	ompC	porin OmpC
ECRA4242												
ECRA7209												
ECRA72015												
ECRA72027												
ECRL10												
ECRL11												

9.7 Appendix 7

Known anti-phage systems in EC958

	system	target.name	hmm.accession	hmm.name	protein.name	full.seq.E.value	domain.iE.value	target.coverage	hmm.coverage	start	end	strand	relative.position
5	RM_type_I	EC958_RS01535	PDLC03104	Specificity_I_00053	Specificity_I	1.10E-302	1.30E-302	0.998	0.998	318664	319912	-	297
5	RM_type_I	EC958_RS01540	PDLC03033	MTase_I_00016	MTase_I	1.30E-304	1.40E-304	0.996	0.998	319901	321539	-	298
5	RM_type_I	EC958_RS01545	PDLC03048	REase_I_00009	REase_I	1.20E-43	1.90E-34	0.484	0.529	321532	324631	-	299
1	AbiE	EC958_RS01550	PDLC02227	AbiEi_WP_068866247.1	AbiEi	1.30E-77	1.40E-77	0.954	0.966	324914	325697	+	300
1	AbiE	EC958_RS01555	PDLC02290	AbiEii_WP_067065479.1	AbiEii	4.30E-115	4.80E-115	0.98	0.986	325683	326604	+	301
4	retron_I-C	NA	-	TypeIC1_IC2	msr-msd	3.80E-25	NA	NA	NA	1349627	1349755	+	1294.011
4	retron_I-C	EC958_RS06845	PDLC02963	retron_type_I_C1_RT_typeIC1	RT-Toprim_I-C	4.80E-214	5.50E-214	0.979	0.989	1349786	1351544	+	1295
7	RM_type_II	EC958_RS11000	PDLC03397	NEase_II_00006	REase_II	2.30E-111	2.50E-111	0.994	0.994	2124720	2125191	-	2060
7	RM_type_II	EC958_RS11005	PDLC03361	MTase_II_00147	MTase_II	1.10E-259	1.20E-259	0.996	0.996	2125171	2126590	-	2061
2	AbiE	EC958_RS16935	PDLC02229	AbiEi_WP_092960020.1	AbiEi	3.90E-52	4.30E-52	0.985	0.969	3358348	3358744	+	3136
2	AbiE	EC958_RS16940	PDLC02297	AbiEii_WP_106546964.1	AbiEii	1.80E-116	2.00E-116	0.993	0.938	3358736	3359630	+	3137
3	brex_type_I	EC958_RS20790	PDLC02439	BrxA_00003	BrxA	2.30E-115	2.50E-115	0.995	0.995	4142003	4142606	+	3858
3	brex_type_I	EC958_RS20795	PDLC02463	BrxB_00005	BrxB	4.50E-68	5.10E-68	0.915	0.964	4142602	4143205	+	3859
3	brex_type_I	EC958_RS20800	PDLC02471	BrxC_00001	BrxC	0	0	0.999	0.999	4143216	4146858	+	3860

3	brex_type_I	EC958_RS20805	PDLC02521	PglX_00007	PglX	0	0	0.992	0.995	4146903	4150509	+	3861
3	brex_type_I	EC958_RS20810	PDLC02547	PglZ_00006	PglZ	0	0	0.999	0.999	4150685	4153283	+	3862
3	brex_type_I	EC958_RS20815	PDLC02506	BrxL_00002	BrxL	0	0	0.968	0.991	4153293	4155378	+	3863
8	RM_type_II	EC958_RS24890	PDLC03365	MTase_II_00151	MTase_II	0	0	0.998	0.971	4977698	4979321	+	4585
8	RM_type_II	EC958_RS24895	PDLC03381	MTase_II_00167	MTase_II	6.10E-293	6.80E-293	0.997	0.997	4979313	4980504	+	4586
8	RM_type_II	EC958_RS24900	PDLC03469	REase_II_00071	REase_II	1.90E-235	2.20E-235	0.976	0.996	4980516	4982256	-	4587
6	RM_type_I	EC958_RS25255	PDLC03040	REase_I_00001	REase_I	0	0	0.995	0.996	5047963	5051227	-	4645
6	RM_type_I	EC958_RS25260	PDLC03168	Specificity_I_00117	Specificity_I	1.70E-154	1.90E-154	0.998	0.998	5051321	5052626	-	4646
6	RM_type_I	EC958_RS25265	PDLC03019	MTase_I_00002	MTase_I	3.40E-193	4.20E-193	0.976	0.536	5052615	5054235	-	4647

9.8 Appendix 8

RNA-seq results: Differentially expressed genes with statistical significance

	logFC	logCPM	PValue	FDR
PIG-L family deacetylase	10.4973699	8.55596928	5.90E-11	2.22E-07
glutamyl-tRNA amidotransferase	-5.7009872	4.23326477	8.43E-10	1.36E-06
acetyltransferase	6.60081899	6.91582251	1.71E-09	1.36E-06
acyl-CoA synthetase FdrA	-3.6077859	7.07477259	1.83E-09	1.36E-06
bifunctional demethylmenaquinone methyltransferase/2-methoxy-6-polyprenyl-1%2C4-benzoquinol methylase UbiE	-2.2776265	7.41356105	2.03E-09	1.36E-06
DUF2877 domain-containing protein	-4.1735526	7.77702753	2.18E-09	1.36E-06
YaiO family outer membrane beta-barrel protein	7.5271942	7.93013256	3.76E-09	2.02E-06
YlcI/YnfO family protein	-3.1226666	4.09410258	7.20E-09	3.39E-06
DUF1116 domain-containing protein	-3.8801796	6.87824193	2.97E-08	1.24E-05
4-aminobutyrate--2-oxoglutarate transaminase	2.6982384	8.63276001	1.39E-07	5.20E-05
gamma-glutamyltransferase	1.83562893	6.19700409	1.57E-07	5.20E-05
proofreading thioesterase EntH	-2.0429151	5.44514497	1.66E-07	5.20E-05
nitrate/nitrite transporter NarU	2.6454008	4.10595435	1.92E-07	5.27E-05
YgdI/YgdR family lipoprotein	1.49879072	5.14338897	2.01E-07	5.27E-05
heme ABC transporter substrate-binding protein ChuT	-2.3964654	6.527836	2.26E-07	5.27E-05
cytosine permease	-2.3166082	7.08040087	2.30E-07	5.27E-05
D-ribose pyranase	-1.2102421	6.62698948	2.46E-07	5.27E-05
glycosyltransferase family 2 protein	3.08401446	9.23912426	2.52E-07	5.27E-05
stress response protein ElaB	2.07341539	8.20399014	2.83E-07	5.28E-05
ClbS/DfsB family four-helix bundle protein	-2.1010678	3.22353275	2.96E-07	5.28E-05
DNA-binding transcriptional regulator CsiR	2.72013326	6.07017295	3.19E-07	5.28E-05

glycine betaine ABC transporter permease YehW	1.75213406	5.67795927	3.30E-07	5.28E-05
GABA permease	2.95008149	7.49300411	3.32E-07	5.28E-05
carbamate kinase	-1.9791943	6.65392286	3.41E-07	5.28E-05
nitrate reductase Z subunit alpha	1.58844508	5.14793013	3.64E-07	5.28E-05
heme ABC transporter ATP-binding protein	-1.6994828	5.12520237	3.65E-07	5.28E-05
carbohydrate porin	-3.5274254	8.03818905	4.03E-07	5.62E-05
ubiquinone biosynthesis protein UbiJ	-1.1612946	7.5474061	4.29E-07	5.76E-05
DDE-type integrase/transposase/recombinase	-3.5191195	2.35159014	5.36E-07	6.61E-05
heme ABC transporter permease ShuU/ChuU	-1.7238843	6.37891005	5.39E-07	6.61E-05
heme anaerobic degradation radical SAM methyltransferase ChuW/HutW	-2.4129741	6.6713732	5.45E-07	6.61E-05
ferredoxin-type protein NapF	-1.9539551	6.04552201	6.27E-07	7.37E-05
alpha-amylase	1.82493293	6.72115861	6.78E-07	7.60E-05
molecular chaperone OsmY	2.18058145	7.93011268	7.12E-07	7.60E-05
2%2C3-dihydro-2%2C3-dihydroxybenzoate dehydrogenase EntA	-2.0196035	5.71436365	7.23E-07	7.60E-05
cysteine hydrolase	-3.1693351	6.99979279	7.27E-07	7.60E-05
lipoprotein toxin entericidin B	2.39190201	10.6206701	7.91E-07	8.04E-05
NADP-dependent succinate-semialdehyde dehydrogenase	2.63752954	7.75642526	8.79E-07	8.53E-05
periplasmic nitrate reductase subunit alpha	-1.2397795	6.69661327	9.07E-07	8.53E-05
phosphoglycolate phosphatase	-1.3116433	6.48422347	9.07E-07	8.53E-05
maltodextrin phosphorylase	3.0830371	7.12928785	1.30E-06	0.00011492
OB fold stress tolerance protein YgiW	1.73549924	6.62450193	1.30E-06	0.00011492
maltose/maltodextrin ABC transporter ATP-binding protein MalK	4.72772318	9.87311849	1.31E-06	0.00011492
quinol dehydrogenase ferredoxin subunit NapH	-1.1255512	5.55922832	1.54E-06	0.00013103
putrescine aminotransferase	1.51672129	7.27877662	1.57E-06	0.00013103
TonB-dependent heme/hemoglobin receptor ChuA/ShuA	-1.6360403	6.77554053	1.63E-06	0.00013103
ribose ABC transporter ATP-binding protein RbsA	-1.1110699	7.11915725	1.64E-06	0.00013103
class I fructose-bisphosphate aldolase	1.97635232	7.01741624	1.67E-06	0.00013103
DUF1328 domain-containing protein	2.39240426	7.2807922	1.77E-06	0.00013604

maltose ABC transporter permease MalF	4.01462102	9.25037275	1.94E-06	0.00014582
iron/manganese ABC transporter substrate-binding protein SitA	-1.1903222	6.7404861	2.30E-06	0.00016873
maltose operon protein MalM	4.54845472	9.37457899	2.37E-06	0.00016873
iron/manganese ABC transporter ATP-binding protein SitB	-1.170712	6.30995666	2.41E-06	0.00016873
transcriptional regulator GlcC	-1.2856149	8.1709576	2.43E-06	0.00016873
hematinate-forming heme oxygenase ChuS	-1.4931481	7.17576671	2.47E-06	0.00016873
2-hydroxy-3-oxopropionate reductase	1.76844126	6.50290667	2.53E-06	0.00017009
regulatory protein GemA	-9.2474728	2.60392582	3.13E-06	0.00020407
DUF3102 domain-containing protein	-4.3979062	1.11358624	3.15E-06	0.00020407
increased serum survival lipoprotein Iss	-2.0812753	5.80454004	3.27E-06	0.00020841
galactarate/glucarate/glycerate transporter GudP	1.32033333	4.54892752	3.51E-06	0.00021861
maltoporin LamB	5.27524595	11.0825803	3.55E-06	0.00021861
DUF1480 family protein	1.19051302	4.7669997	3.64E-06	0.00021861
2-dehydro-3-deoxyglucarate aldolase	1.63633025	4.64358011	3.66E-06	0.00021861
iron/manganese ABC transporter permease subunit SitC	-0.9506804	5.73985252	3.77E-06	0.00022163
GTPase	-2.0824114	7.98205118	4.11E-06	0.00023673
maltose ABC transporter permease MalG	4.36724173	8.9396575	4.20E-06	0.00023673
YbgS-like family protein	1.9156907	4.30071012	4.22E-06	0.00023673
outer membrane protein OmpW	-1.5299945	5.93436079	4.40E-06	0.00024315
amino acid ABC transporter substrate-binding protein	1.64829365	5.31459432	4.56E-06	0.00024868
sucrose-specific PTS transporter subunit IIBC	-2.9391368	7.67239114	4.69E-06	0.00024869
diguanylate cyclase DgcM	1.93361327	6.17543412	4.69E-06	0.00024869
mechanosensitive channel protein	1.23939855	5.92822368	4.76E-06	0.0002489
ubiquinone-dependent pyruvate dehydrogenase	2.17567792	6.32044923	5.19E-06	0.00026633
phage holin family protein	1.57944622	7.93090147	5.24E-06	0.00026633
protein YebF	1.09671873	6.92878102	5.43E-06	0.00027212
sucrose-6-phosphate hydrolase	-2.6119509	8.67484384	5.67E-06	0.0002792
enamine/imine deaminase	1.73344109	5.27927072	5.71E-06	0.0002792

maltose/maltodextrin ABC transporter substrate-binding protein MalE	4.49512659	10.4277174	6.02E-06	0.00029016
enterobactin biosynthesis bifunctional isochorismatase/aryl carrier protein EntB	-1.9797691	5.93819982	6.28E-06	0.00029906
aminobutyraldehyde dehydrogenase	2.00241582	5.56433671	6.53E-06	0.00030727
enterochelin esterase	-1.6173822	8.1129181	6.63E-06	0.00030729
two-component system response regulator BtsR	-0.8418838	6.74940993	6.70E-06	0.00030729
siderophore enterobactin receptor FepA	-2.2649327	8.63055534	6.84E-06	0.00030991
catalase HPII	1.96583361	6.49987948	6.93E-06	0.00030991
L-2-hydroxyglutarate oxidase	2.56387515	8.07381114	7.04E-06	0.00030991
arginine ABC transporter permease ArtM	0.84836444	7.55479363	7.11E-06	0.00030991
nickel ABC transporter permease subunit NikB	-1.1737822	3.82223555	7.17E-06	0.00030991
NADPH-dependent aldehyde reductase Ahr	2.00271854	5.5939665	7.58E-06	0.00032421
YqjD family protein	1.55996319	6.79149997	7.94E-06	0.00033225
sulfurtransferase complex subunit TusB	0.93412545	6.83109884	7.95E-06	0.00033225
cellulase	0.74249629	7.14513662	8.27E-06	0.00034203
YegP family protein	2.16752638	5.25635009	8.59E-06	0.00035144
YqjK-like family protein	1.71792327	8.49641478	8.81E-06	0.00035481
VOC family metalloprotein YjdN	2.12028632	4.99240995	8.87E-06	0.00035481
enterobactin non-ribosomal peptide synthetase EntF	-1.5445664	9.26548998	9.23E-06	0.00035513
SASA family carbohydrate esterase	-1.1129087	4.47877667	9.31E-06	0.00035513
thymidine phosphorylase	1.54086497	6.5848164	9.32E-06	0.00035513
aquaporin Z	1.31037693	3.95818606	9.36E-06	0.00035513
AroM family protein	0.91759517	5.81856043	9.47E-06	0.00035513
cardiolipin synthase ClsB	1.40111484	4.93799974	9.54E-06	0.00035513
putrescine ABC transporter ATP-binding subunit PotG	0.87547008	5.35562382	9.55E-06	0.00035513
protein deglycase HchA	1.06673199	6.16168668	9.63E-06	0.00035513
alpha%2Calpha-trehalose-phosphate synthase	2.01082145	6.47328946	9.98E-06	0.00036456
aldehyde dehydrogenase AldB	2.08118358	7.0196265	1.13E-05	0.00040715
two-component system response regulator RssB	0.78134535	6.85072353	1.14E-05	0.00040715

glycine betaine ABC transporter permease YehY	1.86372688	5.97795503	1.20E-05	0.00042541
carbon starvation induced protein CsiD	2.71610082	8.12923327	1.21E-05	0.0004255
cellulose biosynthesis protein BcsC	0.75763992	8.35391472	1.24E-05	0.00043022
alcohol dehydrogenase AdhP	1.44965773	6.57567255	1.25E-05	0.00043022
cellulose biosynthesis cyclic di-GMP-binding regulatory protein BcsB	0.92383061	8.66271112	1.27E-05	0.00043224
nickel ABC transporter substrate-binding protein	-1.234557	4.81644947	1.28E-05	0.00043224
anaerobilin reductase	-1.7049262	6.32464184	1.32E-05	0.0004448
iron/manganese ABC transporter permease subunit SitD	-0.8684125	6.47961591	1.36E-05	0.00045406
ATP-independent periplasmic protein-refolding chaperone Spy	1.01583725	4.89797381	1.39E-05	0.00045776
ferric-rhodotorulic acid/ferric-coprogen receptor FhuE	-0.8757548	5.7621671	1.42E-05	0.00046073
isopentenyl-diphosphate Delta-isomerase	1.05371216	5.90277423	1.44E-05	0.00046073
Fe2+-enterobactin ABC transporter substrate-binding protein	-0.8642412	7.10148701	1.44E-05	0.00046073
host-nuclease inhibitor Gam family protein	-7.5337989	1.03675786	1.45E-05	0.00046073
deoxyribodipyrimidine photo-lyase	1.00459549	6.9100859	1.46E-05	0.00046116
heme utilization cystosolic carrier protein HutX	-1.6660707	5.899344	1.53E-05	0.00047848
peroxiredoxin OsmC	1.57113587	4.97041284	1.57E-05	0.00048968
trehalose-phosphatase	1.79545382	5.05512455	1.59E-05	0.00048994
aldose sugar dehydrogenase YliI	1.18366721	5.25783707	1.68E-05	0.00050614
tellurite resistance TerB family protein	-1.7711367	4.08896992	1.68E-05	0.00050614
chaperone NapD	-1.5834313	3.47586576	1.68E-05	0.00050614
glycine betaine ABC transporter substrate-binding protein OsmF	1.90967701	7.2133046	1.71E-05	0.00051147
alpha%2Calpha-trehalase	1.41994752	6.93524054	1.74E-05	0.00051655
sn-glycerol-3-phosphate ABC transporter permease UgpE	2.04516608	5.78789231	1.78E-05	0.00052379
trans-aconitate 2-methyltransferase	1.49047653	4.82012306	1.84E-05	0.00053554
allantoinase AllB	0.89952284	4.7970622	1.86E-05	0.00053908
deferrochelatase/peroxidase EfeB	-0.8663105	9.51228898	1.95E-05	0.00055713
Na+/H+ antiporter NhaA	0.86336629	7.74766191	1.95E-05	0.00055713
sn-glycerol 3-phosphate ABC transporter ATP binding protein UgpC	1.37507264	5.63921641	1.97E-05	0.00055855

iron uptake system protein EfeO	-0.7680492	9.13544551	2.06E-05	0.00057343
DNA starvation/stationary phase protection protein Dps	1.48837332	9.34454365	2.06E-05	0.00057343
dipeptide ABC transporter permease DppC	1.13577446	8.71422651	2.21E-05	0.00061031
lipid IV(A) 4-amino-4-deoxy-L-arabinosyltransferase	0.71140314	6.13942421	2.30E-05	0.00063241
cyclic diguanylate phosphodiesterase	1.13079694	3.9668769	2.35E-05	0.00063938
arginine ABC transporter permease ArtQ	1.02597323	7.57711143	2.40E-05	0.00064449
formate hydrogenlyase transcriptional activator FlhA	1.01677314	5.82203816	2.41E-05	0.00064449
amino acid ABC transporter permease	1.00764041	5.1853829	2.42E-05	0.00064449
acid resistance transcriptional activator GadW	1.36399968	5.92879646	2.52E-05	0.00066778
peroxide/acid resistance protein YodD	2.0265061	4.64272112	2.58E-05	0.00067826
stationary-phase-induced ribosome-associated protein	2.49654731	7.88120227	2.60E-05	0.00067826
NADPH-dependent aldehyde reductase YahK	1.4019254	5.65699157	2.61E-05	0.00067826
YbaY family lipoprotein	1.8035409	8.06225036	2.68E-05	0.00069122
glycine betaine ABC transporter ATP binding protein YehX	1.64344656	4.59891476	2.74E-05	0.00069805
YccJ family protein	2.3202628	5.74523803	2.75E-05	0.00069805
NAD(P)H:quinone oxidoreductase	1.54315801	6.23010166	2.80E-05	0.00070809
HTH-type transcriptional regulator GalS	-1.0900727	8.45162371	2.93E-05	0.00073387
osmotically-inducible lipoprotein OsmB	1.97704156	6.27050156	3.05E-05	0.00075751
lipoprotein metalloprotease SslE	2.19865119	8.72339457	3.08E-05	0.00075751
4-alpha-glucanotransferase	2.67389537	7.13188695	3.08E-05	0.00075751
NupC/NupG family nucleoside CNT transporter	1.14165789	4.75207291	3.14E-05	0.00076604
acid resistance transcriptional activator GadX	2.24875814	6.20919118	3.27E-05	0.00079285
(2%2C3-dihydroxybenzoyl)adenylate synthase EntE	-1.867695	7.55430412	3.32E-05	0.00080085
UDP-4-amino-4-deoxy-L-arabinose aminotransferase	0.8536436	5.75944648	3.39E-05	0.00081065
phnA family protein	-0.8366068	7.6438458	3.41E-05	0.00081065
yersiniabactin transcriptional regulator YbtA	-1.1430272	5.74595475	3.43E-05	0.00081065
DUF2786 domain-containing protein	-7.0010015	0.61487269	3.47E-05	0.00081673
pyruvate/proton symporter BtsT	-3.2400695	11.2119303	3.51E-05	0.00082015

oxygen-sensing cyclic-di-GMP phosphodiesterase	0.66501176	5.60086243	3.54E-05	0.00082293
DUF3313 domain-containing protein	0.71889477	6.90483995	3.62E-05	0.00083469
pseudouridine-5'-phosphate glycosidase	1.49267461	5.12335582	3.70E-05	0.00084816
enterobactin biosynthesis protein YbdZ	-1.4130331	5.32548596	3.86E-05	0.00088011
metalloprotease LoiP	0.64936741	7.25933642	3.99E-05	0.0009044
phosphonate metabolism protein PhnP	0.87101784	5.11353402	4.02E-05	0.00090449
glycine betaine/L-proline transporter ProP	1.41121397	8.53178434	4.13E-05	0.00092439
glucarate dehydratase	0.7481489	5.02513593	4.26E-05	0.00094503
stress response membrane protein YncL	1.51267868	8.20088543	4.27E-05	0.00094503
fec operon regulator FecR	-0.945439	7.65468298	4.48E-05	0.00098656
porphyrinogen peroxidase	-0.6132984	5.96931986	4.54E-05	0.0009901
siderophore-iron reductase FhuF	-0.9410386	9.92623167	4.55E-05	0.0009901
glutathione-regulated potassium-efflux system protein KefC	0.92683163	5.62145527	4.61E-05	0.0009901
kinase inhibitor	0.77461245	6.82392154	4.61E-05	0.0009901
galactarate/glucarate/glycerate transporter GarP	1.4941724	4.6787034	4.63E-05	0.0009901
glutathionyl-hydroquinone reductase YqjG	1.31605736	5.26150257	4.87E-05	0.00103436
hemin uptake protein HemP	-1.0282369	7.76048376	4.92E-05	0.0010402
putative adenosine monophosphate-protein transferase Fic	1.34320053	3.98717401	5.24E-05	0.00110037
glycolate permease GlcA	2.9319238	9.58377915	5.26E-05	0.00110037
DUF1090 domain-containing protein	1.53184634	6.65894756	5.47E-05	0.00113632
enterobactin synthase subunit EntD	-2.1237628	5.09550084	5.59E-05	0.00115584
YehE family protein	1.93579535	4.51466103	5.73E-05	0.0011781
pyruvate:ferredoxin (flavodoxin) oxidoreductase	0.68495037	7.0815939	5.94E-05	0.00121365
FAD-NAD(P)-binding protein	1.37584907	4.28343653	6.06E-05	0.00123223
protein YaiA	1.36796042	5.93747012	6.20E-05	0.00125087
malate synthase G	2.25431187	11.7825359	6.22E-05	0.00125087
aminoalkylphosphonate N-acetyltransferase	0.77117215	4.26872795	6.70E-05	0.00134069
sn-glycerol-3-phosphate ABC transporter permease UgpA	2.00720026	6.87370777	6.97E-05	0.00138642

catecholate siderophore receptor Fiu	-1.3163728	4.65557134	7.09E-05	0.00140339
YeaH/YhbH family protein	2.35780955	5.35889348	7.14E-05	0.00140699
exodeoxyribonuclease VII large subunit	0.85794846	7.75908448	7.20E-05	0.00141155
quinoprotein glucose dehydrogenase	1.11744538	7.08909549	7.44E-05	0.00145008
DNA polymerase II	0.6054087	7.27707563	7.79E-05	0.00151106
ferredoxin-type protein NapG	-0.9689148	3.93573109	7.90E-05	0.0015208
polysaccharide deacetylase family protein	0.63983065	5.78640448	7.92E-05	0.0015208
SOS response-associated peptidase family protein	1.2987946	4.50851902	7.99E-05	0.00152487
nitrate reductase cytochrome c-type subunit	-0.895222	3.4251033	8.08E-05	0.00153507
U32 family peptidase	-0.9040777	4.96217495	8.16E-05	0.00154272
C4-dicarboxylate transporter DctC	-0.7671463	9.69814433	8.24E-05	0.00154973
spermidine/putrescine ABC transporter substrate-binding protein PotD	-0.697184	6.85720345	8.30E-05	0.00155349
ribose 1%2C5-bisphosphokinase	0.90720904	4.10757635	8.44E-05	0.00157131
HPr family phosphocarrier protein	0.70664418	3.89320754	8.62E-05	0.00159682
DUF935 domain-containing protein	-1.1672568	3.28881645	8.69E-05	0.00159805
SpoVR family protein	1.7638201	7.05418387	8.71E-05	0.00159805
protein kinase YeaG	1.90431592	6.47335217	8.93E-05	0.00162623
vitamin B12 ABC transporter ATP-binding protein BtuD	0.54127988	6.17498893	8.95E-05	0.00162623
ferrichrome porin FhuA	-0.8149819	9.97784685	8.99E-05	0.00162623
protein YohP	1.76436843	6.96239452	9.23E-05	0.00166207
heme-binding protein	2.07420391	8.93035862	9.53E-05	0.00170708
type I glyceraldehyde-3-phosphate dehydrogenase	1.75968675	4.33412983	9.73E-05	0.00172908
zinc-binding dehydrogenase	0.71132618	3.80360947	9.74E-05	0.00172908
TonB-dependent vitamin B12 receptor BtuB	-0.6578978	7.6851828	9.86E-05	0.00173371
lipocalin Blc	2.0789506	6.0906263	9.86E-05	0.00173371
dipeptide ABC transporter ATP-binding protein	1.03822512	7.83802017	0.00010011	0.00175168
DoxX family protein	1.14164154	4.48268084	0.00010347	0.00180217
glycolate oxidase subunit GlcE	1.55737129	10.6164256	0.00010672	0.0018502

YdiU family protein	0.53855393	6.91134528	0.00011109	0.001917
undecaprenyl-phosphate 4-deoxy-4-formamido-L-arabinose transferase	0.86674238	5.45390275	0.00011219	0.00192515
sulfatase	1.21274442	8.53114823	0.00011297	0.00192515
glycerate 2-kinase	1.06924358	5.41094119	0.00011309	0.00192515
class II aldolase	0.86801313	2.85323813	0.00011483	0.00194582
phosphopentomutase	0.65780968	7.92623669	0.00011808	0.00199202
glycolate oxidase subunit GlcF	1.67571171	10.8787845	0.0001207	0.00202715
YbgA family protein	0.98294621	5.63564568	0.00012724	0.00212746
N-acetylneuraminate epimerase	0.65428062	4.794242	0.00012989	0.00216209
glycerophosphodiester phosphodiesterase	2.79714461	9.13136608	0.00013085	0.00216856
hydrolase	0.6482366	8.49929233	0.00013176	0.00217403
cell-envelope stress modulator CpxP	0.73725871	7.96677686	0.00013823	0.00227076
general stress protein	1.65814923	2.99190214	0.00013942	0.00228041
glutathione-dependent disulfide-bond oxidoreductase	0.58338412	7.43426467	0.00014141	0.00230289
isochorismate synthase EntC	-1.7271016	7.67213325	0.00014787	0.00239118
TMAO reductase system periplasmic protein TorT	-0.6332526	4.35879859	0.0001481	0.00239118
pyridine nucleotide-disulfide oxidoreductase	1.2795318	4.10890633	0.00015312	0.00244996
FTR1 family protein	-0.7053588	9.64109728	0.00015339	0.00244996
glycerol-3-phosphate transporter	4.7612653	9.03251731	0.00015369	0.00244996
acid resistance gamma-aminobutyrate antiporter GadC	2.24815682	4.83380445	0.00016358	0.00259655
GlsB/YeaQ/YmgE family stress response membrane protein	1.27127494	5.80764003	0.00016693	0.0026386
YmiA family putative membrane protein	0.66322139	7.09783863	0.0001693	0.00266486
enterobactin transporter EntS	-0.8730912	7.75573543	0.0001745	0.00272193
glycerol kinase GlpK	4.64654832	10.7538279	0.00017482	0.00272193
mannosyl-3-phosphoglycerate phosphatase-related protein	1.29708717	4.99134639	0.0001751	0.00272193
glutamate--cysteine ligase	0.55289962	9.39246017	0.00018412	0.00284334
CsbD family protein	1.82001917	7.05133265	0.00018442	0.00284334
DUF1161 domain-containing protein	1.07814966	7.02889597	0.00018517	0.00284334

OmpA family protein	0.55566831	5.82254779	0.00018607	0.00284557
small-conductance mechanosensitive channel MscS	0.70797029	6.86379934	0.00019055	0.00290221
spermidine/putrescine ABC transporter substrate-binding protein PotF	0.80952419	6.1002713	0.00019379	0.00293973
ornithine carbamoyltransferase	1.05064436	3.01894119	0.00019748	0.0029836
6-phosphofructokinase II	0.95125467	6.48621618	0.00019903	0.00299502
DUF445 domain-containing protein	0.96579822	6.07294504	0.00020068	0.00300168
biofilm-dependent modulation protein	1.68061334	1.83530267	0.00020155	0.00300168
glycolate oxidase subunit GlcD	1.17482281	11.6063829	0.00020187	0.00300168
PstS family phosphate ABC transporter substrate-binding protein	1.22243187	2.85290274	0.00020325	0.00301034
glutaminase A	2.49621637	3.32042669	0.00020822	0.00307189
lipid kinase YegS	1.43276786	3.5912962	0.00022086	0.00324559
phosphohydrolase	-0.6188363	5.34058451	0.00022554	0.00330152
cyclopropane fatty acyl phospholipid synthase	0.85008082	7.06358168	0.00023303	0.00339785
Fe-S cluster assembly transcriptional regulator IscR	0.52183558	8.37096218	0.00024089	0.00349894
bifunctional UDP-4-amino-4-deoxy-L-arabinose formyltransferase/UDP-glucuronic acid oxidase ArnA	0.6815201	6.12115008	0.00024776	0.00358494
GSH-dependent disulfide bond oxidoreductase	1.42220089	4.06393102	0.00025245	0.00363875
23S rRNA pseudouridine(2457) synthase RluE	0.57313142	6.06300092	0.00025494	0.00366058
YdcY family protein	-0.768651	7.21238941	0.00025806	0.00369128
YIP1 family protein	1.02024365	3.47315162	0.00025975	0.00370148
TonB system transport protein TonB	-0.7055488	8.70671053	0.00026096	0.00370458
YebO family protein	-0.7422151	4.60366893	0.00027573	0.00389625
Fe(3+)-hydroxamate ABC transporter substrate-binding protein FhuD	-0.8350668	7.37072495	0.00027653	0.00389625
lipid-binding membrane homeostasis protein YebT	0.48548574	7.68225524	0.00028672	0.00402474
DNA recombination protein RmuC	-0.5388707	7.48827216	0.0002913	0.00405144
glycerol uptake facilitator protein GlpF	4.74282748	8.06685406	0.00029157	0.00405144
UDP-forming cellulose synthase catalytic subunit	0.75981271	8.96744338	0.00029249	0.00405144
dipeptide ABC transporter ATP-binding subunit DppF	0.73324602	8.36093969	0.00029359	0.00405144
glycerol-3-phosphate dehydrogenase	5.78399218	9.75749731	0.00029641	0.00405144

c-di-GMP phosphodiesterase PdeC	0.82391187	5.58004311	0.00029649	0.00405144
type II secretion system pilot lipoprotein GspS-beta	1.95487156	4.31805435	0.00029667	0.00405144
anaerobic glycerol-3-phosphate dehydrogenase subunit C	4.97539949	6.26035024	0.00029723	0.00405144
2%2C5-didehydrogluconate reductase DkgA	1.61919896	5.22955702	0.00030023	0.0040775
formate/nitrite transporter family protein	1.1377957	4.11014652	0.00030533	0.00411779
low affinity tryptophan permease TnaB	2.80654173	7.07413601	0.00030539	0.00411779
YebC/PmpR family DNA-binding transcriptional regulator	-0.724074	8.61280824	0.00030685	0.00412271
YebY family protein	-0.5595856	5.6497456	0.00031229	0.00418091
Fe3+-hydroxamate ABC transporter ATP-binding protein FhuC	-0.7450432	7.71251979	0.00031564	0.00421072
heat shock chaperone IbpB	0.93357473	3.30489085	0.00031879	0.0042378
purine-nucleoside phosphorylase	0.59553375	8.06435844	0.00033089	0.00438316
N-acetylmuramoyl-L-alanine amidase AmiD	0.72331634	6.7936694	0.00033253	0.00438944
2-ketobutyrate formate-lyase/pyruvate formate-lyase	1.33257841	5.3346491	0.00033978	0.00446944
bifunctional 4-hydroxy-2-oxoglutarate aldolase/2-dehydro-3-deoxy-phosphogluconate aldolase	-0.6910776	6.67069072	0.00034594	0.00453455
glucosamine-6-phosphate deaminase	0.52493875	6.90602442	0.00035108	0.00454868
LacI family DNA-binding transcriptional regulator	-1.035557	7.70609155	0.00035144	0.00454868
AbrB family transcriptional regulator	-0.5866476	4.96509278	0.00035164	0.00454868
prepilin peptidase PppA	1.35134741	6.59641266	0.00035185	0.00454868
SecY/SecA suppressor protein	1.61229751	4.05365207	0.00035515	0.00457557
ribulose-phosphate 3 epimerase family protein	0.73331346	4.13694878	0.00035931	0.00461341
mechanosensitive ion channel YbdG	-0.4527098	6.47578447	0.00036375	0.00465453
glycerol-3-phosphate dehydrogenase subunit GlpB	5.29761045	6.64877344	0.0003687	0.00470181
L-ribulose-5-phosphate 4-epimerase	0.88321321	4.18803278	0.00038569	0.00490185
long-chain acyl-CoA thioesterase FadM	0.79592553	4.83474386	0.00040251	0.00509849
phosphate starvation-inducible protein PsiF	1.4484594	4.89606022	0.00041174	0.00519793
tyrosine transporter TyrP	-0.9234276	6.90668427	0.0004183	0.00526309
HTH-type transcriptional regulator MlrA	1.09412443	4.82478972	0.00042274	0.00530117
phosphotriesterase	0.66709186	4.99930736	0.00042518	0.00530365

Ivy family C-type lysozyme inhibitor	0.90893846	6.39549109	0.00042576	0.00530365
bifunctional glutathionylspermidine amidase/synthase	-0.4638044	6.13163027	0.00043382	0.00538627
serine protease	0.85298311	7.17001179	0.00043767	0.00541623
alpha-glucosidase	2.88879245	6.77834444	0.00045065	0.00555845
preprotein translocase subunit YajC	-0.4931186	8.93507488	0.00045879	0.00564037
DNA polymerase III subunit theta	-0.6870682	5.2186741	0.00046379	0.00568097
iron-sulfur cluster insertion protein ErpA	0.62529854	8.377626	0.00046511	0.00568097
bifunctional allose-6-phosphate isomerase/ribose-5-phosphate isomerase RpiB	-1.1330498	3.71057569	0.00046911	0.00571133
pseudouridine kinase	1.23308166	4.09015162	0.00047891	0.00581177
anaerobic glycerol-3-phosphate dehydrogenase subunit A	4.98013375	7.05251204	0.00048311	0.00584398
putrescine ABC transporter permease PotI	0.65063122	5.55604184	0.00049003	0.00588356
nucleotidyl transferase AbiEii/AbiGii toxin family protein	0.50716303	7.86181776	0.00049033	0.00588356
YbhN family protein	1.1982637	4.19734882	0.00049226	0.00588356
1-deoxyxylulose-5-phosphate synthase YajO	0.79718146	6.24734109	0.00049264	0.00588356
sn-glycerol-3-phosphate ABC transporter substrate-binding protein UgpB	1.81781949	7.39050886	0.00049469	0.00588934
maltodextrin glucosidase	0.87137692	5.3281063	0.00049738	0.00590267
lysine decarboxylase LdcC	0.7149233	6.13213215	0.00050082	0.00592401
Fe(3+) dicitrate ABC transporter substrate-binding protein FecB	-0.4798806	8.99870963	0.00050233	0.00592401
YqaE/Pmp3 family membrane protein	1.99740582	4.94970129	0.00050751	0.00595223
nickel import ATP-binding protein NikD	-0.8844062	3.34710331	0.00050793	0.00595223
osmotically-inducible lipoprotein OsmE	1.48799899	6.42524889	0.00050947	0.00595223
RNA polymerase sigma factor FecI	-0.8488176	8.01500379	0.00051327	0.0059781
YcgL domain-containing protein	-0.6049887	5.87826343	0.00051588	0.00598998
putative cation transport regulator ChaB	1.15604113	3.66280785	0.00053168	0.00615435
4-deoxy-4-formamido-L-arabinose-phosphoundecaprenol deformylase	0.73425179	4.97138531	0.00053567	0.00618151
bifunctional siderophore receptor/adhesin Iha	-0.9608484	6.04936563	0.00054048	0.00621804
UPF0149 family protein YecA	-0.7382702	4.31836295	0.0005428	0.00622563

homoserine kinase	-0.4783593	5.92953304	0.00055184	0.0063101
glutamate decarboxylase	1.15714658	5.71098275	0.00056836	0.00647931
aminoimidazole riboside kinase	-0.903896	4.20464161	0.00057151	0.00649554
7-alpha-hydroxysteroid dehydrogenase	1.18664173	6.05715509	0.00057984	0.0065704
cytochrome c-type protein NapC	-0.5220967	5.07212191	0.0005996	0.00677385
metal-dependent hydrolase	0.43444242	8.6700883	0.00060293	0.00679114
YhfG family protein	1.23995861	4.34129014	0.00060531	0.00679755
DUF2799 domain-containing protein	1.22530739	4.78835362	0.0006204	0.00694623
lipopolysaccharide kinase InaA	2.75472168	5.71715659	0.00062929	0.00702487
outer membrane lipoprotein Slp	2.02413683	3.25378359	0.00063441	0.00705639
Fe-S biogenesis protein NfuA	0.54252963	8.58710827	0.00063586	0.00705639
iron-sulfur cluster-binding protein	1.12767006	5.68202009	0.00064028	0.00708446
selenium metabolism membrane protein YedE/FdhT	-0.9300257	8.76564679	0.00064659	0.00713334
nickel ABC transporter permease subunit NikC	-0.9139673	3.4570619	0.00065248	0.00717725
deoxyribose-phosphate aldolase	0.54977135	5.52176696	0.00065675	0.00718451
DUF1107 domain-containing protein	0.80410494	8.43595163	0.00065696	0.00718451
ketose-bisphosphate aldolase	0.95851884	2.76079116	0.00066415	0.00724213
arginine ABC transporter ATP-binding protein ArtP	0.81386091	7.86518329	0.00066753	0.0072579
LbetaH domain-containing protein	0.73699258	4.42185914	0.000675	0.00731802
protein-methionine-sulfoxide reductase catalytic subunit MsrP	0.94261282	4.14194825	0.00069943	0.00753755
ferrochelatase	0.5674618	7.12977367	0.00069977	0.00753755
9-O-acetyl-N-acetylneuraminic acid deacetylase	1.21857128	3.46963589	0.00070126	0.00753755
DNA repair protein RadA	-0.6181787	7.6420478	0.00071951	0.00771162
barstar family protein	1.2511867	4.07638867	0.00072781	0.0077785
ferredoxin-like diferric-tyrosyl radical cofactor maintenance protein YfaE	-0.6639836	6.40742448	0.00073238	0.00779497
RNA polymerase-binding protein DksA	-0.4448126	9.24126147	0.0007335	0.00779497
glutathione-regulated potassium-efflux system oxidoreductase KefF	0.78863795	4.49601047	0.00073721	0.00781235
cellulose biosynthesis protein BcsF	1.12295912	4.0830139	0.00074235	0.0078447

fimbrial protein	0.52580507	5.29766204	0.00074611	0.0078624
biofilm formation regulator BssR	0.52768533	6.21160726	0.00074912	0.00787205
S-(hydroxymethyl)glutathione dehydrogenase	0.59338963	6.57020578	0.00075763	0.00793926
HI1450 family dsDNA-mimic protein	-0.4339731	5.02218456	0.00076181	0.0079609
catecholate siderophore receptor CirA	-1.6750762	8.31280906	0.00076944	0.00799195
gluconokinase	1.11515391	3.77811395	0.00077101	0.00799195
glutathione transferase	0.77030012	5.11568242	0.00077115	0.00799195
cellulose biosynthesis protein BcsG	0.94376344	7.81100726	0.00077374	0.00799673
bifunctional 3-hydroxydecanoyl-ACP dehydratase/trans-2-decenoyl-ACP isomerase	-0.7335955	9.21454989	0.00079033	0.00814578
DUF853 domain-containing protein	0.82189319	5.40459	0.00081641	0.00838563
oxidative stress defense protein	1.1522397	7.93922712	0.00081806	0.00838563
inner membrane protein YhjD	0.95235268	6.7323878	0.00082743	0.00845871
RpoE-regulated lipoprotein	-0.9688765	6.76025126	0.00084303	0.00859484
iron-enterobactin ABC transporter ATP-binding protein	-0.7282286	7.29474543	0.00085697	0.00871328
adenylosuccinate synthase	-0.6869294	10.8066337	0.00086899	0.00880405
RNA polymerase sigma factor RpoE	-0.5996951	8.34859239	0.00087058	0.00880405
isocitrate lyase	2.73328044	11.0206268	0.00087919	0.00886729
YeaC family protein	-0.5385823	6.95603429	0.00088777	0.00892992
DUF554 domain-containing protein	0.53673352	4.76182141	0.00089494	0.00897449
DNA-binding transcriptional repressor Mlc	-0.5489081	7.43002071	0.00089697	0.00897449
nitrate reductase molybdenum cofactor assembly chaperone	0.7221753	3.56812898	0.0009083	0.00905142
type 1 fimbria switch DNA invertase FimE	-1.0096304	3.55140891	0.00090947	0.00905142
phosphoadenosine phosphosulfate reductase	0.40716971	7.90063061	0.00092063	0.00913832
HTH-type transcriptional regulator	1.92323077	7.01730637	0.00092338	0.00914147
putrescine ABC transporter permease PotH	0.5594582	4.47625764	0.00092605	0.00914381
Na/Pi cotransporter family protein	0.76221074	7.01005238	0.00093303	0.00918865
potassium binding protein Kbp	1.75788501	6.16340335	0.0009379	0.00920874
insulinase family protein	-0.4437514	8.30948582	0.00093997	0.00920874

N-succinylarginine dihydrolase	1.26250775	8.98754885	0.00094613	0.00924507
histidinol dehydrogenase	-0.6523786	5.82820905	0.00095099	0.00926846
patatin-like phospholipase RssA	0.50918114	6.63582999	0.00097089	0.00942762
YciK family oxidoreductase	-0.497687	5.23943558	0.00097233	0.00942762
D-xylose ABC transporter substrate-binding protein	1.28090558	4.53864155	0.00098903	0.00955107
glutaredoxin 2	0.95370599	7.47798551	0.00099014	0.00955107
Fe(3+) dicitrate transport protein FecA	-0.4869289	10.4577564	0.00099461	0.00956958
acid-activated periplasmic chaperone HdeB	2.46174669	5.8073326	0.00101136	0.00970595
chitin disaccharide deacetylase	-0.4467976	5.71034667	0.00102272	0.00975815
DNA-binding transcriptional activator AdiY	1.6848552	0.78109923	0.00102401	0.00975815
cob(I)yrinic acid a%2Cc-diamide adenosyltransferase	-0.4472104	6.3333408	0.00102526	0.00975815
DUF1778 domain-containing protein	-0.6446509	5.4639506	0.00102717	0.00975815
acid-resistance protein HdeD	1.50660442	4.54472224	0.00103235	0.00978266
N(6)-hydroxylysine O-acetyltransferase lucB	-0.628163	7.24481804	0.00104084	0.00983827
catabolite repressor/activator	-0.4353248	8.60306702	0.00104937	0.00989407
large-conductance mechanosensitive channel protein MscL	0.91685142	7.23181152	0.00105698	0.00994091
F0F1 ATP synthase subunit B	-0.6328612	10.2253299	0.00106488	0.00996299
cation/acetate symporter ActP	1.04552729	9.95575361	0.00106558	0.00996299
ribose ABC transporter permease	-0.4599123	7.66402086	0.00106727	0.00996299
elongation factor P hydroxylase	-0.5612099	6.17715881	0.00107476	0.010008
succinyl-CoA--3-ketoacid-CoA transferase	-1.4408503	0.78463483	0.00108198	0.0100336
malonyl-ACP O-methyltransferase BioC	-0.7250213	2.86304122	0.00108589	0.0100336
trimeric intracellular cation channel family protein	0.41002157	7.58017044	0.00108641	0.0100336
transcriptional regulator MelR	-0.5063572	5.52489726	0.00108817	0.0100336
ribonucleoside-diphosphate reductase subunit alpha	-0.4292897	9.20134943	0.00109165	0.01004105
HTH-type transcriptional repressor AllR	0.42001705	8.44734387	0.00110683	0.0101558
signal peptide peptidase SppA	-0.3993686	7.71951529	0.00112562	0.01027067
two-component regulatory system sensor histidine kinase BtsS	-0.6494829	8.81587673	0.00112723	0.01027067

protein YgjJ	3.36792886	5.06852048	0.00112753	0.01027067
1%2C4-dihydroxy-2-naphthoyl-CoA hydrolase	-0.5951718	6.59695201	0.00113 62	0.01031257
tryptophanase	2.08777	7.71599741	0.00113762	0.01031257
stress response protein AzuC	0.93564028	2.52463242	0.00114661	0.01036907
excisionase	0.64450381	3.68742091	0.00115871	0.01045 34
thiosulfate sulfurtransferase YnjE	-0.5100236	5.74480074	0.00117 35	0.01056 15
superoxide response transcriptional regulator SoxS	0.8318313	5.72684787	0.00120164	0.01078899
cytochrome ubiquinol oxidase subunit I	0.45723962	9.51700349	0.00121124	0.01082448
DUF2756 family protein	1.19096992	4.77309878	0.00121135	0.01082448
IS66 family insertion sequence element accessory protein TnpB	0.4323034	4.74938224	0.00122241	0.01089744
6-phosphogluconolactonase	0.91477726	7.78919545	0.00123226	0.01095927
bifunctional phosphoribosyl-AMP cyclohydrolase/phosphoribosyl-ATP diphosphatase HisIE	-0.5642991	6.82099579	0.00124001	0.01100218
YbjO family protein	0.45733982	5.34815248	0.00124469	0.01101771
Fe(3+)-hydroxamate ABC transporter permease FhuB	-0.83251	7.73354365	0.00124812	0.01102216
respiratory nitrate reductase subunit gamma	0.60177615	4.21741 62	0.00125 96	0.01109749
arginine ABC transporter substrate-binding protein	0.82061508	7.14377951	0.00126783	0.01114388
30S ribosomal protein S12 methylthiotransferase accessory protein YcaO	-1.2540414	7.27576152	0.00127418	0.01117357
diguanylate cyclase DgcN	0.43475806	5.98012211	0.00128383	0.01123199
bifunctional histidinol-phosphatase/imidazoleglycerol-phosphate dehydratase HisB	-0.4627765	5.93807534	0.00128717	0.01123512
threonine ammonia-lyase%2C biosynthetic	-0.8104321	8.53078592	0.00130969	0.01140522
type II secretion system protein GspC	1.70153082	4.59053439	0.00131688	0.01143 79
phosphoserine phosphatase	-0.6127847	7.32250195	0.00131952	0.01143 79
metal-binding protein ZinT	-0.698441	2.68830031	0.00133344	0.01153195
DUF2254 domain-containing protein	0.60612966	3.90375481	0.00133719	0.01153784
bifunctional thioredoxin/glutathione peroxidase	0.57497845	5.57983914	0.00134525	0.01158086
ribokinase	-0.47988	7.84545481	0.00135357	0.01162583
DNA-binding protein	-0.493553	4.59454831	0.00136163	0.01166849

6-N-hydroxylaminopurine resistance protein YcbX	-0.4813277	6.4060174	0.00136976	0.01171145
sulfurtransferase-like selenium metabolism protein YedF	-0.9431562	7.05248711	0.00139297	0.01188287
bifunctional isocitrate dehydrogenase kinase/phosphatase	2.51753084	10.0162069	0.00141204	0.01201828
NIS family aerobactin synthetase IucC	-0.5671004	8.07771514	0.00142326	0.01208649
acid-activated periplasmic chaperone HdeA	1.74121762	5.87630679	0.00142753	0.01209546
methionine ABC transporter substrate-binding lipoprotein MetQ	-0.6371209	8.2074502	0.00143393	0.01211694
peptide-methionine (R)-S-oxide reductase MsrB	-0.4444774	8.11032674	0.00143651	0.01211694
stationary phase inducible protein CsiE	1.29566462	8.41476958	0.00144727	0.0121804
host cell division inhibitor Icd-like protein	-0.4889672	6.19567989	0.00147396	0.01235622
PhoP/PhoQ regulator MgrB	-0.7133625	3.71692077	0.00147473	0.01235622
rpoE leader peptide RseD	-1.1188573	7.90420002	0.00149628	0.01250891
serine protease autotransporter toxin Sat	0.56470878	7.34982296	0.00153954	0.012842
electron transfer flavoprotein subunit alpha	-1.1806522	1.68357087	0.00154442	0.01285421
two-component system sensor histidine kinase RstB	-0.3573606	6.16816283	0.00156054	0.01293193
als operon DNA-binding transcriptional repressor AlsR	-0.5686331	7.39338482	0.00156483	0.01293193
DNA repair protein RecN	0.58204579	7.33401527	0.00156823	0.01293193
LacI family transcriptional regulator	-0.4487191	8.0669611	0.00157041	0.01293193
YiiQ family protein	-0.5953128	6.42755579	0.00157094	0.01293193
L%2CD-transpeptidase LdtE	0.92581918	4.0483577	0.0015961	0.0130825
7-methyl-GTP pyrophosphatase	0.44528257	7.31719817	0.00159961	0.0130825
YobF family protein	-0.7090988	12.9154229	0.00159967	0.0130825
class II fructose-bisphosphatase	1.31867386	7.26513538	0.00160869	0.01312775
VOC family protein	0.63718091	7.61111837	0.00166494	0.01355737
cellulose biosynthesis protein BcsQ	0.92125693	7.24483012	0.00166906	0.01356156
1%2C4-alpha-glucan branching enzyme	0.75934947	7.92203926	0.00167942	0.01361634
YoaK family small membrane protein	-0.5255786	4.3690696	0.00169986	0.01374686
protein-methionine-sulfoxide reductase heme-binding subunit MsrQ	0.71339438	4.10270036	0.00170283	0.01374686
nitrate reductase subunit beta	0.69861443	4.74217676	0.00170887	0.01376612

porin OmpC	-0.7433158	12.8716219	0.00172337	0.01385323
glycogen synthase GlgA	0.67994035	8.87337301	0.00173393	0.01390838
thioesterase family protein	-0.5364313	5.04922785	0.00175419	0.01402786
argininosuccinate synthase	0.8479961	7.15128653	0.0017604	0.01402786
succinylglutamate-semialdehyde dehydrogenase	1.0785255	8.89838889	0.00176236	0.01402786
outer membrane channel protein TolC	0.4185036	9.36820026	0.00176374	0.01402786
disulfide bond formation protein DsbB	-0.3458618	8.09122728	0.00178226	0.01414524
(Fe-S)-binding protein	1.18664576	3.9885309	0.0017883	0.01416332
succinyl-diaminopimelate desuccinylase	-0.4138056	6.01896597	0.00180277	0.01424797
class II glutamine amidotransferase	-0.3401331	7.29293111	0.00181718	0.0143206
crossover junction endodeoxyribonuclease RuvC	-0.8638444	7.03339182	0.00181958	0.0143206
peptidoglycan glycosyltransferase PbpC	0.36237733	6.90127488	0.00182452	0.01432953
DUF454 family protein	-0.6024114	7.74674187	0.00185154	0.01451141
heme o synthase	-0.500828	10.6577412	0.00186977	0.01460875
nucleoside diphosphate kinase regulator	-0.3919198	8.0567349	0.00187236	0.01460875
propionate catabolism operon regulatory protein PrpR	1.11860891	6.38334932	0.0018756	0.01460875
phosphoethanolamine transferase EptA	0.43656596	6.24573403	0.00188065	0.01461775
CDP-diacylglycerol diphosphatase	-0.3878983	5.1901528	0.00188977	0.0146584
ribonucleotide-diphosphate reductase subunit beta	-0.4425598	8.53220535	0.00190064	0.01471235
RidA family protein	-0.4344988	7.25033739	0.00194891	0.01505503
biofilm formation regulator BssS	0.57251061	5.04720602	0.00199004	0.01534126
succinylglutamate desuccinylase	1.12134547	7.66116451	0.0020174	0.0155204
tol-pal system-associated acyl-CoA thioesterase	-0.4632026	9.30435213	0.00203847	0.01565046
DNA-binding transcriptional regulator HexR	-0.4732525	7.2230318	0.00205052	0.01571089
peptide IlvX	-1.1279395	2.3383798	0.00207063	0.01583273
pyridoxal kinase PdxY	-0.4933612	6.78005678	0.00210246	0.01604351
histidinol-phosphate transaminase	-0.5724308	5.50006051	0.00211369	0.01609654
50S ribosomal protein L36	-0.8732167	10.1419587	0.00214515	0.01630314

pyruvate dehydrogenase complex dihydrolipoyllysine-residue acetyltransferase	-1.0936262	8.57271494	0.00215778	0.01633456
YpfN family protein	-0.5514105	4.90945636	0.00215797	0.01633456
tyrosine--tRNA ligase	-0.476021	8.32768203	0.00216927	0.01638715
class 1b ribonucleoside-diphosphate reductase subunit alpha	-0.704491	7.13200346	0.00218933	0.01650 55
malate dehydrogenase (quinone)	-1.0675583	7.09453 84	0.00222285	0.01669501
SDR family oxidoreductase UcpA	-0.4928262	9.46901465	0.00222334	0.01669501
cytochrome b562	0.48961144	7.29595483	0.00223479	0.01671724
DUF441 domain-containing protein	-0.3879319	5.73115399	0.00223519	0.01671724
copper homeostasis membrane protein CopD	-0.4224931	6.82972876	0.00224 76	0.01675462
DNA-binding transcriptional regulator CytR	-0.3690763	8.51520 27	0.00224909	0.01675462
superoxide dismutase [Cu-Zn] SodC2	0.78304603	5.75526519	0.00226985	0.01687582
phosphoribosylglycinamide formyltransferase	-0.8680642	8.28881226	0.00227584	0.01688701
PTS mannitol transporter subunit IICB	0.82265212	2.50149 72	0.00229061	0.01696314
peptidylprolyl isomerase PpiC	-0.4791542	6.09191769	0.00229818	0.01698576
tryptophan permease	-0.4323213	5.43595887	0.00230374	0.01699345
DUF1456 family protein	-0.3701708	7.41182886	0.00231845	0.01705769
YbdD/YjiX family protein	-0.56062	7.95547858	0.00232151	0.01705769
flagellar basal body rod protein FlgB	-1.4349419	1.36146 35	0.00235743	0.01728779
outer membrane permeability protein SanA	-0.4150253	6.15017481	0.00237019	0.01734758
quaternary ammonium compound efflux SMR transporter SugE	0.44433313	5.50616571	0.00238 12	0.01739431
DUF485 domain-containing protein	0.95734525	8.24389729	0.00241047	0.01757 4
BtpA family protein SgcQ	0.88519014	5.07584412	0.00244924	0.01782211
4-amino-4-deoxy-L-arabinose-phosphoundecaprenol flippase subunit ArnF	0.64200564	3.80074	0.00247525	0.01790857
imidazole glycerol phosphate synthase subunit HisH	-0.5831201	4.39003 79	0.00247777	0.01790857
macrodomain Ter protein MatP	-0.50005	5.08893653	0.00247965	0.01790857
protein translocase subunit SecF	-0.5715398	8.86985161	0.00248016	0.01790857
sugar ABC transporter permease YjfF	1.22300731	6.31972022	0.00248678	0.01792198

anti-sigma-E factor RseA	-0.5101827	9.13700368	0.0024927	0.01793029
molybdopterin-dependent oxidoreductase	0.32858993	7.23553322	0.00252713	0.01814328
sigma-E factor regulatory protein RseB	-0.3926782	8.99277786	0.0025332	0.01814641
dihydroxy-acid dehydratase	-0.6815807	8.30174165	0.00253722	0.01814641
CidA/LrgA family protein	0.5289141	4.28752551	0.00255756	0.01825719
two-component system sensor histidine kinase PmrB	0.40317145	7.17124512	0.0025948	0.01848795
NAD-dependent dihydropyrimidine dehydrogenase subunit PreT	0.6826402	3.7728865	0.00262036	0.01863477
membrane-bound lytic murein transglycosylase EmtA	-0.3507953	5.40605748	0.00262784	0.01865272
cyclic-guanylate-specific phosphodiesterase PdeF	0.41136831	5.62356804	0.00268058	0.01899125
galactofuranose ABC transporter substrate-binding protein YtfQ	1.08642633	7.82364602	0.00269208	0.01903687
BCCT family transporter	0.48863742	5.71567657	0.00271677	0.01917539
leucine efflux protein LeuE	-0.6652917	5.98270367	0.00277058	0.01951859
NADPH-dependent L-lysine N(6)-monooxygenase IucD	-0.3519724	7.36219706	0.00281336	0.01977393
DUF883 domain-containing protein	1.28466226	3.83813528	0.00281734	0.01977393
putative DNA-binding transcriptional regulator	-0.4357653	8.11679384	0.0028341	0.01979987
diaminopimelate decarboxylase	1.95237732	6.0541886	0.00283447	0.01979987
DNA-binding protein HU-beta	-0.42813	11.1816825	0.00283974	0.01979987
peptidylprolyl isomerase B	-0.3648175	9.39283161	0.00284209	0.01979987
YidB family protein	1.18759369	5.16007024	0.0029219	0.02031827
YqaJ viral recombinase family protein	0.42366584	4.30228956	0.0029917	0.02074788
dTDP-4-dehydrorhamnose 3%2C5-epimerase	-0.7061028	3.92996645	0.00299471	0.02074788
G/U mismatch-specific DNA glycosylase	0.51457914	7.26126356	0.00304871	0.02108315
diguanylate cyclase	0.44428446	8.06810864	0.00310414	0.0214266
galactose/methyl galactoside ABC transporter ATP-binding protein MglA	-0.7953223	9.2081869	0.00310976	0.0214266
hexitol phosphatase HxpB	-0.3399922	6.87945768	0.0031351	0.0215234
YjcZ-like family protein	0.86922019	4.34048454	0.00313525	0.0215234
heme exporter protein CcmC	-0.4098041	5.17546782	0.00318031	0.02179293
DUF2633 family protein	0.36399799	8.07387808	0.00320906	0.02194023

Zn(II)/Cd(II)/Pb(II) translocating P-type ATPase ZntA	0.34091024	7.93552254	0.00321347	0.02194023
50S ribosomal protein L7/L12	-0.9239963	12.3393868	0.00325692	0.02219392
F0F1 ATP synthase subunit C	-0.451411	10.1394718	0.00326242	0.02219392
zinc ABC transporter ATP-binding protein ZnuC	-0.4276463	5.53862268	0.00327495	0.02221377
arylsulfatase AslA	0.42669482	4.17864433	0.00327715	0.02221377
glucose-6-phosphate dehydrogenase	-0.4348222	8.39235716	0.00331254	0.0223821
aconitate hydratase AcnA	0.65747016	8.46639355	0.00331804	0.0223821
porin OmpA	0.52908381	11.4716971	0.00331983	0.0223821
phosphate ABC transporter substrate-binding protein PstS	0.46276379	5.24039703	0.00335572	0.02258359
ABC transporter substrate-binding protein	0.49787702	8.63949773	0.00336422	0.02258375
anthranilate synthase component I	-0.5407827	3.6384388	0.00336888	0.02258375
class Ib ribonucleoside-diphosphate reductase assembly flavoprotein NrdI	-0.8427813	5.57740552	0.00337708	0.02258375
DUF3343 domain-containing protein	-0.6685116	4.01868984	0.00337976	0.02258375
SLC13 family permease	-0.3596967	5.97828533	0.00340469	0.02271001
arabinose ABC transporter substrate-binding protein AraF	0.92091566	3.94307904	0.00341367	0.02272962
cysteine synthase B	-0.5565225	5.18134389	0.0034221	0.02274545
3-phosphoshikimate 1-carboxyvinyltransferase	-0.5667512	6.4068587	0.00344031	0.02282616
trp operon repressor	-0.3565801	6.73663276	0.00345373	0.0228473
nucleoside triphosphatase NudI	-0.6538614	7.3356923	0.00345564	0.0228473
bifunctional hydroxymethylpyrimidine kinase/phosphomethylpyrimidine kinase	-0.6766289	6.18097296	0.00352544	0.02326788
bifunctional DNA-binding transcriptional regulator/O6-methylguanine-DNA methyltransferase Ada	0.59076416	6.12844697	0.00353637	0.02329918
glutamate/aspartate:proton symporter GltP	-0.5619547	8.77549786	0.00355375	0.02337274
DUF421 domain-containing protein	0.68351425	4.08724701	0.00356786	0.0233864
3-oxoacyl-ACP reductase FabG	-0.4397099	9.57943491	0.00356826	0.0233864
flavin reductase family protein	0.59498274	4.64928655	0.00366703	0.02399193
dipeptide ABC transporter permease DppB	1.02947438	7.10996076	0.00369663	0.02414358
FKBP-type peptidyl-prolyl cis-trans isomerase	-0.373842	10.071389	0.00370888	0.02416604
acetyl-CoA carboxylase biotin carboxyl carrier protein	-0.5010968	7.89178348	0.00371291	0.02416604

scaffolding protein MipA	-0.5464628	7.79237594	0.00378675	0.02460405
excinuclease ABC subunit B	0.32331083	7.17262361	0.00379582	0.02462044
peptidoglycan DD-endopeptidase MepH	-0.4012965	8.30025544	0.00381962	0.02473218
IS3-like element ISEc24 family transposase	0.44535389	4.64544494	0.00384865	0.02487442
DeoR/GlpR family DNA-binding transcription regulator	-0.3647481	9.57739061	0.00385481	0.02487442
YtjB family periplasmic protein	-0.4187056	4.89169283	0.00387043	0.02493244
NADP-specific glutamate dehydrogenase	-0.6152383	7.7426051	0.00390153	0.02506447
cysteine desulfurase	0.59286191	8.18625947	0.00390536	0.02506447
CidB/LrgB family autolysis modulator	0.54319903	3.96435022	0.00391091	0.02506447
excinuclease ABC subunit UvrA	0.40582969	8.68014657	0.00395156	0.02528194
protein/nucleic acid deglycase	1.49886307	1.57701202	0.00397306	0.02537629
exodeoxyribonuclease VII small subunit	-0.3516761	7.50623442	0.00401663	0.02561115
two-component system response regulator RstA	-0.5087165	4.4991795	0.00404941	0.02577646
6-phosphogluconate phosphatase	-0.40966	6.86436178	0.00406326	0.0257928
DUF2766 domain-containing protein	-0.5965784	6.39967433	0.00406667	0.0257928
SPFH/Band 7/PHB domain protein	0.35117501	5.89169787	0.00407255	0.0257928
aspartate carbamoyltransferase	2.37402467	6.13454505	0.00409006	0.02586021
Na(+)/H(+) antiporter NhaB	-0.3634907	7.66637885	0.00411943	0.02600217
aromatic amino acid efflux DMT transporter YddG	-0.327466	5.17348455	0.00412843	0.02601531
glycogen phosphorylase	0.53349982	9.26823385	0.00413837	0.02603436
PTS maltose transporter subunit IICB	-0.5036171	6.97442488	0.00414992	0.02606344
phosphonate C-P lyase system protein PhnL	0.84430507	2.50914466	0.00417073	0.02615048
nickel import ATP-binding protein NikE	-0.5162348	3.8893237	0.00418937	0.0261981
50S ribosomal protein L27	-0.777908	9.60255436	0.00419225	0.0261981
adenylate kinase	-0.5138518	9.8307668	0.00423264	0.02640663
gluconate transporter	0.69759568	7.47791428	0.00426212	0.02654652
ribosome-associated protein	-0.3599196	7.15890235	0.00435601	0.02708649
copper homeostasis protein CutC	-0.7801039	6.61446449	0.00437162	0.02713865

PTS glucitol/sorbitol transporter subunit IIA	1.12646362	4.56342706	0.00440958	0.02728991
glutaredoxin-like protein NrdH	-0.941047	6.41601583	0.00441049	0.02728991
asparagine synthase B	-1.019872	7.87609739	0.00442889	0.02735877
anaerobic ribonucleoside-triphosphate reductase	-0.4216838	6.33452568	0.00445888	0.02749883
oligopeptidase B	0.48262621	5.61956568	0.0044717	0.0275328
acetyl-CoA carboxylase biotin carboxylase subunit	-0.6287993	10.2587812	0.00449008	0.02757966
Nramp family divalent metal transporter	0.38002906	8.33633067	0.00449397	0.02757966
bifunctional anthranilate synthase glutamate amidotransferase component TrpG/anthranilate phosphoribosyltransferase TrpD	-0.5493794	4.12951902	0.00451668	0.02767385
xylonate dehydratase YjhG	0.40563237	5.64945257	0.00452771	0.02769632
inosine/xanthosine triphosphatase	-0.3321044	5.61550568	0.00454692	0.02776871
redox-sensitive transcriptional activator SoxR	0.57177344	3.92885683	0.00456633	0.02784205
1-(5-phosphoribosyl)-5-[(5-phosphoribosylamino)methylideneamino]imidazole-4-carboxamide isomerase	-0.5327225	4.74928281	0.00458497	0.02786819
tRNA uridine 5-oxyacetic acid(34) methyltransferase CmoM	-0.3852753	7.31267785	0.00459056	0.02786819
carnitine operon protein CaiE	-0.47538	3.42309304	0.00459284	0.02786819
aldo/keto reductase	0.52246202	6.0019079	0.00461787	0.02797184
acetolactate synthase 2 small subunit	-1.0284209	4.38063607	0.0046248	0.02797184
putative acyl-CoA thioester hydrolase	-0.6268862	8.35187578	0.00477112	0.0288105
cellulose biosynthesis regulator YedQ	0.43752488	6.38274149	0.00479584	0.02888825
ribose-5-phosphate isomerase RpiA	0.41819829	9.41676367	0.00479935	0.02888825
RNA 2'%2C3'-cyclic phosphodiesterase	-0.327048	5.89752963	0.00481513	0.02890357
membrane integrity lipid transport subunit YebS	0.34469023	6.69163794	0.00481726	0.02890357
glutathione ABC transporter permease GsiD	0.42123696	5.38577956	0.00484903	0.02904782
LuxR C-terminal-related transcriptional regulator	1.76450048	1.29976646	0.00486586	0.02910234
multidrug DMT transporter permease	1.00664444	4.64049068	0.00491153	0.02932882
arginine decarboxylase	-0.3878507	4.23005351	0.00496214	0.02955192
galactitol-specific PTS transporter subunit IIC	0.57349381	5.07852953	0.0049646	0.02955192
ABC transporter substrate-binding protein ArtJ	0.74260082	4.93651189	0.00500179	0.02970015

type 1 fimbria switch DNA invertase FimB	-0.7326986	4.08835512	0.00500529	0.02970015
sorbitol-6-phosphate dehydrogenase	1.22576999	6.81420007	0.00501422	0.02970629
acetate--CoA ligase	0.67081151	10.8557086	0.00506507	0.02996037
translation elongation factor Ts	-0.9487016	10.421851	0.00508409	0.03002568
UDP-N-acetylmuramate:L-alanyl-gamma-D-glutamyl-meso-diaminopimelate ligase	-0.3211809	8.33394943	0.00513793	0.03029609
aspartate--ammonia ligase	-1.4359727	6.92273802	0.0051497	0.03031798
GyrI-like domain-containing protein	0.58586298	3.92192842	0.00517716	0.03041309
transcriptional regulator BolA	0.9104411	9.22081178	0.00518203	0.03041309
long-chain-fatty-acid--CoA ligase FadD	-0.3747201	8.83650678	0.00519393	0.03043545
iron-enterobactin ABC transporter permease	-0.525381	8.16375643	0.00524973	0.03071459
DUF2754 domain-containing protein	-0.5985374	6.90966446	0.00535302	0.03123201
MDR efflux pump AcrAB transcriptional activator MarA	-0.8577877	2.15867177	0.00535477	0.03123201
acetate CoA-transferase subunit alpha	-1.3235529	1.03272795	0.0054299	0.03162116
curved DNA-binding protein	0.55225265	6.00360473	0.00544443	0.03162403
cell division inhibitor SulA	0.4390968	7.55274534	0.0054472	0.03162403
YfcL family protein	-0.5709021	7.27361116	0.00546826	0.03169736
type VI secretion system ATPase TssH	0.52963375	2.98382831	0.00549689	0.03181429
peptide antibiotic transporter SbmA	0.30757889	5.77597431	0.00552954	0.03195411
beta-galactosidase subunit beta	2.79150804	5.64051137	0.00554598	0.03199994
restriction endonuclease subunit S	-0.3684664	7.42133178	0.00557181	0.03209975
DUF1788 domain-containing protein	-0.3100105	6.11621513	0.00566758	0.03258286
threonine synthase	-0.4996149	7.58616808	0.00567299	0.03258286
sialic acid transporter NanT	0.39885663	5.24405835	0.00572458	0.0328291
DUF1889 family protein	0.90704232	3.24162368	0.00575687	0.03294148
lipopolysaccharide biosynthesis protein	0.65300043	3.18655871	0.00576169	0.03294148
SH3 domain-containing protein	-0.7329368	6.78565243	0.0058106	0.03315314
dynamin family protein	-0.9016295	2.95718274	0.00581634	0.03315314
F0F1 ATP synthase subunit epsilon	-0.5051999	9.91296176	0.00582643	0.03316041

bacterioferritin-associated ferredoxin	-0.6296617	7.16841136	0.00587463	0.03332452
bacterioferritin	0.50423741	6.82164904	0.00587708	0.03332452
yersiniabactin ABC transporter ATP-binding/permease protein YbtP	-0.5429617	3.17635792	0.00588184	0.03332452
DUF1471 domain-containing protein	0.4189939	8.7652171	0.00591561	0.03346543
fatty acyl-AMP ligase	0.66501878	3.03517326	0.00597991	0.03377843
Tat proofreading chaperone DmsD	-0.3243515	6.54877345	0.00599735	0.03382612
multifunctional transcriptional regulator/nicotinamide-nucleotide adenylyltransferase/ribosylnicotinamide kinase NadR	-0.2907486	7.63282353	0.00611452	0.03443538
cellulose biosynthesis protein BcsE	0.76991615	7.90714436	0.00614314	0.03454486
nucleoside triphosphate pyrophosphohydrolase	0.32742957	7.87445978	0.00623269	0.03499143
twin-arginine translocase subunit TatE	-0.5940945	6.06691423	0.00624116	0.03499143
DUF2534 family protein	-0.3953694	9.424795	0.00625507	0.03501721
tryptophan synthase subunit alpha	-0.4283451	6.11136569	0.00627817	0.03507275
YibL family ribosome-associated protein	-0.3241964	8.48928351	0.00628363	0.03507275
PTS glucitol/sorbitol transporter subunit IIC	1.01214233	6.42570292	0.0063499	0.03537143
phage recombination protein Bet	0.52012523	5.18316062	0.00635595	0.03537143
two-component system response regulator CreB	-0.4335058	5.84870618	0.00636729	0.03538219
ATPase RavA stimulator ViaA	0.39285713	7.50384767	0.00642335	0.03559951
tRNA (uridine(34)/cytosine(34)/5-carboxymethylaminomethyluridine(34)-2'-O)-methyltransferase TrmL	-0.4019019	5.1385404	0.00642532	0.03559951
aspartate 1-decarboxylase	-0.3616405	9.42750336	0.00645627	0.03571835
threonine/serine transporter TdcC	0.99277085	5.94762676	0.00646955	0.0357393
lactate utilization protein C	1.01673386	3.82057204	0.0065772	0.03628068
transcription antiterminator/RNA stability regulator CspE	-0.5051381	13.756295	0.00663209	0.0365299
type IV toxin-antitoxin system AbiEi family antitoxin domain-containing protein	0.42558217	8.03909935	0.00664376	0.03654066
DUF1190 family protein	0.29547345	7.62718798	0.00675505	0.03709855
NADH-quinone oxidoreductase subunit NuoF	-0.3736817	9.14617678	0.0067895	0.03721076
glucose-1-phosphate adenylyltransferase	0.52028626	8.24132932	0.00679527	0.03721076

type II toxin-antitoxin system antitoxin ChpS	-0.6635856	1.84563399	0.00681236	0.03723192
energy-coupling factor ABC transporter ATP-binding protein	0.47231328	3.46308829	0.00681892	0.03723192
Rha family transcriptional regulator	0.56814169	3.16938648	0.00684 85	0.03729185
23S rRNA pseudouridine(2604) synthase RluF	-0.2716728	6.83764991	0.00685618	0.03729185
two-component system sensor histidine kinase ZraS	-0.5407836	5.28801321	0.00685964	0.03729185
FGGY-family carbohydrate kinase	-0.522057	5.54876827	0.00688876	0.03739612
tRNA(1)(Val) (adenine(37)-N(6))-methyltransferase TrmN	-0.5573849	5.44476455	0.00690357	0.03742252
YdgA family protein	0.49601993	7.32983903	0.00696797	0.03771725
glycogen debranching protein GlgX	0.50220235	8.36452506	0.00697816	0.03771816
D-xylose ABC transporter ATP-binding protein	0.84951833	3.45292368	0.00700322	0.03779931
DUF3300 domain-containing protein	0.47120498	4.1406736	0.00704405	0.03787194
hemolysin activation protein	-0.3672569	3.76210059	0.00704625	0.03787194
D-glycero-beta-D-manno-heptose 1%2C7-bisphosphate 7-phosphatase	-0.3668733	5.77420066	0.00705541	0.03787194
DUF2058 domain-containing protein	-0.372874	6.38258874	0.00706102	0.03787194
PKHD-type hydroxylase YbiX	-0.4604994	4.14648532	0.00706701	0.03787194
protein YliM	0.71817283	3.25416922	0.00709485	0.03796705
chromosome partition protein MukF	-0.2862688	6.79250504	0.00712464	0.03807229
hypoxanthine phosphoribosyltransferase	-0.3380097	6.89505859	0.00714853	0.03814578
L-rhamnonate dehydratase	0.5865001	3.4480324	0.00719052	0.0383155
galactarate dehydratase	0.65676174	5.46601909	0.00721726	0.03838538
ATP phosphoribosyltransferase	-0.5036172	5.53866241	0.00722404	0.03838538
DUF1449 family protein	0.7355149	2.67476851	0.00727139	0.03858244
ABC-F family ATPase	-0.4533528	6.77177513	0.00733894	0.03888604
serine endoprotease DegP	-0.4133248	7.77413672	0.00739855	0.03904618
DUF1398 domain-containing protein	-0.574827	4.19073811	0.00739956	0.03904618
hydroxyacylglutathione hydrolase GloC	-0.3473299	8.12615201	0.0074003	0.03904618
P2 family phage major capsid protein	1.10964492	1.52682984	0.00743455	0.03917196
phage encoded cell division inhibitor protein	0.49254534	5.36518135	0.00747291	0.03931902

PTS trehalose transporter subunit IIBC	-0.6217232	8.23161763	0.00750671	0.03944167
penicillin-insensitive murein endopeptidase	-0.4094745	7.18027242	0.00756706	0.03970333
Fe(3+) dicitrate ABC transporter ATP-binding protein FecE	-0.3696165	7.74170898	0.0075825	0.0397289
N-acetylneuraminic acid outer membrane channel NanC	1.01736978	1.73979925	0.00759855	0.03975762
chaperone modulator CbpM	0.62870807	6.13543434	0.00762508	0.03984103
uracil/xanthine transporter	0.53040211	2.94794721	0.00764243	0.03987629
nucleoside-specific channel-forming protein Tsx	-0.3265496	8.15615448	0.00767861	0.04000958
cold shock-like protein CspH	1.24372173	3.24502309	0.00771333	0.04013494
phosphatidylglycerol--membrane-oligosaccharide glycerophosphotransferase	-0.3972394	8.58321468	0.00777581	0.04040414
type I toxin-antitoxin system toxin Ldr family protein	0.3528711	7.27193004	0.00786244	0.04075781
sodium-potassium/proton antiporter ChaA	0.29952402	8.14097354	0.00786554	0.04075781
DUF2773 domain-containing protein	0.47041427	3.13676985	0.00788216	0.04078773
hydrogenase maturation carbamoyl dehydratase HypE	0.27116312	6.23776507	0.00793066	0.04098236
sugar ABC transporter ATP-binding protein	0.73864371	7.94511569	0.00808394	0.04164311
glutathione S-transferase	0.65084064	6.89807968	0.00808524	0.04164311
5-formyltetrahydrofolate cyclo-ligase	0.53021883	6.48828265	0.00809174	0.04164311
tRNA/rRNA methyltransferase	-0.3381409	7.75701375	0.00819382	0.04206156
bacteriophage adsorption protein NfrA	0.3389279	6.03607626	0.00819541	0.04206156
YsaB family lipoprotein	1.11816575	2.53216989	0.00825495	0.04230942
phosphotransferase RcsD	-0.2693874	8.07350129	0.00826963	0.04232701
NADH-quinone dehydrogenase	0.33680336	4.56100314	0.00842492	0.04306323
YbaB/EbfC family nucleoid-associated protein	-0.287236	7.23009138	0.00847256	0.04324801
cell surface composition regulator GlgS	0.67598048	7.81790974	0.00853515	0.04350447
3-oxo-tetronate kinase	0.59414645	3.7497408	0.00854593	0.04350447
multiple antibiotic resistance protein MarB	-0.6419465	2.05897257	0.00866839	0.04401457
adenine phosphoribosyltransferase	-0.8028771	7.88845653	0.00866954	0.04401457
YncE family protein	-0.6125164	9.50704832	0.00872734	0.04424834
helix-turn-helix transcriptional regulator	-0.2611711	7.3581747	0.00874791	0.04429291

IS110 family transposase	0.56662148	2.50881254	0.0087637	0.04431321
primosomal protein DnaT	0.37784993	6.2296731	0.00877562	0.04431392
dienelactone hydrolase family protein	0.57785432	7.23487467	0.00879707	0.04436269
exo-alpha-sialidase	0.44327307	2.63879014	0.00886632	0.04465208
GntP family transporter	0.41692001	4.77245588	0.00892642	0.04489463
translation initiation factor IF-3	-0.6578058	11.9967005	0.00895065	0.0449564
flagellar transcriptional regulator FlhD	-0.4656385	4.18939742	0.008965	0.04496842
CcdB family protein	0.30728355	6.02233877	0.00898867	0.04502714
protein translocase subunit SecD	-0.3254738	9.78047677	0.00905523	0.04526987
flagellum-specific ATP synthase FliI	-0.7171041	2.15736944	0.00906119	0.04526987
alpha%2Calpha-phosphotrehalase	-0.596008	7.54466109	0.00908797	0.04534344
selenide%2C water dikinase SelD	-0.3618145	6.84856721	0.00910356	0.04536104
glutamate synthase subunit GltD	-0.5855168	7.12709401	0.00917406	0.04565187
PTS glucitol/sorbitol transporter subunit IIB	1.00715302	6.02367292	0.00927063	0.04607148
MurR/RpiR family transcriptional regulator	-0.2548326	7.3814621	0.00933057	0.04625009
branched-chain-amino-acid transaminase	-0.6735212	7.3667895	0.00933116	0.04625009
autonomous glycyl radical cofactor GrcA	-1.2725987	6.41550188	0.00938805	0.04647083
beta-aspartyl-peptidase	-0.271228	7.11285904	0.00950369	0.04698146
sodium/proline symporter PutP	-0.5402948	7.79088664	0.00952415	0.04702082
tRNA epoxyqueuosine(34) reductase QueG	0.27069963	7.05284711	0.00954479	0.04706095
DUF1481 domain-containing protein	-0.2548181	8.37404034	0.00957238	0.04709452
copper response regulator transcription factor CusR	-0.5388679	4.6105986	0.00957664	0.04709452
transcriptional regulator LrhA	-0.3247044	8.73752308	0.0096408	0.04734815
molybdate ABC transporter permease subunit	-0.3195861	5.54036571	0.00971593	0.04753777
ion channel protein	0.55065284	4.98178006	0.00972138	0.04753777
arginine N-succinyltransferase	0.85234011	8.17629278	0.009728	0.04753777
lipoprotein	0.44372102	9.66145584	0.00972995	0.04753777
type I pantothenate kinase	-0.3092468	8.1452695	0.00975359	0.04759142

phosphatidate cytidylyltransferase	-0.2753563	8.20672322	0.00978783	0.04769664
zinc transporter ZntB	0.44398681	5.26141725	0.00982464	0.0478141
non-heme ferritin	0.44281024	6.73962657	0.00989895	0.04811348
DNA topoisomerase III	-0.2707936	8.21685356	0.00993415	0.04822226
YfeK family protein	-0.9826381	2.64575504	0.01000381	0.04849783
macrodomain Ori organization protein MaoP	-0.3438527	8.91473713	0.01008321	0.04873036
aspartate:alanine antiporter	0.34658145	7.54542855	0.01008715	0.04873036
sulfur carrier protein ThiS	-0.7470738	2.43235516	0.01009063	0.04873036
DUF1819 family protein	-0.3177784	6.88189225	0.01012634	0.04884013
integrase arm-type DNA-binding domain-containing protein	0.2690559	6.19671947	0.01030229	0.04962513
molybdopterin-dependent oxidoreductase Mo/Fe-S-binding subunit	0.28612822	5.56405011	0.01034654	0.04968393
N-acetylneuraminic acid channel protein	0.71895955	1.43240913	0.0103622	0.04968393
F0F1 ATP synthase subunit delta	-0.4341437	10.0318778	0.01036515	0.04968393
2-dehydro-3-deoxygalactonokinase	-0.4736393	6.05454375	0.01036733	0.04968393
propionate kinase	1.25251754	5.3929461	0.01039052	0.0497317

9.9 Appendix 9

Clinical monitoring sheet				
	Healthy **Normal (N)**	**Mild illness** **(MI)**	**Moderate illness (MO)**	**Severe illness (S)**
Rectal temperature	37.8 – 39.8°C	Pyrexia: >39.8°C		Drop of temperature to <37°C
Bladder inflammation	Normal urination	Stanguria: frequent small urinations	Bloody urine	Persistent bloody urine despite NSAIDs
Body condition	BCS = 3 or higher	BCS = 2 or 3	BCS = 2	BCS = 1
Food consumption	Normal food consumption	Reduced food consumption	Anorexia for 24 hours	Anorexia for 48 hours
Activity	Curious and engaged with peers	Subdued but normal when provoked	Subdued even when provoked. Apart from cage mates	Unresponsive or vocalises or reacts violently when provoked
Respiration	Normal breathing	Altered breathing	Slightly laboured breathing	Laboured breathing
Recumbancy	Stands without need to provoke	Stands when provoked	Requires assistance to stand	Persistent
Dehydration	Skin and eyes are normal		Mildly wrinkled skin	Wrinkled skin or sunken eyes

Day 1	Before procedure			End of Day 1		
	Pig 1	Pig 2	Pig 3	Pig 1	Pig 2	Pig 3
Rectal temperature						
Temp (thermal imaging)						
Bladder inflammation						
Body condition						
Food consumption						
Activity						
Respiration						
Recumbancy						
Dehydration						
Day 2	AM			PM		
	Pig 1	Pig 2	Pig 3	Pig 1	Pig 2	Pig 3
Rectal temperature						
Temp (thermal imaging)						
Bladder inflammation						
Body condition						
Food consumption						
Activity						
Respiration						
Recumbancy						
Dehydration						
Day 3	AM			PM		
	Pig 1	Pig 2	Pig 3	Pig 1	Pig 2	Pig 3
Rectal temperature						
Temp (thermal imaging)						
Bladder inflammation						
Body condition						
Food consumption						
Activity						
Respiration						
Recumbancy						
Dehydration						
Day 4	AM - before procedure			PM		
	Pig 1	Pig 2	Pig 3	Pig 1	Pig 2	Pig 3
Rectal temperature						
Temp (thermal imaging)						
Body condition						
Food consumption						
Activity						
Respiration						
Recumbancy						
Dehydration						